ANL-92/15

Chemical Technology Division

Annual Technical Report

1991

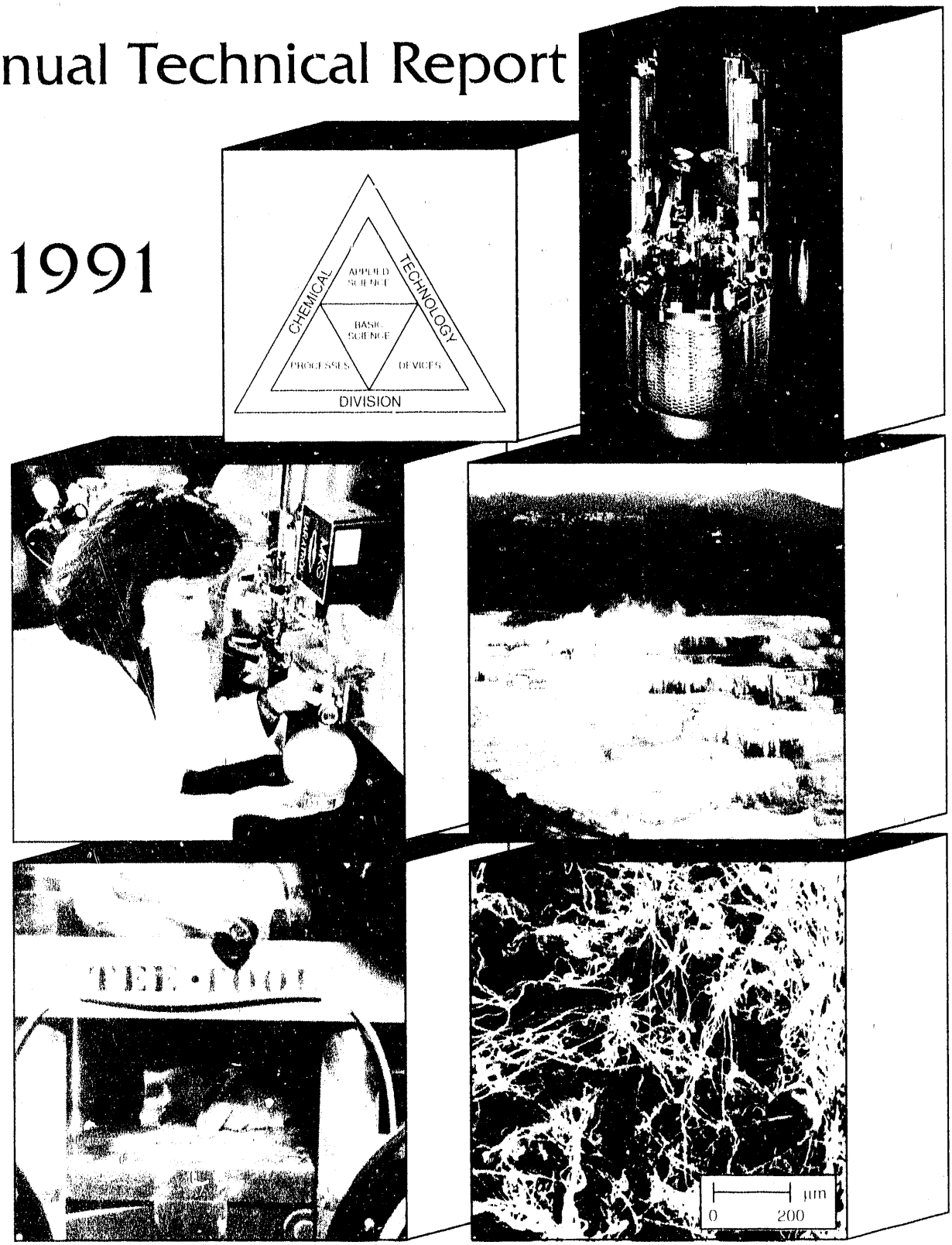

Argonne National Laboratory

Operated by The University of Chicago for the U.S. Department of Energy under Contract W-31-109-Eng-38

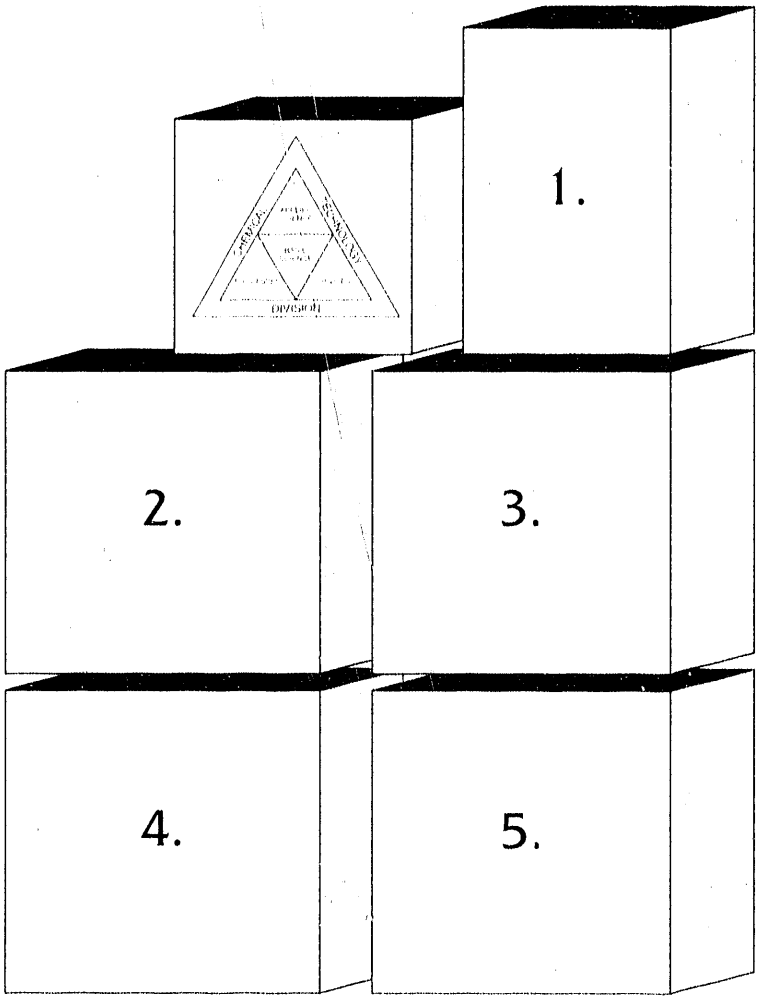

Cover Description

1. The electrorefiner in this photograph will be used in the EBR-II Fuel Cycle Facility to demonstrate the reprocessing of spent fuel from an Integral Fast Reactor.

2. Researcher is preparing canister for gas analysis as part of the Waste Isolation Pilot Plant project, the objective of which is to demonstrate the safe disposal of defense-generated radioactive waste.

3. Samples are being analyzed to investigate the geochemistry and evolution of the hydrothermal system shown in this photograph – Mammoth Hot Springs (Minerva Terrace), Yellowstone National Park, Wyoming.

4. Researcher is pointing to peripheral seal ring developed for bipolar lithium/sulfide cell to be used in electric-vehicle and other energy-storage applications.

5. Micrograph shows ceramic fibers formed by new electrode fabrication process developed for molten carbonate fuel cells.

Disclaimer

Printed in the United States of America

This report has been reproduced from the best available copy.

Available to DOE and DOE contractors from the Office of Scientific and Technical Information
P.O. Box 62
Oak Ridge, TN 37831
Prices available from (615) 576-8401,
FTS 626-8401

Available to the public from the National Technical Information Service
U.S. Department of Commerce
5285 Port Royal Road
Springfield, VA 22161

Distribution Category:
General Energy Research (UC-400)
General, Miscellaneous, and Progress
Reports (Nuclear) (UC-500)

ANL-92/15

ANL--92/15

DE92 014059

ARGONNE NATIONAL LABORATORY
9700 South Cass Avenue
Argonne, IL 60439

CHEMICAL TECHNOLOGY DIVISION
ANNUAL TECHNICAL REPORT
1991

M. J. Steindler — Division Director
P. A. Nelson — Deputy Division Director
J. E. Battles — Associate Division Director
D. W. Green — Associate Division Director

March 1992

Previous reports in this series

ANL-91/18	January-December 1990
ANL-90/11	January-December 1989
ANL-89/15	January-December 1988
ANL-88-19	January-December 1987

TABLE OF CONTENTS

	Page
ABSTRACT	1
SUMMARY	1
I. **ELECTROCHEMICAL TECHNOLOGY**	18
A. U.S. Advanced Battery Consortium	18
B. Advanced Battery Research and Development	19
1. Lithium/Iron Sulfide System	19
2. Sodium/Metal Chloride System	24
C. Analysis and Diagnostics Laboratory	29
1. Performance and Life Evaluations	29
2. Post-Test Analyses	33
D. Fuel Cell Research and Development	35
1. Solid Oxide Fuel Cell	35
2. Molten Carbonate Fuel Cell	42
E. Development of Fuel Cell Systems for Transportation Applications	46
1. Fuel Cell/Battery Powered Bus System	46
2. Proton Exchange Membrane Fuel Cell	48
3. Fuel Reforming Technology	48
II. **FOSSIL FUEL RESEARCH**	51
A. Fluidized-Bed Combustion Studies	51
1. Metal Wastage in Fluidized-Bed Combustors	51
2. Atmospheric Fluidized-Bed Cogeneration Air Heater Experiment	54
3. Development of Regenerable Activated-Bauxite Sorbent Alkali Monitor	55
4. Parametric Study of N_2O Emissions from FBC	57
5. Evaluation of Illinois Limestones for Reducing SO_2 and HCl Emissions	58
B. Magnetohydrodynamic Studies	60

TABLE OF CONTENTS (contd)

		Page
III.	**HAZARDOUS WASTE RESEARCH**	64
	A. Aqueous Biphase Process for Actinide Recovery from Solid Wastes	64
	B. Microwave-Assisted Detoxification	68
	C. New Initiatives	70
	1. Electrokinetic Processes	70
	2. Combined Physical and Biochemical Treatment of Uranium-Contaminated Soils	71
	3. Chemically Bonded Ceramic Waste Forms	71
IV.	**NUCLEAR WASTE PROGRAMS**	72
	A. Glass Testing Program for Environmental Restoration and Waste Management	72
	1. Critical Review	72
	2. Long-Term Testing of Radioactive Glasses	73
	3. Effects of Radiation	75
	4. Effects of SA/V Ratio	76
	5. Formation and Characterization of Colloids	79
	6. Natural Analogues	81
	7. Analytical Support	82
	B. Yucca Mountain Site Characterization Project	82
	1. Unsaturated Glass Testing	82
	2. Spent Fuel Testing	86
	3. Radiation Effects Studies	87
	C. Actinide Speciation Studies	90
	D. Radiation Effects Studies for Waste Isolation Pilot Plant	91
V.	**SEPARATION SCIENCE AND TECHNOLOGY**	94
	A. TRUEX Technology-Base Development	94
	1. Improvements to Generic TRUEX Model	94
	2. Development of Data Base and Modeling Capability	96
	3. Monitoring and Control of TRUEX Processes	99
	4. Centrifugal Contactor Development	103

TABLE OF CONTENTS (contd)

		Page
B.	Treatment of Plutonium Waste Solution by TRUEX Process	104
C.	Treatment of Rocky Flats Plant Waste by TRUEX Process	108
D.	Decontamination of Groundwaters Containing Volatile Organic Compounds	111
E.	Advanced Evaporator Technology	113
VI.	**INTEGRAL FAST REACTOR PYROCHEMICAL PROCESS**	114
A.	Process Flowsheet and Chemistry Studies	114
B.	Process Development Studies	116
1.	Zirconium Behavior Studies	116
2.	Laboratory-Scale Electrorefiner	119
C.	Engineering-Scale Process Development	119
1.	Dissolution of Spent Fuel	120
2.	Electrotransport to Solid Cathode	120
3.	Electrotransport to Liquid Cadmium Cathode	120
4.	Experiments with Pulsed Liquid Cadmium Cathode	122
5.	Cover-Gas Treatment System	123
6.	Equipment Testing	124
7.	Zirconium Behavior in the Engineering-Scale Electrorefiner	125
D.	Waste Treatment Processes	128
1.	Salt Extraction	128
2.	Salt Stripping	129
3.	Salt Immobilization	130
4.	Metal Waste Handling	132
5.	Waste Form Assessment	133
VII.	**ACTINIDE RECOVERY**	134
A.	Flowsheet Development	134
B.	Materials Development	135
C.	Laboratory-Scale Testing	136

TABLE OF CONTENTS (contd)

		Page
	D. Development of Calcium/Salt Recovery Method	137
	E. Engineering-Scale Testing	138
VIII.	**APPLIED PHYSICAL CHEMISTRY**	140
	A. Liquidus-Solidus Temperatures and Viscosities of Core-Concrete Mixtures	140
	1. Differential Thermal Analysis Experiments	141
	2. Viscosity Experiments	144
	B. Metal Fuel Property Studies	145
	1. Phase Studies of U-Fe-Zr System	145
	2. Thermal Conductivity Studies	146
	3. Behavior of Actinide and Lanthanide Alloys	147
	C. Fusion-Related Research	149
	1. Temperature-Programmed Desorption from $LiAlO_2$	150
	2. Lithium Vaporization Behavior of Lithium Ceramics	153
	3. Tritium Release Studies	155
	D. Support Studies for New Production Reactor	158
IX.	**BASIC CHEMISTRY RESEARCH**	162
	A. Fluid Catalysis	162
	1. Catalytic Chemistry in Supercritical Media	162
	2. Hydrocarbon Activation Chemistry	168
	B. Materials Chemistry	170
	1. Studies of High-T_c Superconductors	170
	2. Quantum Chemical Studies	173
	C. Interfacial and Corrosion Science	175
	1. Interface Structure and Dynamics	175
	2. Research on Molecular Sieve Materials	179
	3. Preparation of High-T_c Films by Alloy Oxidation	182
	D. Geochemistry	183
	1. Radium Geochemistry and Isotopy of Thermal Waters in Yellowstone National Park, Wyoming	184

TABLE OF CONTENTS (contd)

Page

2. Origin and History of Petroleum: Compound-Specific Isotopic Evidence 186

3. New Facilities 187

X. **ANALYTICAL CHEMISTRY LABORATORY** 188

XI. **R&D PROGRAM COORDINATION OFFICE** 205

A. Private-Sector Contracts 205

B. Hazardous Substance Research Centers 208

XII. **COMPUTER APPLICATIONS** 210

XIII. **ADDENDUM. CHEMICAL TECHNOLOGY DIVISION PUBLICATIONS --- 1991** 213

CHEMICAL TECHNOLOGY DIVISION
ANNUAL TECHNICAL REPORT
1991

ABSTRACT

Highlights of the Chemical Technology (CMT) Division's activities during 1991 are presented. In this period, CMT conducted research and development in the following areas: (1) electrochemical technology, including advanced batteries and fuel cells; (2) technology for fluidized-bed combustion and coal-fired magnetohydrodynamics; (3) methods for treatment of hazardous and mixed hazardous/radioactive waste; (4) the reaction of nuclear waste glass and spent fuel under conditions expected for an unsaturated repository; (5) processes for separating and recovering transuranic elements from nuclear waste streams; (6) recovery processes for discharged fuel and the uranium blanket in the Integral Fast Reactor (IFR); (7) processes for removal of actinides in spent fuel from commercial water-cooled nuclear reactors and burnup in IFRs; and (8) physical chemistry of selected materials in environments simulating those of fission and fusion energy systems. The Division also conducts basic research in catalytic chemistry associated with molecular energy resources; chemistry of superconducting oxides and other materials of interest with technological application; interfacial processes of importance to corrosion science, catalysis, and high-temperature superconductivity; and the geochemical processes involved in water-rock interactions occurring in active hydrothermal systems. In addition, the Analytical Chemistry Laboratory in CMT provides a broad range of analytical chemistry support services to the technical programs at Argonne National Laboratory (ANL).

SUMMARY

Current programs within CMT are briefly summarized below. These programs are discussed in greater detail in the remainder of the report.

1. *Electrochemical Technology*

The CMT Division is engaged in a variety of activities related to the development of advanced batteries for vehicle propulsion, utility load-leveling, and other energy storage applications. These activities include research, performance and lifetime testing, post-test examinations, modeling, technology transfer, and technical management of industrial contracts from the Department of Energy (DOE). Work is also being conducted on advanced fuel cells for power plant and transportation applications.

During 1991, DOE's battery R&D program underwent a major restructuring because a partnership among the three major U.S. automakers was formed with the objective of accelerating the development of advanced battery systems for electric-vehicle applications. This new partnership--designated the U.S. Advanced Battery Consortium (USABC)--has pooled its financial resources with the Electric Power Research Institute (EPRI) and DOE. Several briefings were given by CMT staff to members of the USABC regarding the relative capabilities and limitations of various advanced battery systems, as well as the capabilities of CMT to provide R&D support to future USABC-sponsored programs.

Over the past 19 years, CMT has been conducting in-house R&D on lithium/iron sulfide batteries, which have a molten-salt electrolyte and operate at high temperature (375-425°C). In 1990, DOE signed an industrial R&D contract with SAFT America, Inc., to develop lithium/iron sulfide batteries for electric-van applications. The contract specifies delivery of three full-size Li/FeS batteries for testing in the third year of the contract. In support of this project, CMT provided technology transfer to SAFT, technical management for DOE, and R&D on critical technical issues. Full-size EV cells (prismatic design) built by SAFT are undergoing evaluation in performance and lifetime tests at SAFT and CMT.

In the past year, CMT undertook performance modeling studies for lithium/sulfide batteries with various designs. The performance projections indicated that the "bipolar" Li/FeS_2 battery (i.e., cylindrical cells stacked so that the positive and negative electrodes of adjacent cells have a common current collector) has the best prospects of meeting the USABC long-term performance objectives (specific power of 400 W/kg and specific energy of 200 Wh/kg).

Our in-house research program on the lithium/iron sulfide system has been concentrated on further improving the bipolar design. A critical component in the bipolar battery is the hermetic seal formed at the cell periphery. We have developed sealant materials that are electronic insulators and bond tenaciously to metals and ceramics in the molten-salt cell environment. This seal was successfully tested in a stack of four small-scale (3-cm dia) bipolar cells, which operated for >500 cycles with >98% coulombic efficiency. Effort in the past year was concentrated on scaling up the bipolar cell from the small-scale electrode diameter of 3 cm to a battery prototype size of 13 cm. To that end, prototype FeS and FeS_2 bipolar cells with our new sealant technology were fabricated and tested. These prototype cells have exhibited approximately 30% increased specific energy and doubled specific power compared with the earlier prismatic cells. Testing is continuing.

In-house research is also being conducted on the sodium/nickel chloride battery, which normally operates at 260°C. Recent efforts have focused on improving the performance of the Ni/$NiCl_2$ positive electrode, which limits the cell performance in the present construction. As a result of this work, we achieved a significant breakthrough by development of a "synergistic" Ni/$NiCl_2$ electrode in which the usable capacity was increased by four times and the area-specific impedance was reduced to one-third that of a baseline Ni/$NiCl_2$ electrode. This significant performance improvement was achieved by the use of additives and a modified morphology in the Ni/$NiCl_2$ electrode. For exact measurements of usable capacity and area-specific impedance in these studies, we designed and operated small research cells with 0.6-1.8 Ah capacity. These cells simulate the components and operational conditions of a full-size

$Na/NiCl_2$ cell. We also developed a method to measure the dynamic performance of the research cells and project energy and power for full-size batteries of various specified designs when discharged under dynamic load profiles, such as the Simplified Federal Urban Driving Schedule. In other work, performance projections with a computer model developed in CMT indicated that an advanced bipolar design containing $Ni/NiCl_2$ electrodes with the same capabilities as the synergistic design would nearly reach the USABC long-term performance objectives.

The Analysis and Diagnostics Laboratory (ADL) in CMT includes a test laboratory to conduct battery evaluations under simulated application conditions and a post-test analysis laboratory. In the test laboratory, cells and multicell modules of six battery systems (Na/S, Li/FeS, Ni/Cd, Ni/Fe, nickel/metal hydride, and lead-acid) fabricated by various industrial firms underwent performance and lifetime testing during 1991. Three battery systems (Li/FeS, Na/S, and lead-acid) representing the efforts of five different developers were also subjected to post-test analysis. The information gained from the performance and lifetime tests and the post-test evaluations provides a measure of the technical progress made by the battery developers and identifies specific areas where changes in design or the materials of construction would improve battery performance.

Two advanced fuel cells are being studied at CMT: the solid oxide fuel cell and the molten carbonate fuel cell. Work is underway to develop a monolithic solid oxide fuel cell (MSOFC) design, which shows promise of achieving more power than any conventional hydrocarbon-fueled energy system of the same weight. Since 1988, Allied Signal Aerospace/AiResearch has been conducting development work on the MSOFC with technical support from ANL. In the past year, our support work was focused on understanding and modeling the electrochemical performance of single MSOFCs. Polarization curves for a typical MSOFC operated at 1000°C with oxygen partial pressures on the cathode side of the fuel cell between 0.035 and 1.0 atm (3.5 and 100 kPa) revealed complex, unexpected behavior at high oxygen partial pressure. An electrochemical model is being developed to examine possible mechanisms that would describe the observed polarization curves and would be consistent with other electrochemical studies in our laboratory and others. We also determined that competing cracking reactions could be a problem in MSOFCs operated with a high-molecular-weight hydrocarbon fuel, and that the presence of small amounts of sulfur in hydrocarbon fuel could react with the anode and cause performance degradation.

A project is underway to develop new materials which permit operation of ceramic solid-state fuel cells at lower temperatures (500-800°C vs. 1000°C currently required), which would increase flexibility in cell stack design and would improve cell efficiency. Our approach is to start with a search for a new electrolyte to replace the present yttria-stabilized zirconia. Tests to date have shown that $Bi_2Al_4O_9$ and La-Al-Bi-O have promise of achieving the necessary conductivity and thermodynamic stability for the lower temperature operation. A search is also underway for improved sealants to be used in a stack of solid oxide fuel cells (along the edges of each electrode and between the manifold and the stack).

The work on molten carbonate fuel cells is focused on developing conductive materials that are stable in the high-temperature (650°C) cell environment and testing these materials as cell components. The cathode development effort in 1991 was focused on testing

$LiFeO_2$ as the cathode material. This stable material is being considered as an alternative to the present NiO because NiO cathodes have dissolution/precipitation problems that limit cell lifetime. We have formulated an alternative oxidant mixture (95% air-5% CO_2) that is expected to improve the performance of $LiFeO_2$ cathodes. When this oxidant is coupled with a 675°C operating temperature, Co-doped $LiFeO_2$ cathodes tested in half cells attained similar performance to state-of-the-art NiO cathodes at 650°C. This performance level still needs to be demonstrated in full molten carbonate fuel cells. Alternatives are also being sought for the present nickel anode, because this component suffers from compaction and creep during cell operation. Present emphasis is on determining the in-cell performance of doped and undoped iron- and manganese-based anodes. In addition, ceramic bipolar separators are being evaluated as an alternative to the present metal separators, which could exhibit corrosion problems and add significantly to cell cost.

The Division provides technical support to DOE for developing fuel cell and fuel cell/battery systems for transportation applications. This work included technical management of contractor efforts to develop a phosphoric acid fuel cell/battery system (for use in an urban bus) and a proton exchange membrane fuel cell. In addition, in-house studies are being conducted on fuel reformers for converting alternative fuels (e.g., methanol, ethanol) to a hydrogen-rich gas mixture for powering fuel cells in automotive applications.

2. *Fossil Fuel Research*

The Chemical Technology Division is the lead division for several projects in the ANL Fossil Fuel Program. These projects involve studies on fluidized-bed combustion (FBC) and magnetohydrodynamic (MHD) power generation.

Metal loss from in-bed heat-transfer tubes in FBC is a recurring problem that is impeding commercialization. To address this problem, a cooperative R&D venture was formed with ANL and seven other organizations. Activities undertaken in 1991 included fluidized-bed experiments at Foster Wheeler Development Corp. and the University of Illinois at Urbana-Champaign to determine solids motion around immersed tubes and their erosion in a fluidized bed. Data from these experiments were analyzed using ANL-developed computer models of the fluidized-bed hydrodynamics and erosion processes. The model predictions and experimental data from this and earlier work have been translated into simple guidelines for the design and operation of fluidized-bed combustors with minimal metal loss.

Argonne is managing the Atmospheric Fluidized-Bed Cogeneration Air Heater Experiment for DOE. The objective is to assess materials and process performance of in-bed air heaters for cogeneration of electricity and hot air in an atmospheric fluidized-bed combustor (AFBC). Corrosion tests of 60 types of alloys at 875°C for 2000 h were conducted in a large-scale AFBC unit at a Rockwell International site in El Segundo, CA. These results, together with those reported for an earlier laboratory test, were used to determine the role of key variables that contribute to accelerated corrosion of the candidate alloys and assess the long-term performance of these materials for air heater applications.

The presence of vapor-phase alkalis in the exhaust of pressurized fluidized-bed combustors (PFBCs) can lead to unacceptable corrosion of the gas-turbine blade materials. Work is in progress to develop a regenerable activated-bauxite sorber alkali monitor (RABSAM) for the *in situ* measurement of alkali vapor in PFBC off-gas. The monitor will use commercial-grade activated bauxite, which contains some clay impurities that can react with alkali vapors. Impregnating the bauxite with LiCl solution was found to deactivate these impurities completely. In the RABSAM, the adsorbed alkalis will be recovered from the activated bauxite by water leaching. To prevent leachate contamination, complete removal of water-soluble alkali compounds in the LiCl-treated activated bauxite is necessary. This was accomplished by a series of steps involving heat treatment, water leaching, acid leaching, and Soxhlet extraction. A batch of regenerable activated bauxite was tested in a pressurized alkali-vapor sorption unit using a simulated PFBC flue gas with no SO_2. After testing, analysis of the activated bauxite indicated that NaCl vapor was captured by the adsorbent through (1) physical adsorption as NaCl, which was easily leached out by water extraction, and (2) chemical reactions that form sodium meta-aluminates and silicates. Tests of regenerable activated bauxite in simulated PFBC flue gas with SO_2 are in progress.

In tests conducted with the laboratory-scale FBC unit (15-cm dia) at ANL, we determined that N_2O emissions from FBC are probably higher than from other types of combustors, and that SO_2 and NO_x emissions could be reduced by staged FBC combustion, as compared with conventional single-stage combustion.

Two materials evaluation studies were conducted for the MHD topping cycle, where an easily ionized seed material will be injected into a coal combustor, and the resulting electrically conductive gas will flow through a magnetic channel. In one study, we found that the design specification for the dissolved oxygen concentration in the combustor cooling water should be set at 15 ppb to avoid metal corrosion problems. In the other study, we determined that the use of silicon nitride to replace boron nitride as the insulating material in the MHD channel may be advantageous with regard to chemical compatibility, mechanical integrity, and electrical properties.

3. *Hazardous Waste Research*

The CMT research on hazardous wastes was focused on two major projects: (1) aqueous biphase processing for recovering actinides from solid radioactive waste and (2) microwave-assisted detoxification for remediating hazardous waste streams.

In the first project, we are investigating the wet grinding of radioactive solids to a particle size of 1 μm followed by aqueous biphase extraction in order to maximize plutonium recovery and minimize waste volume by producing an actinide-bearing concentrate that would more effectively integrate with existing chemical recovery processes. A particularly attractive feature of aqueous biphasic extraction is the ability to achieve single-stage separation factors $>10^6$ between silica and a wide variety of metal oxides. For example, we determined that, with a biphase system consisting of 15% polyethylene glycol (PEG)/7.5% Na_2SO_4, >99.9% of metal oxides such as Fe_2O_3 and Al_2O_3 partitions to the sulfate phase, while >99.9% of the SiO_2 partitions to the PEG phase. The partitioning of SiO_2 and the metal oxides was found to be

quantitatively related to the heat of immersion. We also determined the separation factors for the partitioning of polymeric Pu(IV) and either silica or graphite with 15% PEG/7.5% sodium sulfate. (Graphite and silica are the major constituents of certain foundry residues and incinerator ash, respectively.) The separation factors were quite high: greater than 10^6 for the Pu(IV)/silica system and 10^4 for the Pu(IV)/graphite system (with 0.01% Aerosol OT added to the biphase solution). Work is underway to evaluate separation capabilities of aqueous biphase extraction using actual plutonium residues.

In the second project, we are investigating the use of a microwave discharge plasma reactor for remediating hazardous waste streams containing chlorinated compounds. In experiments with a 7-kW microwave generator, we studied the reaction of trichloroethane (TCA) and oxygen in an argon plasma with varying operating parameters (O_2/TCA molar feed ratio of 1.5 to 165 and microwave power input of 300 to 600 W). The results indicated that the degradation of TCA is nearly complete in the presence of excess oxygen (O_2/TCA ratio greater than two) and power levels above the minimum required to sustain the plasma (450 W). Similar experiments with trichloroethylene (TCE) and an argon plasma indicated that TCE does not have sufficient hydrogen to convert all of the chlorine to HCl under the test conditions. However, this was not a problem when O_2 and H_2O were added to the argon plasma. Future work will focus on the reaction of TCA and TCE with O_2 and H_2O in an air plasma.

Work was started on three new projects: (1) use of electrokinetics for remediating soils contaminated with metals and hazardous organics, (2) use of combined physical and biochemical methods for treating uranium-contaminated soils, and (3) development of chemically bonded ceramic waste forms for underground disposal.

4. *Nuclear Waste Programs*

The volcanic tuff beds at Yucca Mountain, Nevada, are being studied as a potential site for locating the U.S. high-level nuclear waste repository. The potential site at Yucca Mountain is unique among sites that have been considered previously in that it lies several hundred meters above the local water table in a hydrologically unsaturated zone. Because only water vapor or small volumes of liquid water in the repository horizon are expected to contact the waste forms, traditional test methods used to assess glass durability may not be appropriate for the Yucca Mountain environment. Therefore, we have designed alternative test methods which better represent the expected repository environment and are using them to study the interactions that may occur and to project the long-term behavior of emplaced waste. These tests have resulted in valuable insight into the nature of the waste/repository interactions, primarily through analyses of leachates and reacted solids. The latter are done with advanced surface analytical techniques such as analytical electron microscopy.

Several tasks are in progress to assist DOE's Environmental Restoration and Waste Management Program in demonstrating that the Defense Waste Processing Facility and the West Valley Demonstration Project will produce a waste glass product that will perform well in an unsaturated environment typical of what is expected at Yucca Mountain. A detailed review of the literature is being undertaken to critically evaluate the available theoretical and experimental results relevant to the long-term stability of waste glass. To date, a critical review has been

completed on the effects of temperature on glass durability. Reviews of the other important parameters are in progress. In addition, long-term tests are underway to (1) evaluate the reactivity of fully radioactive glasses in a high-level waste repository environment and compare it to the reactivity of nonradioactive glasses of similar composition, (2) assess the effect of radiation on the durability of waste glasses at high glass surface area-to-liquid volume (SA/V) ratios, and (3) compare the extent of reaction for waste glasses at various SA/V ratios. The following observations were made from test results obtained in the past year: (1) elemental releases to solution differed for the radioactive and nonradioactive glasses, and these differences could be explained by taking the controlling reaction mechanism into account; (2) irradiated glasses reacted 5-10 times faster than similar nonirradiated glasses, but remarkable similarity was seen in the sequence of minerals that formed on both the irradiated and nonirradiated glasses; and (3) elemental releases to solution did not scale as SA/V multiplied by the reaction time, as previously believed.

The potential formation of colloids in dissolution of waste glass and the role of colloids in transporting radionuclides are important issues in evaluating waste glass behavior after disposal in a geological repository. A study was therefore initiated to examine the characteristics of colloidal particles formed during waste glass testing. Tests with actinide-doped glasses showed that most (up to 100%) of the Pu, Am, and Cm isotopes in the leachates are associated with particulates in the colloidal size range. The colloids are fragments of a hydrated layer that spalled off the glass during testing.

Experiments involving the reaction of glass and spent fuel under simulated repository conditions are being performed in support of DOE's Yucca Mountain Site Characterization Project. Previous unsaturated glass testing revealed that, as the glass hydrates, elemental segregation occurs, secondary phases form on the original glass surface, and a hydrated layer simultaneously penetrates into the glass. Test results in the past year indicated that (1) Ca, P, Th, and other actinides redistribute within the hydrated layer to form discrete brockite inclusions, and (2) actinide redistribution preferentially concentrates Th, U, Pu, and Am from the glass into the inclusions, which are subsequently mobilized as colloids. Long-term experiments are also being conducted with simulated spent fuel under repository-relevant conditions. In this effort, we have exposed two sets of Zircaloy clad-unirradiated UO_2 pellets to EJ-13 well water under conditions that simulate unsaturated repository conditions. Tests have been underway for 2.25 and 6.5 yr, respectively. A pulse of uranium release from the UO_2 solid, in conjunction with the formation of several uranyl oxide hydrate mineral phases across the sample surface, was observed after one to two years of testing. Thereafter, the uranium release decreased, and a second set of secondary phases was observed.

In other repository-related work, photoacoustic spectroscopy is being employed to study the solubility and speciation of radionuclides in groundwaters. This work has yielded information concerning complexant and temperature effects on the solubilities of important radionuclide species. Recent emphasis has been on the Pu(VI) hydrolysis in near neutral aqueous systems.

Work is underway to investigate the effect of ionizing radiation on the potential for gas generation in the Waste Isolation Pilot Plant (WIPP) site. In this report period, experiments

were initiated to study the gas evolved from WIPP brine spiked with Pu(VI) at concentrations of 10^{-4}, 10^{-6}, and 10^{-8} M over a 160-day test period. Hydrogen was determined to be the primary gaseous product of radiolytic origin. Gas generation rates were determined to be 0.14, 0.002, and <0.0003 mol/(m^3•yr) for Pu(VI) concentrations of 10^{-4}, 10^{-6}, and 10^{-8} M, respectively.

5. *Separation Science and Technology*

The Division's work in separation science and technology is mainly concerned with developing the TRUEX process for removing and concentrating actinides from acidic waste streams contaminated with transuranic (TRU) elements. The objectives of TRUEX processing are to recover valuable TRU elements and to lower disposal costs for the non-TRU waste product of the process. The major thrust of the development efforts has been the Generic TRUEX Model (GTM), which is used with Macintosh or IBM-compatible computers for designing TRUEX flowsheets and estimating cost and space requirements for installing TRUEX processes for treating specific waste streams.

Version 2.4.1 of the GTM was released in 1991 with several enhancements over the earlier versions. These enhancements include increased number of possible feed components; improved calculation of speciation and activities (hydrogen, nitrate, and water) for the aqueous feed solution; greater compatibility between the versions for the Macintosh and IBM-compatible computers; and the capability to complete multiple GTM runs without user intervention.

The data base generated for developing the GTM contains information (from the literature and our own laboratory measurements) on the solution and extraction behavior of important feed components over a wide range of possible waste-stream and processing conditions. Our recent efforts on expanding the data base and adding extraction models have focused on chemical species from (1) the nuclear waste housed in the single-shell storage tanks at Hanford, WA, and (2) waste generated by the Idaho Chemical Processing Plant (ICPP) from the reprocessing of naval nuclear fuel. The chemical species include PO_4^{3-}, Bi^{3+}, and Cr^{3+}, which are important constituents of the Hanford storage tanks, and Cd^{2+}, BF_4^-, and $B(OH)_3$, which are found in the ICPP process stream but have not previously been included in the GTM.

The GTM was used in performing a sensitivity analysis to determine the effect of perturbations in feed composition and flow rates for a base-case flowsheet with regard to meeting the goals set for processing a typical nuclear waste generated at the Plutonium Finishing Plant (operated by Westinghouse Hanford Co.). Of all the perturbations analyzed, only one of them, a change in the flow rate for the aqueous extraction feed, resulted in the most important process goal (TRU concentration in the raffinate <10 nCi/mL) being exceeded. Even then, the flow rate could be up to four times the base value of 400 mL/min without exceeding this goal. The tightest bounds were calculated for the organic-feed flow rate and the concentration of HNO_3 in the aqueous feed to the scrub and first strip sections of the flowsheet. In these cases, the upper value could not exceed 1% and 2%, respectively, of the base value before another process goal (<0.3 mol % americium in the effluent from the second strip) was exceeded. The base-case flowsheet was then redesigned to increase the operating range for these two cases.

An effort is underway to redesign the ANL centrifugal contactor so that its throughput is increased by a factor of four to eight yet it remains safe with respect to nuclear criticality. This super high throughput is being accomplished by increasing the rotor length and rotational speed. The contactor design was evaluated to determine the effect that such super high throughput will have on contactor hydraulics and vibrations. Plans are to build and test a prototype contactor with super high throughput.

The GTM was used to design a TRUEX flowsheet for treating plutonium-containing waste (approximately 200 L) generated at ANL and the New Brunswick Laboratory. Processing of this waste with the calculated flowsheet reduced the TRU concentration by a factor of 22,000, producing a raffinate with an activity of 2 nCi/mL. After processing the first batch, we were informed by Waste Management Operations in ANL's Plant Facilities and Services (PFS-WMO) that the waste acceptance goal had been lowered from 100 to 0.1 nCi/mL. To meet this more stringent goal, we developed another TRUEX flowsheet for treating the raffinate from the first batch. This processing reduced the TRU concentration to 0.2 nCi/mL, which was considered acceptable by PFS-WMO.

The GTM was also used to develop a TRUEX flowsheet for recovering TRU elements (Am and Pu) from a nitrate waste stream at Rocky Flats Plant. This nuclear waste stream, which can contain as much as 0.001 to 0.1 g plutonium per liter and similar amounts of americium, differs from previous TRUEX feeds in that the acid concentration is very high, 5.0 to 7.5 M HNO_3. Sensitivity analysis of this flowsheet showed it to have the desired robustness to meet the process goals.

Two other projects have recently been initiated in separation science and technology. The objectives of these projects are to develop (1) a membrane-assisted solvent extraction method for treating natural and process waters contaminated by volatile organic compounds and (2) evaporation technology for concentrating radioactive waste and product streams such as those generated by the TRUEX process.

6. *Integral Fast Reactor Pyrochemical Process*

The Integral Fast Reactor (IFR) is an advanced reactor concept proposed by, and under development at, ANL. One of its distinguishing features is an "integral" fuel cycle in which the discharged reactor core and blanket materials are processed and fabricated into new fuel elements in an on-site facility. The CMT Division has the responsibility for developing the on-site process for recovering plutonium and uranium from the core and blanket, removing fission products, reenriching the core alloy with plutonium bred in the blanket, and immobilizing fission product wastes in suitable media for disposal.

The IFR pyrochemical process flowsheet accepts any mix of spent fuel from the reactor, removes fission products and cladding, and yields a product from which fresh fuel can be fabricated. The reference process for the planned demonstration of the pyrochemical process in the Fuel Cycle Facility at Experimental Breeder Reactor-II (EBR-II) will utilize anodic dissolution of 20 kg of chopped spent fuel (10 kg/basket assembly), solid cathodes for collecting

the uranium product, and a liquid cadmium cathode for collecting the U-Pu product. A detailed mass balance flowsheet applicable to commercial operations is being prepared.

As part of supporting chemistry studies, the separation factors for pairs of the rare earth elements up to atomic number 64 (gadolinium) and for neodymium vs. plutonium are being measured. The separation factors are being determined by measuring the distribution of these elements between LiCl-KCl eutectic salt and cadmium phases as a function of electrorefiner operating conditions at 500°C. The data from these measurements have been used to construct a chart of the distribution coefficients as a function of the oxidation state in the system. The behavior of the most metallic (readily oxidized) rare earth elements is of interest in salt purification steps, where the salt is treated with Cd-Li or Cd-U alloy for removal of TRU elements.

In the normal transport of uranium to a solid cathode and U-Pu to a liquid cathode, the bulk of the zirconium from the fuel is left in the electrorefiner. Experimental studies of the zirconium behavior in the electrorefiner have shown that anodic dissolution and transport of zirconium to a cadmium pool cathode are possible; the transport current density is about 100 mA/cm^2. Also, these studies showed that zirconium could be electrotransported from the cadmium pool to a solid cathode, provided that the uranium concentration in the cadmium pool and salt is low. X-ray diffraction analysis of samples taken from these experiments indicated that $ZrCd_2$ had formed. This finding agrees with that obtained from examination of the laboratory-scale electrorefiner that we used in earlier tests.

A new, laboratory-scale electrorefiner has been designed, fabricated, and installed in a glovebox. The major design change was in the cathode impeller assembly, which can now accommodate both axial and rotational motion.

In our engineering-scale electrorefiner, anodic dissolution of chopped, clad U-Zr alloy pins has become a routine operation at the 10 kg per batch level. To date, about 200 kg of uranium has been anodically dissolved in this electrorefiner. Electrotransport of about 10 kg of uranium from a cadmium pool to a single mandrel cathode has also become a routine operation, as evidenced by five successive, successful runs. In addition, the important process control parameters for uranium transport have been determined. Major development efforts are now focused on establishing the process parameters for U-Pu transport to the liquid cadmium cathode. A pulsed current is being investigated as a means to reduce formation of uranium dendrites and increase electrotransport of U-Pu mixtures to liquid cadmium cathodes. A device for harvesting the solid cathode product in the Fuel Cycle Facility has been designed and successfully tested. Other prototype equipment for the Fuel Cycle Facility are undergoing testing in the engineering-scale electrorefiner.

Processes are being developed to treat the spent salt and metal from the electrorefiner to recover TRU elements and then to convert the treated salt and metal into disposable high-level waste forms. The spent salt contains the alkali metal, alkaline earth, rare earth, and halide fission products. It also contains small, but significant amounts of uranium and TRU elements. The spent metal consists of cadmium from the electrorefiner pool, which contains zirconium and noble metal fission products, and the cladding hulls. Efforts have been

concentrated on developing the processes needed to treat and immobilize salt. Key features in the treatment of spent salt are the countercurrent extraction apparatus for removing low-level transuranics, the salt stripper vessel for removing rare earth elements and residual transuranics, and a method for immobilization of the salt waste into a form suitable for disposal. The construction of the countercurrent extractor apparatus is nearly complete, and it should be ready for operation in the first half of 1993. Similarly, the salt stripper vessel has been fabricated and is undergoing bench-top testing. This apparatus will be installed in the engineering-scale electrorefiner for demonstration of the salt stripping process. The major effort for immobilizing waste salt has focused on testing salt-occluded zeolites as the immobilization matrix. Tests have been conducted to determine the leach resistance and radiation and thermal behavior of zeolites loaded with simulated fission products from the salt (e.g., Cs and Sr). The results have been encouraging. Also, efforts have been initiated to develop a suitable waste form for the metallic waste from the IFR pyroprocess.

7. *Actinide Recovery*

Spent fuel from commercial light-water reactors (LWRs) contains a considerable quantity of unreacted fissile uranium as well as TRU elements (mainly Pu, Np, Am, and Cm). These elements (actinides) constitute a valuable energy resource, and the purpose of the current work is to develop pyrochemical processes for their recovery for use as fuel in the IFR. We expect these processes to be simple and efficient and to provide a cost-effective method for recovering actinides from LWR spent fuel.

Two high-temperature (~800°C) processes are being examined. In both processes, the LWR oxide spent fuel is reduced to metal, and the actinide elements are separated from the fission products. Both processes use calcium metal to reduce the oxide fuel, forming CaO. In one process, molten salt is used to selectively recover the TRU elements, while the other process uses liquid magnesium metal for this recovery. Calcium metal is recovered from the CaO in the reduction salt by electrochemical methods and recycled along with the salt to minimize process wastes. Mass balance flowsheets have been developed for the salt transport and magnesium extraction processes.

Development work this past year was focused on laboratory-scale testing of each of the process steps with 25-100 g of simulated LWR fuel. Results indicated that the oxide reduction, actinide metal separations, and electrochemical reduction of CaO should perform as expected. Materials for containment of the process liquids are being developed and tested under the chemical and temperature conditions of the processes, and equipment is being designed for scaling up the process steps to the engineering scale (~20 kg of simulated LWR spent fuel).

8. *Applied Physical Chemistry*

The program in applied physical chemistry involves studies of the thermodynamic, thermophysical, and transport behavior of selected materials in environments simulating those of fission and fusion energy systems.

We are experimentally determining the thermophysical properties of core-concrete mixtures expected to occur during the molten core-concrete interaction phase of severe accidents in LWRs. Our current experiments are concerned with two important properties of the core-concrete mixtures: liquidus-solidus temperatures and viscosities. The liquidus-solidus temperatures of core-concrete mixtures are being determined by differential thermal analysis (DTA). Our DTA measurements with UO_2-CaO samples indicated a eutectic temperature of 1945°C and eutectic composition of 37 mol % UO_2-63 mol % CaO. These data helped resolve significant differences in the previously published phase diagrams for the UO_2-CaO system. We also measured viscosities for mixtures of concrete (27.5 wt %) and UO_2-ZrO_2 (72.5 wt %). The viscosity data differed significantly (typically two orders of magnitude) from the viscosity estimates in a thermal hydraulic code (CORCON) that treats core-concrete interactions in hypothetical severe reactor accidents and is an integral part of the Nuclear Regulatory Commission's Source-Term Code Package.

Measurements and calculational analyses are being performed to provide needed information on the thermodynamic and transport properties of IFR fuel. One study focused on determining phase relations with fuel-cladding systems over a wide temperature range. The DTA curves derived from several U-Fe-Zr samples were found to be similar to those previously determined for the U-Fe system and showed a eutectic at 725°C. In other work, we are analyzing some of the basic chemistry and phase relations in metallic fuel systems containing actinides and lanthanides. Lanthanides appear to accumulate in the neighborhood of the cladding during irradiation, and the possible significance of this to fuel performance should be understood. The buildup and intentional addition of actinides to fuel also need to be considered. We are investigating several theoretical approaches to calculation of needed binary phase diagrams for lanthanide and actinide systems.

A critical element in the development of the fusion reactor is the blanket for breeding tritium fuel. Several studies are underway with the objective of determining the feasibility of using lithium-containing ceramics as breeder material.

In one such study, temperature-programmed desorption (TPD) experiments are in progress to provide data that describe the kinetics of desorption of $H_2O(g)$ and $H_2(g)$ from the surface of ceramic tritium breeders. These data are needed for modeling tritium release from such breeders. During the past year, TPD experiments were run with $LiAlO_2$ that had been pretreated at 650°C in a helium gas stream containing hydrogen at several concentrations. During the runs, the sweep gas was either pure helium or the same He-H_2 mixture that was used in the pretreatment, and the temperature was increased from 200 to 800°C at a rate of 5.6°C/min. The results showed that the rates and amounts of H_2O desorption for the runs with He-H_2 sweep gas were substantially higher than the values for desorption into pure helium. The results also indicated that the desorption process can be related to different kinds of sites on the $LiAlO_2$ surface. A method is given on how to apply these results to practical questions of blanket design and tritium-release modeling.

Another study addressed LiOH vaporization loss from ceramic breeders, which is viewed as a possible problem under some operating conditions in fusion reactors. This potential problem is greatest for Li_2O breeder material, and less so for the other candidate ceramic

breeders ($LiAlO_2$, Li_4SiO_4, and Li_2ZrO_3). To assess the need for further experimental work on lithium losses from Li_2O, the existing literature studies were placed on a common basis for comparison by expressing the individual data points as a ratio relative to what would be predicted thermodynamically for equilibrium at the same conditions of temperature and $H_2O(g)$ partial pressure. The results indicated that sweep-gas flow rates under expected reactor conditions will be (1) high enough so that diffusional contributions to mass loss will be negligible and (2) in the range in which one can assume thermodynamic equilibrium conditions. We also concluded that existing studies provide adequate replication and consistency, and that further experimental studies would not be cost effective.

In another breeder study, we employed the TPD method to investigate the tritium release behavior of single crystals of $LiAlO_2$, Mg-doped $LiAlO_2$, and Pt-coated $LiAlO_2$. The TPD plot for the pure $LiAlO_2$ had five peaks, each associated with a different activation energy. Doping the $LiAlO_2$ with magnesium shifted the peaks to lower activation energy; this suggested that the magnesium doping provided low-energy MgO surface sites from which the tritium desorbs. Use of the platinum coating also shifted the peaks to lower activation energies and improved the tritium release. This finding suggests that the rate-controlling step in tritium release from the pure $LiAlO_2$ involves the surface and not bulk diffusion. Based on the TPD results, we developed a tritium release model that accounts for diffusion and simultaneous desorption from several sites on the breeder material and, unlike earlier models, contains no adjustable input parameters. Calculated results showed excellent agreement with measurements from an in-pile tritium release experiment with $LiAlO_2$.

The DOE initiated the New Production Reactor (NPR) Program to plan, design, and construct safe and environmentally acceptable new reactor capacity for an assured supply of tritium. The CMT Division supported this program by conducting two projects on an NPR that is a heavy water reactor. The first project entailed calculational and experimental studies in preparation for transpiration experiments to determine fission product release from Al-U fuel and Al-Li target in a severe accident. Results indicated that formation of an oxide layer on molten aluminum may be a barrier to transport of gaseous aluminum species in the transpiration experiments. In the second project, a conceptual design was developed for the modifications needed to a hot cell at ANL-West so that irradiated fuel and target tubes could be handled there with minimal tritium contamination.

9. *Basic Chemistry Research*

Fluid Catalysis. This research explores new catalytic chemistry and catalytic reaction mechanisms to activate small gaseous molecules (e.g., CO, CO_2, H_2, CH_4) and produce useful products. Kinetic, thermochemical, and structure vs. reactivity studies of catalytic reaction chemistry are conducted in the *in situ* mode under industrial process conditions. Our current effort is focused on investigating homogeneous catalysis in supercritical fluids and hydrocarbon activation chemistry.

In the area of catalytic chemistry in supercritical media, olefin hydroformylation catalysis in supercritical CO_2 is being investigated using ^{59}Co, ^{13}C, and ^{1}H nuclear magnetic resonance (NMR) spectroscopy at high pressure. In earlier research, we had shown that the

cobalt carbonyl catalyzed process works well in supercritical CO_2 and yields a higher selectivity for linear products from propylene hydroformylation than previously obtained in any liquid medium. More recently, we have uncovered several new dynamic NMR processes which indicate that radical chemistry predominates for the cobalt catalyst under hydroformylation process conditions in the absence of olefin.

In the area of hydrocarbon activation chemistry, we are exploring catalytic complexes containing rhodium centers bound to solubilized phthalocyanine ligands. Using this approach, we have recently activated methane by means of the rhodium center's ability to form reasonably strong, but still reactive, metal-carbon and metal-hydrogen bonds.

Materials Chemistry. This research involves experimental and theoretical studies of novel materials that are expected to contribute to significant advances in fields such as energy conservation and utilization and microelectronics. The materials investigated in the past year were high-temperature superconducting (high-T_c) oxides and silicon hydrides.

Electromotive force studies performed on the high-T_c material $NdBa_2Cu_3O_x$ showed no sign of the miscibility gap observed in our prior studies of $YBa_2Cu_3O_x$. However, interesting new evidence was seen for structural transformations and order-disorder effects in the region $x = 6.15$-6.00. In related work, the growth and stability of $(Bi_{2-x}Pb_x)$ $Sr_2Ca_2Cu_3O_y$ from precursor powders fabricated into silver-sheathed wires have been investigated by a combination of equilibration, X-ray diffraction, and electron microscopy methods. Modeling of the equilibration data indicated two sequential kinetic regimes: one (5 to ~80% conversion) controlled by a liquid-phase diffusion process, and the second (~85 to 100% conversion) controlled by a solid-state process.

The powerful Gaussian-2 (G2) *ab initio* theoretical procedure, developed in prior years, has been used to study the thermodynamic properties of silicon hydrides, Si_2H_n ($n = 0$-6) and $Si_2H_n^+$ ($n = 0$-7). The results for the neutral species are in agreement with recent experimental data reporting the existence of stable silicon hydrides having $n = 2$-5. Calculated structures for several of the neutral and cationic species are characterized by unusual hydrogen bridges between silicon atoms.

Interfacial and Corrosion Science. The research in interfacial and corrosion science is focused on the kinetics and mechanisms of aqueous corrosion, the catalytic activity and selectivity of novel molecular sieve materials, and the synthesis of high-T_c superconducting films and interfaces by oxidation of liquid alloy precursors.

In our aqueous corrosion work, surface-enhanced Raman techniques were applied to the characterization of the thin passive films that form on nickel and chromium in aqueous solutions. The film on nickel was determined to be a bilayer structure consisting of a NiO layer between the metal surface and an outer $Ni(OH)_2$ layer, while the film on chromium was found to contain Cr_2O_3 under open-circuit conditions, with the oxidation of Cr(III) to Cr(VI) at more positive potentials.

Our combined experimental/theoretical investigation of the $Cu^{2+} \rightarrow Cu^0$ electron transfer process in aqueous solution has continued. This process is being investigated because copper deposition is one of the most troublesome cathodic reactions occurring during corrosion in LWRs. Experimental kinetics measurements at room temperature have reproduced results reported in the literature, but numerical modeling of the $Cu^{2+} \rightarrow Cu^0$ transient response data has indicated that earlier conclusions regarding the rate-controlling step in the reaction sequence may be in error. *Ab initio* calculations were conducted to determine the energetics of the Jahn-Teller effect for Cu^{2+} and to examine the stability of the Cu^0 species in a water environment. These results will be used to develop a model for the Cu^{2+}/Cu^0 electron transfer reaction.

Our application of synchrotron X-ray radiation to problems in corrosion and interface science has continued. A study of the oxidation of the Pt(111) single-crystal surface in aqueous media revealed a critical anodic potential beyond which the Pt(111) surface became irreversibly roughened. Charge calculations from voltammetric measurements indicated that the critical oxygen coverage necessary to induce the surface disorder associated with the roughening is approximately one monolayer. In work related to elucidating phenomena in the electrical double-layer region, the X-ray reflectivity from a Pt(111) electrode surface immersed in CsF solution was found to vary in a systematic way with electrode potential. This variation is believed to be a signature of the reconstruction of the double layer following a voltage change.

The research on molecular sieve materials has produced two significant findings. First, *ab initio* molecular orbital methods were used to compute the energetics of the Bronsted acid site in TSi_nO_m clusters (where T is either another silicon atom or an aluminum atom) having zeolite-like structures, and several key properties of such structures that are strongly correlated with the acid catalyst performance of zeolite materials were calculated with unprecedented accuracy. Second, zeolite frameworks containing sulfided metal clusters in the intracrystalline void regions were determined to have catalytic activity for the conversion of methane to higher hydrocarbons (C_{2+}) in a reducing environment at temperatures between 300 and 400°C. The reaction rates are still relatively low, but the selectivity to production of C_{2+} hydrocarbons is near 100%.

Work on the development of an alloy oxidation procedure for producing high-T_c superconducting oxide films and interfaces was completed during the past year. Processing parameters were refined to the point where high-quality, epitaxial $YbBa_2Cu_3O_x$ films (10- to 20-μm thick) could be prepared with critical temperature and critical current density of $\geq$80 K and ~1000 A/cm^2, respectively. A method for thinning the liquid precursor alloy layer prior to oxidation was identified as a key objective for any future process development effort.

Geochemistry. This research program includes studies of the geochemistry and evolution of hydrothermal systems and the compound-specific isotopic geochemistry of petroleum. The approach being taken is to investigate specific problems through detailed chemical and isotopic analysis of rock, mineral, water, and gas sampled from appropriate field areas.

During the past year, a study of the geochemistry and isotopy of radium in the hydrothermal system of Yellowstone National Park demonstrated that radium concentration in

thermal waters is largely controlled by barite saturation and zeolite-water ion exchange in thermal water aquifers. Radium isotope ratios ($^{228}Ra/^{226}Ra$) in thermal waters were found to be similar to those of aquifer rocks, indicating predominance of chemical exchange over α-recoil input. Also, techniques for determining carbon isotope ratios of specific organic molecules within complex mixtures were developed and applied to measurements of n-alkanes in a variety of crude oil samples. These measurements allow interpretation of characteristics and migration histories for oil source rock.

10. *Analytical Chemistry Laboratory*

The Analytical Chemistry Laboratory (ACL) is administratively within CMT, the principal user, but collaborates with most of the technical divisions and many of the programs at ANL as a full-cost-recovery service center. In addition, the ACL conducts research in analytical chemistry and provides analytical services for governmental, educational, and industrial organizations.

During the past year, the ACL was involved in a diverse array of activities, including the following: several types of analyses in support of the development of the IFR pyrochemical process; development of procedures for determining uranium and uranium isotopes in high silica soils and total ^{10}B in a novel neutron absorber; measurement of nitrous oxide emissions from fluidized-bed combustors; analyses of limestone and marble briquettes exposed to a variety of atmospheric conditions throughout the U.S.; analyses of samples from a study of molten core-concrete interactions during a degraded-core reactor accident; measurement of radium isotopes in waters and soils for geoscience studies; analyses of environmental samples (waters, soils, sediments, filters, air) taken from DOE sites; development of an extraction chromatography method to analyze environmental radioactive samples for americium; analyses of cores from the pressure vessel of the Experimental Boiling Water Reactor, which is undergoing decommissioning and decontamination; field testing of Fourier transform infrared spectroscopy for characterizing soil samples contaminated with explosives or selected volatile and semivolatile organic species; development of methods for remote detection of chemical agents (related precursors and degradation products) and illegal drug laboratories; development of a Fourier transform infrared spectrometer for the continuous monitoring of incinerator emissions; determination of volatile organic and inorganic compounds in the headspace of storage bins to be placed in the Waste Isolation Pilot Plant site; development of supercritical fluid extraction/gas chromatography for analysis of organic compounds from soil samples; and measurement of volatile organic compounds at a former grain storage facility.

11. *R&D Program Coordination Office*

The R&D Program Coordination Office is assisting DOE in establishing and maintaining a national program of applied R&D in the environmental restoration and waste management area. In the past year, this Office provided technical management and oversight to assist 15 contractors (13 private firms, 1 university, and 1 government laboratory) in performing R&D on new technologies for DOE to meet its compliance and cleanup goals. The R&D projects encompass development of technologies in four general areas: groundwater contamination, soil remediation, site characterization, and containment of contamination. This

Office also provided technical and administrative support to five Hazardous Substance Research Centers, which are co-funded by DOE and the Environmental Protection Agency. Each center is located at a main participant university but consists of a consortium of several universities in the same region. Research at the centers includes projects on biotechnology for waste remediation; pollutant transport mechanisms; chemical and thermal destruction of organics; and remediation of contaminated soils, groundwater, sediments, and dredged materials.

12. *Computer Applications*

The Computer Applications Group assists CMT staff in many aspects of computer-related activities, including laboratory data acquisition and control, computer modeling and simulation studies, analysis of experimental results, graphics, information management and data-base development, computer networking, and procurement of automatic data processing equipment. The Group has responsibility for software maintenance and development for several major minicomputer data acquisition systems, the Division's Local Area VAX cluster (consisting of 11 VAXs), and both Macintosh and IBM-compatible personal computer networks. Additionally, the Group provides hardware maintenance for various small computer systems and peripherals.

I. ELECTROCHEMICAL TECHNOLOGY

The Electrochemical Technology Program in CMT undertakes (1) in-house research, development, testing, post-test analysis, and technical evaluation studies of advanced battery and fuel cell systems and (2) support research, technology transfer, and technical management for industrial R&D contracts to develop these systems. To date, in-house battery R&D has focused on two advanced technologies, lithium/iron sulfide and sodium/metal chloride. The testing, evaluation, and post-test analysis of a variety of advanced batteries (i.e., lead-acid, nickel/iron, nickel/metal hydride, lithium/sulfide, sodium/sulfur) fabricated by industrial firms are performed in CMT's Analysis and Diagnostics Laboratory (ADL). Potential uses of these battery technologies include vehicle propulsion, utility load-leveling, and other energy storage applications. In-house R&D is also being conducted on fuel cells (with solid oxide, molten carbonate, or polymer electrolytes) for power plant and transportation applications.

A. *U.S. Advanced Battery Consortium*

Historically, CMT has conducted R&D on advanced battery systems for DOE, and as technologies have reached an appropriate level of development maturity, they have been transferred to industrial firms for hardware scaleup and engineering development. After that point, typically, CMT has continued to offer R&D support on critical technical issues and provided technical management of the industrial R&D projects for DOE. During 1991, DOE's battery R&D program underwent a major restructuring because a partnership among the three main U.S. automobile manufacturers (General Motors, Ford, and Chrysler) was formed to accelerate the development of selected advanced battery systems for electric-vehicle (EV) applications. This new partnership--designated the U.S. Advanced Battery Consortium (USABC)--has pooled its financial resources with the electric utility industry and DOE. The utility industry joined the USABC in August 1991 through an agreement between the Electric Power Research Institute (EPRI) and USABC.

During the second half of FY 1991, CMT adjusted its R&D efforts to conform with new directives from DOE and align them with the technologies of interest to the USABC. Several briefings were given to members of the USABC regarding the relative capabilities and limitations of various advanced battery systems, as well as the capabilities of CMT to provide R&D support to future USABC-sponsored programs. Technologies that CMT has discussed with USABC include lithium/sulfide, sodium/sulfur, nickel/metal hydride, and lithium/polymer batteries. Also in 1991, CMT achieved a technical breakthrough that significantly increased the power and energy characteristics of the positive electrode for the sodium/nickel chloride battery (Sec. I.B.2); this breakthrough has been acknowledged by the USABC as a significant contribution toward making this technology a viable candidate for meeting its long-term objectives. Based on the interest expressed by the USABC, it appears that DOE will continue to support an R&D project by CMT on the sodium/nickel chloride system.

B. *Advanced Battery Research and Development*

This effort is directed toward developing advanced battery systems and transferring the technology to industry. Current work is focused on attaining major improvements in the performance and cycle life of lithium/iron sulfide and sodium/metal chloride systems.

1. Lithium/Iron Sulfide System

a. Industrial Contracts

For more than 19 years, CMT has been conducting in-house R&D on lithium/iron sulfide batteries, which have a molten-salt electrolyte and operate at 375-425°C. To date, the Li/FeS technology has been developed to the sub-scale battery level for EV applications, while the Li/FeS_2 technology has been advanced to the level of full-size EV cells.

In April 1990, DOE signed an industrial R&D contract with SAFT America, Inc. (Cockeysville, MD) to develop lithium/iron sulfide batteries for EV applications. In support of this three-year, cost-shared contract, CMT has provided technology transfer to SAFT and technical management of the project for DOE. Also, CMT conducted R&D on critical technical issues related to this industrial contract.

Work during the first 17 months of the DOE/SAFT contract was primarily directed at developing Li/FeS technology into full-size batteries for use in electric vans. The performance and life milestones established for this effort are given in Table I-1. The contract specifies delivery of three full-size batteries in the third year of the contract--two for evaluation in the process of developing full-size EV batteries and one for final laboratory testing. The technology transferred from CMT to SAFT during 1990 and 1991 was used to design and build baseline and improved prismatic cells, which are being tested in CMT's Analysis and Diagnostics Laboratory (Sec. I.C) as an independent means of tracking technical progress toward meeting the contract goals. In tests at SAFT, a baseline cell had accumulated 299 cycles and an improved cell, 289 cycles, through the end of FY 1991. Both cells continue to perform well. Also, SAFT built nine baseline cells that will be used to fabricate a 12-V module for evaluation in 1992.

The DOE/SAFT contract included a one-year R&D effort on Li/FeS_2 technology. During 1990-1991, CMT transferred this technology to SAFT, who then designed and built full-scale FeS_2 prismatic cells employing 11.7 x 17.3 cm electrodes. These cells are being tested by SAFT to verify the high performance and long life achieved in smaller prismatic cells at CMT.[1] Through the end of FY 1991, a large prismatic Li/FeS_2 cell continues to perform well after 303 cycles at SAFT.

---

[1]M. J. Steindler et al., *Chemical Technology Division Annual Technical Report, 1988*, Argonne National Laboratory Report ANL-89/15, p. 15 (1989).

Table I-1. Performance and Life Development Milestones for Li/FeS EV Cells and Batteries[a]

Technology	Energy, Wh/kg	Power		Life	
		W/kg	W/L	Cycles	Years
Baseline Cells	90	100	195	300	2
Baseline Sub-Scale Battery	62	80	90	140	1
Improved Cells	100	105	215	600	4
Improved Sub-Scale Battery	80	95	120	370	2
Prototype Cells	125	137	270	800	5
Full-Size Batteries	100	110	150	600	4

[a]All milestones are for simulated driving profiles on the Simplified Federal Urban Driving Schedule (SFUDS). The power is required to 100% depth-of-discharge (DOD), while the cycle-life goal is for operation to 80% DOD.

In the area of support research, CMT conducted detailed performance modeling studies for lithium/sulfide batteries with prismatic and "bipolar" designs. (In a bipolar battery, cylindrical cells form a series-connected stack in which adjacent cells share a current collector, the bipolar plate. This design is described further in Sec. I.B.1.b.) Figure I-1 illustrates the projected performance bands for prismatic Li/FeS, bipolar Li/FeS, and bipolar Li/FeS_2 batteries. The filled circles represent the projected performance levels for batteries designed to meet different power-to-energy requirements. Also shown are the mid-term and

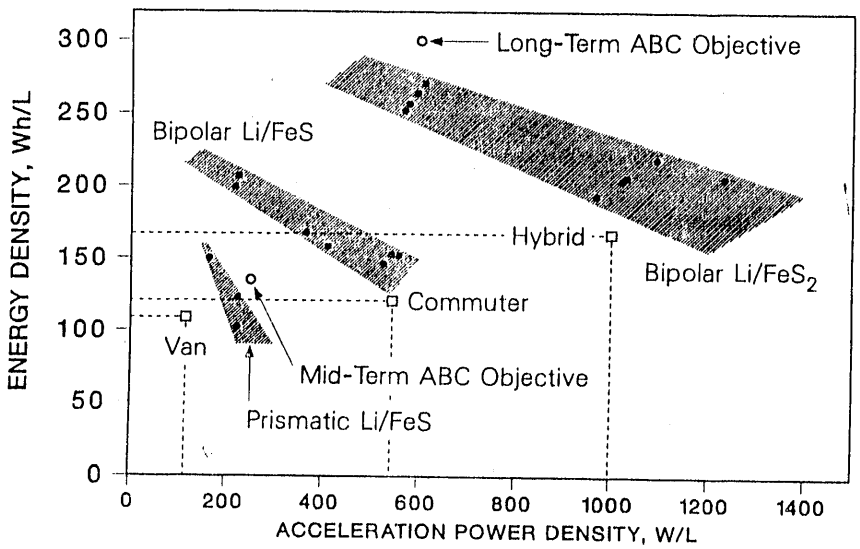

Fig. I-1. Projected Performance of Prismatic Li/FeS, Bipolar Li/FeS, and Bipolar Li/FeS_2 Batteries, along with Performance Objectives of the USABC and Requirements for Electric-Vehicle Applications

long-term performance objectives of the USABC, as well as typical requirements for three different EV applications: a light-duty van with a 160-km range, a high-performance commuter vehicle with a 240-km range, and a small hybrid-vehicle battery that can provide full power for vehicle acceleration. The results indicate that the bipolar Li/FeS_2 batteries have the potential to meet the USABC long-term objectives.

b. In-house Research

The objective of this effort is the development of a prototype bipolar battery that will attain high performance (~200 Wh/kg and 500 W/kg) and long cycle life (>1000 cycles) with the potential for low-cost fabrication. Lithium/sulfide (Li/FeS_2 or Li/FeS) cells with molten-salt electrolyte are well suited to the development of a bipolar battery because long strings of series-connected cells can be assembled, and the individual cells always fail in a short-circuit condition. (When cells fail in the short-circuit mode in a series-connected array of cells, the remaining cells can continue to function normally, and the only loss of energy is that associated with the failed cell.) To maintain the electrolyte molten, cells are normally operated at temperatures of 375 to 425°C. The high-temperature bipolar battery operation provides advantages, as well as engineering and materials development challenges.

A unique feature of the bipolar battery is that the positive and negative electrodes share a common current collector. Because of this arrangement, measures have to be taken to avoid the appreciable self-discharge that would result from an electrolyte path connecting the negative and positive electrodes. Our earlier work on bipolar batteries concentrated on forming gaskets between the two electrode assemblies to retain the electrolyte; these batteries were short-lived. In our present bipolar cell design, a peripheral seal for each cell is formed prior to cell/battery assembly.

As part of a project jointly funded by DOE and the State of Illinois, we are scaling up the sealed bipolar cell from the small-scale electrode diameter of 3 cm to a battery prototype size of 13 cm. The development of a fabrication method for 13-cm-dia peripheral seals in the bipolar lithium/sulfide cell is a key element of this scaleup effort. The development of sealant materials at ANL has led to metal/ceramic bonds about ten times stronger than obtainable with commercially available sealants for service at over 300°C. Additionally, the new ceramic materials, which are chemically stable to the molten-electrolyte cell environment, have been engineered to match thermal expansion coefficients of metal components. Our innovative design approach, in which each cell in the bipolar stack is hermetically sealed, promises to provide long-term stability (capacity and coulombic efficiency). A 500-cycle test of a stack of four 3-cm-dia bipolar cells has demonstrated the extended cycle-life capability of a bipolar Li/FeS_2 battery with our peripheral seal.[2]

---

[2]T. D. Kaun, M. J. Duoba, W. P. Johll, V. Luong, F. C. Mrazek, D. J. Palkon, and D. R. Simon, "Development of Prototype Sealed Bipolar Lithium/Sulfide Cells," Proc. of 26th Intersoc. Energy Conversion Eng. Conf., Boston, MA, August 4-9, 1991, Vol. 3, p. 417 (1991).

During the past year, prototype FeS and FeS_2 bipolar cells and seal components were fabricated and tested at CMT. These Li/FeS and Li/FeS_2 bipolar cells are operated at 425°C with LiCl-LiBr-KBr electrolyte. These bipolar cells have 13-cm-dia electrodes, are 7-mm thick, and have a total weight of 0.25 kg (including the weight of two full current collectors). The electrode materials account for 48% of the total bipolar cell weight. The bipolar Li/FeS cell has a steel/ceramic/steel peripheral seal, whereas the bipolar Li/FeS_2 cell has a steel/ceramic/molybdenum peripheral seal (Fig. I-2), which is more technically challenging to develop. These large-diameter metal/ceramic seals have successfully undergone thermal cycling. The initial prototype seal design uses a simple stacked assembly (Fig. 1-3), which allows for testing several current-collector materials options. We also designed the seal to facilitate bipolar cell integration into a stack through a simple steel/steel weldment. A steel welding flange for the FeS_2 bipolar cell is incorporated into the seal, which is coupled with the molybdenum current collector (positive bipolar cup). Further, a successful cell test of TiN-coated steel for the FeS_2 current collector (40 cycles, 500 h at 415°C) suggests its potential as a substitute for the expensive molybdenum current collector.

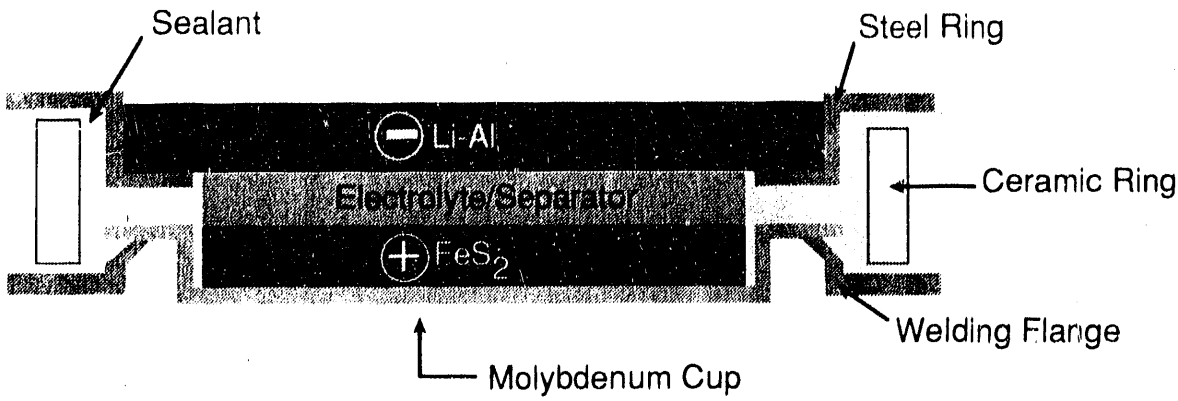

Fig. I-2. Cross Section of Sealed Bipolar Li/FeS_2 Cell

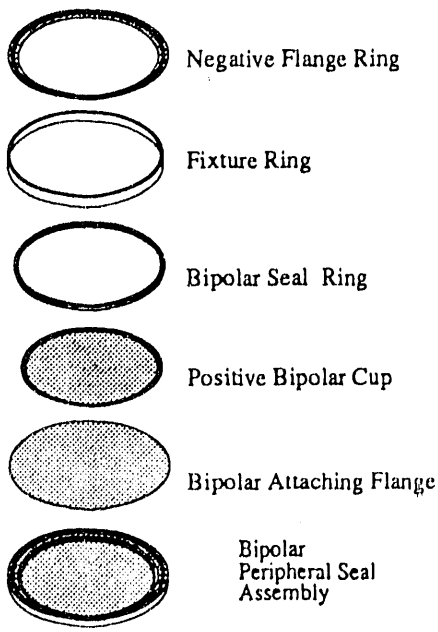

Fig. I-3.

Exploded View of a Bipolar Peripheral Seal Assembly

The first prototype cells are exhibiting approximately 30% increased specific energy and more than doubled specific power over earlier prismatic "monopolar" cells (i.e., separate current collectors for the positive and negative electrodes). They also have attained about 90% utilization of the FeS_2 theoretical capacity (on upper voltage plateau) and 70% utilization for the FeS theoretical capacity. These utilizations are similar to those attained with the 3-cm-dia bipolar cells. The prototype bipolar Li/FeS_2 cell delivers a specific energy of 180 Wh/kg at a 30 W/kg discharge rate, while the prototype Li/FeS cell delivers 130 Wh/kg at a 25 W/kg discharge rate.

The bipolar-cell scaleup actually improved the specific power as a result of lower internal impedance. (It was generally more difficult to provide uniform surface contact to the 3-cm-dia bipolar cells.) Cell impedance was measured by a current-interrupt method with voltage relaxation recorded from 25 ms to 15 s. As shown in Fig. I-4a, the impedance of the Li/FeS cell is impressively low, with only 0.4 $\Omega \cdot cm^2$ values at up to 50% of the discharge capacity, which is equivalent to a peak specific power of ~360 W/kg. As is characteristic of Li/FeS cells, impedance climbs at higher depths of discharge (DOD), up to 0.7 $\Omega \cdot cm^2$

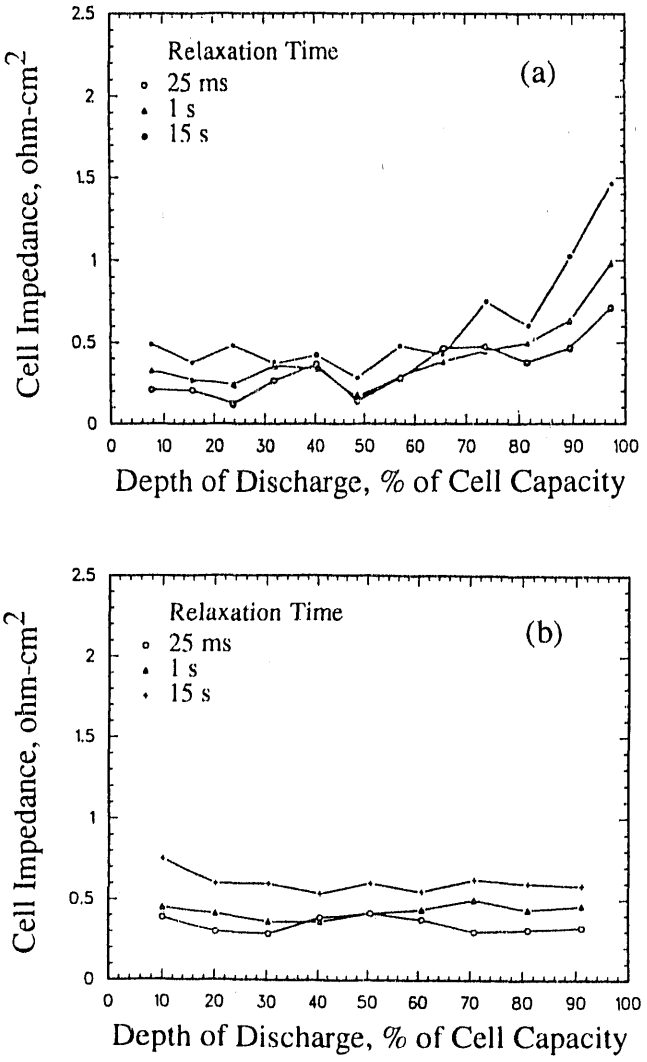

Fig. I-4.

Area-Specific Impedance vs. Depth-of-Discharge for a Prototype Bipolar (a) Li/FeS Cell and (b) Li/FeS_2 Cell at 425°C

at 80% DOD (240 W/kg). Even higher specific power was achieved for the bipolar Li/FeS_2 cell because of its high average discharge voltage and impedance stability to 80% DOD. As shown in Fig. I-4b, this prototype cell had a cell impedance of 0.5 to 0.6 $\Omega \cdot cm^2$ at 80% DOD, equivalent to a peak specific power above 400 W/kg. Because of its excellent performance characteristics, future work will be concentrated on continued development of the bipolar Li/FeS_2 system.

2. Sodium/Metal Chloride System

The purpose of this research is to generate the scientific and technical base needed for development of sodium/metal chloride (Na/MCl_2) batteries for EV propulsion. Of the metal choices, nickel offers the technically most viable cell couple. The cell system can be represented as

$$Na//\beta''\text{-}Al_2O_3//NaAlCl_4/NiCl_2/Ni \qquad (1)$$

and the cell reaction is

$$2Na + NiCl_2 \rightleftharpoons 2NaCl + Ni \qquad (2)$$

The cell uses a β''-alumina solid electrolyte. Moreover, $NaAlCl_4$ is added to the porous Ni/$NiCl_2$ positive electrode to transport sodium ions from the surface of the β''-alumina electrolyte to the reaction sites at the interior of the electrode. The $NaAlCl_4$ is molten at the operational temperature (250 to 400°C) of the cell, but the other constituents of the positive electrode are solid.

These cells are under intensive development in England, Germany, and South Africa because of the attractive high voltage (2.58 V at 300°C) and theoretical specific energy (790 Wh/kg). Also attractive are the mid-temperature range and the reliability of the battery construction because cells fail in the short-circuited mode. The specific power of the present battery construction, however, is only moderate due to the performance-limiting positive electrode. To overcome this problem, we sought to improve the performance of this electrode and to better understand its charge and discharge processes.

Our earlier potentiometric, coulometric, and cyclic-voltammetric investigations on nonporous nickel electrodes[3,4] suggested that a $NiCl_2$ layer formed on the electrode and limited

---

[3]L. Redey and D. R. Vissers, "Investigations of Ni/$NiCl_2$ Electrodes in Basic Chloroaluminate Melt," Extended Abstracts, 176th Electrochem. Soc. Meeting, Hollywood, FL, October 15-20, 1989, Vol. 89-2, p. 143 (1990).

[4]J. Prakash, L. Redey, and D. R. Vissers, "Investigation of Ni/$NiCl_2$ Electrode Process," Extended Abstracts, 177th Electrochem Soc. Meeting, Washington, DC, May 5-10, 1991, Vol. 91-1, p. 4 (1991).

the available capacity (C/cm^2 of the true surface area of the nickel electrode) and power (as a result of high impedance). Our earlier studies also suggested that an electrode with tailored porosity would improve performance by providing high surface area and sufficient pore cavities to support an effective mass transport. Also, we found indications with these experiments that chemical additives to the nickel chloride electrode would improve the properties of the electrochemically forming $NiCl_2$ layer.

Based on the earlier work, we initiated a systematic effort to improve the $Ni/NiCl_2$ positive electrode. As a result, we achieved a breakthrough in which the usable capacity was increased by four times and the area-specific impedance was reduced to one-third that of a baseline $Ni/NiCl_2$ electrode. Figure I-5 shows the area-specific impedance (ASI_{15s}), measured by an interrupted galvanostatic method, as a function of discharged capacity per unit volume for several $Ni/NiCl_2$ electrodes. The baseline electrode represents our electrode fabricated without additives using a sintering process characteristic for mid-1990. The defined usable capacity in this figure is the discharged capacity where the area-specific impedance of the $Ni/NiCl_2$ electrode is $<4\ \Omega \cdot cm^2$. The termination points of the curves at progressively higher utilized capacities indicate increased available energy density (Wh/cm^3), and the lowered area-specific impedance of the $Ni/NiCl_2$ electrode indicates higher power capability (W/kg).

Use of a single chemical additive significantly improved electrode performance, as shown by the higher available capacity and much lower area-specific impedance in Fig. I-5. The morphology of the sintered $Ni/NiCl_2$ electrode was modified by using a pore former during fabrication to attain controlled pore-size distribution. This modified morphology along with an additive further improved performance. Recently, we found that a combination of additives in the modified-morphology electrode has a significant synergistic effect, producing even more

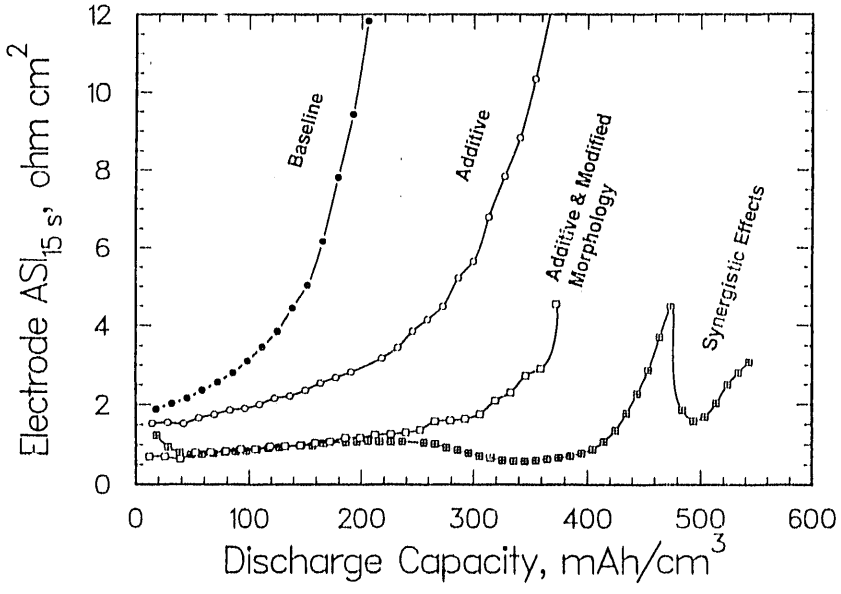

Fig. I-5. Performance Characteristics for Different Designs of $Ni/NiCl_2$ Electrode (0.5-cm thick, discharged at 20 mA/cm^2 and 300°C)

energy per unit volume and even lower area-specific impedance. The chemical additives produce high utilization and low electrode impedance of the nickel matrix, apparently due to doping effects. By an optimal combination of additives, we were able to increase the utilization of the nickel matrix from 15% to about 45%. Even higher utilization of the nickel matrix would not be advantageous because the remaining metal skeleton of the fully charged electrode serves as a current collector and is needed to provide good electronic conduction. The results in Fig. I-5 also indicate that the total capacity of the "synergistic" $Ni/NiCl_2$ electrode can be used in a $Na/NiCl_2$ cell since the area-specific impedance remains below 4 $\Omega \cdot cm^2$.

For exact measurements of the energy density and area-specific impedance in these studies, we designed and operated small research cells with about 0.6-1.8 Ah capacity (Fig. I-6). The research cell simulates the components and operational conditions of a full-size $Na/NiCl_2$ cell. By providing one-dimensional current density distribution in the $Ni/NiCl_2$ electrode, we can precisely measure the important electrochemical engineering parameters necessary for the modeling and performance-projecting calculations that we use to evaluate designs of full-size batteries.

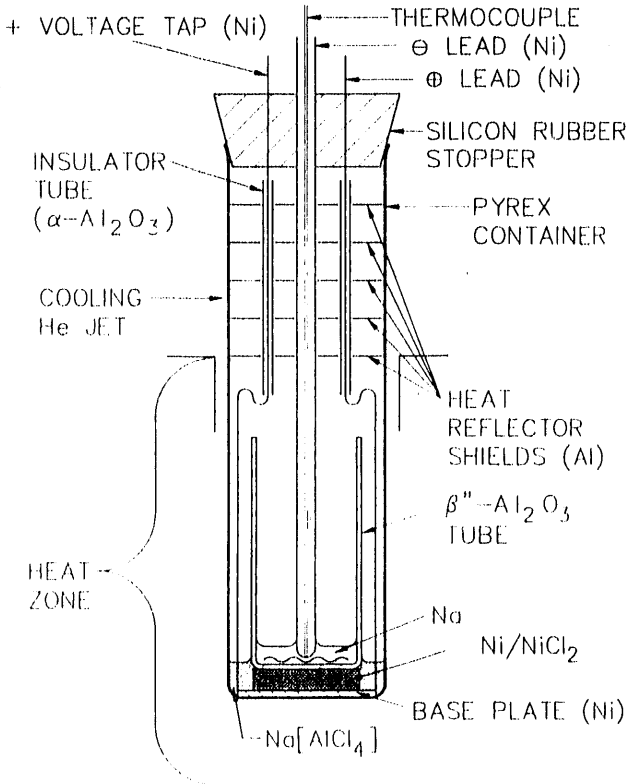

Fig. I-6.

Research Cell Used to Assess Performance of Full-Size $Na/NiCl_2$ Cells

Chemical additives also influence the solubility of $NiCl_2$. Our extensive solubility measurements showed that, for example, in NaCl-saturated (basic) $NaAlCl_4$ melt (the cell electrolyte), sulfur additive reduces the solubility of $NiCl_2$. In the basic melt, the dissolved nickel salt is present as $(NiCl_4)^{2-}$ complex anion. The low concentration and the complex-ion form of the dissolved nickel are important factors because both reduce the rate of the deleterious

cation exchange between the Na^+ ion in the β"-alumina and the Ni^{2+} ion in the melt, resulting from the dissociation of the complex anion. These two factors, thus, facilitate longer cycle life of the $Na/NiCl_2$ cell.

Increased temperature (from 260 to 340°C) was found to significantly improve the energy density and lower the impedance for the $Ni/NiCl_2$ electrode (Fig. I-7). The trend indicates more improvement at even higher temperatures, but, because of the higher solubility of the nickel species, this performance-improving approach has questionable value. To date, our research cells have achieved about 400 deep cycles at 300°C without failure.

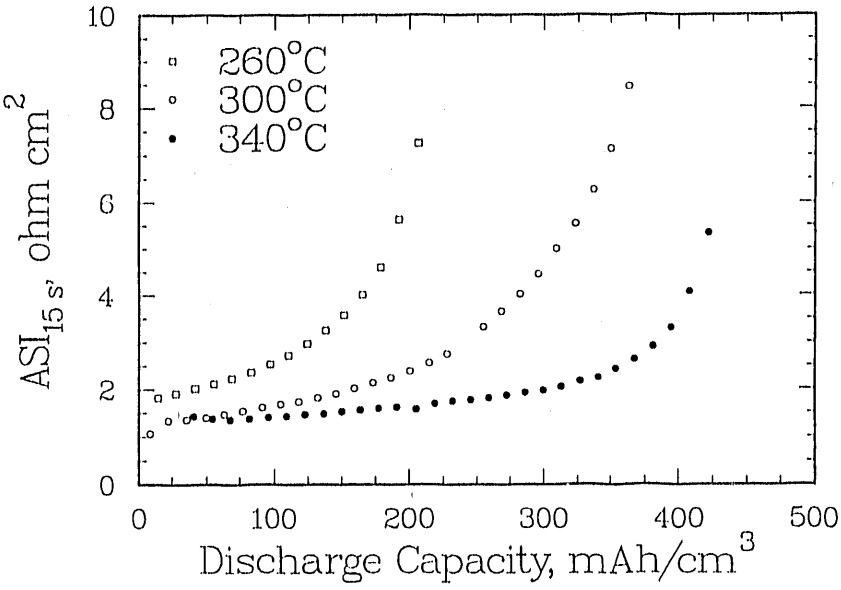

Fig. I-7. Effect of Temperature on Impedance and Discharge Capacity of $Ni/NiCl_2$ Electrode (0.5-cm thick, discharged at 20 mA/cm^2)

We studied the effects of pore-size distribution on electrode performance by measuring the capacities of model electrodes with various porosities (nonporous Ni, Ni felt, and Ni powder sintered with and without a pore former) under identical conditions. From the results, we determined the optimum pore-size distribution of the nickel electrode. Results also indicated that capacity density (mAh/cm^3) improved with increased BET surface area. These measurements provided a firm theoretical basis for the improvement of the modified-morphology $Ni/NiCl_2$ electrodes shown in Fig. I-5.

To better understand parameters that influence electrode performance and direct our research more effectively toward development of an EV battery, we have developed a method (see Ref. 5) to (1) measure the dynamic performance of research cells and (2) project specific

---

[5]L. Redey, "Dynamic-Performance Measurements of Battery Cells for Electric Vehicle and Other Applications," Proc. of 180th Electrochem. Soc. Meeting, Phoenix, AZ, October 13-18, 1991, Vol. 91-10, p. 38 (1991).

energy and power for full-size batteries of various specified designs when discharged under dynamic load profiles, such as SFUDS. Static discharge and different dynamic discharge profiles produce significant differences in cell performance. Hence, our dynamic-performance measuring method should be extremely useful even at the early stage of battery R&D, when systems intended for dynamic application, such as EV propulsion, are being evaluated. Using this method, we measured and evaluated the dynamic performance of $Na/NiCl_2$ research cells in various power profiles in which the duration, intensity, and ratio of the power levels (mW/cm^2) in SFUDS-like profiles were varied. The projected energy and power values indicate that EV batteries built with our synergistic $Ni/NiCl_2$ electrodes would easily surpass the mid-term USABC objectives given in Fig. I-1.

A modeling procedure has been developed to predict the impedance of the positive electrode for different designs of $Na/NiCl_2$ cells.[6] The model requires the adjustment of a single diffusion constant to correlate experimental data on impedance versus depth of discharge. The performance of a conventional $Na/NiCl_2$ battery (tubular electrode design) that had been tested by AEG Anglo Battery Holdings (AABH, formerly Beta Research and Development Ltd.)[7] was modeled with the use of (1) the above modeling procedure for determining the area-specific impedance of the positive electrode and (2) data provided by AABH on dimensions of the battery's internal parts. This effort produced a computer program that will calculate the cell and battery performance, as well as the dimensions and weights for all components, including the insulating case. The results of the calculation for the AABH battery performance are shown in Table I-2. These calculated results are virtually the same as the measured results by AABH. Also shown in Table I-2 are the USABC objectives and our calculated results (1) for a battery based on tubular electrodes having the same area-specific impedance as our recently developed synergistic $Ni/NiCl_2$ electrodes (Fig. I-5) and (2) an advanced bipolar design containing $Ni/NiCl_2$ electrodes with the same capabilities as the ANL synergistic design. As shown in Table I-2, the tubular design with ANL electrodes would yield significantly higher performance than the AABH battery and would easily meet the USABC mid-term objectives. The improvement over the AABH battery is even more marked for the advanced bipolar design. The USABC long-term objectives are considered extremely stringent and difficult to meet, especially the specific energy. This battery design comes closer to meeting the USABC goals than any other battery for which we have made performance calculations. For the near future, we are planning to experiment with hermetically sealed $Na/NiCl_2$ cells (5-Ah capacity) to study cycle-life limiting factors of the improved positive electrode and corrosion of cell components.

---

[6] I. Bloom, P. A. Nelson, L. Redey, S. K. Orth, C. L. Hammer, R. S. Skocypec, D. W. Dees, M. C. Hash, and D. R. Vissers, "Design Considerations for the Development of Advanced Sodium/Metal-Chloride Cells," Proc. of 25th Intersoc. Energy Conversion Eng. Conf., Reno, NV, August 12-17, 1990, Vol. 3, pp. 341-347 (1990).

[7] W. G. Bugden and R. N. Bull, "Reliability Testing of Zebra Cells with a New Diffusion Bond Seal," Proc. of DOE/EPRI Beta Battery Workshop, Chester, England, June 12-14, 1990, pp. 33-1 to 33-22 (1990).

Table I-2. Calculated Performance of $Na/NiCl_2$ Batteries Compared with USABC Objectives

	Specific Power		Specific Energy	
	W/kg	W/L	Wh/kg	Wh/L
USABC Objectives				
Mid-Term	200	250	100	135
Long-Term	400	600	200	300
Tubular Design				
AABH	68	86	78	99
ANL	235	380	110	180
Adv. Bipolar Design	390	700	170	315

C. *Analysis and Diagnostics Laboratory*

The Analysis and Diagnostics Laboratory (ADL) was established in CMT to study advanced battery systems for EV and utility load-leveling applications. The facilities include a test laboratory to conduct battery experimental evaluations under simulated application conditions and a post-test analysis laboratory to determine, in a protected atmosphere if needed, component compositional changes and failure mechanisms. Evaluations are performed for DOE, EPRI, and others to provide insight into those factors that limit the performance and life of advanced battery systems. The results of these evaluations help identify the most-promising R&D approaches for overcoming these limitations and provide battery users, developers, and program managers with a measure of the progress being made in battery R&D programs, a comparison of battery technologies, and basic data for modeling.

1. Performance and Life Evaluations

As shown in Table I-3, performance and life evaluations were conducted on six battery systems (Na/S, Li/FeS, Ni/metal hydride, Ni/Cd, Ni/Fe, lead-acid) from seven manufacturers in 1991. These results and others for each system are discussed below.

a. Sodium/Sulfur

Two Na/S systems are undergoing evaluation: one is a one-half sized (22-kWh) Na/S EV battery fabricated by ASEA Brown Boveri (ABB), and the other is an 8-V Na/S module from Chloride Silent Power Ltd. (CSPL). The 240-Ah, 90-V battery of ABB was shipped to ANL at operating temperature (310°C) with thermal and safety management systems in May 1990. It contains 360 cells (30-Ah rating) configured into three series-connected banks. Each bank contains eight parallel-connected strings of 15 series-connected cells. Performance characterization tests were completed, and life testing initiated in October 1990. This battery system exhibited the highest specific energy (and provided the greatest simulated vehicle driving

Table I-3. Summary of Selected Test Results from EV Battery Evaluations in ADL for 1991

Battery Description			Module Wt., kg	Initial Module Capac.,[a] Ah	Specific Energy,[a] Wh/kg	Volumetric Energy Density,[a] Wh/L	Peak Power,[b] W/kg	Battery Efficiency,[a] %		Battery Life,[c] cycles	Van Range,[d] mi (km)
Technology	Manufacturer	Model						Coulombic	Energy		
Sodium/Sulfur	ABB	B-11	253	238	81	83	152	100	91	592	154 (246)
	CSPL	PB-MK3	29.2	292	79	123	90	100	88	>800	150 (240)
Lithium/ Monosulfide	SAFT	Prismatic	2.94	203	66	133	64	95	81	>125[e]	93 (149)
Nickel/Metal Hydride	Ovonics	C-cell	0.081	3.6	54	186	158	92	80	333	97 (155)
	Ovonics	ExLC-cell	0.093	4.5	57	209	105	90	74	108	–
	Ovonics	H-cell	0.628	28.0	55	152	175	90	80	>170[e]	97 (155)
Nickel/ Cadmium	SAFT	STM5-200	24.5	217	55	104	175	90	78	>700[f]	102 (163)
Nickel/Iron	Eagle-Picher	NIF200	25	203	51	118	99	74	58	>825[e,f]	87 (139)
Lead-Acid	Chloride	3ET205	32.8	185	33	78	68	87	68	149	47 (75)

[a]Determined for 3-h discharges at constant current.
[b]Determined from driving profile discharge data at 80% DOD.
[c]Determined with SFUDS to 100% DOD unless otherwise noted. Ongoing life tests are indicated with the ">" sign.
[d]Determined for IDSEP Van with 695 kg battery on SFUDS.
[e]Determined with 80% DOD cycles.
[f]Determined with J227aC discharges.

range) of any battery technology examined to date. Because the internal heat losses were low, the cooling system was not used during driving profile discharges. The average heater power needed to maintain a battery temperature of ~310°C over an open-circuit period of 72 h was 176 W (enclosure heat loss). This heat loss would cause a capacity decline of about 0.8%/h if the battery were used to power its heaters (self-discharge loss). Life testing was terminated in August 1991 because the battery operating temperature could not be maintained at 310°C. The module had completed 589 cycles and retained ~81% of its initial 238-Ah capacity when the temperature started to decline. After 592 cycles, the battery was returned to ABB for post-test analysis. A cursory inspection when the battery was opened revealed that three cells had failed and a hole existed in the thermal enclosure wall (below one of the failed cells) that appeared to be the result of sodium-polysulfide corrosion. Researchers at ABB are conducting a more detailed post-test analysis and will furnish a report of their findings.

The 8-V Na/S module from CSPL has been under test since June 1990. The module contains 120 cells (10-Ah each) configured into 30 parallel-connected strings of four series-connected cells. This module is of the same design and assembly as those (24 series-connected modules) in the battery system for the ETX-II vehicle (a light-duty van based on the Ford Aerostar). Performance characterization tests were completed, and life tests initiated in October 1990. Test results indicate that the performance of this module is similar to that of the ABB battery. However, the CSPL module has a higher internal resistance and, therefore, cannot achieve as high a peak power. The CSPL module has completed more than 800 cycles in this ongoing life test and still retains ~85% of its initial 292-Ah (3-h rate) capacity. The specific energy obtained with SFUDS discharges has held at ~80% of its initial value for the past 100 cycles. The total capacity loss with life indicates that four of the four-cell strings are no longer operational (~40-Ah loss).

b. Lithium/Iron Sulfide

The first Li/FeS cell delivered under the DOE R&D contract with SAFT (Sec. I.B.1.a) was received and placed on test in May 1991. At an operating temperature of 470°C, a capacity of 182.5 Ah was obtained at the 3-h rate. This was ~14% below the capacity measured at SAFT using an operating temperature of 485°C. At ADL, the operating temperature was raised in 5°C steps to 485°C to observe the effect on cell capacity. The results showed that cell capacity, internal resistance, iR-free voltage, and peak power capability were sensitive to temperature. After completing 30 cycles of operation, the cell still retained 98% of its initial capacity but was removed from test to undergo post-test analysis.

A second cell was delivered from SAFT and placed on test in July 1991. Based on preliminary test results, the cell is being operated at a temperature of 465°C. Because the clamping arrangement used in the test fixture for this cell was modified to allow more compression on the electrode face, this cell performed much better than the first. Performance characterization tests were completed, and life tests started in December 1991 after 120 cycles were accrued. Life tests are being conducted with SFUDS discharges to 80% DOD. The cell has completed >125 cycles and retains ~96% of its initial 203-Ah capacity.

c. Nickel/Metal Hydride (H-Cells)

Performance and life tests are being conducted on two 25-Ah nickel/metal hydride H-cells from Ovonic Battery Co. These cells represent an intermediate step in an Ovonics program to fabricate and develop large, full-size EV battery cells. The two cells were delivered to ANL in June 1991. Performance characterization tests were completed, and life evaluation started in November 1991. Life tests are being conducted with SFUDS discharges to 80% DOD. Test results show that these H-cells have very low resistance and exceptionally high peak power capability (~200 W/kg at 50% DOD). This peak-power capability is the highest measured at the ADL, and it provides full capacity and maximum vehicle range for all driving profile discharges. The cells have completed about 170 and 80 cycles and retain all of their initial 100% DOD capacity.

d. Nickel/Cadmium

Life tests are being conducted on a 6-V, 190-Ah Ni/Cd module manufactured by SAFT (Industrial Storage Battery Division), France. The module was received in April 1990 after completing 35 performance characterization cycles at the Idaho National Engineering Laboratory. Life testing was started at ADL in June 1990 after 78 cycles of performance testing were accrued. Life evaluation is being conducted with 100% DOD driving profile discharges (J227aC schedule for a Chrysler TEVan). The module has completed more than 700 cycles and retains ~100% of its initial capacity at the 3-h discharge rate.

e. Nickel/Iron

Life tests are being conducted on several advanced Ni/Fe modules (NIF200) from Eagle-Picher Industries, Inc. The NIF200 design provides a capacity of 200 Ah in the same module package as the 170-Ah module developed for the dual-shaft electric propulsion (DSEP) vehicle developed by Eaton Corp. Performance characterization tests were completed in early 1990, and three NIF200 modules were placed on life tests. Since that time, another five NIF200 modules have been placed on life tests.

A charging study was conducted to determine the optimal charge regime for the NIF200. The study evaluated three charge methods: one-step constant current (CI), two-step constant current (CI/CI), and constant current/constant voltage/constant current (CI/CV/CI). Also investigated were charge returns (overcharge) of 115 and 135%; constant and pulsed charge currents as the final charge structure with CI/CV/CI charging; and a range of overcharge levels to determine the 50% "charge acceptance point" (i.e., 50% of charge current used for electrochemical recharge and 50% used for electrolysis). During these studies, the total outgas volume was measured with each charge regime to indicate charging efficiency. The results of this study showed that charge method and charge current structure had no significant impact on NIF200 module performance. Only the charge return level affected available module capacity and efficiency. At the 50% charge acceptance point, both efficiency and available capacity were maximal. Hence, we recommended a CI/CI charge regime (for simplicity) and a charge return of 111% (50% charge acceptance point). A life test has been initiated using the ANL recommended charge regime.

f. Lead-Acid

Life tests using SFUDS discharges to 100% DOD were performed on a three-cell 3ET205 module manufactured by Chloride Motive Power. The 3ET205 is an advanced lead-acid module having tubular positive electrodes and is representative of battery packs being vehicle tested. The test was terminated after 149 cycles because the energy obtained with SFUDS discharges had declined to less than 80% of its initial level. At that time, cycling the module with 3-h rate discharges returned the capacity to 175 Ah (92% of its initial 191 Ah). However, returning to SFUDS discharges resulted in a decline in energy from ~88% to 78% of the initial level in only a few cycles. Test data showed that the internal resistance had steadily increased with life. End-of-life diagnostic tests were performed using intercell connectors to provide individual cell voltage monitoring. The weak and strong cells were identified with 3-h rate discharges, and then a reference electrode was used to determine the limiting electrode. These data showed that the center cell was the weak-performing cell, and the cell closest to the positive terminal had the highest capacity. The reference electrode data showed that the negative electrode was limiting capacity in all three cells. This module has undergone post-test teardown analysis.

2. Post-Test Analyses

Detailed examinations are conducted on selected cells, modules, and batteries that have completed testing either at the ADL or at other centers of battery research. The information gained from post-test analyses provides a measure of the technical progress made by the battery developers and identifies specific areas where changes in design or the materials of construction would improve battery performance. In this report period, we examined three different battery systems (Li/FeS, Na/S, and lead-acid) representing the efforts of five different developers.

a. Lithium/Iron Sulfide

Three prismatic Li/FeS cells built by SAFT were analyzed; two cells completed approximately 200 cycles each, and the third cell was voluntarily terminated after 53 cycles. The short circuits that developed in the two failed cells were traced to similar sources: the rupture of the retainers around the central (positive and negative) electrodes. The ruptures developed at the first line of photoetched holes along the side walls of the cells. An electrical pathway developed in separator regions next to the failed retainers due to the buildup of conductive corrosion products. Degradation of the separators was also noted for cell sections with good cold resistances. Protrusion of positive active material extended 20 to 25% into the separator, and areas of iron deposition extended an additional 50% through the separator. The lithium-depleted negative electrodes were severely agglomerated, and galvanic corrosion of the related hardware produced extensive aluminum-rich intermetallic layers. In short-circuited areas, the negative current collectors were perforated as a result of the galvanic corrosion. The extensive galvanic reaction was promoted by the low negative-to-positive capacity ratio and by the high operating temperature.

Examination of the voluntarily terminated cell identified the causes for its lower-than-projected power and energy levels. Inadequate welding of the current collector and electrode retainer led to higher-than-expected internal resistance. In addition, the compositional gradients in the charged positive and negative electrodes revealed that an electrolyte deficiency caused lower-than-expected capacity. The manufacturer initiated measures to remedy both conditions in subsequent cells. This cell's hardware was also studied to provide baseline corrosion data at an early stage in cycle life.

b. Sodium/Sulfur

Two Na/S cells (XPB design) built and tested by CSPL were examined. Cell 10352 suffered from discharge polarization on cycle 459 and was removed from test three cycles later at the point of polarization, 24.0 Ah into discharge. Cell 10359 had been operated successfully for 52 cycles before it was removed from the test for comparison purposes. A reduced sodium level in the electrolyte annulus was the cause of discharge polarization in cell 10352. Radiography revealed voids in the electrolyte annulus of cell 10352 that were not present in cell 10359. Gravimetric measurements made on sections of the electrolyte assembly before and after methanol dissolution confirmed that less sodium was present in the electrolyte annulus for cell 10352. The distribution of sodium (in terms of mg/cm^2) within the annulus was relatively uniform, except for the head space at the top. Physical and chemical analyses of the two electrolytes indicated that the discharge polarization of cell 10352 had no deleterious effect on its electrolyte, at least not over the brief period of operation (3 cycles) with this condition. The maintenance of a relatively uniform distribution of sodium within the annulus, even in the sodium-depleted condition, would reduce the likelihood of excessive high currents over a small localized area of the electrolyte. These findings, however, do not preclude the possibility of electrolyte damage in cells exhibiting discharge polarization and operated for extended time periods.

c. Lead-Acid

Examinations were completed on six lead-acid modules: a 3ET205 module from Chloride Motive Power, a 6V160 module from Sonnenschien Battery Co., and four absorbed-electrolyte modules from GNB Batteries, Inc. The first two modules were evaluated with different driving profiles as part of a larger assessment of this technology for EV applications. The GNB modules were part of a test matrix to establish expected cycle life under conditions likely to be encountered in utility applications.

As noted previously (Sec. I.C.1.f), the 3ET205 module completed 149 cycles on a modified SFUDS algorithm to 100% DOD. The immediate cause of capacity decline of the module was antimony poisoning of the negative electrodes. High concentrations were found in all negative electrode samples, especially the samples from the weak-performing cell. The concentrations reached sufficient levels to reduce the charging efficiency and thereby decrease the effective capacity of the module. Corrosion of the Sb-Pb alloy used for the positive grids proved to be the primary source of this antimony. A strong correlation existed between the degree of positive grid corrosion and the antimony levels in the corresponding negative electrodes. Grid corrosion also was the primary source of increased internal resistance. The

effective reduction in cross-sectional area for the grid wires and the thick corrosion scales led to the progressive cell resistance rise noted during the performance evaluation. This factor is especially critical in an SFUDS evaluation because maintenance of adequate power is essential to longevity.

The Sonnenschien 6V160 module completed 370 cycles during a life evaluation using the J227aC profile. Positive grid corrosion was found to be the primary cause of the performance decline in the weak-performing cell of this three-cell module. The accelerated corrosion in the weak cell resulted in greater grid growth and increased resistance between the positive active material and the adjacent grid wires. As a consequence, by cycle 370, the module could no longer generate 80% of its initial capacity under the variable power demands of the J227aC profile, even though this performance level was still achievable at the constant-current discharge rate of 3 h. Cell-to-cell variations in the oxygen-recombination efficiency were responsible for the different rates of grid corrosion and thus the wide divergence in final capacity for the cells.

Life evaluations were completed on four GNB lead-acid modules operated using different depths-of-discharge and temperatures. The baseline condition, 80% DOD and 30°C, resulted in a lifetime of 850 cycles. Increasing the DOD to 100% caused a moderate reduction in cycle life, but raising the temperature to 50°C decreased cycle life by a factor of three. Our diagnostic tests established that the positive electrodes limited performance at end-of-life (<80% of initial capacity). Teardown and examination of the weak-performing cells in the modules determined that corrosion of the positive grids was the primary cause of failure. The data also established a linear dependence of grid corrosion on accumulated overcharge. The role of DOD as a moderate accelerant of grid corrosion was interpreted in terms of the quantitatively higher overcharge imparted to a module for each cycle. The role of elevated operating temperature in accelerating end-of-life could also be related to accumulated overcharge.

D. *Fuel Cell Research and Development*

We are developing two types of high-temperature fuel cell: one with a solid oxide electrolyte, and the other with a molten carbonate electrolyte.

1. Solid Oxide Fuel Cell

The solid oxide fuel cell (SOFC) has an oxide-ion conducting electrolyte material, yttria-stabilized zirconia (YSZ). The electrode materials are strontium-doped lanthanum manganite (LM) on the air side (cathode) and nickel-YSZ on the fuel side (anode). The material that connects the individual cells in electrical series (bipolar plate) is strontium-doped lanthanum chromite. These components are all oxide-ceramic materials. On the fuel side, at the nickel-electrolyte-gas (three-phase electrochemically active) interfacial area, hydrogen and carbon monoxide in the fuel gas react with oxide ions from the electrolyte to form water and carbon dioxide, giving up electrons to the external circuit. Similarly on the air side, at the LM-electrolyte-gas interfacial area, oxygen in the air accepts electrons from the external circuit to form oxide ions, which are conducted through the electrolyte to the anode interface. These cells operate at temperatures of 800 to 1000°C. At these temperatures, hydrocarbon fuels (e.g.,

methanol, ethanol, natural gas) can reform on the nickel cermet anode to form electrochemically active fuels, such as hydrogen and carbon monoxide.

Solid oxide fuel cells are being developed under sponsorship of DOE, EPRI, and the Gas Research Institute (GRI) as a potential future energy conversion technology for utilities and private power generators. The principal industrial developers in the U.S. are the Westinghouse Electric Corp. and Allied Signal Aerospace/AiResearch.

In support of the SOFC Program, we have served as advisors to DOE in managing industrial R&D contracts and have done laboratory research. In 1991, almost all of our effort was in research, but we also advised the transportation branch of DOE to consider SOFC as a potential power source for vehicles. In the laboratory, we are conducting research (1) in support of Allied Signal's program to develop the monolithic solid oxide fuel cell and (2) for an effort aimed at developing new electrolytes and sealing materials for SOFCs in general.

a. Monolithic Solid Oxide Fuel Cell

The monolithic solid oxide fuel cell (MSOFC), developed in CMT and the ANL Materials and Components Technology Division, is based on the premise that the thin solid components of oxide cells can be fabricated into compact shapes having power-to-weight ratios that are much higher than those of conventional fuel cells. The MSOFC concept was transferred to Allied Signal in 1988, and since that time, we have played a support role in its development. In the past year, work in CMT was focused on understanding and modeling the electrochemical performance of single MSOFCs.

One measure of the overall electrochemical performance of a fuel cell is its voltage as a function of current density ("polarization curve"). Polarization curves obtained for a typical MSOFC at 1000°C and three different oxygen partial pressures on the cathode side of the fuel cell are given in Fig. I-8. These curves indicate that the fuel cell voltage (and thus the performance) increases with the oxygen partial pressure at constant current density. This effect is normally attributed to a decrease in the diffusion overpotential for oxygen in the air electrode. However, the polarization curve for an oxygen partial pressure of 1 atm (100 kPa) is nonlinear, and the calculated resistance from this curve approaches that of the electrolyte alone. This indicates that the diffusion and activation potentials are close to zero for the anode and cathode. This complex, atypical behavior suggests that mathematical modeling of the fuel cell is needed to explain the observed polarization curves.

An electrochemical model is thus being developed to examine possible mechanisms that would describe the observed polarization curves for MSOFCs and would also be consistent with other electrochemical studies conducted in this laboratory and others. Some of the processes occurring in the fuel cell are generally well established and are included in the model. These include the bulk properties of the electrolyte and the porous mixed-conductor anode and cathode. However, the importance of other processes, such as the many transport and kinetic phenomena associated with the three-phase electrochemically active area in each electrode, is not as well established. Of the many postulated interfacial phenomena, three have been included in the model so far: surface adsorption of reactants and products, their diffusion,

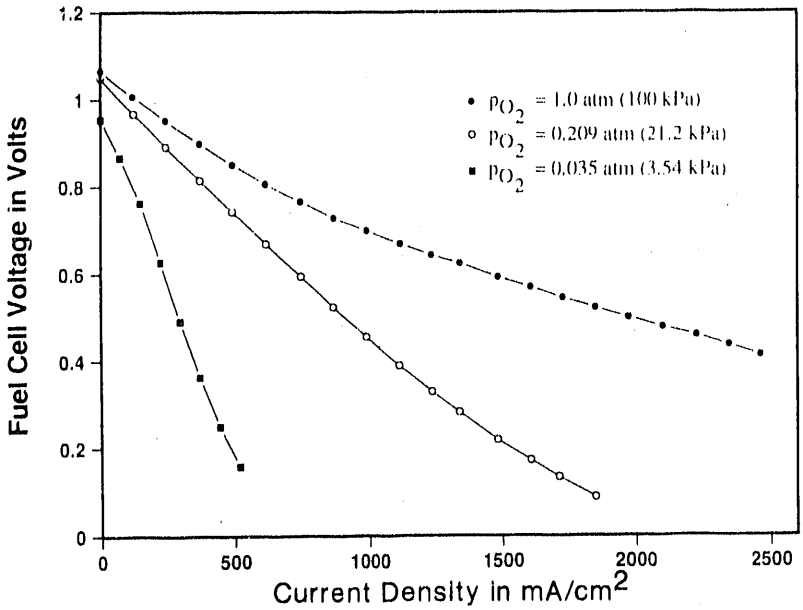

Fig. I-8. Polarization Curves for Single MSOFC with H_2/H_2O Fuel and the Indicated Oxygen Partial Pressure at 1000°C

and electrochemical kinetics. In the present form, the electrochemical model consists of seven nonlinear coupled differential equations that must be solved simultaneously. Several observations were made from polarization curves calculated to show the effect of interfacial transport and electrochemical kinetics for the anode and cathode in a typical MSOFC. First, bulk gas transport in the porous electrodes is very fast and does not limit the electrode reaction. Second, the curves showing the effect of electrochemical kinetics for the electrodes are linear over the current density range of interest (<1000 mA/cm^2). Therefore, electrochemical kinetics cannot be used to explain the observed nonlinear behavior of the polarization curve in Fig. I-8 at 1-atm (100-kPa) oxygen partial pressure (the other two curves are approximately linear in this current density range). Third, the observed MSOFC behavior cannot be adequately modeled by a single reaction mechanism at each electrode. Thus, dual reaction mechanisms are being investigated.

We also examined the consequences of operating an MSOFC with a high-molecular-weight hydrocarbon fuel such as hexadecane. Theoretically, at the MSOFC's high operating temperature, the internal reform of hydrocarbon fuels and subsequent water gas-shift reaction can supply enough electrochemically active hydrogen and carbon monoxide to operate the fuel cell. The polarization curve determined for an MSOFC operating on hexadecane/water fuel is given in Fig. I-9. As shown, the slope of this polarization curve is similar to that for an MSOFC operated with H_2/H_2O fuel. The lower voltage with the hexadecane fuel was a result of the high water content in the inlet fuel stream. The water was added to support the internal reform reaction and to suppress the formation of coke and tars resulting from cracking reactions. The test results indicate that the MSOFC can operate on hydrocarbon fuels, but that competing cracking reactions can be a problem with high-molecular-weight hydrocarbons.

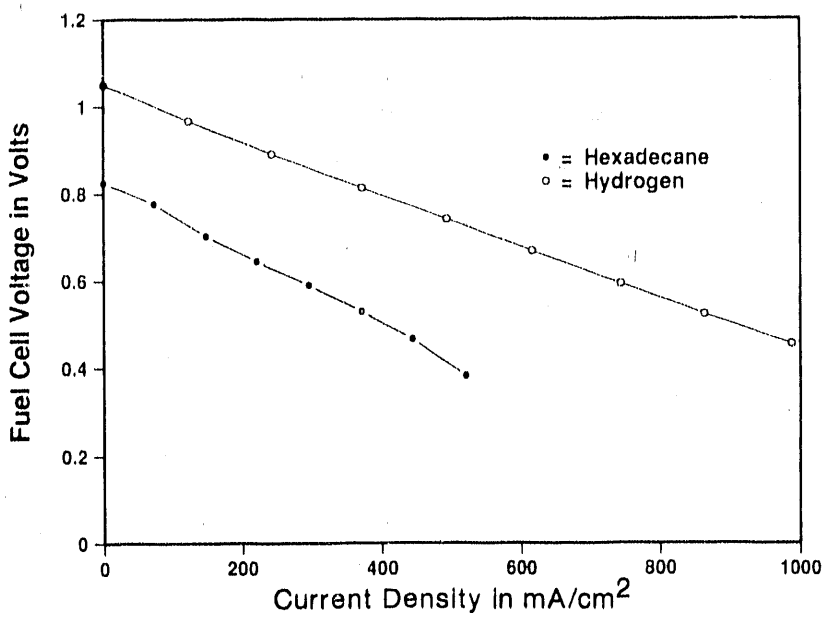

Fig. I-9. Polarization Curves for a Single MSOFC with Indicated Humidified Fuel and Air as Oxidant at 1000°C

A concern with operating the MSOFC on petroleum-derived fuels is the effect of sulfur in the hydrocarbon fuel on the performance of the anode. Earlier studies[8] with anode/electrolyte/anode composites operated with sulfur in the fuel indicated a slow, steady decrease in performance, which was associated with the yttria-stabilized zirconia in the anode. We then conducted a literature review of possible reaction mechanisms involving ZrO_2 and Y_2O_3 with H_2S and completed thermodynamic calculations on the possible reactions. While there are many possible reactions, reliable thermodynamic information on the sulfide and oxysulfide products is somewhat limited. Therefore, the thermodynamic calculations were done on three known reactions, given below, with the assumption that these reactions are the most favored or at least typical of other reactions in the system:

$$ZrO_2 + H_2S \Leftrightarrow ZrOS + H_2O \quad (3)$$

$$ZrO_2 + 2H_2S \Leftrightarrow ZrS_2 + 2H_2O \quad (4)$$

$$Y_2O_3 + H_2S \Leftrightarrow Y_2O_2S + H_2O \quad (5)$$

[8]M. J. Steindler et al., *Chemical Technology Division Annual Technical Report, 1990*, Argonne National Laboratory Report ANL-91/18, pp. 33-34 (1991).

The free energies at 1000°C were calculated to be -37 kJ for reaction 1, -180 kJ for reaction 2, and -37 kJ for reaction 3. In general, the oxides of zirconium and yttrium are more stable than their corresponding oxysulfides and sulfides, but the overall reactions are thermodynamically favored at standard fuel cell conditions because H_2O is much more stable than H_2S.

After establishing the possibility of sulfur reacting with the yttria-stabilized zirconia, we conducted thermogravimetric analysis and other analytical studies on this material to determine if the sulfur actually reacts at significant rates in reducing environments at 1000°C. No appreciable reaction of yttria-stabilized zirconia with H_2S at concentrations in the fuel of up to 50 ppm was detected. This result indicates that reactions 3-5 are kinetically limited.

A study of our present MSOFC stack testing procedures was conducted to determine if they are causing undue stress on the stacks. Three similar MSOFC stacks (before testing) were X-rayed for cracks, and none was apparent. Destructive analysis of one stack confirmed the absence of cracks. The other two stacks were brought up to the operating temperature (1000°C). One of them was tested on air and H_2/H_2O, while the other was brought back down to room temperature without testing. Post-test studies revealed numerous cracks in both stacks, which exhibited the same general condition. This suggested that, at least initially, most cracks are introduced during loading of the stacks into the experimental apparatus and/or raising of the temperature before testing.

Work on the development of the MSOFC concept is continuing. Much of the work on the electrochemical modeling has been transferred to the University of Oklahoma for further development. The need for additional work on internal reforming of hydrocarbon fuels, as well as associated sulfur effects, has been clearly established. Improved testing procedures are being evaluated. New areas of work include examining the use of alternative ceramic materials in the MSOFC. This could be done by replacing the present $LaMnO_3$ material in the cathode and possibly the nickel in the anode by $LaCrO_3$. While this could cause an overall decrease in the performance of the fuel cell, it would greatly simplify the fabrication procedures.

b. Advanced Materials and Sealants

The objectives of the SOFC materials program are to develop (1) electrolytes and electrodes that permit the operation of a ceramic fuel cell at temperatures of 500-800°C instead of the 1000°C now used and (2) electronically insulating sealants for use in state-of-the-art fuel cells and in newer cell designs.

(1) Advanced Materials

Lowering the operating temperature of the fuel cell to 500-800°C has several advantages, such as increasing the efficiency of the cell (i.e., increased cell voltage at the lower temperature) and decreasing thermal stresses and interdiffusion of cell components. The present focus is to develop new candidates for electrolyte materials. Once suitable electrolytes have been identified, compatible electrodes and interconnect materials will be developed. The new electrolyte materials must be chemically stable to both fuel (e.g., hydrogen or methane) and oxygen and have conductivities close to the target value of 0.05 $\Omega^{-1}cm^{-1}$ in the 500-800°C

temperature range. Our approach to finding new electrolyte materials is to identify and test materials which exhibit oxygen substoichiometry or have some crystallographic features which might facilitate ionic transport. This search includes materials which contain both strong and weak metal-oxygen bonds.

Oxide-ion-conducting materials exhibit a direct correlation between bond strength and conductivity. That is, those oxides with greater free energy of formation (ΔG_f) tend to be more conductive. The ΔG_f values and conductivities at 700°C of yttria-doped ZrO_2 are -920 kJ/mol-O_2 and 1.8 x 10^{-2} $\Omega^{-1}cm^{-1}$, respectively[9,10]; and those of yttria-doped Bi_2O_3 are -240 kJ/mol-O_2 and 1.6 x 10^{-1} $\Omega^{-1}cm^{-1}$, respectively.[10,11] Both crystallize with the fluorite structure, but doped Bi_2O_3 is more conductive. However, lower bond strengths also tend to make this oxide unstable in H_2. We thus decided to investigate compound formation between Bi_2O_3 and Al_2O_3, along with incorporation of Bi_2O_3 into a refractory host lattice ($LaAlO_3$). These compounds have the potential of circumventing the problem of thermodynamic instability in H_2 and represent compromises between high conductivity and thermodynamic stability. The conductivity of the candidate electrolyte materials, $Bi_2Al_4O_9$ and La-Al-Bi-O, was determined with platinum electrodes under humidified H_2/O_2 gas at 500-800°C.

The test results indicated that $Bi_2Al_4O_9$ has an intrinsic conductivity of about 8 x 10^{-3} $\Omega^{-1}cm^{-1}$ and an ionic transference number (i.e., fraction of the total conductivity due to ionic transport) of 0.65 at 800°C. This conductivity is on the order of that of yttria-stabilized zirconia (present SOFC electrolyte) but still below our goal. The conductivity of $Bi_2Al_4O_9$ was also measured under equilibrium conditions and successively lower oxygen partial pressures [1 atm (0.1 MPa), 0.2 atm (0.02 MPa), 10^{-4} atm (10 Pa), and 10^{-6} atm (0.1 Pa)] to gauge the size of the electrolytic domain. The conductivity versus oxygen partial pressure at 600, 700, and 800°C is shown in Fig. I-10. Based on the shapes of these curves, the material has an electrolytic domain extending from about 0.2 atm (0.02 MPa) to at least 10^{-6} atm (0.1 Pa). At 1 atm (0.1 MPa), the beginning of a p-conduction branch is seen.

In Bi-substituted $LaAlO_3$ materials, X-ray powder diffraction (XRD) patterns of sintered and annealed pellets (800°C) indicated that a perovskite was the major phase. However, because of the similarity in size of La^{3+} and Bi^{3+}, these patterns did not indicate that Bi^{3+} was incorporated into the lattice. Also, $Bi_2Al_4O_9$ and $Bi_{24}Al_2O_{39}$ were detected as minor phases. In the ion microprobe, the major phase contained La, Bi, and Al in approximately a 0.8:0.14:1.00 ratio, respectively. These results and those from the XRD pattern are consistent with Bi^{3+} incorporation into the $LaAlO_3$ lattice. The conductivity of $La_xBi_{1-x}AlO_3$ (x = 0.9, 0.8, 0.7, and 0.6) materials was found to depend on bismuth concentration. At 800°C, the conductivity values range from 5.5 x 10^{-3} $\Omega^{-1}cm^{-1}$ (x = 0.9) to 1.6 x 10^{-2} $\Omega^{-1}cm^{-1}$ (x = 0.6), with all ionic transference numbers near 0.5. Doping with 5 mol % Zn^{2+} on the Al^{3+} site

---

[9]D. Strickler and W. Carlson, J. Am. Ceram. Soc. **48**, 286 (1965).

[10]T. R. Reed, *Free Energy of Formation of Binary Compounds: An Atlas of Charts for High Temperature Chemical Calculations*, MIT Press, Cambridge, MA (1971).

[11]T. Takahashi, H. Iwakawa, and T. Arao, J. Appl. Electrochem. **5**, 187 (1975).

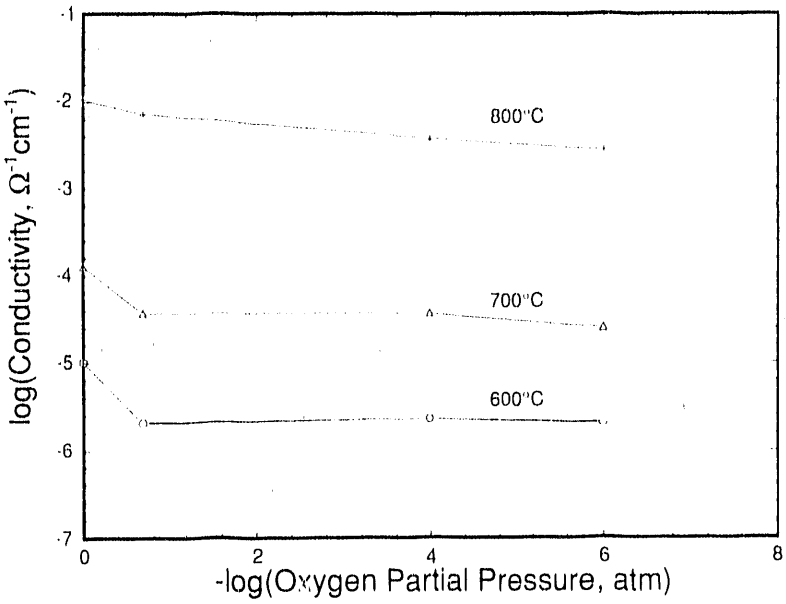

Fig. I-10. Conductivity vs. Oxygen Partial Pressure for $Bi_2Al_4O_9$ Candidate Electrolyte at 600-800°C

improved the conductivity of all materials studied. As a result, the conductivities range from 9.3×10^{-3} to 1.2×10^{-1} $\Omega^{-1}cm^{-1}$, with ionic transference numbers again near 0.5, at 800°C. The last conductivity value is an order of magnitude higher than that of yttria-stabilized zirconia.

In future work, we plan to increase the conductivity of $Bi_2Al_4O_9$ and La-Al-Bi-O by doping and to develop compatible electrodes for fuel cell testing. We will also continue to search for better electrolyte materials for 650°C operation.

(2) Sealants

The sealants in an SOFC stack must form gas-tight seals along the edges of each electrode and between the manifold and stack. The sealants should also be chemically and thermally stable at 1000°C in H_2, O_2, and water vapor and must be compatible with the fuel cell components. The key to developing such sealants is the matching of chemical and thermal properties of the materials involved.

During the first phase of the project, commercially available, high-temperature cements were surveyed. Most of them contain high levels of SiO_2 (10-50 wt%). Because SiO_2 is volatile under fuel cell conditions, these cements were considered not acceptable and were not tested. We did find two commercial cements that the manufacturers claim are free of silicon. After firing at 1000°C, these cements formed strong bonds between disks of cathode, electrolyte, and anode materials. Examination of the bonded disks by electron microscopy showed, however, that neither cement was free of silicon. If the silicon is present as silicates, it may not be a problem. Nevertheless, these cements are unsuitable because they contain regions of high porosity in the bonding area. For fuel cell applications, neither silicon nor porosity is acceptable.

Reactive glasses were selected as the first type of novel sealant to evaluate. We fabricated three different glasses (designated A, B, and C) and characterized them in terms of their coefficient of thermal expansion (CTE) and compatibility with yttria-stabilized zirconia. The CTE values for these glasses were in the 7-8 x 10^{-6}/°C range, which is lower than that of yttria-stabilized zirconia, 10^{-5}/°C. Even though there is a difference in CTE, the difference does not seem to be a problem; the glasses wet yttria-stabilized zirconia very well. Under the optical microscope, differences in interactions between the glasses and yttria-stabilized zirconia were seen. Glass A formed a thin reaction zone; Glass B formed a more extensive reaction zone, about 1.5 μm thick; and Glass C showed clear evidence of intermediate compound formation along the glass/yttria-stabilized zirconia interface. The extent of interaction was found to be glass-composition dependent. We concluded from this study that surface and materials chemistry seems to be more important than an exact matching of CTEs. Issues which still need to be addressed include controlling the interaction between the glasses and yttria-stabilized zirconia and determining glass compatibility with the other fuel cell components.

2. Molten Carbonate Fuel Cell

The present molten carbonate fuel cell comprises a porous nickel anode, a porous nickel oxide cathode, a liquid electrolyte of lithium and potassium carbonates retained by a ceramic matrix of $LiAlO_2$, and appropriate metal separator sheets. The cell operates at an average temperature of about 650°C. The objective of our work on this fuel cell is to develop new, conductive materials and to produce structures from these materials for use as components, i.e., electrodes and separator sheets. The current focus of this effort is on cell testing of electrodes made from previously developed materials found to be electronically conductive and chemically stable. The work on developing a new separator material emphasizes the effect of fuel gas and oxidant on the electronic conductivity and material properties and on the integrity of the structure produced from candidate materials.

a. Cathode Cell Testing

Alternatives to the currently used NiO cathode are being sought because NiO has dissolution/precipitation problems that are projected to limit its lifetime in the fuel cell environment. The current cathode work focuses on the performance and reaction kinetics of $LiFeO_2$, a material which we experimentally determined to have the same nominal composition in the both the anode and cathode environments.[12]

Previous tests with full-size (25-cm^2) cells and smaller diagnostic cathode half cells showed that significant gains in performance could be realized with $LiFeO_2$ cathodes by increasing both the operating temperature and the surface area.[12] The magnitude of this improvement with increasing temperature from 650 to 700°C was larger than predicted from the behavior of NiO cathodes. This suggested that a different mechanism controls the reaction rate with the $LiFeO_2$ cathode.

---

[12]M. J. Steindler et al., *Chemical Technology Division Annual Technical Report, 1990*, Argonne National Laboratory Report ANL-91/18, pp. 37-42 (1991).

To gain insight into the $LiFeO_2$ electrode reactions, we conducted half-cell tests with the following experimental variables: temperature, O_2 partial pressure, CO_2 partial pressure, electrode thickness, and electrolyte composition.

The influence of temperature on the performance of Co-doped $LiFeO_2$ cathodes is shown by the polarization curves in Fig. I-11. The half cells were operated using an oxidant of 15% O_2-30% CO_2-balance N_2 and an electrolyte containing 70 mol % Li_2CO_3-30 mol % K_2CO_3. These data show that increasing the temperature at a given current density results in a significant decrease in the cathode overpotentials (i.e., performance increases). At 160 mA/cm^2, a decrease in overpotential of about 250 mV is obtained by increasing the temperature from 650 to 700°C; with a state-of-the-art NiO cathode, the reduction in overpotential is less than 20 mV for the comparable temperature change. The effect of changing the O_2 partial pressure in the oxidant at 650°C is similarly beneficial for performance. At a current density of 160 mA/cm^2 and a CO_2 partial pressure of 0.3 atm (30 kPa), the overpotential is reduced by ~300 mV with an increase in the O_2 partial pressure from 0.05 to 0.7 atm (5 to 70 kPa). The effect on performance of changing the CO_2 partial pressure at 650°C is less dramatic (Fig. I-12). At current densities less than about 125 mA/cm^2, the performance decreases when the CO_2 content in the oxidant is increased from 15% to 60%; at higher current densities, the effect is reversed. At 5% CO_2, however, the performance is better than with the higher CO_2 oxidants for current densities up to ~200 mA/cm^2. Taken together, the test results suggest that the electrode reaction consists of two independent, simultaneous mechanisms. One mechanism is attributed to a slow, kinetically limited reaction, and the other to a much faster, diffusion-controlled reaction.

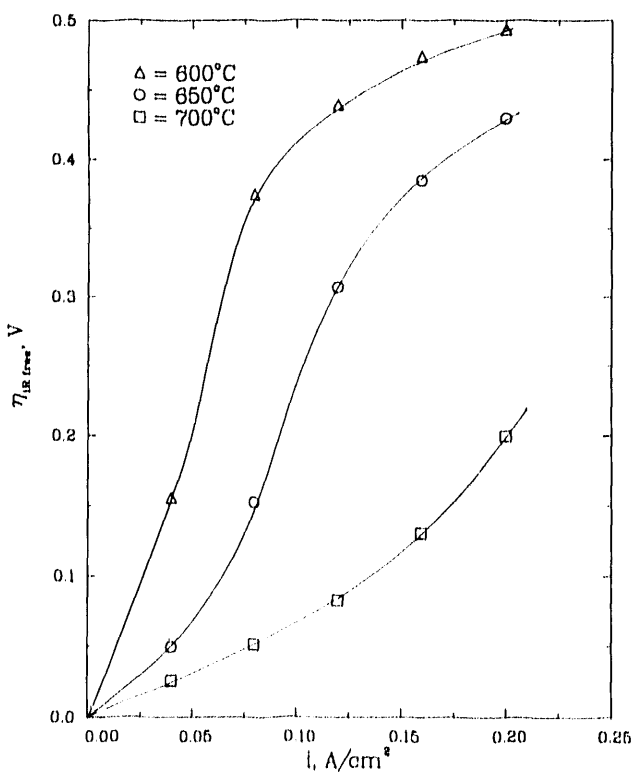

Fig. I-11.

Cathode Overpotential ($\eta_{IR\ free}$) as Function of Current Density (i) and Temperature for Co-Doped $LiFeO_2$ Cathode in Half Cell Operated with 15% O_2-30% CO_2-55% N_2 Oxidant

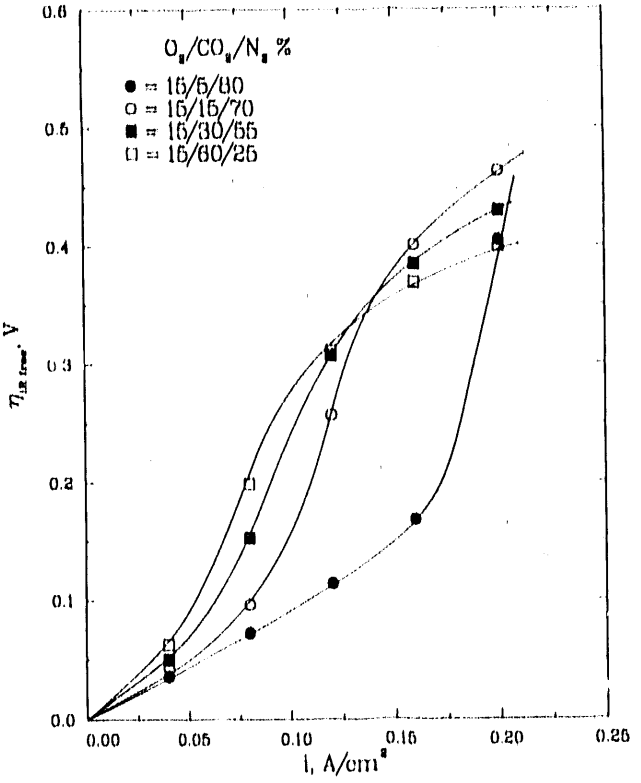

Fig. I-12.

Cathode Overpotential ($\eta_{IR\ free}$) as Function of Current Density (i) and CO_2 Content in Oxidant for Co-Doped $LiFeO_2$ Cathode in Half Cell

In other half-cell tests, the electrode thickness (between 0.015 and 0.030 cm) and the lithium content of the electrolyte (between 50 and 70 mol % Li_2CO_3) were found to be relatively unimportant parameters with regard to cathode performance at 650°C.

With the above results as a guide, we formulated an alternative oxidant mixture that is expected to improve $LiFeO_2$ cathode performance. The new mixture is 95% air-5% CO_2, i.e., 20% O_2-5% CO_2-balance N_2. When this oxidant is coupled with an operating temperature of 675°C, a Co-doped $LiFeO_2$ cathode in the half cell will perform comparably to a state-of-the-art NiO cathode at 650°C (Fig. I-13). However, it remains to be demonstrated that state-of-the-art NiO performance can be obtained with a $LiFeO_2$ cathode in a full molten carbonate fuel cell. Future half-cell tests will include determining the effect of dopants (Cu, Mn, and Ni) on the behavior of $LiFeO_2$ cathodes and the effect of oxidant composition and temperature on the performance of Mg- and Nb-doped Li_2MnO_3, another material under consideration for use as the cathode.

b. Anode Cell Testing

As in the case of the presently used cathodes, alternatives are also being sought for the nickel anodes because this metallic component suffers from compaction and creep during cell operation. The present emphasis in this effort is on determining the in-cell performance of doped and undoped iron- and manganese-based electrodes.

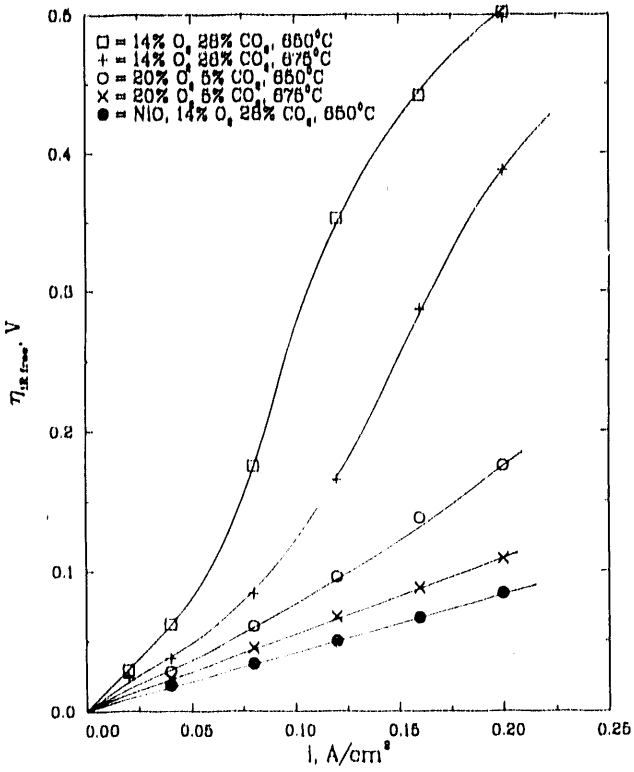

Fig. I-13.

Effect of Temperature and Modified Oxidant on Cathode Overpotentials ($\eta_{IR\ free}$) for Co-Doped $LiFeO_2$ Cathode in Half Cell at Current Densities (i) up to 200 mA/cm^2. Performance of NiO cathode also shown for comparison.

Previously, we reported that the conductivity of the iron- and manganese-based materials was sensitive to reaction conditions.[12] In these materials, the O_2 partial pressure and temperature determine their stoichiometry and, therefore, the conductivity of the anode. In an operating cell, changes in O_2 partial pressure are expected as the load and fuel utilization are changed; thus, changes in the number of electronic charge carriers will result and are likely to have an adverse effect. Doping will produce a fixed number of charge carriers and can minimize this effect by keeping the charge carriers and conductivity nearly constant.

To determine the impact of doping on the performance of $LiFeO_2$ anodes, full- and half-cell tests are being performed. The first of these cells to be operated was a full cell with Mn-doped $LiFeO_2$ anode operated under standard conditions (temperature of 650°C, an oxidant of 14%O_2-28% CO_2- balance N_2, and a fuel of 80%H_2-20%CO_2 humidified at 60°C). The cell contained the conventional NiO cathode and 70 mol % Li_2CO_3- 30 mol % K_2CO_3 electrolyte. The cell voltage was stable for current densities up to 60 mA/cm^2; beyond that point, however, the voltage decreased steadily with time. From the limited data, it is not possible to understand what electrode conditions are responsible for the observed behavior. Further cell studies using Co- and Nb-doped $LiFeO_2$ anodes are planned. In addition, we will examine the performance of an undoped anode under similar conditions.

c. Ceramic Separator Development

Metal bipolar separators add significantly to the cost of molten carbonate fuel cells, and their corrosion in fuel cell stacks can result in high contact resistance and component

degradation. Ceramics offer the potential for eliminating this corrosion problem and reducing the cost by lowering materials cost and allowing use of new design options. The emphasis of this effort has been on assessing the property changes that are likely to occur in ceramic separator sheets as hydrogen and oxygen diffuse into the component. The properties include stoichiometry, crystalline form, and conductivity.

The initial focus is on the iron- and manganese-based materials because of the understanding gained through our cathode and anode studies. We examined the property changes in anode-prepared Nb- and Mg-doped MnO and Mn- and Nb-doped $LiFeO_2$ when exposed to oxidant gas (14% O_2-28% CO_2-balance N_2) at 650°C. The conductivity of Nb- and Mg-doped MnO increased to 5 $\Omega^{-1}cm^{-1}$ from 0.06 and 0.2 $\Omega^{-1}cm^{-1}$, respectively. The MnO also oxidized to Mn_2O_3; this change in composition was accompanied by a 12% change in volume. The Mn- and Nb-doped $LiFeO_2$ under similar conditions showed a decrease in conductivity, from 3 $\Omega^{-1}cm^{-1}$ to about 0.03 and 0.01 $\Omega^{-1}cm^{-1}$, respectively. The crystalline form of $LiFeO_2$ remains the same in both anode and cathode gas, but the crystal volume undergoes a 3% change. These volume changes did not appear to be detrimental to the structural integrity with respect to cracking; however, the manganese-doped specimen warped badly.

These results indicate that a manganese-based separator is likely to undergo stresses that will damage its structure in the fuel cell environment. On the other hand, a separator based on $LiFeO_2$ shows promise. Other materials that have nominally the same composition in both the anode and cathode environment are being explored as potential separators. At this time, experiments with the iron- and manganese-based materials are being continued to determine the extent of enhanced electronic conductivity with doping.

E. *Development of Fuel Cell Systems for Transportation Applications*

Fuel cells, operating on nonpetroleum fuels, have the potential to provide propulsion systems with nearly twice the fuel efficiency and greatly reduced emissions and noise compared with the internal combustion engine. The CMT Division conducts in-house research on advanced fuel cell technology for transportation applications and provides technical management of DOE contracts with industrial developers.

1. Fuel Cell/Battery Powered Bus System

a. Technical Management

The CMT Division provides overall technical management for the Fuel Cell/Battery Powered Bus Program co-sponsored by DOE, the U.S. Department of Transportation, and the California South Coast Air Quality Management District. The objective is to develop an urban transit bus powered by a methanol-fueled, phosphoric acid fuel cell combined with a battery. In Phase I (1988-90), two industrial contractors each built and tested a fuel cell/battery power system that was one-half the size needed for the bus. In both systems, the test results verified the performance predicted by the design analyses and confirmed the feasibility of the fuel cell bus concept. During 1991, Phase II was initiated. As part of this phase, three fuel cell/battery powered buses (~8-m long, capacity of 25 passengers) will be built,

and the design for a full-size (~12-m long) transit bus will be developed. A 30-month contract for the Phase II work was awarded to H-Power Corp. (Bloomfield, NJ) through a competitive procurement. H-Power will assemble and test fuel cell/battery systems in its laboratory before they are installed on buses. Key subcontractors on the H-Power team are Transportation Manufacturing Corp. (the largest US bus manufacturer); Bus Manufacturing USA, Inc.; Booz-Allen & Hamilton, Inc.; Fuji Electric Co.; and Soleq Corp. The involvement of major bus manufacturers and their willingness to share in the development costs is evidence of their support for this project.

b. In-house R&D

In support of the fuel cell bus program, we conducted systems analyses and modeling to determine the expected overall efficiency of the fuel cell/battery propulsion system as a function of fuel and oxidant flow rates and utilizations, and the degree of thermal integration included in the system. Typical results for liquid- and air-cooled phosphoric acid fuel cell (PAFC) systems are shown in Fig. I-14. These results show that, for the thermally well integrated liquid-cooled PAFC system, peak efficiencies of 41.7% (based on higher heating value of methanol) can be achieved. For the air-cooled PAFC system, which is less well integrated but simpler than the liquid-cooled PAFC, the peak efficiency is only 31.2%.

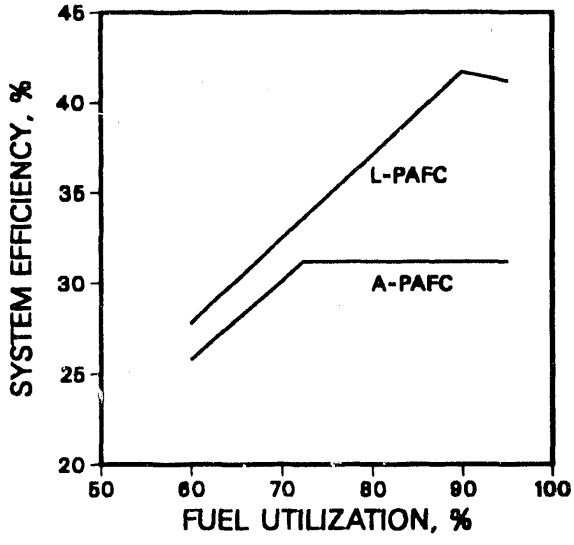

Fig. I-14.

Effect of Electrochemical Fuel Utilization on the Efficiencies of Liquid-Cooled (L) and Air-Cooled (A) Phosphoric Acid Fuel Cell (PAFC) Systems

While previous R&D efforts on fuel cell/battery propulsion systems have emphasized the development of the fuel cell portion of the hybrid system, additional work is required to identify the best battery type and battery size for this bus application. Since the battery is used to level the power demand load on the fuel cell, it is never deeply discharged, but it must be capable of providing and accepting power at high rates. Thus, the requirements of the battery in this application are quite different from those of battery-powered vehicles. To address this need, we initiated testing in 1991 on high-power batteries using a load profile designed to simulate the anticipated duty cycle in the fuel cell bus.

2. Proton Exchange Membrane Fuel Cell

a. Technical Management

The proton exchange membrane (PEM) fuel cell, also known as the polymer electrolyte fuel cell, offers significant advantages over the phosphoric acid fuel cell for transportation applications. These include reduced size and weight, faster start-up, increased reliability, and potentially lower cost. During 1991, the Allison Gas Turbine Division of General Motors (GM) carried out the first year of a two-year R&D contract sponsored by DOE and managed by CMT. Allison is the prime contractor and responsible for overall system integration. Support subcontractors are Los Alamos National Laboratory for fuel processor development and fuel cell testing, Dow Chemical Co. for membrane fabrication and testing, Ballard Power Systems for fuel-cell stack fabrication, GM Research Laboratories for electrode and catalyst studies, and GM Advanced Engineering Staff for vehicle system engineering.

Under this program, a conceptual design for a PEM fuel-cell powered passenger car is being developed, state-of-the-art stacks (5 kW) of PEM fuel cells are under test, and system modeling is being carried out for trade-off analyses. This effort will culminate with the integration and testing of a complete PEM fuel cell system (10 kW), which is expected to demonstrate the feasibility of PEM fuel cells for transportation, thereby laying the groundwork for future engineering scaleup.

b. In-house R&D

In support of PEM technology development, we developed a comprehensive systems simulation model for the PEM fuel cell system in 1991. Using this model, we carried out thermodynamic and engineering analyses of the PEM fuel cell system being developed by Allison. In preliminary investigations, we used the model to assess the effects on system efficiency of the following: ambient temperature, water tank temperature, current density, fuel utilization, and efficiency of the air-moving equipment (compressor, expander, and fans). For example, Fig. I-15 illustrates the variation of system efficiency with the average current density in the cell. As shown, the system efficiency varies from a low of 24% at a current density of 1.4 A/cm^2 to over 50% at a current density of 0.05 A/cm^2. The efficiency of air-moving equipment was found to have a significant effect on the system efficiency. The latter drops from 39.6% to 29.7% as the former changes from an ideal 100% to the more commonly achievable 50%. Our future analyses will examine the effects of system operating pressure and projected improvements in the electrochemical performance of PEM fuel-cell stacks. In addition, we have set up in-house experimental facilities for conducting small-scale testing of PEM electrodes and cells.

3. Fuel Reforming Technology

To use hydrocarbon fuels such as methanol, ethanol, or natural gas as the energy source for PAFC and PEM fuel cells, these fuels must first be converted (reformed) to a hydrogen-rich gas mixture, since the cell reaction is the electrochemical oxidation of hydrogen to

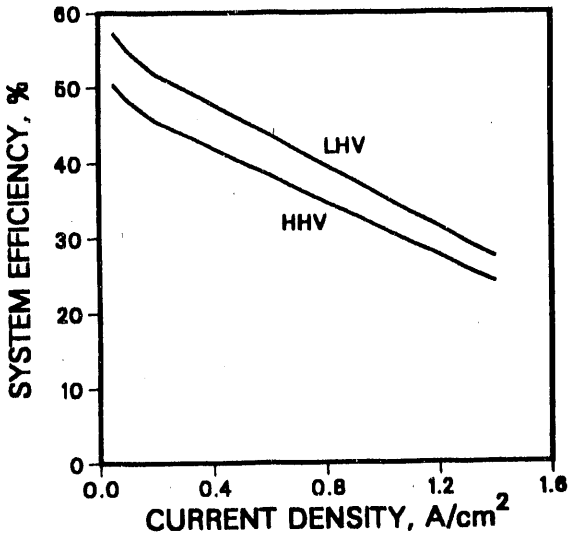

Fig. I-15.

Variation of PEM Fuel Cell System Efficiency with the Average Cell Current Density [based on the lower heating value (LHV) and the higher heating value (HHV) of methanol fuel]

water. Our fuel-reforming efforts include three activities: catalysis and kinetics studies for reforming ethanol and methanol; the design and analysis of partial oxidation reformers that are compact and responsive to dynamic loads; and technical support to DOE for a major industrial contract to fabricate an advanced multifuel reformer.

a. Catalysis and Kinetics Studies of Alcohol Reforming

The objective of this effort is to develop improved catalysts for the partial oxidation and steam reforming of ethanol and methanol. According to the literature,[13] the oxides of copper and zinc give satisfactory conversion of methanol in steam reforming; however, little has been discussed in the literature regarding the reforming of ethanol. We set up an experimental apparatus to study the steam reforming of ethanol and methanol under various feed (steam/alcohol ratio) and thermal conditions. With steel wool as the catalyst material and methanol/water solution as the fuel, preliminary experiments showed 450°C to be the lowest temperature at which noticeable gas production was achieved. However, the flow rate of the product gases was extremely small compared to the feed rate and thus represented a very low conversion. With nickel as the catalyst, discernible conversion to gaseous products was achieved only at temperatures approaching 500°C. Future work will evaluate catalyst materials to determine their effectiveness in reforming alcohol fuels.

b. Design and Analysis of Reformer Systems

A fuel reformer may produce hydrogen from hydrocarbon fuels by either steam reforming, partial oxidation, or a combination of the two. The dynamic-response and start-up performance of the partial oxidation reformer can be much superior to that of the steam

---

[13]N. E. Vanderborgh, B. E. Goodby, and T. E. Springer, "Oxygen Exchange Reactions during Methanol Reforming," Proc. of 32nd Int. Power Sources Symp., Cherry Hills, NJ, June 9-12, 1986, p. 623 (1986).

reformer for transportation applications. This is because the partial oxidation reformer uses direct heat transfer, which provides very high heat fluxes; therefore, the required heat transfer loads can increase or decrease rapidly. In contrast, a steam reformer must use indirect heat transfer, which limits heat fluxes. The partial oxidation reformer is an intrinsically simple device due to the absence of burners, baffles, heat transfer surfaces, and combustion manifolding and ducting. We have begun some conceptual design and analysis studies to devise reformer systems to exploit these potential advantages of partial oxidation reformers.

c. Technical Management

During 1991, CMT provided technical support to DOE to implement a competitive procurement for development of multifuel reformer systems to reform methanol, ethanol, natural gas, or other hydrocarbons into hydrogen for use in transportation fuel cell systems and for development of advanced systems for on-board hydrogen storage. The Department of Energy plans to award a 30-month development contract in 1992 and has assigned the responsibility for its technical management to CMT. The work will be divided into two phases: (1) a feasibility study and (2) the fabrication and test of proof-of-concept reformer and hydrogen storage systems.

II. FOSSIL FUEL RESEARCH

The Chemical Technology Division is the lead division for several projects in the ANL Fossil Fuel Program. These projects involve studies on fluidized-bed combustion (FBC) and open-cycle, coal-fired magnetohydrodynamic (MHD) power generation.

A. *Fluidized-Bed Combustion Studies*

Fluidized-bed combustion involves a process in which coal is burned under atmospheric or pressurized conditions in a fluidized bed of limestone or dolomite, which reacts with most of the SO_2 released during combustion. The FBC projects at CMT include investigations into (1) metal wastage on FBC heat exchanger surfaces, (2) materials performance in an atmospheric fluidized-bed cogeneration air heater, (3) alkali vapor emissions in the off-gas from pressurized fluidized-bed combustion (PFBC), (4) N_2O and NO_x emissions from PFBC, and (5) the use of Illinois limestones for reducing SO_2 and HCl emissions during the PFBC of an Illinois coal with high S and Cl content.

1. Metal Wastage in Fluidized-Bed Combustors

Metal loss from in-bed heat-transfer tubes in FBCs is a recurring problem that is impeding the commercialization of this technology. To address this problem, a cooperative research and development venture was formed with the following organizations: DOE, Electric Power Research Institute (EPRI), Center for Research on Sulfur in Coal (CRSC), Tennessee Valley Authority (TVA), ASEA Babcock PFBC, Foster Wheeler Development Corp. (FWDC), and ABB Combustion Engineering Systems (ABB/CE). The overall objectives are to (1) develop models and computer codes that will predict hydrodynamics and metal wastage of tubes in fluidized beds and (2) translate model predictions and experimental data into simple guidelines for the design and operation of FBCs with minimal metal loss. The ANL divisions involved in this project are CMT, Energy Systems (ES), and Materials and Components Technology (MCT).

Activities undertaken in 1991 include fluidized-bed experiments at FWDC and the University of Illinois at Urbana-Champaign (UI-UC) to determine solids motion around immersed tubes and their erosion at ambient conditions. Data from these experiments were analyzed using ANL-developed computer models of the fluidized-bed hydrodynamics and erosion processes. As reported previously,[1,2] the ANL computer models predict hydrodynamics of the solids and bubble motion and the erosion of tubes resulting from the impaction and abrasion by particles.

---

[1]M. J. Steindler et al., *Chemical Technology Division Annual Technical Report, 1988*, Argonne National Laboratory Report ANL-89/15, p. 49 (1989).

[2]R. W. Lyczkowski, J. X. Bouillard, D. Gidaspow, and G. F. Berry, *Computer Modeling of Erosion in Fluidized Beds*, Argonne National Laboratory Report ANL/ESD/TM-1 (January 1990).

In 1991, FWDC continued testing in a "cold-model" fluidized bed (room temperature, no combustion). The bed material was ash recovered from a circulating FBC unit operated by FWDC. Before the 400-h test, 21 tubes (51-mm OD and 3.75-mm wall thickness) were installed horizontally in the arrangement shown in Fig. II-1. A vertical partition plate was fixed to the floor of the existing fluidized bed to create two equal-sized beds. A superficial fluidizing velocity of 0.2 m/s was maintained in one-half of the fluidized bed, while a velocity of 0.3 m/s was maintained in the other half. Each tube was marked at 45° increments on the circumference and at five locations along the length. Differences in measurements of wall thickness at the marked locations, before and after the test, were used to assess material loss caused by erosion. Wall-thickness loss measurements ranged from 0.0 to 0.33 mm. Figure II-2 shows the path of greatest wear in the half of the fluidized bed that was operated at the higher superficial fluidizing velocity. The measured erosion wear in this half was greater than that of the other half, which was operated at lower superficial fluidizing velocity. Pressure fluctuation data were taken at the locations shown in Fig. II-1 to obtain information on bubble behavior for comparison with ANL computer model calculations.

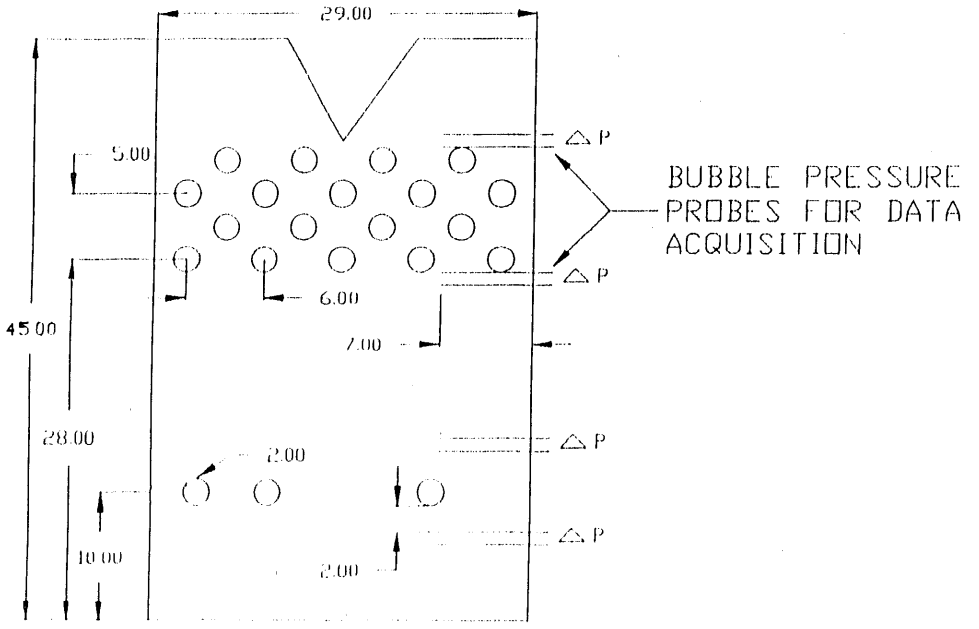

Fig. II-1. Arrangement of Tubes in Cold-Model Fluidized Bed of Foster Wheeler Development Corp. (All dimensions in inches; 1.00 in. = 2.54 cm)

The experiments at UI-UC investigated erosion and particle velocity in a fluidized bed, 30.5-cm square in cross section. For the erosion experiments, the tube array consisted of two rows of 5-cm (2-in.) OD tubes (two tubes per row), simulating a small section in the FWDC bed. The bed particles were Molochite (mainly SiO_2 and Al_2O_3), which was also used in earlier FWDC erosion studies. The Molochite particles are irregularly shaped and have a wide size distribution (predominantly 1.0-1.4 mm). Since the Molochite particles were recycled over and over in the fluidizing bed, they were subject to breakage and attrition. Accordingly, the change in their size distribution was monitored. Although changes were observed during the initial 10 h of testing, subsequent changes were small. Erosion data expressed in terms of the loss of local

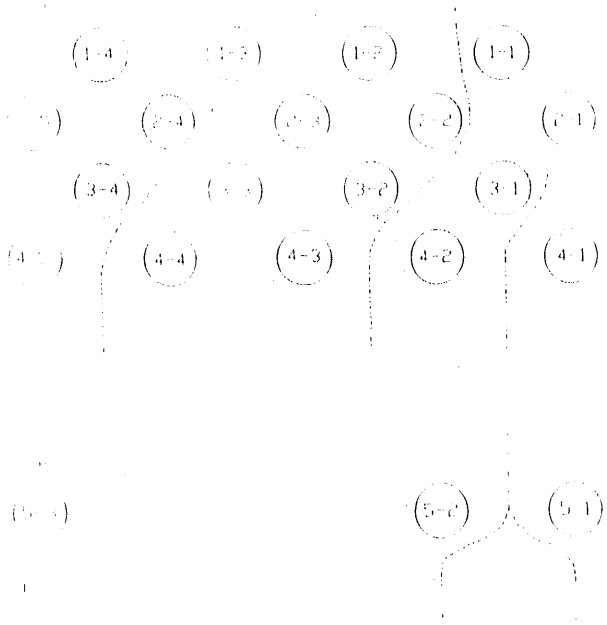

Fig. II-2.

Paths of Greatest Wear for Foster Wheeler Experiments in Cold-Model Fluidizing Bed. (View from opposite end of facility from that shown in Fig. II-1.)

tube wall thickness were obtained over a 450-h period. It was found that, for a given axial location on a tube, the erosion rate was highly nonuniform in the circumferential direction. On the other hand, for a given circumferential location, the variations in erosion rate were small in the axial direction.

In the UI-UC fluidized bed, the particle velocity of soda lime glass beads (dia = 1.0-1.4 mm) was measured by using the Computer-aided Particle Tracking Facility.[3] (The glass beads were used to eliminate dust formation experienced in tests with the Molochite.) Velocity data were collected for 95 h of experimental runs. Because of the presence of the tube array, the contribution of the averaged particle velocities in the axial direction was small, indicating that the averaged particle velocity field was approximately two dimensional. This is in agreement with the approximately two-dimensional character of the erosion behavior just described. From a vector plot of the averaged particle velocities in a plane normal to the tube axis, regions of the tube surface where high particle impact velocities occurred were readily identified. The confidence level of the measured data in those regions was examined, and the results were found acceptable. The high erosion regions of the immersed tubes coincided with those of high particle speed and high hitting frequency.

The ANL computer models and experimental data acquired in this project were employed to develop easy-to-use mechanistic models that designers can apply to determine the effect of various operating and design parameters on metal erosion in FBCs. From these models, guidelines were derived for the design, operation, and scaleup of FBCs with minimal erosion wear. In the next year, additional data analysis and model validation will be conducted for the British Coal Corp. and CISE (Milan, Italy), which recently joined the consortium.

---

[3]J. S. Lin, M. M. Chen, and B. T. Chao, AIChE J. **31**(3), 465 (1985).

2. Atmospheric Fluidized-Bed Cogeneration Air Heater Experiment

Argonne is managing the Atmospheric Fluidized-Bed Cogeneration Air Heater Experiment (ACAHE) for DOE. The objective of this project is to assess materials and process performance of in-bed air heaters for cogeneration of electricity and hot air in an atmospheric fluidized-bed combustor (AFBC). The ANL divisions involved in this effort are CMT and MCT.

Rockwell International was subcontracted for the experimental testing of heat-exchanger tube bundles in the DOE-owned AFBC unit (1.8-m square cross section) located at a Rockwell site in El Segundo, CA. Test articles made from a wide variety of metal alloys (including weldments, coated materials, and cladding materials) were supplied by ANL, Babcock & Wilcox (B&W), FWDC, and ABB/CE (the latter three, under subcontract to Westinghouse Electric Corp.). The test articles were intended to provide material wastage information that will enable projections of service life in an AFBC environment. Several types of articles were tested: platen specimens assembled into in-bed tube bundles, cylindrical specimens inserted into internally cooled probes, specimens of various geometries attached to uncooled probes, and tube clamps made from a candidate alloy. More than 60 types of alloys were exposed to the AFBC environment for ~2000 h at temperatures of ~1150 K. Argonne and the three subcontractors performed data analysis and an assessment of the heat-exchanger performance. These results, together with those reported earlier from a laboratory test program in support of ACAHE,[4] were used to determine the role of key variables that contribute to accelerated corrosion of materials and assess the long-term performance of candidate materials for air heater applications.

The following conclusions were drawn with regard to candidate material performance:

1. Austenitic stainless steels (e.g., Types 304, 310, and 330) and alloys such as HR 3C, FW 4C, and 8XX exhibited little corrosion after exposure in the Rockwell facility, as well as in a laboratory test under gas-cycling conditions between high and low oxygen partial pressures (~100 Pa/~3 x 10^{-7} Pa) and a more severe laboratory test at low oxygen partial pressure.

2. Long-term laboratory tests (3000 h) revealed that alloys such as HS 188, HS556, HK 40, and 800H exhibited catastrophic corrosion in the presence of sustained low oxygen partial pressures and bed-material deposit. Even though the test conditions were more severe than expected in a typical well-run FBC system, the data suggest the susceptibility of these materials to accelerated corrosion.

3. Alloys such as HH, HP 50, 253 MAX, XM 19, Sanicro 33, HS 556, and HS 188 were susceptible to unacceptable corrosion when in contact with the bed material.

---

[4]K. Natesan, S. A. Miller, and W. F. Podolski, *An Assessment of the Performance of Heat Exchanger Materials in Fluidized-Bed Combustors*, Argonne National Laboratory Report ANL-86/42 (1987).

4. Among the weldments, filler metals 25-35R, 21-33, and 308 exhibited superior corrosion resistance, whereas filler metals Nicro 82, 188, and 25-35 showed acceptable corrosion resistance.

5. Among the coated specimens, the performance of aluminized coatings was poor. In general, this is more due to difficulty in the development of a crack-free coating than to exposure in the FBC environment. However, the cracked regions, if present initially, exhibited accelerated oxidation, and the coating integrity declined.

6. Among the cladding alloys, Type 310 stainless steel on Type 304 stainless steel or Alloy 800H exhibited superior performance.

A final report describing the results from these experiments in more detail is in preparation.

3. Development of Regenerable Activated-Bauxite Sorbent Alkali Monitor

Vapor-phase alkalis in the flue gas from pressurized fluidized-bed combustion (PFBC) of coal are of concern because they are known to cause corrosion of turbine blade materials. The objective of this work is to develop a regenerable activated-bauxite sorbent alkali monitor (RABSAM) that will allow *in situ* measurement of alkali vapors in PFBC flue gas.

The key to the RABSAM is the development of a regenerable activated-bauxite adsorbent such that (1) the alkali vapors in the PFBC flue gas are captured by the adsorbent purely through physical adsorption, and (2) the adsorbed alkalis can be totally recovered by simple water leaching. The RABSAM will use commercial activated bauxite, which contains clay impurities that can react with alkali vapors; therefore, these clay impurities need to be either removed or deactivated. Our earlier work[5] indicated that NaCl solution is effective in deactivating clay impurities; however, the rate of residual alkali removal in the regenerable activated bauxite was low and needed to be improved. This past year, efforts were concentrated on (1) investigating a LiCl-solution impregnation method for deactivation of the clay impurities and (2) testing LiCl-treated activated bauxite for its ability to capture NaCl vapor from a simulated PFBC flue gas.

a. Method Development

On the basis of the amount of clay impurities in the raw activated bauxite, we selected a 6 M LiCl solution for impregnation of the activated bauxite at 3 mL LiCl per 5 g activated bauxite. Test results confirmed that the clay impurities in raw activated bauxite were completely deactivated by impregnating this material with 6 M LiCl solution, followed by heat treatment of the impregnated activated bauxite at 973 K for ~50 h.

---

[5]M. J. Steindler et al., *Chemical Technology Division Annual Technical Report, 1990*, Argonne National Laboratory Report ANL-91/18, p. 51 (1991).

In the RABSAM, the adsorbed alkalis will be recovered by a simple water leaching process. To prevent contamination of the water leachate for alkali analysis, complete removal of residual water-soluble alkali compounds in the LiCl-treated activated bauxite is necessary. Figure II-3 summarizes the steps employed for this purpose. A batch of activated bauxite impregnated by 6 M LiCl solution was subjected to these leaching steps to evaluate their effectiveness in removing residual alkalis from the sample. Spectroscopic analysis of the leachates and extracted bauxite indicated complete removal of the residual water-soluble sodium and potassium in the regenerable activated bauxite.

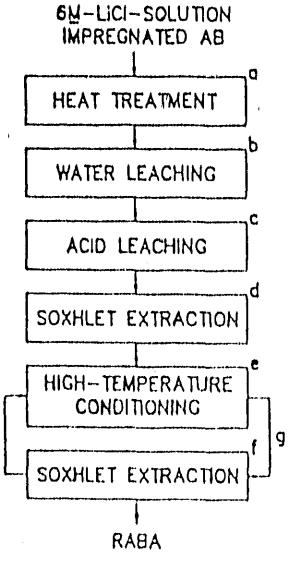

a Conducted at 973 K for 50 h.

b Conducted in a beaker at gentle boiling temperature for two minutes. Three leachings were made.

c Conducted in a beaker at gentle boiling temperature for ten minutes. Three leachings were made.

d Extracted with deionized water for 48 h.

e Conducted in a muffle furnace at 1173 K for 12 h.

f Extracted with deionized water for 4 h.

g Five cycles.

Fig. II-3. Procedures for Preparing Regenerable Activated Bauxite Adsorbent (RABA) after 6 M-LiCl Impregnation

c. High-Temperature/High-Pressure Testing

A batch of regenerable activated bauxite was prepared according to the procedures shown in Fig. II-3 and tested with a simulated PFBC flue gas in a pressurized alkali-vapor sorption test unit at a bed temperature of ~1175 K and a system pressure of ~1 MPa. The simulated PFBC flue gas was free of SO_2 and had a composition of 3% O_2, 16% CO_2, 5-7% H_2O vapor, 0.1-38.2 ppmW NaCl vapor, and the balance N_2. After testing, the activated bauxite was subjected to Soxhlet extraction with deionized water to remove water-leachable sodium. A portion of this extracted bauxite was then analyzed by atomic absorption spectrometry for its sodium content. Results of the analyses indicated that the NaCl vapor was captured by the adsorbent through (1) physical adsorption as NaCl, which was easily leached out by water extraction, and (2) chemical reactions that form sodium meta-aluminates and silicates. These alkali capture mechanisms are the same as those observed with untreated activated bauxite. The results of our earlier studies[6] with untreated activated bauxite suggest that, when SO_2 is present

[6]I. Johnson and S. H. D. Lee, *Alkali Metal Vapor Removal from Pressurized Fluidized-Bed Combustion Flue Gas, Annual Report for October 1980-September 1981*, Argonne National Laboratory Report ANL/FE-81-59 (1982).

in the simulated PFBC flue gas, NaCl vapor should be captured by the regenerable activated bauxite by physical adsorption as Na_2SO_4. High-temperature/high-pressure testing of the regenerable activated bauxite in simulated PFBC flue gas with SO_2 will be undertaken to confirm this observation.

4. Parametric Study of N_2O Emissions from FBC

In FBCs, the amount of N_2O existing in off-gases and the operating factors affecting N_2O levels are not well known. A parametric study of N_2O emissions from the laboratory-scale (15-cm dia) FBC at ANL was carried out to determine whether N_2O emission from FBCs is a problem that could impede their continued development and what influence operating parameters, such as pressure and combustion temperature, have on N_2O formation.

Nitrous oxide is considered to be one of the gaseous pollutants contributing to the greenhouse effect and the depletion of ozone in the upper atmosphere. It is stable in the troposphere and is eventually transported to the stratosphere, where it is converted to NO, which subsequently reacts with ozone. The increase in N_2O in the atmosphere has been attributed to the denitrification of chemical fertilizer, biomass burning and decomposition, and the combustion of fossil fuels. Currently, some confusion exists as to whether N_2O is subject to emissions regulations. The regulations limit the class of compounds, oxides of nitrogen, without designating specific species. However, the analytical method used for determining NO_x emissions compliance is not sensitive to N_2O. In addition, N_2O is not detected by the chemiluminescent NO_x analyzers currently used to monitor stack gas nitrogen oxides. Therefore, if FBC units produce substantial amounts of N_2O, additional regulations on its release could be forthcoming.

We combusted two Illinois coals (from Kerr-McGee Coal Co. and Peabody Coal Co.) in the laboratory-scale FBC unit and measured the N_2O emissions by means of an on-line infrared analyzer and gas chromatograph. Also determined were the SO_2 and NO_x levels. Data were obtained for a range of temperatures, excess air levels, fluidizing velocities, and pressures.

The results of these tests are summarized in Table II-1. Several observations were made from these data. First, the N_2O concentration decreased substantially as the temperature increased (other operating conditions constant). The decrease in N_2O level may be due to thermal destruction reactions or reactions with H and OH radicals. Second, the N_2O concentration increased with increasing excess air, although the relationship does not appear linear. Since NO_x levels also generally increase with excess air, running the combustor at the lowest excess air feasible would tend to decrease NO_x and N_2O levels and maximize boiler efficiency. Third, increasing residence time (inversely related to fluidizing velocity) tends to decrease N_2O emissions. If reactions with char are at least partly responsible for N_2O reduction, then increasing residence time should result in lower N_2O emissions. Increasing char loadings in the freeboard could also have the same effect; however, char loadings were not independently varied in these experiments. Fourth, increasing pressure appears to increase N_2O levels somewhat. Fifth, increasing SO_2 level (decreasing sorbent feed rate) tended to increase the N_2O

level. Finally, the levels of N_2O measured in the ANL FBC unit appear consistent with other reported FBC measurements and are higher than other types of combustors.

Table II-1. Emissions from Fluidized-Bed Combustion of Kerr-McGee and Peabody Coals

Run No.	Temp., K	Excess Air, %	Fluidizing Velocity, m/s	Pressure, kPa	Conc.,[a] ppm		
					SO_2	NO_x	N_2O
Kerr-McGee							
1	1173	30	1.6	101	230	649	61
2	1123	30	1.6	101	327	477	77
3	1073	30	1.6	101	341	378	92
4	1223	30	1.6	101	304	616	39
5	1173	50	1.6	101	250	639	78
6	1173	100	1.6	101	397	658	87
7	1173	30	1.2	101	448	552	86
8	1173	30	0.9	101	366	608	43
9	1173	30	0.9	505	235	159	62
10	1173	30	0.9	910	263	60	69
Peabody							
11	1173	25	1.6	101	293	551	77
12	1173	32	1.6	101	159	554	78
13	1173	32	1.6	101	682	590	113
14	1073	35	1.6	101	358	445	138
15	1173	70	1.6	101	392	632	125
16	1173	185	1.6	101	554	770	153
17	1173	30	0.9	101	326	495	53
18	1173	25	0.9	505	330	129	111
19	1173	25	0.9	910	370	83	82

[a]Normalized to 3.5% O_2 in flue gas.

5. Evaluation of Illinois Limestones for Reducing SO_2 and HCl Emissions

In this two-year study for the Center for Research on Sulfur in Coal (CRSC), two Illinois dolomites (Racine and Racine/Sugar Run) and an Illinois limestone (Fredonia) were tested for reducing the emissions of SO_2 from the laboratory-scale FBC at ANL. In the first year, 1990, the tests were conducted with Herron No. 6 coal (2.6 wt % S) under the excess-air conditions typical of a single-stage PFBC (3.5% O_2 in flue gas, pressure of 0.8 MPa, and temperatures of 1080-1180 K). Sulfur retentions ranged from a low of 67.4%, with the limestone at a Ca/S ratio of 1.3, to a high of 98.0%, with the limestone at a Ca/S ratio of 4.6.[7] The Racine/Sugar Run dolomite was the most reactive sorbent tested, the Racine dolomite the next most reactive, and the Fredonia limestone the least reactive. This finding was in qualitative

[7]M. J. Steindler et al., *Chemical Technology Division Annual Technical Report, 1990*, Argonne National Laboratory Report ANL-91/18, pp. 54-44 (1991).

agreement with the results of laboratory tests of the relative sorbent reactivity reported previously by the Illinois State Geological Survey (ISGS).[8]

In work completed this past year, the relative reactivity of the sorbents observed in the excess-air combustion tests was determined to be consistent with the physical characteristics of the sorbents, as determined by mercury porosimeter and nitrogen BET measurements (surface area and pore size distribution) on samples of the sorbents and their calcines. The combustor test results with the Racine/Sugar Run dolomite at 1123 K were also found to be in good agreement with the predicted performance of the sorbent obtained with the Westinghouse sulfur-removal model[9] using the ISGS laboratory data[8] on the reactivity of the sorbent (see Fig. II-4). This agreement confirmed the validity of employing laboratory test data in the selection of sorbents for FBC testing. Analysis of flue-gas HCl measurements during the combustion tests with excess air indicated that the sorbents were not effective in reducing HCl emissions, an expected result.

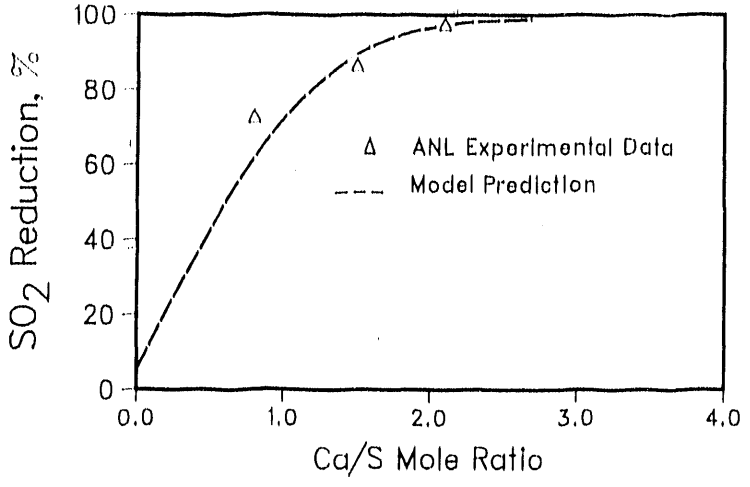

Fig. II-4. Comparison of Model Predictions of Sulfur Retention with Experimental Data for Racine/Sugar Run Dolomite. For predictions, data from ISGS[8] were used in the Westinghouse sulfur-removal model,[9] assuming that the SO_2 released uniformly throughout the fluidized bed.

The Fredonia limestone sorbent was also tested under fuel-rich conditions (air-to-fuel ratio <1.0) typical of staged PFBC concepts. Operating conditions included a bed temperature of 1123 K and pressure of 0.6 MPa. Parameters varied were air-to-fuel ratio (0.6 to 1.2) and Ca/S ratio (1.4 to 3.1). Figure II-5 shows the sulfur retention vs. first-stage stoichiometry (air-to-fuel ratio) obtained in these tests. Sulfur retention varied from 80 to 96%

---

[8]M. Rostam-Abadi et al., *Sorbent Evaluation for Pressurized Fluidized-Bed Combustors*, Final Report to the Center for Research on Sulfur in Coal, Illinois State Geological Survey (1989).

[9]R. A. Newby et al., "A Technique to Project the Sulfur Removal Performance of Fluidized-Bed Combustors," Proc. of Sixth Int. Conf. on Fluidized-Bed Combustion, Atlanta, GA, April 9-11, 1980, pp. 803-814 (1980).

and improved with increasing Ca/S ratio and decreasing air-to-fuel ratio. The results indicate that the quantity of sorbent required for a given sulfur retention v ould be less with staged combustion, as compared with conventional single-stage FBC. Also determined in these tests was that the NO_x emissions decreased from 125 ppm at an air-to-fuel ratio of 1.06 (excess air) to between 60 and 70 ppm at ratios less than 0.7 (fuel rich). These results indicate that NO_x emission can also be reduced by staged combustion under fuel-rich conditions. Hence, staged FBC may offer significant environmental and operational advantages over conventional FBC systems. Considerably more testing needs to be conducted, however, with additional sorbents to confirm the findings of this study. No additional tests are planned at this time, however.

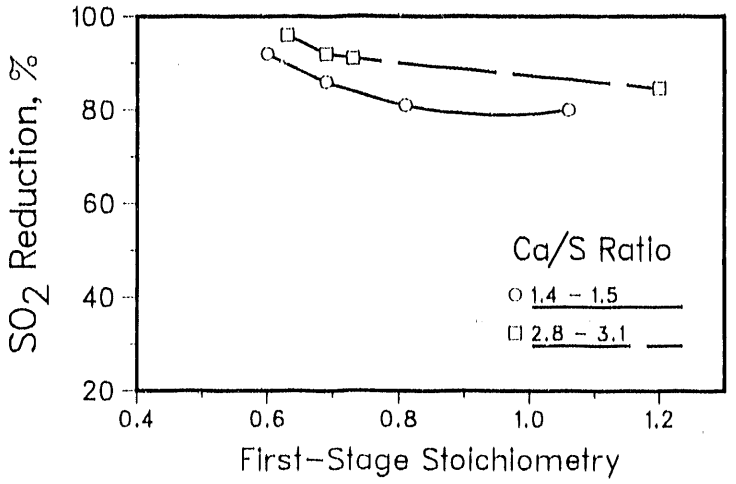

Fig. II-5. Effect of First-Stage Stoichiometry and Ca/S Ratio on Sulfur Retention at Bed Temperature of ~1123 K

B. *Magnetohydrodynamic (MHD) Studies*

Open-cycle MHD is a developing technology with the potential to improve substantially the electrical efficiency of coal-fired power plants and to reduce their environmental impact. In the coal-fired concept of MHD, an easily ionized seed material (usually a potassium salt) is injected into a high-temperature, slag-rejecting coal combustor. The resulting electrically conductive combustion gas then flows through a high-velocity channel in the presence of a strong magnetic field. An electrical potential develops across electrodes in contact with the gas stream in the channel walls and produces an electrical current. The fuel-rich combustion gas leaves the MHD topping cycle at approximately 2300 K and enters a bottoming cycle that is similar in function to the steam bottoming cycle of a conventional coal-fired power plant. However, the MHD steam plant must not only extract heat from the combustion gas to produce high-pressure steam, but also separate the seed from the ash, recover the seed material for reuse, preheat the primary combustion air to at least 1000 K, lower nitrous oxide emissions to acceptable levels, and inject secondary air to complete combustion of the fuel.

Materials evaluation studies are in progress in support of development of the MHD bottoming cycle. These studies include laboratory autoclave tests of candidate alloys to

determine their corrosion behavior under conditions expected for the intermediate temperature air heater in the bottoming cycle. Results from these tests are being analyzed and will be presented in a future report. In addition, we are analyzing tube materials from proof-of-concept tests for the MHD bottoming cycle at the Coal-Fired Flow Facility (CFFF) with Illinois No. 6 (high-sulfur) coal.

Materials evaluation studies for the topping cycle were conducted this past year for TRW Applied Technology Division in support of a proof-of-concept design for an MHD slagging-coal combustor. Specifically, water corrosion tests were conducted with T11 steel (Fe-1.25Cr-0.5Mo) to evaluate the performance of this material in the combustor cooling water supply system. In two separate tests, eight specimens of T11 obtained from TRW were exposed to water (pH = ~7.0) at a temperature of 368 K and pressure of 2.1 MPa for 305-310 h. In the first test, the dissolved oxygen in the feedwater was controlled at 3.0 ppm by bubbling an O_2/N_2 gas mixture through the feedwater. In the second test, the dissolved oxygen was controlled to 15.0 ppb by sparging the feedwater with nitrogen. Subsequent to the tests, the specimens were weighed and their thicknesses measured, before and after the removal of surface scales, to evaluate the corrosion rate.

Figure II-6 presents the normalized weight loss rates for the T11 specimens from both tests. Based on the weight-change data obtained in the first test (O_2 level of 3.0 ppm), the maximum general corrosion rate was calculated as ~5 x 10^{-5} mg/(mm^2•h). This translates to a maximum metal recession of only 20 μm (0.8 mils) during a 2000-h test in a prototypical combustor. However, scanning electron micrographs of the exposed specimens revealed localized pitting of the specimen surfaces, with pit depths much larger than the general corrosion.

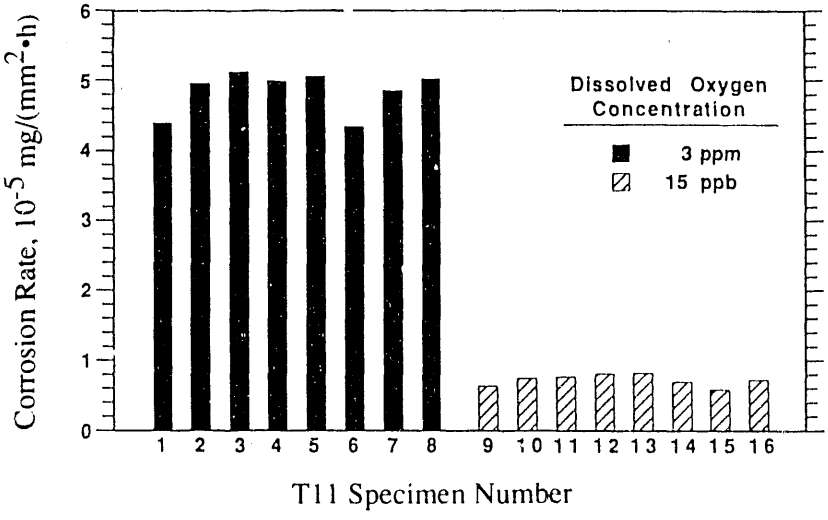

Fig. II-6. Normalized Weight Loss Rates of T11 Test Specimens

As indicated in Fig. II-6, the general corrosion rate was lower by a factor of approximately six in the second test (O_2 level of 15 ppb). The average weight loss in the second test was ~8 x 10^{-6} mg/(mm^2•h), which translates to a metal recession of 3.2 μm in a 2000-h test of the prototypical combustor. Examination of cross sections of exposed specimens showed minor

pitting, with pit depths in the range of 2-4 μm, substantially smaller than in the first test. As a result of these tests, the design specification for the dissolved oxygen concentration in combustor cooling water has been set at 15 ppb.

Tests were also conducted to evaluate the corrosion resistance of boron nitride and silicon nitride insulating materials in a potassium environment (liquid and vapor) at temperatures of 811 and 1033 K and to measure the electrical conductivity of the specimens before and after exposure to potassium. The objective was to determine the suitablility of replacing boron nitride by silicon nitride as the insulating material in an MHD channel.

Detailed microstructural analyses of the tested specimens after exposures up to 250 h were conducted using a scanning electron microscope. A preliminary visual examination showed a number of cracks in the boron nitride samples exposed under all conditions. The microscopic examination revealed substantial cracking and spallation of material from the surface. The potassium had penetrated the boron nitride specimens in their entire cross sections. The exposed samples were very fragile and disintegrated even with careful handling. The silicon nitride samples, however, were relatively unaffected. Potassium was evident in isolated areas on the surface of the specimens, but no cracks were observed, indicating much better resistance of this material toward potassium attack. Although there was evidence of potassium on the surface of the silicon nitride samples, none was detected in their cross sections.

The conductivity results for the boron nitride samples as a function of temperature are shown in Fig. II-7. Results are given for boron nitride after exposure to potassium vapor and liquid at 1033 K (760°C) for 250 h and for unexposed boron nitride. As can be seen, the effect of potassium penetration of the boron nitride specimens was to increase the conductivity of the

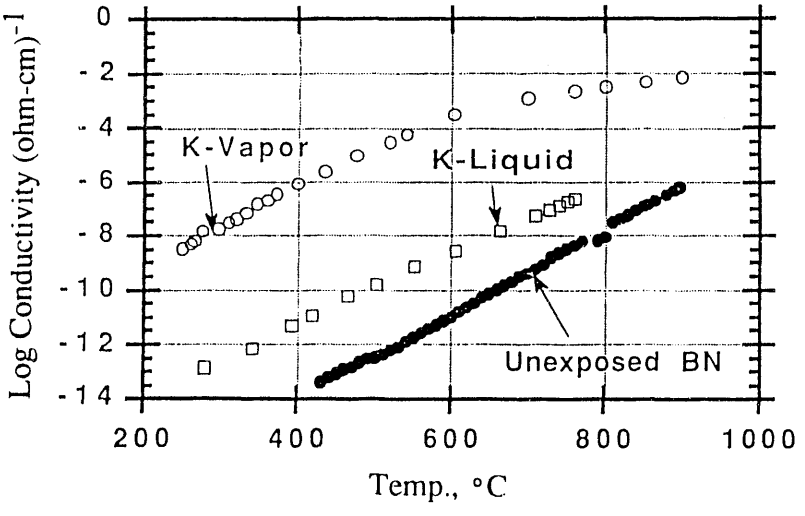

Fig. II-7. Electrical Conductivity of Boron Nitride Samples as Function of Temperature. [Results are given for samples before and after exposure to potassium liquid and vapor at 1033 K (760°C) for 250 h.]

material by three (potassium liquid) to seven (potassium vapor) orders of magnitude. In the case of the silicon nitride specimens, however, the exposure to potassium had very little effect on their electrical conductivity. Hence, the use of silicon nitride to replace boron nitride as the insulating material in the MHD channel may be advantageous with regard to chemical compatibility, mechanical integrity, and electrical properties.

During the coming year, support work for the topping cycle is expected to continue as additional areas of concern are identified by TRW, the prime topping-cycle contractor.

III. HAZARDOUS WASTE RESEARCH

During the past year, the CMT hazardous waste research was concentrated on two processes: (1) aqueous biphase extraction for recovering actinides from solid radioactive waste and (2) microwave-assisted detoxification for remediating hazardous waste streams. In addition, work was started on three initiatives: (1) use of electrokinetics for remediating soils contaminated with metals and hazardous organics, (2) use of combined physical and biochemical methods for treating uranium-contaminated soils, and (3) development of chemically bonded ceramic waste forms for underground disposal.

A. *Aqueous Biphase Process for Actinide Recovery from Solid Wastes*

The objective of this project is to explore the possible application of aqueous biphasic extraction for treating solid radioactive wastes. Wet grinding of the solids to a particle size of 1 μm or less followed by aqueous biphasic extraction will produce (1) a solid waste that would meet or exceed "economic discard limits" (i.e., plutonium concentration below the point where plutonium recovery costs exceed the value of the recovered plutonium) and (2) an actinide-bearing concentrate that would more effectively integrate with existing chemical recovery processes.

Aqueous biphase systems are heterogeneous, liquid/liquid systems that result from the appropriate combination of inorganic salts and water-soluble polymers, such as polyethylene glycol (PEG). Colloid-size particles, when suspended in an aqueous biphase system, will partition to one phase or the other, depending on a complex balancing of particle interactions with the surrounding solvent. With regard to waste treatment, aqueous biphase systems have similarities with conventional solvent extraction systems but do not utilize an organic diluent, which may generate concern as a source of pollution or a potential fire hazard. The water-soluble polymers used in biphase formation are inexpensive, nontoxic, and biodegradable.

The heterogeneous particle structure of many plutonium residues makes these materials attractive candidates for the use of ultrafine grinding as a means of liberating the plutonium from the particle matrix. Plutonium(IV) is known to be extremely abrasive, having a Moh's hardness greater than 9.[1] The PuO_2 can therefore be expected to be much more resistant to fracture than the surrounding particle matrix, giving rise to preferential breakage and enhanced liberation. The extreme hardness of PuO_2 should not present a problem during grinding since the plutonium in many residues is present as discrete grains that are about 1 μm in diameter. We do not expect that micron-size PuO_2 grains would require any further size reduction to be compatible with aqueous biphasic extraction. During the past year, our separation work was focused on investigating the partitioning of silica and metal oxides in aqueous biphase systems, the use of water-soluble complexants for promoting particulate extractions, and separation of binary systems containing colloidal PuO_2 and either SiO_2 or graphite.

---

[1] R. E. Skavdahl and T. D. Chikalla, in *Plutonium Handbook*, Vol. 1, ed., O. J. Wick, Gordon and Breach, New York, p. 259 (1967).

A particularly attractive feature of aqueous biphasic extraction is the ability to achieve single-stage separation factors $>10^6$ between silica and a wide variety of metal oxides. For example, we have determined that, with a biphase system consisting of 15% PEG/7.5% Na_2SO_4 at pH = 3, greater than 99.99% of metal oxides such as Fe_2O_3 and Al_2O_3 partitions to the bottom (sulfate-containing) phase, while greater than 99.99% of the SiO_2 particles partition to the top (PEG-containing) phase.

The partitioning of SiO_2 and the metal oxides between the sodium sulfate and PEG phases can be qualitatively related to the heat of immersion (ΔH_i). A large exothermic heat of immersion indicates very strong adsorption of water. Adsorption of PEG takes place through hydrogen bond formation between ethylene oxide and surface OH groups[2] and, therefore, must compete with water of hydration for surface adsorption sites. We have found that solids having low ΔH_i values, such as graphite and silica, partition into the PEG phase with partition coefficients >200, while those solids with large ΔH_i values, such as the metal oxides, have partition coefficients <0.005.

The partitioning behavior of silica is highly dependent upon pH and is directly related to the ionization of surface SiOH groups. Previous studies[2] have shown that only uncharged silanol groups can form hydrogen bonds with electron donor groups like ethylene oxide, and that, between pH values of approximately 1.5 and 3.5, silica carries a low charge density. It is in this pH range that we have observed maximum silica partition coefficients in the PEG/sulfate biphase system.

If PEG adsorption onto a silica surface occurs through hydrogen bonding only, the oxygens would be oriented toward the SiOH surface, and the hydrocarbon groups would be oriented outward, away from the silica surface. It is believed that the hydrophobic surface regions that would be generated by this preferential orientation are responsible for the partitioning of silica into the PEG layer. In going from pH = 2 to 4, there is only a slight increase in surface charge, but at pH $\geq$ 5 the surface charge becomes increasingly negative much more rapidly.[2] As the pH is raised, counter-cation adsorption at the silica surface increases in proportion to surface charge. Because of the relatively large size of hydrated cations such as $Na(H_2O)_6^+$, surface ionization also prevents polymer adsorption to neutral silanol groups that are in the immediate vicinity of SiO^- surface sites. We will be undertaking molecular modeling studies to gain further insight into the mechanism for PEG adsorption onto silica surfaces.

Selective adsorption of water-soluble surfactants onto the desired metal oxide surfaces can be used to render the solids sufficiently hydrophobic that they partition into the PEG phase. However, we have found that surfactants which adsorb through physical interactions, such as electrostatic attraction and hydrophobic bonding, tend to be ineffective phase transfer agents. In contrast to the poor performance of physically adsorbed collectors, we have found that surfactants which chemisorb through covalent bonding are quite effective at promoting solids partitioning from aqueous sulfate solutions into PEG phases. For example, oleic acid promotes the transfer of Fe_2O_3 and TiO_2 into the PEG-rich phase with partition coefficients >200. The

---

[2]R. K. Iler, *The Chemistry of Silica*, Chapter 3, John Wiley & Sons, New York (1979).

chemisorption of oleic acid onto hematite and rutile has been demonstrated by an infrared spectroscopy study, which indicates surface hydroxyl displacement by oleate.[3]

As with other metal oxides, polymeric Pu(IV) partitions to the sulfate layer with partition coefficients less than 10^{-3}. In experiments carried out thus far, polymeric Pu(IV) has been used as a stand-in for particulate PuO_2. Previous X-ray diffraction measurements at ANL showed that this plutonium polymer has a PuO_2 crystal lattice structure, while small-angle neutron scattering (SANS) measurements indicated that the polymer is approximately 22 Å in diameter and 120 Å long.[4] We are attempting to further characterize this polymer by dynamic laser light scattering to determine if the polymer size has remained stable since the SANS data were collected.

It is expected that the surface properties of the plutonium polymer and ground, micron-size PuO_2 particles are similar. The surfaces of both contain hydrated Pu-OH sites and should therefore display similar partitioning behavior. We are investigating the partitioning behavior of monomeric Pu(IV), polymeric Pu(IV), and micron-size PuO_2 particles. Thus far, we have shown that the partitioning behavior of monomeric and polymeric Pu(IV) is quite similar. Both species have extremely low partition coefficients in 15% PEG/7.5% Na_2SO_4 and 15% PEG/15% $(NH_4)_2SO_4$ biphase systems, and both are extracted into the PEG phase when the metal complexing dye Arsenazo III is used as phase transfer agent. Extraction data for polymeric Pu(IV) are shown in Fig. III-1. Above pH = 3.5, the partition coefficients are >300; and at pH = 2 the partition coefficient is about 0.15. Thus, efficient extraction and recovery of polymeric plutonium from alkaline solutions can be achieved by aqueous biphasic extraction. We are screening other water-soluble metal complexants for use as phase transfer agents in the aqueous biphase extraction of plutonium.

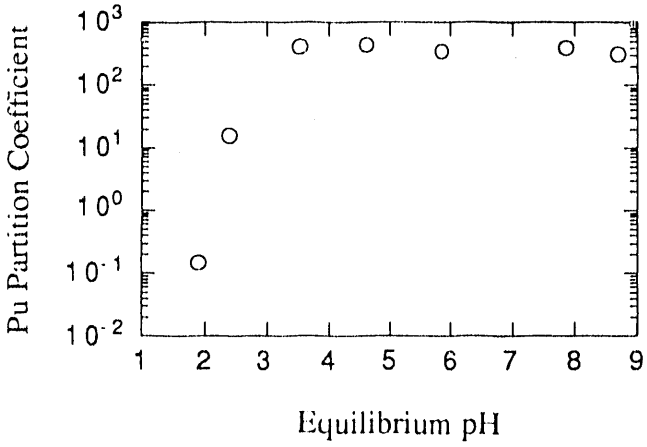

Fig. III-1.

Extraction of Polymeric Pu(IV) by 0.01% Arsenazo III as Function of Bottom-Phase pH in 15% PEG/15% $(NH_4)_2SO_4$ Biphase System

[3]D. W. Fuerstenau, Pure Appl. Chem. **24**, 135 (1970).

[4]P. Thiyagarajan, H. Diamong, L. Soderholm, E. P. Horwitz, L. M. Toth, and L. K. Felker, Inorg. Chem. **29**, 1902 (1990).

Graphite and silica are the major constituents of certain foundry residues and incinerator ash, respectively. Therefore, separations of PuO_2/graphite and PuO_2/SiO_2 mixtures are of interest and were investigated using a PEG/sodium sulfate biphase system and polymeric Pu(IV).

During the extraction of polymeric Pu(IV) in the presence of ground amorphous silica, the silica partitioned into the top phase (PEG), leaving the bottom phase with no trace of cloudiness. The size of the ground silica was between 0.2 and 1.0 μm. Since the bottom phase was clear, the silica concentration in that phase was estimated as less than 10^{-4} wt %. Based on the total amount of silica added, slightly greater than 99.99% of the silica had partitioned into the top phase. With greater than 99% of the polymeric Pu(IV) remaining in the bottom phase, a separation factor greater than 10^6 was obtained in a single stage [partition coefficients of $>10^4$ for silica and 0.009 for polymeric Pu(IV), as shown in Table III-1].

Table III-1. Partitioning of Polymeric Pu(IV) in Binary Particulate Systems[a]

		Partition Coeff.		
Systems	Reagent	Pu(IV)	SiO_2	Graphite
Pu(IV)/SiO_2	None	0.009	$>10^4$	
Pu(IV)/Graphite	None	4.0		$>10^3$
Pu(IV)/Graphite	0.01% AOT[b]	0.04		$>10^3$

[a]Aqueous biphase system: 15% PEG-3400/7.5% sodium sulfate at pH = 3.
[b]Sodium bis(2-ethylhexyl)sulfosuccinate, Aerosol OT.

In the polymeric Pu(IV)/graphite mixture, the naturally hydrophobic graphite was extracted into the upper PEG phase, leaving no visible trace of color or cloudiness in the bottom sulfate layer. Given a particle size of 1 to 2 μm, the graphite concentration in the lower phase was estimated to be less than 10^{-4} wt %. The partition coefficient of the polymerized Pu(IV) was 4 in this case (Table III-1). This large partition coefficient for plutonium is probably due to adsorption of the plutonium polymer onto the graphite particles. By the addition of 0.01% Aerosol OT to the biphase system, the partition coefficient of plutonium was reduced to 0.04 (Table III-1). It is possible that the partition coefficient could be reduced even further by optimizing the dispersant structure and concentration.

Interestingly, the Aerosol OT was effective only when it was added as a dodecane solution. Using an aqueous Aerosol OT stock solution actually resulted in plutonium partition coefficients larger than 4. The reason for this peculiar behavior is not clear at this time.

Work is underway to evaluate separation capabilities of aqueous biphase extraction using actual plutonium residues. Grinding studies with several different types of residues are being performed to evaluate the extent of plutonium liberation during particle-size reduction. Wet residues will be ground to an average particle size of 1 μm or less by using a vibratory ball mill. If separation factors as large as those obtained with the model systems are attainable, we believe that economic discard limits could be met for a significant portion of the residue volume. The

plutonium concentrates remaining could then be more economically processed by chemical means to recover highly purified plutonium as either the metal or the oxide.

B. *Microwave-Assisted Detoxification*

The thermal combustion of chlorinated hydrocarbons, such as trichloroethylene (TCE) and 1,1,1-trichloroethane (TCA), is the method approved by the Environmental Protection Agency for chemically detoxifying this class of compounds. Chemical detoxification is defined in this instance as the conversion of chlorinated hydrocarbons into (1) nonhazardous compounds, such as CO_2 and H_2O, which can be readily discharged to the environment, or (2) less hazardous compounds, such as HCl, which can be removed from the effluent stream by caustic scrubbing. However, because of the flame-inhibiting properties of chlorine radicals and the potential for forming oxygenated hydrocarbons, such as dioxins, in the oxidative atmosphere of an incinerator, considerable effort has been placed on finding alternative technologies for remediating hazardous waste streams containing chlorinated compounds. One potential new technology is the microwave discharge plasma reactor.

The microwave discharge plasma reactor uses microwave radiation (for this work, at 2.45 GHz) to sustain a glow discharge plasma. The alternating microwave radiation accelerates free electrons present in the plasma to energies one to two orders of magnitude greater than the average energies of the ions and molecules, resulting in a highly nonthermal equilibrium environment. Through collisional processes, the free electrons can generate the highly reactive radical species necessary for the detoxification reactions to occur. Owing to this nonthermal equilibrium energy distribution, a much greater radical concentration can be generated in a plasma reactor compared to an incinerator operating at the same gas-phase temperature. In addition, the reactive atmosphere in a plasma reactor can be either oxidative or reductive, whereas it can only be oxidative in an incinerator.

The reaction of TCA and O_2 in an argon plasma was investigated in our 7-kW microwave generator with varying operating parameters (O_2/TCA molar feed ratio of 1.5 to 165 and microwave power input of 300 to 600 W) to determine their influence on the overall TCA conversion and the resulting product distribution. The TCA conversion ranged from 75% at 300 W and an O_2/TCA ratio of 1.5 up to >99% at 600 W and an O_2/TCA ratio of 150.

The primary reaction of TCA and O_2 in an argon plasma can be described by an overall reaction which is identical to that observed in thermal combustion:

$$C_2H_3Cl_3 + 2O_2 \longrightarrow 2CO_2 + 3HCl \qquad (1)$$

The experimental results showed that this reaction is applicable in the presence of excess oxygen, i.e., O_2/TCA ratio greater than 2, and a power input of 600 W, which is above the minimum power (450 W) required to sustain the plasma under these conditions. As the concentration of O_2 was decreased to levels below that required for complete TCA oxidation, CO and soot were formed at the expense of CO_2. Moreover, as the power input to the reactor approached the minimum required to sustain the plasma (450 W), CO, soot, and nonparental hydrocarbons were

detected even in the presence of a large O_2 excess (O_2/TCA molar feed ratio of 165). This indicates incomplete oxidation of the TCA.

We also investigated the degradation of TCE in our microwave generator with an argon plasma (power input of 600-800 W and O_2/TCE molar ratio of 13 to 190). The TCE conversion was >96%. However, unlike TCA, TCE does not have sufficient hydrogen to convert all of the chlorine to HCl. As a consequence, the excess chlorine is eliminated as Cl_2:

$$C_2HCl_3 + 2O_2 \longrightarrow 2CO_2 + HCl + Cl_2 \qquad (2)$$

Our experimental results indicated that only ~30-40% of the chlorine was recovered as HCl, which is in good agreement with the overall stoichiometry of reaction 2.

To increase the hydrogen concentration, we investigated addition of water vapor to the argon plasma. In these experiments, the power input was 600 W, and the H_2O/TCE ratio was varied from 10.3 to 173. Ideally, the reaction of TCE and H_2O would occur according to

$$C_2HCl_3 + 4H_2O \longrightarrow 2CO_2 + 3HCl + 3H_2 \qquad (3)$$

However, our results indicate that the complete conversion of carbon to CO_2 does not occur. As the H_2O/TCE molar feed ratio was decreased from 173 to 10.3, the $CO_2/(CO_2 + CO)$ ratio decreased from 0.905 to 0.528. One possible explanation for the incomplete conversion of carbon to CO_2 is the water-gas shift reaction:

$$CO_2 + H_2 \longrightarrow CO + H_2O \qquad (4)$$

At the gas-phase temperatures anticipated for plasmas under these conditions, on the order of ~1000°C, the equilibrium constant is 3.7 for reaction 4. The observed increase in CO concentration in the effluent stream as the H_2O/TCE molar feed ratio was decreased is consistent with the equilibration of the water-gas shift reaction under these conditions.

When we reacted the TCE with a mixture of O_2 and H_2O in an argon plasma, we observed both the complete oxidation of carbon to CO_2 and the complete conversion of chlorine to HCl. This reaction is given by

$$C_2HCl_3 + 1.5O_2 + H_2O \longrightarrow 2CO_2 + 3HCl \qquad (5)$$

No CO, soot, or nonparental hydrocarbons were formed under the reaction conditions investigated (power input, 800 W; H_2O/TCE ratio, 2.40 to 25.7; and O_2/TCE ratio, 18.8 to 202).

Experimental work to be conducted in 1992 will focus on the reaction of TCA and TCE with O_2 and H_2O in an air (O_2/N_2) plasma. One of the major problems to be addressed is the formation of NO_x, which occurs more readily in a plasma reactor than an incinerator under similar gas-phase temperatures. We will also strive to develop a reactor system, such as the

slow-wave plasma reactor, with an effective plasma volume on the order of 500-1000 cm^3, which is approximately two orders of magnitude greater than the plasma volume (~7 cm^3) of the present reactor system. This new plasma reactor system will be capable of treating waste stream volumes expected in a field demonstration.

C. *New Initiatives*

1. Electrokinetic Processes

Soils contaminated with metals, in particular actinides and transuranics, or hazardous organic compounds, such as chlorinated and aromatic hydrocarbons, are a major environmental problem at DOE Defense Program sites. Considerable R&D on new technologies has been done to restore these contaminated soils to an acceptable level of decontamination. Electrokinetics is a potential technology for the *in situ* remediation of such contaminated soils. (Electrokinetics is the general term applied to the movement of charged particles through a continuous medium under the influence of an applied electric field. Two principal phenomena, electroosmosis and electrophoresis, comprise electrokinetics.) We have initiated two tasks to investigate electrokinetics technology for soil decontamination. The first is to investigate the enhanced migration of metals, and possibly organic compounds, under the influence of oscillating waves superimposed on a normal dc electric field. The second task is to develop electrokinetics-based processes that will enhance the molecular transport rates in novel "environmental" catalytic systems for the *in situ* destruction of organic contaminants.

Isotron Advanced Coating Technology (New Orleans, LA) is developing a soil decontamination process based on electrokinetic technology, and DOE has asked ANL to investigate this process. The process, marketed as the Electrosorb Soil Decontamination Process, differs from other electrokinetics processes in that oscillating waves, either electromagnetic (e.g., microwave or electrical power waves) or mechanical (e.g., sonic or ultrasonic waves), are superimposed on the normal dc electric field. We will perform experiments to verify whether or not a superimposed oscillating wave enhances the electrokinetic recovery of metals from soils. If the initial tests are positive, a more comprehensive research program will be undertaken to gain an understanding of this phenomenon and the optimal operating conditions for actual field tests.

We are also proposing, independent of the Isotron investigation, to develop electrokinetic processes to enhance the molecular transport rate in novel "environmental" catalytic remediation systems. This task will involve process development utilizing novel catalysts, currently under development at ANL, to destroy or detoxify hazardous organic chemicals in contaminated soils and groundwaters.

One of the major engineering problems in developing *in situ* catalytic remediation processes is bringing the catalyst and contaminant in contact to allow the reaction to proceed. This problem is particularly acute with soils. The complex nature of the soil matrix results in low transport rates and nonuniform flow distributions in the absence of an external driving force. Electrokinetics has the potential to minimize these problems because electroosmosis can cause the flow of groundwater under the influence of an electric potential. Since numerous contaminants are soluble or miscible to some extent in water, an electroosmotic flow pattern

could be developed to direct the contaminated groundwater through a catalyst bed implanted in the soil. Surfactants could be dispersed through the soil by using electrokinetics to increase the miscibility of hydrophobic compounds. The ability to destroy hazardous organic compounds in soils by a single-stage, *in situ* remediation process should compare favorably to the multiple-stage remediation processes currently under investigation.

2. Combined Physical and Biochemical Treatment of Uranium Contaminated Soils

The objective of this new initiative is to develop combined physical separation and selective leaching techniques to remove uranium from contaminated soils. The work is in support of an integrated demonstration for uranium removal from soils near Fernald, Ohio, and is being carried out jointly with researchers at Los Alamos National Laboratory. The extraction systems will use "biochelators" (siderophores) to bring about the dissolution of uranium oxides. A major portion of this project will be devoted to (1) increasing the water solubility of the biochelators and (2) minimizing the adsorption of the uranium-chelator complex onto soil particles.

We will attempt to increase the water solubility of siderophores and their metal complexes through molecular encapsulation of the hydrophobic regions of the biochelator molecule. Cyclic carbohydrates, such as gamma-cyclodextran, will be used as the encapsulating agent. The cyclodextrins have a conical structure with a hydrophobic internal cavity and a hydrophilic exterior. Enhanced solubility of hydrophobic solutes occurs through inclusion of guest molecules within the internal cavity. Gamma-cyclodextrin would be capable of encapsulating only the hydrophobic portion of the siderophore, leaving the chelating groups exposed and available for metal complexation.

Other planned activities include the development of (1) a hydrocyclone separator for the production of uranium concentrates from soils and (2) aqueous biphasic extraction for the recovery of ultrafine uranium oxide particulates from clay. Preliminary work has shown that micron-size kaolinite and montmorillonite can be separated from metal oxide particles by aqueous biphase extraction. We found that, in a 15%PEG/7.5% sodium sulfate system at pH = 3, the clay particles partition into the PEG layer with a partition coefficient >200, while the metal oxide particles partition into the sodium sulfate layer with partition coefficients <0.005. Thus, the separation factor is $>10^4$ in a single stage. Experiments to verify the performance of the aqueous biphase system will be carried out using Fernald soil samples. If successful, this will be the only commercially viable extraction technique available for treating 2-μm soil particles.

3. Chemically Bonded Ceramic Waste Forms

In anticipation of emerging needs for improved methods of stabilizing wastes for underground disposal, we are initiating work on development of chemically bonded ceramic materials. These materials offer potential as either final waste forms or as grouts for *in situ* stabilization of buried waste. Initial focus is on phosphate-bonded materials, such as magnesium orthophosphate and magnesium polyphosphate cements, which appear to be attractive for stabilizing buried transuranic waste.

IV. NUCLEAR WASTE PROGRAMS

Work is being performed in CMT to support the development of the first U.S. high-level waste repository. Programs are in progress to test the behavior of high-level nuclear waste glass and spent fuel upon exposure to liquid water or water vapor and characterize the reaction products. The alterations in the repository environment caused by the emplaced radioactive waste are also being investigated since these will also affect the waste behavior.

A. *Glass Testing Program for Environmental Restoration and Waste Management*

The Unsaturated Glass Testing Program at CMT is part of the technology support provided to DOE's Environmental Restoration and Waste Management. The purpose is to evaluate, before startup of the Defense Waste Processing Facility (DWPF) and the West Valley Demonstration Project (WVDP), factors that are likely to affect glass reaction in an unsaturated environment typical of what may be expected for the candidate repository site at Yucca Mountain (in southwestern Nevada). As part of this program, we are (1) reviewing the current understanding of parameters (e.g., temperature, glass composition) important to evaluating glass performance, (2) performing tests to further quantify the effects of important parameters, and (3) performing long-term tests designed to bound glass performance under the range of conditions identified in the Yucca Mountain Project Scientific Investigation Plan.[1] The data from the latter tests can be used to validate models developed to predict long-term performance of nuclear waste glass.

1. Critical Review

The predicted repository environment at Yucca Mountain has been described as hydrologically unsaturated with possible air exchange with the neighboring biosphere. We have identified several environmental conditions that can affect the durability of waste emplaced in such an unsaturated environment over repository-relevant time periods. To date, much of the information regarding what is known about these conditions has not been synthesized for use within the waste-glass research community. Thus, the need to perform such a critical review was identified, and this review is underway.

During the projected lifetime of an unsaturated repository, large amounts of liquid water are not expected to come into contact with the waste; however, water vapor or small volumes of transient water may contact the waste during the emplacement. We have identified the amount of water contacting the glass waste to be a primary parameter affecting waste glass durability. Other identified primary parameters include temperature, radiation field, glass composition, ratio of glass surface area to leachant volume (SA/V), and alteration phases resulting from glass hydration. We are conducting detailed critical reviews of how each

---

[1] R. D. Aines, *Plan for Glass Waste Form Testing for NNWSI*, Lawrence Livermore National Laboratory Report UCID-21190 (1987).

parameter affects waste glasses. The results from these reviews will be used in support of the DWPF and WVDP startup.

Our technical approach is to assemble all known and pertinent sources of scientific literature relevant to the critical parameters and then to assess the current state of knowledge as to how each parameter affects the waste glass reaction. When desirable, we have included reviews and discussions of studies of materials other than nuclear waste glasses, but this ancillary information is used to relate waste glass reaction to the parameter being reviewed. Existing data are synthesized, where possible, to provide a framework for comparing the results obtained from different studies. All references used in the critical reviews are collected in a computerized data base, which lists the reference, along with keywords and the ANL reviewer's comments regarding the reference.

A preliminary critical review was previously performed in order to provide a foundation for subsequent detailed review of each parameter.[2] The first such report, detailing the effects of temperature on waste glass performance, has been issued.[3] This report concluded that reaction mechanisms for waste glass dissolution in water are complex and involve multiple simultaneous reaction processes. The temperature dependence of each reaction process can be described by the Arrhenius equation, a relationship derived from empirical observations. In cases where the reaction mechanism changes as a function of time or temperature (i.e., the dominant reaction process changes), the Arrhenius equation is less useful in interpreting the temperature dependence of the overall reaction mechanism. Understanding the interplay of the reaction processes and their temperature dependences for nuclear waste glasses requires a clear understanding of the overall reaction mechanism, which has not yet been achieved. Until this understanding is gained, caution should be exercised in using temperature as an accelerating parameter in nuclear waste glass studies.

The next parameter to undergo a detailed critical review is the effect of glass composition on glass durability. This review is in progress. Models of glass structure are being investigated to help understand the fundamentals of how water may interact with glass. Brief reviews of models of glass dissolution are combined with this information to form a basis for critically reviewing theoretical and empirical models relating glass composition to glass durability. Reviews of the remaining parameters (radiation, SA/V ratio, surface layers, and unsaturated environments) are also being initiated.

2. Long-Term Testing of Radioactive Glasses

Most testing to evaluate the performance of high-level nuclear waste (HLW) glasses has been done using simulated nonradioactive analogues of the same general composition as the radioactive glass. To apply the knowledge gained in those studies to a fully radioactive

---

[2]M. J. Steindler et al., *Chemical Technology Division Annual Technical Report, 1990*, Argonne National Laboratory Report ANL-91/18, pp. 70-71 (1991).

[3]J. J. Mazer, *Temperature Effects on Waste Glass Performance*, Argonne National Laboratory Report ANL-91/17 (1991).

production glass, we have to demonstrate that the simulated-glass experiments are an adequate representation of reactions that will occur with the actual glasses to be generated by the glass producers.

We are thus conducting long-term leaching tests (for up to eight years) on fully radioactive glass to (1) allow comparison between the reaction of nonradioactive and radioactive glass and (2) collect long-term data relevant to conditions that may exist in an unsaturated environment. The glass samples are in the form of monoliths (SA/V = 340 m^{-1}) and powders (SA/V = 2000 m^{-1} or 20,000 m^{-1}) and have one of three compositions (designated 131/11, 165/42, and 200). The 131/11 glass is lowest in silicon and is in the lower portion of the stability range of waste glasses. The 165/42 glass is higher in silicon and is expected to be near the best range for durability. The 200 glass is poorer in silicon than the 165/42 glass, and a glass with this composition could be produced in the DWPF. The test temperature is 90°C, and the leachant is J-13 well water equilibrated with tuff rock (EJ-13), representative of the Yucca Mountain site. To monitor the reaction progress, solution and glass samples are periodically taken for analysis (see Sec. IV.A.7).

The solution analysis on the leachates from the fully radioactive (R) and simulated nonradioactive (S) glasses (SA/V = 2000 m^{-1}) reacted for 70 to 280 days indicated some differences in their normalized leach rates. Boron leaching from the glass was used to assess the extent of glass reaction. The 131/11R powder leached 150% less boron than 131/11S during the 280-day testing period. Similarly, the 200R powder leached 30-250% less boron than 200S up to the 70-day period. On the other hand, 165/42R powder leached almost 50% more boron than 165/42S for the 280-day period.

In spite of these differences, the solution kinetics analysis indicated that the radioactive and simulated glasses generally followed the same controlling mechanism in the glass reaction. The leaching for the 165/42R and 165/42S glasses entailed preferential alkali release, and the normalized lithium concentrations in the leachates were always the highest. The dissolution of 200R and 200S glasses was more characteristic of matrix dissolution, and the normalized boron and sodium concentrations were usually higher than the corresponding lithium concentrations. The 131/11R and 131/11S glasses underwent leaching characteristic of matrix dissolution over the extended time period but an alkali-dominated leaching in the early reaction, where normalized lithium concentrations fell between those of sodium and boron. On the basis of the solution analyses, the relative glass durability observed for both the radioactive and simulated glasses follows the order 165/42 > 131/11 > 200.

The reacted glass samples were further characterized using transmission electron microscopy (TEM). Those results indicated that the reacted layer thickness ranged from a few nanometers for 165/42S monoliths to about 200 nm for 200R and 200S powders. The durability measured by reacted layer thickness follows the order 165/42 > 131/11 > 200 for simulated glasses (the radioactive glasses have not been analyzed yet). This durability order agrees with that derived from the solution analyses. For all three glass types, the reacted layer thickness decreased when SA/V was increased from 340 m^{-1} (monolith) to 2000 m^{-1} (powder) or 20,000 m^{-1} (powder). This probably results from the element concentrations in the higher SA/V

solutions approaching saturation more rapidly because more glass surface area is available for reaction. Solution saturation is expected to reduce reaction affinity and glass dissolution.

The pH's for the radioactive glasses were usually lower than those for the simulated glasses due to the formation of nitrogen-related acids in the leachates as a result of radiation. This reduction in solution pH for the radioactive glasses, combined with the controlling mechanisms revealed above, helps explain the observation that radioactive glass leached less than the corresponding simulated glass for 131/11 and 200 glasses, but leached more for 165/42 glass. The controlling reaction mechanism for both 131/11 and 200 glasses was matrix dissolution, where the leach rates were proportional to the concentration of the nucleophilic species, hydroxide. Since the pH's were lower in the solutions leached from the radioactive glasses, the 131/11R and 200R glasses had lower leach rates. On the other hand, 165/42 glasses were leached mainly through an ion-exchange reaction mechanism, where the reaction rate depended on the hydronium ion concentration. As the pH was lowered for 165/42R glass, the increased concentration of hydronium ions promoted the ion exchange process between hydronium ions in solution and the alkalis in glass, resulting in a faster leaching. Therefore, the 165/42R glass leached more than the 165/42S glass. These long-term tests will be continued with periodic monitoring of effluent and reacted glass.

3. Effects of Radiation

Long-term tests are underway to determine the effects of radiation on glass behavior under the high SA/V conditions expected at a geologically unsaturated repository site. The objective of these tests is to (1) examine radiolytic product formation in a moist-air system, without the presence of glass (blank tests), (2) examine glass reaction in a radiolytic field as a function of glass composition and SA/V ratio, and (3) identify the influence of radiation and the radiolytic products on the formation and stability of the glass alteration phases.

To determine the effects of radiolysis, blank tests were carried out in pressure vessels containing deionized water under gamma and alpha radiation at 25-200°C. The results from the blank tests with gamma radiation indicate $G(NO_3^-)$ yields [where G(X) is the number of molecules converted per 100 eV absorbed] of 3.4 ± 0.8 at 25°C, 1.2 ± 0.4 at 90°C, and 0.5 ± 0.1 at 200°C. These results suggest an inverse temperature relationship for NO_3^- formation. In blank tests with alpha radiation, the $G(NO_3^-)$ yield was 2.2 ± 0.3 at 25°C. The reduced yield relative to the gamma blank tests at 25°C may reflect partial attenuation of the alpha particles in thin films of water that form on the Am-241 foils in our test vessel.

The effect of radiolytic product formation on glass reaction is being studied by exposing identical glass samples to both irradiated (~3.7×10^3 rad/h) and nonirradiated humid air at 150-200°C. These vapor hydration tests have been completed for periods of up to 56 days. Cross-section profiles indicated that glasses exposed to the irradiation field react five to ten times faster than their nonirradiated counterparts. Although cursory examination suggested completely different surface behavior, detailed microscopic examinations indicated a remarkable similarity in the sequence of minerals that form on both the irradiated and nonirradiated glasses. The results in Fig. IV-1 for a Type 202 waste glass show that, given enough time, the nonirradiated sequence of secondary phases will progress to the point where they are identical to those of the

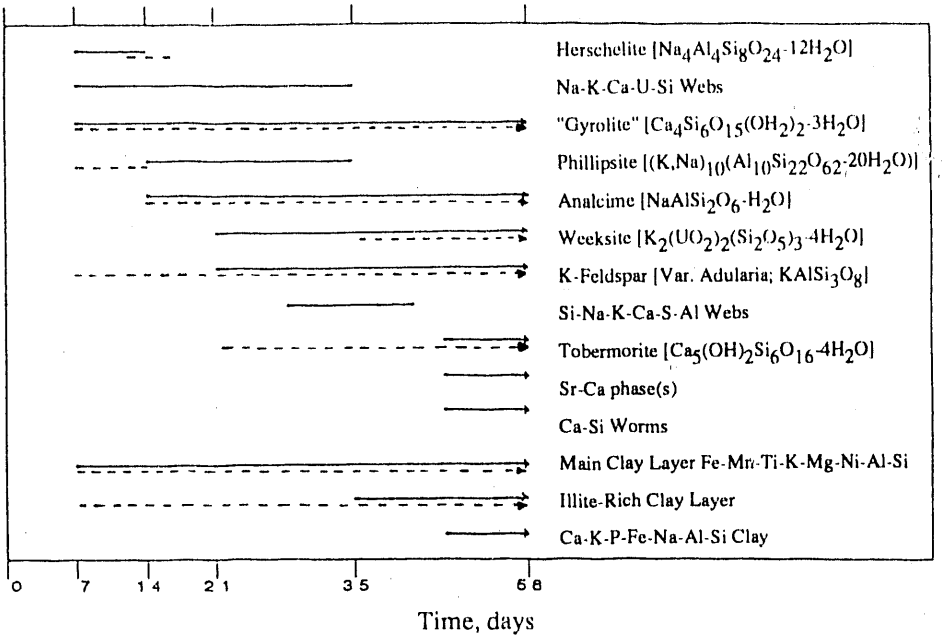

Fig. IV-1. Secondary Phases Formed on Surfaces of Type 202 Glass Monoliths Hydrated at 200°C. Tick marks on horizontal scale indicate periodic sampling intervals. Paths show mineral paragenetic sequence for actinide-doped glass exposed to an external gamma radiation field (dashed lines) and uranium-doped glass without external radiation (solid lines).

irradiated tests. This observation is important in that the surficial chemistry of the irradiated samples, especially in relation to solution pH, remains similar to that of the nonirradiated tests. An increase in glass reaction products apparently has neutralized the formation of radiolytic products. The stability of these secondary phases in the radiation field may be important in the retention of radionuclides dissolved from the reacting glasses.

Irradiated leach tests were also conducted for periods up to one year with glass monoliths (SA/V = 340 m^{-1}) immersed in EJ-13 water at 90°C and dose rates of 3500 rad/h. Plots of normalized element release vs. time display parabolic release curves for Si, Ca, Mg, Na, K, Li, and B. This trend may reflect a decrease in glass dissolution rates as concentrations of the leached elements increase. For some samples, Ca, Mg, B, Si, and U concentrations may also decrease after one year of reaction. These decreased concentrations may result from the precipitation of phases that have relatively low solubilities for these elements. These tests will continue to monitor glass reactions for up to two years, and in the future will also include analysis of secondary phases that form on the altered glass surfaces.

4. Effects of SA/V Ratio

Static leach tests are being performed to assess the effects of SA/V ratio on the extent and nature of the glass reaction. The glass compositions (Types 202 and 131) are

representative of waste glass to be produced at DWPF. All tests are conducted at 90°C with deionized water or groundwater solution (EJ-13), and reaction times range from 3 to 1820 days.

The SA/V ratios include those used in standard MCC-1 tests (10 m^{-1}) and the Product Consistency Test (2000 m^{-1}). These conditions result in dilute or concentrated leachate and measure different glass responses. The interpretation of these tests forms the basis for modeling glass reaction in long-term computer simulations. It is thus important to understand how the glass reaction might be affected by these SA/V ratios and how tests at different SA/V ratios are related. Tests are also being conducted at SA/V ratios of 340 and 20,000 m^{-1}. These SA/V ratios are the highest values which permit complete solution analyses with monolithic and powder glasses, respectively. Some tests employ glasses doped with actinides to determine how the SA/V affects their release and distribution.

Tests have been completed through one year with glasses having SA/V ratios of 10, 2000, and 20,000 m^{-1}. The measured leachate pH values are plotted as a function of the reaction time in Fig. IV-2 for Type 202 glass. The results indicate that the major influence of SA/V is dilution of hydroxide produced by ion exchange reactions releasing alkali metals. If the same amount of hydroxide were generated at all SA/V ratios, differences in dilution would yield pH values which differ by 2.3 units for tests at 10 and 2000 m^{-1} and 1 unit for tests at 2000 and 20,000 m^{-1}. This is observed in the data for Fig. IV-2 through about 200 days. Beyond about 200 days, the behavior is more complex. Figure IV-3 shows the normalized boron release as a function of reaction time for Type 202 glass. The release is low at all SA/V ratios through about 300 days, but is greatly accelerated in tests at 20,000 m^{-1} between 182 and 364 days. The acceleration of the reaction at 20,000 m^{-1} is also evident in the appearance of the reacted glass. For times up to 182 days, the glass looks virtually unreacted, but after 364 days the glass is covered with a chalky white residue. Accelerated reaction was found to occur in previous tests in water vapor upon precipitation of secondary mineral phases.[4] Analysis of the reacted powder glass from the tests at 364 days is in progress to identify the secondary phases that had formed.

Other workers[5-7] have noted an apparent correspondence in the solution compositions of tests performed for equivalent values of SA/V multiplied by the reaction time (t). This is an apparent corollary of the dilution effect noted in the pH measurements. Figure IV-4 shows the measured boron concentration as a function of (SA/V)t for tests at 10, 2000, and 20,000 m^{-1}. Clearly, the solution concentrations do not scale as (SA/V)t. The difference appears to be due to a quenching of the reaction at longer times at all SA/V ratios. More tests are needed to clarify the scaling behavior.

---

[4]M. J. Steindler et al., *Chemical Technology Division Annual Technical Report, 1989*, Argonne National Laboratory Report ANL-90/11, p. 81 (1990).

[5]L. R. Pederson, C. Q. Buckwalter, and G. L. McVay, Nucl. Technol. **62**, 151 (1983).

[6]L. R. Pederson, C. Q. Buckwalter, G. L. McVay, and B. L. Riddle, Mater. Res. Soc. Symp. Proc. **15**, 47 (1983).

[7]S. O. Bates, G. F. Piepel, and J. W. Johnston, *Leach Testing of Simulated Hanford Waste Vitrification Plant Reference Glass HW-39*, Pacific Northwest Laboratory Report PNL-6884 (1989).

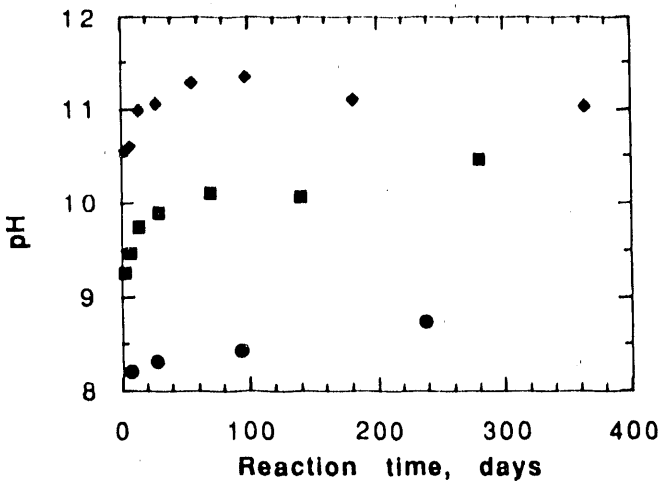

Fig. IV-2.

Leachate pH (25°C) vs. Reaction Time for Type 202 Glass at SA/V = 10 m^{-1} (circles), 2000 m^{-1} (squares), and 20,000 m^{-1} (diamonds)

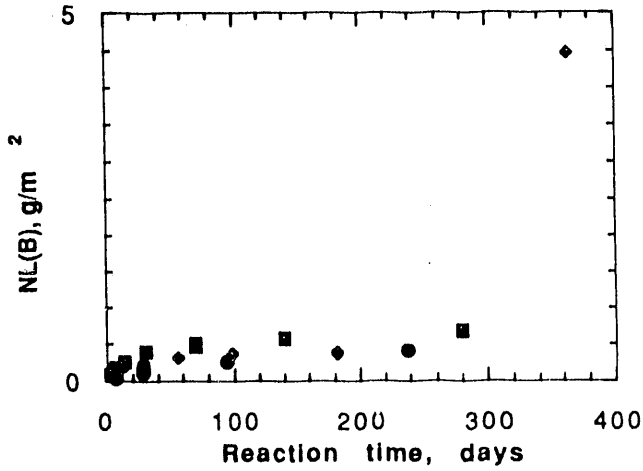

Fig. IV-3.

Normalized Boron Release vs. Reaction Time for Type 202 Glass at SA/V = 10 m^{-1} (circles), 2000 m^{-1} (squares), and 20,000 m^{-1} (diamonds)

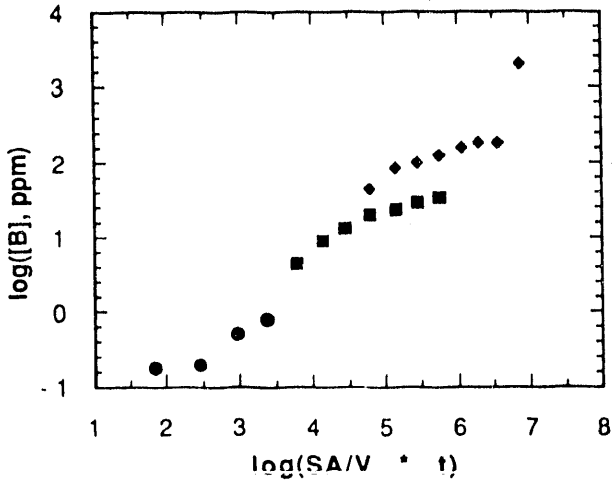

Fig. IV-4.

Boron Concentration vs. (SA/V)t for Type 202 Glass at SA/V = 10 m^{-1} (circles), 2000 m^{-1} (squares), and 20,000 m^{-1} (diamonds)

5. Formation and Characterization of Colloids

The potential formation of colloids in nuclear waste-glass dissolution and the role of these colloids in transporting radionuclides are important issues in evaluating the behavior of nuclear waste glass (and indeed other waste forms) after disposal in a geologic repository. In particular, the assumption that the concentrations of most sparingly soluble radionuclides would be "solubility limited" needs to be checked. A study was, therefore, initiated to examine the characteristics of colloidal particles formed under a variety of waste-glass testing conditions (see also Sec. IV.B.1).

a. Radionuclide Behavior

Samples of waste glasses, in the form of actinide-doped monolithic disks or crushed powders, were leached in J-13 well water at 90°C. The test duration ranged from 14 to 1460 days. A leachate solution from each test was filtered sequentially through a series of Nuclepore (pore size of 5, 1, 0.1, and 0.015 μm) and Amicon Diaflo (pore size of approximately 3.8 nm) filters. After filtration, the amount of filtrate collected was weighed, and an aliquot was deposited and dried on a stainless steel planchette for alpha counting. Also, the filters were removed from the filter housing and mounted on steel planchettes in a configuration suitable for counting by alpha spectroscopy. The observed count rates for the alpha peaks characteristic of ^{237}Np, ^{239}Pu, ^{238}Pu, ^{241}Am, and ^{244}Cm were used to calculate the filterable and nonfilterable concentrations for each isotope. Samples suitable for TEM examination were prepared from selected leachate solutions by carefully wicking a small droplet of the leachate through a "holey" carbon TEM grid.

The data for neptunium indicate that less than 15% of the solution concentration is filterable, even at the 3.8-nm filter pore size. This result is consistent with neptunium results reported previously.[8] The data for neptunium are consistent with the expectation that its concentration is dominated by the material truly dissolved in solution, and that colloidal formation and transport may not play an important role in neptunium release from waste packages or engineered barrier systems.

In contrast, most (up to 100%) of the Pu, Am, and Cm isotopes in the leachate were associated with particulate in the colloidal size range. The size distribution changed significantly from test to test. The TEM results indicate two distinct types of particles (Fig. IV-5). The larger particles (Fig. IV-5b) are believed to result from exfoliation of the reacted layer on the glass surface. The particles illustrated in Fig. IV-5a are believed to be typical of those that account for the filtration results and may be formed and grown in the leachate. The size distributions are probably influenced by a broad range of factors (including glass type, test duration, and test conditions), which are not well understood at this point. However, the fractions of Pu, Am, and Cm isotopes associated with the different size particles appear to follow the same trend.

---

[8] J. C. Cunnane and J. K. Bates, Mater. Res. Soc. Symp. Proc. **212**, 885-892 (1991).

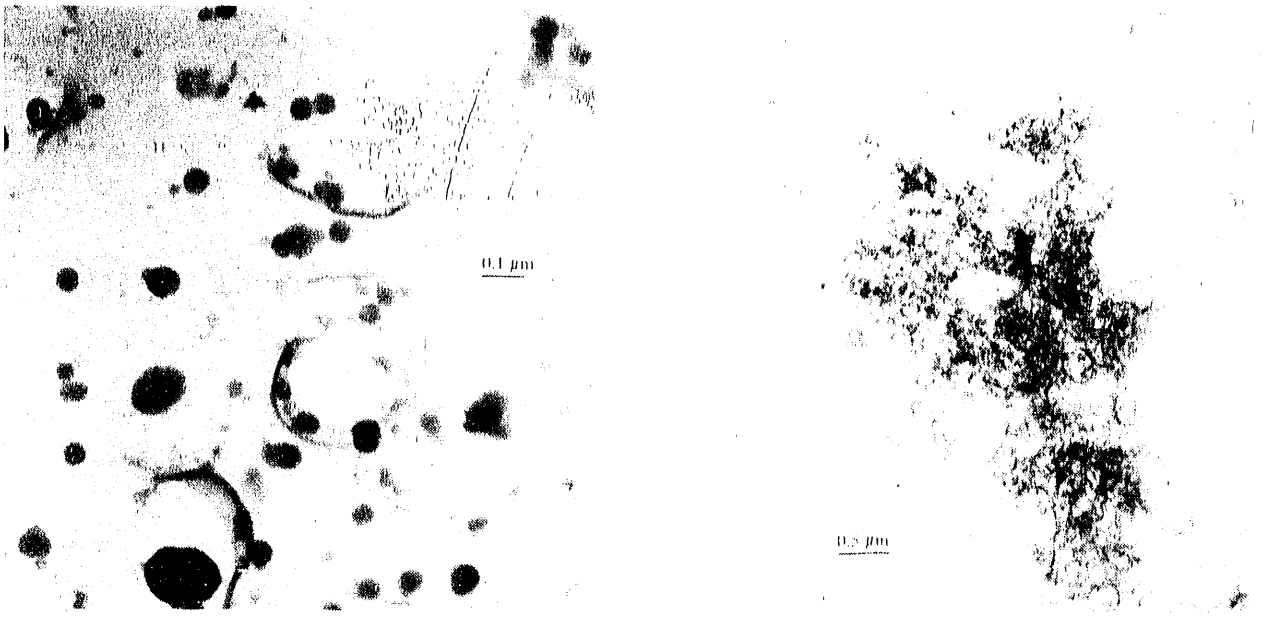

(a) (b)

Fig. IV-5. Transmission Electron Micrograph of Particulate Materials Isolated on a Holey Carbon Grid

Although preliminary, these test results indicate that the assumption that groundwater concentrations of actinide elements will be solubility limited should be reexamined. This conclusion applies particularly to modeling the release of Pu, Am, and Cm isotopes from waste packages containing nuclear waste glass.

b. Colloid Characterization

Analysis of the filtered leachates from some reacted glasses tested earlier has shown that the glasses were depleted in Al and Fe. The TEM examination of the colloidal particles from the leachates revealed the presence of Al- and Fe-rich colloids. Concentrations of particular elements within colloids were often greatly increased, and we observed colloids rich in Pb, Sn, Cr, Fe, Al, and Hg. Moreover, many different phases were identified, such as phosphates, which have the potential to take up actinides. The most common types of clay colloidal particles found appeared to be smectite and kaolinite; however, many other types of phases were observed. Most of these were unidentifiable.

Two tentative conclusions were drawn from these analyses: smectites are the most common type of colloid found, and colloidal phosphate phases only appear in samples reacted over long periods of time. These studies clearly show the need to carry out investigations with fully radioactive production glasses to predict the leach rate of radionuclides away from the proposed repository.

6. Natural Analogues

The reaction of naturally occurring rhyolitic glass (obsidian) with water under conditions where the SA/V ratio is large (i.e., reaction in water vapor) has a relatively simple reaction process, molecular water diffusion. A detailed study of this reaction process has been undertaken to assist in understanding more complicated reaction mechanisms for nuclear waste glasses. Although obsidians are enriched in silica and depleted in alkalis and boron, relative to nuclear waste glasses, their survival in nature for extensive periods of time (up to millions of years) can offer insights into the long-term corrosion of glass in a geologic setting.

Fourteen different obsidians and one tektite were hydrated in vapor between 110 and 180°C for up to 400 days at relative humidities (RH) of 60, 90, 95, or 100%. Reaction progress was monitored by the growth rate of the birefringent hydration layer, thought to be caused by the formation of a strained glass network as molecular water diffuses into the glass. In all cases, the growth rate was proportional to the square root of time, a dependence consistent with a diffusion process. We found that the hydration rate of obsidian is significantly affected by relative humidity, an effect previously believed to be negligible. The RH dependence could be correlated to the amount of water sorbed onto the glass surface; this suggests that the diffusion process is driven by chemical potential differences between the glass and the sorbed water. We also found that the isothermal hydration rate of obsidian strongly depends on the obsidian composition, specifically the intrinsic water content. Our correlation between intrinsic water content and hydration rate is superior to previously proposed models.[9,10] Our plot of the temperature dependence of obsidian hydration rates conformed to an Arrhenius equation in which the activation energy strongly depends on the intrinsic water content.

As a test of our model, we also considered the experimental hydration of tektite. Tektite is a natural glass, somewhat similar in composition to obsidian, but containing a very small (~0.01 wt %) amount of water. The tektite data are consistent with the diffusion process being controlled by the intrinsic water content, whereas the other compositional models could not successfully incorporate the tektite values.

These results suggest that obsidian hydration dating,[11,12] a chronometric tool utilized extensively by archaeologists, has the potential to be accurately calibrated. The technique currently relies on experimental determinations of the activation energy of hydration for each obsidian being studied. Our results will allow practitioners of obsidian hydration dating to estimate the ages of obsidian artifacts or features from the intrinsic water content. Furthermore, better age estimates will also result when the effects of RH are taken into account.

---

[9] I. Friedman and W. Long, Science **191**, 247 (1976).

[10] J. Ericson, J. D. MacKenzie, and R. Berger, "Physics and Chemistry of the Hydration Process in Obsidians. I: Theoretical Implications," in *Advances in Obsidian Glass Studies*, ed., R. E. Taylor, Noyes Press, Park Ridge, NJ (1976).

[11] I. Friedman and R. L. Smith, Am. Antiq. **25**(4), 476 (1960).

[12] I. Friedman and F. W. Trembour, Am. Sci. **66**, 44 (1978).

The results of this study indicate that water diffusion is not the rate-controlling reaction process under the conditions investigated. It is unknown whether water diffusion becomes rate controlling at longer times or under different reaction conditions. The quantitative nature of the results obtained to date can be incorporated into developing more realistic and mechanistic models of glass/water dissolution reactions.

7. Analytical Support

For the above tests, we used analytical electron microscopy (AEM) to examine the structure of the reacted glasses and obtain accurate information as to the reaction process. This analytical method involves a combination of transmission electron microscopy (TEM), X-ray energy dispersive spectroscopy (EDS), electron energy loss spectroscopy (EELS), and electron diffraction (ED). Point-to-point resolution for images obtained with the TEM approaches 3 Å, and the smallest region that can be investigated using EDS, EELS, and ED is about 200 Å. The AEM is a very powerful tool for investigating samples with very small inclusions, thin layers, and intercalated materials.

For AEM identification of secondary phases to be successful, one must have extremely thin samples, 500 Å or thinner. Since reaction layers are much thicker, frequently >50 μm, transverse cross sections must be prepared. Ultramicrotomy, i.e., thin sectioning with a specially designed diamond knife, has proven successful in preparing ultrathin sections of a wide variety of reacted glasses. Ultramicrotomy preparation artifacts do not interfere with the analyses required, and the layer structure of the reaction products is preserved.

In addition to the reaction layers that adhere to the glass, colloidal particles are spalled from the glass reaction layers into the reaction effluent or form from solution. We have thus collected colloidal particles from the leachate of many samples and analyzed them by AEM (see Sec. IV.A.5). With AEM, one not only obtains information about the size of colloidal particles but also compositions and diffraction information.

B. *Yucca Mountain Site Characterization Project*

The Yucca Mountain Site Characterization Project (YMP) is evaluating the suitability of Yucca Mountain as a site for a potential HLW repository. Work at CMT supported by the YMP includes tests involving the reaction of glass and spent fuel under simulated repository conditions and tests to determine the effects of radiation on the gas-phase composition near the buried waste.

1. Unsaturated Glass Testing

The current reference design[13] for the Yucca Mountain site calls for spent nuclear fuel from commercial reactors and HLW glass to be contained in an engineered barrier system

---

[13]U.S. Department of Energy, *Site Characterization Plan: Yucca Mountain Site, Nevada Research and Development Area, Nevada*, DOE-RW-1099, 7 Vols., Office of Civilian Radioactive Waste Management, Washington, DC (1988).

(EBS) that is surrounded by the natural host rock. Ideally, this multiple barrier system (waste form, EBS, rock) will limit radionuclide release from the waste material. In addition, radionuclide migration will be retarded due to chemical and physical interactions with the rock.

Evaluation of the total repository performance has been based on two premises: the release of actinides (e.g., Pu and Am) from the waste form will be controlled by the solubility of individual elements in groundwater, and subsequent radionuclide transport will be determined by factors such as water flow and radionuclide retardation processes (e.g., sorption). Under this scenario, the waste form itself can react relatively rapidly, yet the transport of radionuclides will be limited by geohydrologic factors.

We have examined the solubility-controlled assumption by determining the release of Np, Pu, and Am from waste glass under simulated storage conditions. While radionuclides may form colloids that could affect transport properties,[14,15] it is generally assumed that colloids result either from hydrolysis of dissolved species in solution ("radiocolloids"), or from adsorption of dissolved radionuclides onto suspended mineral particles existing in the groundwater ("pseudocolloids"). Both of these processes of colloid formation occur independently of the waste form and EBS and may be considered as secondary processes. However, since glass is a metastable solid, it may transform into a more stable phase assemblage under repository storage conditions.[16,17] This assemblage may be a new source of colloidal material, i.e., primary colloids, and would form by a process that is waste-form dependent. The radionuclide content of these colloids, their sources, and the mechanism of formation must be accurately known to assess the transport of radionuclides from the EBS to the accessible environment. Thus, we have studied the primary colloids that form during glass reaction. The results provide insight into the dynamics of radionuclide mobilization in an HLW repository.

Tests with simulated glasses nave been ongoing for 50 months. The test method involves dripping water onto a cylindrically shaped glass-metal assemblage that is suspended in an enclosed test vessel at 90°C. The water that collects in the bottom of the test vessel provides information regarding (1) the form and rate by which radionuclides are released from the glass and (2) synergistic effects that occur in the glass-metal-water system.

During the most recent liquid collection period, the test solution was filtered to determine whether the actinide fraction was associated with particulate material or could be considered truly dissolved in solution. Solution was passed sequentially through filters having pores that are from 1.0 μm to 1 nm in size. The liquid that passed through each filter and the filters were analyzed for radionuclides. The filters were then dissolved; the resulting suspension was dried and exposed to alpha-particle sensitive films to locate the source of alpha activity. When alpha tracks were observed, the specific particles producing those tracks were identified

---

[14]J. D. F. Ramsay, Radiochim. Acta **44/45**, 165 (1988).

[15]M. B. ten Brink, D. L. Phinney, and D. K. Smith, Mater. Res. Soc. Symp. Proc. **212**, 641 (1991).

[16]J. K. Bates, W. L. Ebert, and T. J. Gerding, in *High-Level Radioactive Waste Management Proceedings*, Vol. 1, American Nuclear Society, La Grange Park, IL, pp. 1095-1102 (1990).

[17]T. A. Abrajano, J. K. Bates, A. B. Woodland, J. P. Bradley, and W. L. Bourcier, Clays and Clay Miner. **38**, 537 (1990).

and transferred to a TEM grid. The structure and composition of the radioactive particle were then determined.

The results of the tests indicate that 70% of the neptunium passed through all filter sizes and can be considered truly dissolved in solution. On the contrary, over 99% of the Am and Pu was retained as colloidal solids. In these tests, most of the alpha radiation was due to the ^{241}Am decay; however, in samples where ^{239}Pu was also detected, its behavior mirrored that of americium. Thus, we discuss Pu and Am release together. In general, the ratio of radioactivity in the filtered to dissolved fraction was greater than 1000:1.

We employed a combination of particle micromanipulation procedures, autoradiography, and AEM to characterize the colloidal particles. The colloids were found to be a matrix of clay that contains submicrometer inclusions. The clay is Na- and Fe-rich aluminosilicate (with minor amounts of Ca, Ti, and Ni), which exhibits a basal lattice spacing of 1012 Å. This basal spacing, combined with X-ray diffraction data, suggests that the clay is Na-rich smectite.[18] The submicrometer inclusions contain major amounts of Ca, Th, P, and O and minor amounts of U and Pb. Electron and X-ray diffraction analyses indicated that the inclusions are the mineral brockite (ideally $[Ca,Th](PO_4)\cdot H_2O$).[19]

We compared the densities of the alpha tracks originating from brockite-rich vs. clay-rich material and established that the Am (and Pu) is carried in the brockite inclusions rather than the clay matrix. (Both Am and Pu are present at levels $<<0.1$ wt % and are, therefore, undetectable by EDS.)

The Am (and Pu) bearing colloidal particles form via a different mechanism than radiocolloids and pseudocolloids. Whereas radiocolloids and pseudocolloids develop from solution, the colloids studied here are fragments of a hydrated layer that spalled from the glass surface during aqueous alteration. This spallation mechanism can generate primary colloidal particles with highly elevated radionuclide levels. We examined the spallation mechanism of colloid formation by exposing a glass to water vapor. Exposure to water vapor is known to accelerate glass reaction[20] and thus provides an ideal method to examine redistribution of elements during glass reaction. Additionally, water vapor is also likely to be more prevalent in the Yucca Mountain environment than liquid water. In the presence of water vapor, a thin film of water sorbs onto the glass surface, where it becomes concentrated in cations leached from the glass. We have determined that mineral phases nucleate from the film and form on the surface of the glass, and at the same time, a hydrated or leached layer penetrates into the glass (Fig. IV-6). Since this layer is analogous to the hydrated layer that forms during the dripping-water tests, its mineralogy should be similar to that of the primary colloids filtered from the groundwater. Scanning electron microscopy and AEM were used to study polished thick and ultramicrotomed thin sections of the vapor-exposed specimen. We identified inclusions that exhibited the same

---

[18]G. W. Brindley, in *Crystal Structure of Clay Minerals and their X-ray Identification*, eds., G. W. Brindley and G. Brown, Mineralogical Society, London, p. 125 (1984).

[19]J. L. Fisher and D. S. Meyrowitz, Am. Mineral. **47**, 1364 (1962).

[20]J. K. Bates, L. J. Jardine, and M. J. Steindler, Science **218**, 51 (1982).

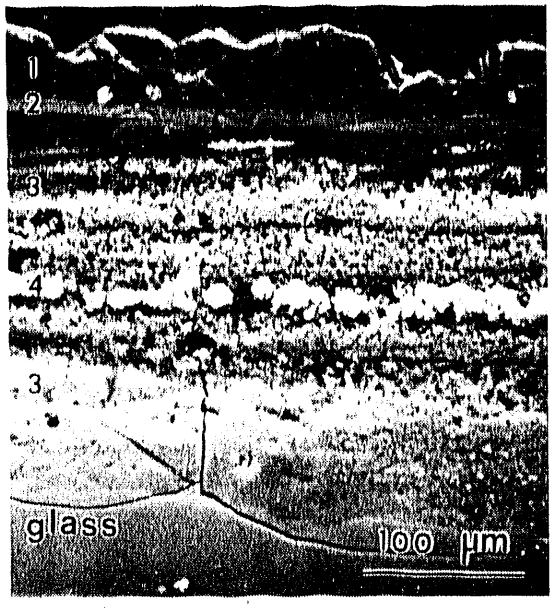

Fig. IV-6.

Backscattered Electron Image of Cross Section of Glass Exposed to Water Vapor. As the glass hydrates, elemental segregation occurs, secondary phases (1) form on the original surface (2) of the glass, and a hydrated layer (3) simultaneously penetrates into the glass. Calcium, phosphorus, thorium, and other actinides redistribute within the hydrated layer to form discrete brockite inclusions (4) as small as 10 nm. Actinide redistribution preferentially concentrates Th, U, Pu, and Am from the glass into the inclusions, which are subsequently mobilized as colloids.

compositional and diffraction characteristics as the Pu- and Am-bearing inclusions in the colloids, and determined that the clay in the hydrated layer was Na-rich smectite. This correspondence in phases confirms that the reacted glass layer is the source of the primary colloidal particles.

These results provide insight into the process of actinide release from glass waste forms. They also highlight the importance of engineered and natural barriers in retarding radionuclide migration. The majority of neptunium is truly in solution, as shown by its passage through the smallest filter size. Therefore, neptunium performance in the repository appears to be adequately treated using current assumptions of solubility-controlled transport. However, nearly 100% of the Pu and Am was found in small (<200 nm) insoluble inclusions associated with colloidal-sized clay particles. This observation has two ramifications. First, since the colloids form from the glass, as opposed to forming by precipitation in solution, the actinides in the glass become highly concentrated in these colloids. In addition, these colloids are readily generated from reacted glass, and transport of Pu and Am from the glass may be dominated by their movement. Thus, the EBS should be designed to inhibit colloid transport in the case of unexpected liquid water contact with the waste. Assessments of the ability of the environment near the repository to retard radionuclide transport should also consider colloid migration and trapping processes. Secondly, a conservative performance assessment should be based on the identity and transport properties of specific actinide-bearing phases that result from waste-form reaction. The colloid phases generated will likely vary depending on the type of waste form (spent fuel or glass) and on the glass composition.

The approach taken in the present study also has applications to cleanup of sites contaminated with hazardous wastes. The identity of small radionuclide-bearing phases may help in determining transport rates, developing remediation methods, and supporting risk assessment studies.

2. Spent Fuel Testing

In addition to glass studies, experiments designed to determine radionuclide release rates by exposing simulated spent fuel to repository-relevant conditions are being performed in CMT.

a. UO_2 Unsaturated Drip Tests

We have exposed two sets of Zircaloy clad-unirradiated UO_2 pellets to dripping EJ-13 water under conditions that simulate reactions expected for spent reactor fuel in an unsaturated repository environment. The two sets of experiments examine reactions of UO_2 samples at 90°C and variable SA/V ratios in the presence of stainless steel and Teflon support plates and have been continuing for periods of 2.25 yr (stainless steel plate) and 6.5 yr (Teflon plate). Goals for these tests are to develop procedures for studies conducted with actual spent fuel, identify secondary alteration phases, and describe parameters that control the release of uranium from the waste package assembly.

Results to date indicate that the UO_2 matrix readily reacts under liquid water/oxidizing conditions. Reactions are characterized by a large pulsed release of uranium, and the formation of several uranyl oxide hydrate mineral phases (schoepite, dehydrated schoepite, and becquerelite) across the sample surface after one to two years (Fig. IV-7). Surface examinations indicate that the UO_2 pellets have undergone extensive corrosion, with spallation of fine UO_{2+x} particulates being responsible for much of the uranium released during this period. After two years, reactions are characterized by reduced uranium release; dissolution of uranyl oxide hydrate phases; the formation of uranyl silicate phases (soddyite and uranophane); and depletion of alkali, alkaline earth, and silicon concentrations from the EJ-13 solutions.

Filtration of the leachate indicated that the concentration of the <20 Å particle component averages 0.28 ± 0.10 ppm (~1.2×10^{-6} M). This "soluble component" represents ~50% of the total uranium released from tests during slow uranium release, while it represents <5% of the fraction from tests entering a rapid release period. These findings support the above evidence that identifies spalled UO_{2+x} particulates as being responsible for the pulse of uranium release. These experiments will continue to monitor the reaction of UO_2 with liquid water under unsaturated conditions.

b. UO_2 Saturated Tests

Tests were also completed to determine the dissolution characteristics of UO_2 powder samples in J-13 well water under saturated conditions at room temperature. The tests were initiated by adding 80 g of ^{235}U-enriched powder to 250 mL of J-13 water and allowing the solution to equilibrate for 161 days. The test solution was next spiked with a uranyl salt solution containing uranium with a natural isotopic abundance. The dissolution rate kinetics from UO_2 powders was determined over the next 93 days using an isotope dilution technique that measures the re-equilibration rate between the solution and the powder. Anomalously high uranium concentrations (17 to 74 ppm) detected from the test solutions were attributed to the large initial

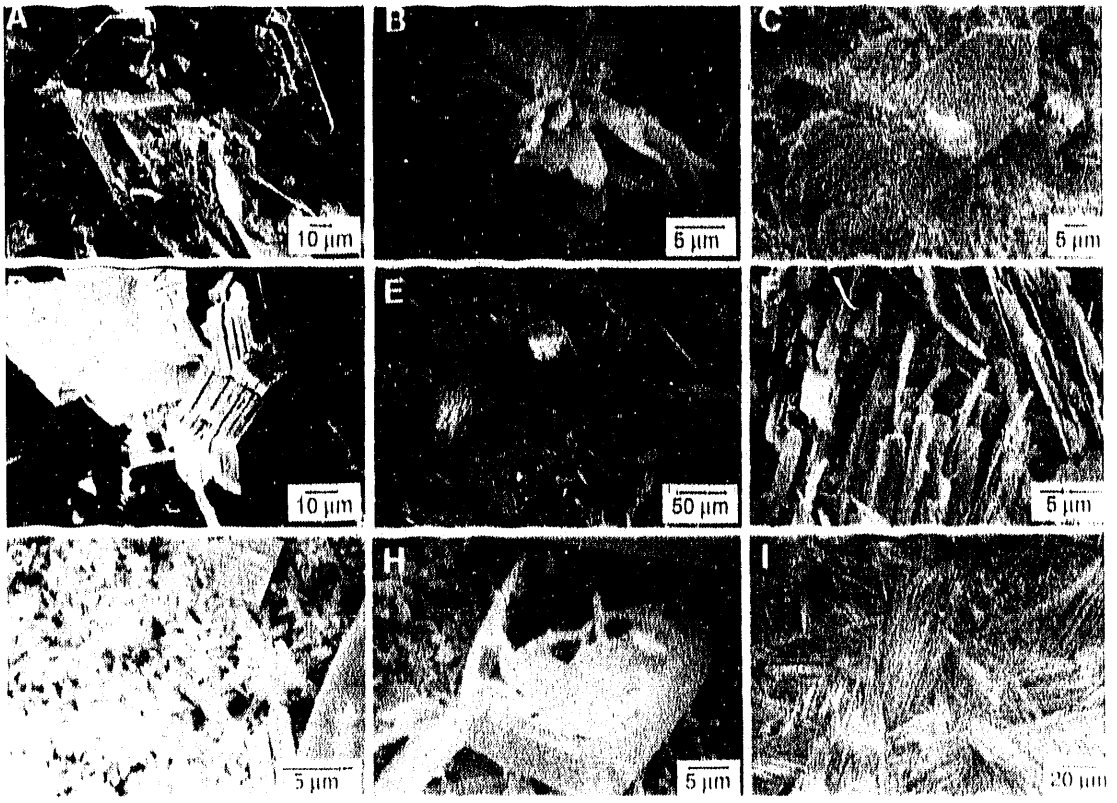

Fig. IV-7. Scanning Electron Photomicrographs of Various Alteration Phases Formed on Surface of UO_2 Samples Over Time. (A) Fine-grained particulate matter deposited on surface of hydrated schoepite crystals and underlying UO_{2+x} surface (2.25 yr); (B) stellar-shaped accumulation of dehydrated schoepite crystals (2.25 yr); (C) dehydrated schoepite with pitted surface suggestive of dissolution event (1.5 yr); (D) tabular books of schoepite (3.5 yr); (E) large tabular becquerelite crystal (3.5 yr) showing development of dissolution pits, along with individual bunches of acicular uranophane crystals, and the granular UO_{2+x} surface; (F) bladed soddyite crystals (3.5 yr); (G) very fine-grained soddyite (3.5 yr); (H) U-Si coating formed over unidentified blocky phase (3.5 yr); and (I) dense mat of uranophane bundles and exposed granular UO_{2+x} substrate (3.5 yr).

surface area of the powder and its high initial oxidation states (O/U = 2.16). Modeled results suggest that the elevated uranium concentrations are controlled by secondary uranyl mineral phases such as schoepite. The experiments also helped to derive appropriate filtering procedures, sampling intervals, leachant replenishment techniques, and uranium spiking procedures to be used for future studies with spent fuel.

3. Radiation Effects Studies

The emplacement of a nuclear waste container in a high-level waste repository would subject the near-field environment to significant levels of gamma radiation (>0.1 Mrad/h)

in the current waste package design. The presence of gamma radiation will lead to the formation of gaseous species that may affect container durability. The effect of gamma radiation is, therefore, an important factor in assessing the overall performance of the waste package.

The near-field environment of the waste package will be an air-water vapor gas throughout most of the repository history. The composition of the gas phase, as long as the repository remains unsaturated, will be a function of the initial gas phase present, the temperature of the waste package, the gamma radiation level, material-specific surface interactions, and gas exchange/transport throughout the repository horizon.

A series of experiments was performed in high-humidity air systems to establish the yield trends as a function of water vapor content. The experimental conditions included temperatures of 30-240°C, air/water vapor ratios of 0.1-10, absorbed doses of 2-16 Mrad, and times up to 30 days. These experiments extend past work to higher humidity contents and lower absorbed dose to obtain initial yields.

The most important effect of increased amounts of water vapor in the gas phase is the more efficient oxidation of NO_2 to nitric acid:

$$NO_2 + OH \rightarrow HNO_3 \qquad (1)$$

In previously performed long-term experiments at low humidity (air/water vapor ratios of >100),[21] we determined the levels of nitrate on the vessel wall and nitrate as nitric acid in the gas phase. The former was obtained by rinsing the vessel walls, and the latter by condensing the gas phase into a secondary vessel. When detectable amounts of water vapor were in the gas phase, nitrogen-containing acids, which appeared mostly in the vessel rinse, were the only fixation products of importance. Only a small buildup of NO_2 was observed in the gas phase. The long-term nitric acid yields were linear with absorbed dose up to 300 Mrad, with a net yield between 0.8 and 1.2 molecules/100 eV in the 30-210°C temperature range investigated.

To establish the initial yield of nitric acid, we performed high-humidity experiments to low absorbed doses (up to 16 Mrad). In these experiments, nitric acid remained as the predominant nitrogen fixation product generated. The initial concentration of nitric acid increased nearly linearly with absorbed dose (Fig. IV-8a), while the N_2O formed increased nonlinearly (Fig. IV-8b) after an induction period. The initial NO_x yields, based on energy absorbed by nitrogen gas alone, correspond to 2.75 ± 0.14 molecules/100 eV at 150°C and 2.84 ± 0.15 molecules/100 eV at 180°C.

---

[21] M. J. Steindler et al., *Chemical Technology Division Annual Technical Report, 1989*, Argonne National Laboratory Report ANL-90/11, p. 87 (1990).

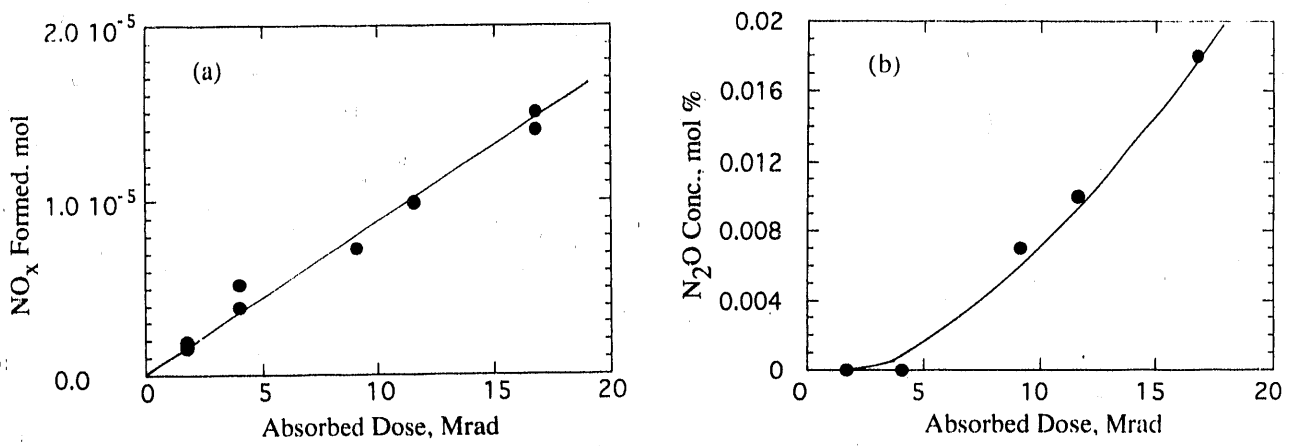

Fig. IV-8. Formation of (a) Nitric Acid and (b) N_2O in 1:1 Water Vapor-Air Mixture at 180°C as Function of Absorbed Dose

Our initial yield data agree with those reported by others,[22,23] even though our experimental methodology differed. The decrease in $G(HNO_3)$ from an initial value of 2.8 molecules/100 eV to ~1 molecule/100 eV at long irradiation times occurs because of product buildup in the gas phase and thermal/radiolytic degradation of the nitric acid once it is generated. The initial nonuniformity in the nitrous oxide and nitric acid yields is reflected in Fig. IV-8. Here, OH radicals that are radiolytically generated from the water vapor effectively compete with atomic nitrogen to oxidize nitrogen dioxide to nitric acid at the expense of nitrous oxide formation. In the long term, the buildup of nitrous oxide itself scavenges OH radicals and helps reduce the overall yield of nitric acid.

The presence of water vapor in the gas phase had a significant effect on both the extent of nitrogen fixation and the nature of the radiolytic products formed. In the high-humidity experiments (at room temperature and 90°C), N_2O yield was suppressed, NO_x yields were increased, and detectable levels of ammonia were generated. This is in contrast to the results of others,[24,25] who reported no effect of water content on N_2O and NO_x yield and the absence of ammonia formation, even when only trace amounts of oxygen were present in the irradiated gas phase.

Another observation concerning the yield data is that steady-state concentrations of the major molecular products were not established in either dry air or high-humidity air systems at the highest absorbed doses. Nitrous oxide and NO_x buildup continued at a linear rate beyond absorbed doses of 300 Mrad, provided that no significant change in the bulk composition of the gas phase occurred. Under repository-relevant conditions (in an open system), a steady-state

---

[22]A. R. Jones, Rad. Res. **10**, 655 (1959).

[23]J. K. Linacre and W. R. Marsh, *The Radiation Chemistry of Heterogeneous and Homogeneous Nitrogen and Water Systems*, Chemistry Division, AERE Harwell Report AERE-R 10027 (1981).

[24]A. R. Jones, Rad. Res. **10**, 655 (1959).

[25]C. H. Cheek and V. J. Linnenbom, J. Phys. Chem. **62**, 1475 (1958).

condition may be established due to a balance between the radiolytic formation of products, their diffusion or advective transport away from the waste package, and their interaction with the components of the waste package and the host rock. This, however, is determined by site-specific characteristics and waste package design rather than radiolytic considerations alone.

C. *Actinide Speciation Studies*

We have continued investigations of actinide speciation in groundwater-relevant systems. In these investigations, we are using high-sensitivity laser techniques, primarily laser photoacoustic spectroscopy, as well as the more conventional techniques of absorption spectrometry and potentiometry. This work is supported by the DOE Subsurface Science Program in the Office of Health and Environmental Research.

Our emphasis continues to be the environmental chemistry of plutonium, which is of interest because of its predominance as a radioactive contaminant at DOE waste sites. Plutonium(VI), as PuO_2^{2+}, is often of little importance in deep geologic media, which tend to be reducing, but is expected to be an important species in determining the initial near-surface chemistry of plutonium at the point of its release to the environment.

We have experimentally determined the initial hydrolysis of Pu(VI) as a function of pH, total plutonium concentration (6.9×10^{-5} M to 1.2×10^{-2} M) in sodium perchlorate, and temperature (10-45°C). Plutonium(VI) hydrolysis is known to be complex and does not proceed reversibly at high plutonium concentrations and pH. This has been attributed to the formation of polynuclear/polymeric species. The initial hydrolysis of Pu(VI), as reported by others, proceeds by one or both of the following reactions:

$$PuO_2^{2+} + H_2O = PuO_2OH^+ + H^+ \tag{2a}$$

where

$$-\log \beta_{11} = -\log \left[\frac{[PuO_2OH^+]\,[H^+]}{[PuO_2^{2+}]} \right] = 3.3 \text{ to } 5.9 \tag{2b}$$

and

$$2PuO_2^{2+} + 2H_2O = (PuO_2OH)_2^{2+} + 2H^+ \tag{3a}$$

where

$$-\log \beta_{22} = -\log \left[\frac{[(PuO_2OH)_2^{2+}][H^+]^2}{[PuO_2^{2+}]^2} \right] = 8.0 \tag{3b}$$

The published literature on these and other hydrolytic reactions has been reviewed by Baes and Mesmer[26] and summarized by Katz et al.[27]

The initial product observed, in our work, at total plutonium concentrations greater than 6×10^{-5} M in sodium perchlorate was identified as a polynuclear species and proposed to be the $(PuO_2OH)_2^{2+}$ complex (reaction 3a). The formation constant determined for the hydrolytic reaction is $5.0 \pm 1.5 \times 10^{-8}$ M, corresponding to a -log β_{22} value of 7.3 ± 0.2. The effect of temperature on the relative concentration of the aquo ion and the $(PuO_2OH)_2^{2+}$ complex is small and at or near the detection limits of the methodology utilized. From our data, we have estimated an enthalpy of formation of -11 ± 10 kJ/mol and an entropy of 170 ± 30 J/(mol•K) for this hydrolytic reaction.

The conclusions that we reached in this study do not agree with most existing literature in three respects. First, we have concluded that polynuclear hydrolytic species are more important than predicted by existing data. We have proposed that this discrepancy is, in part, due to slow hydrolysis kinetics, which has not been fully recognized in other work reported. This effect needs to be investigated further using other experimental methods. Second, we have seen no spectroscopic evidence for the formation of the PuO_2OH^+ hydrolytic species (reaction 2a) and suggest that the formation constant for this reaction is $<3 \times 10^{-7}$ M. Third, we have measured a much smaller effect of temperature than is predicted by current theoretical estimates.[28] Since we are the first to report temperature-effect experimental data for the Pu(VI) hydrolytic system, further work is needed to validate our results before a definitive explanation can be given.

Future plans are to use spectroscopic methods to measure formation constants of Pu(VI) with organic complexants and extend the work to real groundwater systems. Investigations to establish the applicability of photoacoustic spectroscopy to uranyl in groundwater systems are underway and will also be completed.

D. *Radiation Effects Studies for Waste Isolation Pilot Plant*

In support of the Waste Isolation Pilot Plant (WIPP) in New Mexico, we are investigating the effect of ionizing radiation on aspects of importance to the long-term performance of this repository. This work is part of an overall effort, coordinated through Sandia National Laboratories, to assess the performance of WIPP for the disposal of transuranic (TRU) waste. Ionizing radiation will be present in WIPP primarily as alpha particles associated with the radioactive decay of the TRU waste.

Three principal technical issues, related to the presence of ionizing radiation, were identified by researchers for the WIPP project: (1) radiolytically induced conversion of non-biodegradable plastics to those that are biodegradable, (2) the gas generation due to the

---

[26]C. F. Baes and R. E. Mesmer, *The Hydrolysis Cations*, John Wiley and Sons, New York (1976).

[27]J. J. Katz, G. T. Seaborg, and L. R. Morss, *The Chemistry of the Actinide Elements*, 2nd ed., Vol. 1, Chapman and Hall, New York, pp. 787-797 (1986).

[28]R. J. Lemire and P. Tremaine, J. Chem. Eng. Data **25**, 361 (1980).

interaction of alpha particles with WIPP waste and brine, and (3) the general effect of radiolysis on the redox conditions in the site, with particular emphasis on the speciation of dissolved transuranics.

In 1990, we experimentally addressed the first issue. This past year we have focused on gas generation due to the direct interaction of ionizing radiation with WIPP brine. This will occur should the WIPP become inundated with brine and dissolve radionuclides in the waste. The objective is to establish the extent and nature of gas evolved due to the interaction of truly dissolved ^{239}Pu with WIPP brine.

The gas generation rate was established for WIPP brine A spiked with Pu(VI) at concentrations of 10^{-4}, 10^{-6}, and 10^{-8} M. Total pressure buildup and gas phase composition were monitored as a function of time for as long as 160 days. Hydrogen was the predominant gaseous product of radiolytic origin. Oxygen, initially present in the gas phase, was consumed by radiolytic processes in the higher concentration samples [$>10^{-4}$ M Pu(VI)]. Gas generation rates were determined to be 0.14, 0.002, and <0.0003 mol/m^3/yr for Pu(VI) concentrations of 10^{-4}, 10^{-6}, and 10^{-8} M, respectively. The corresponding hydrogen yields were 1.1, 1.4, and <20 molecules/100 eV.

To support interpretation of the gas generation experiments, we also performed stability experiments with synthetic brines (WIPP brine A and ERDA-6) and actual brine samples (DH-36 and G-SEEP). The initial absorption spectra of plutonium(VI) in these brines were obtained and were interpreted in light of existing spectroscopic data. In the carbonate-free systems (ERDA-6, DH-36, and G-SEEP), the plutonium appeared to exist primarily as a hydrolyzed species, with some chloride complexation evident. When carbonate was present (WIPP brine A), a Pu(VI) carbonate complex was observed. This complex was shown to be stable for periods longer than 180 days (Fig. IV-9), and this reflects the overall long-term redox stability of Pu(VI) that we observed in this brine at Pu(IV) concentrations above 10^{-4} M. We also established that Pu(VI) can be kept in solution, as the hydrolyzed species, for periods longer than 90 days in G-SEEP brine. For WIPP brine A and G-SEEP, no evidence of plutonium precipitation was observed. For WIPP brine A, we counted both unfiltered solutions and those passed through a 0.2 μm filter and found no difference in the total plutonium content. Over the long term, however, both brines exhibited some indications that slow aggregation of the Pu(VI) may be occurring.

Autoreduction of Pu(VI) to Pu(V) was observed only in the samples with Pu(VI) concentrations above 10^{-4} M. Initial rates of reduction were 0.011%/day, which contrasts with the zero reduction rate observed with acidic chloride systems.[29] The reduction rates are, however, comparable to those observed in acid systems when an OH scavenger is not present. The higher pH (>6) of the brines permits the formation of oxidizing species, even though high chloride concentrations are present. Over the entire test period, the autoreduction rate decreased

---

[29]F. M. Cleveland, *The Chemistry of Plutonium*, 2nd ed., American Nuclear Society, Lagrange Park, IL, pp. 415-417 (1979).

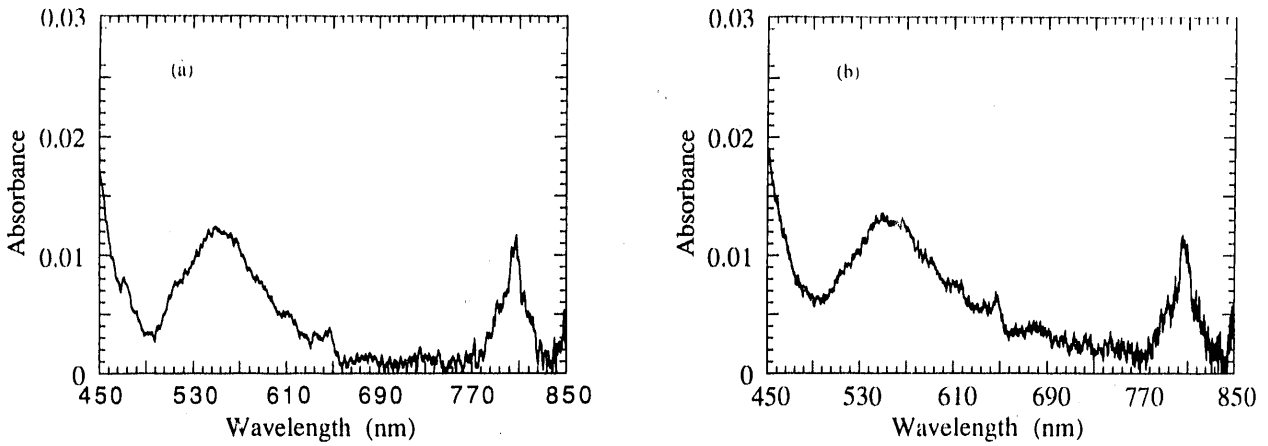

Fig. IV-9. Absorption Spectra for 2.3×10^{-4} M Plutonium in WIPP Brine A: (a) Initial Spectrum and (b) Spectrum at 189 Days

and a steady-state oxidation state was observed. This is consistent with observations reported by others in experiments with brine systems.[30,31]

This work directly supports WIPP performance assessment and provides data that will be used to evaluate the contribution of radiolytic processes to the overall gas generation rate. The issue of gas generation due to dissolved radionuclides is closely tied to the solubility and speciation of that radionuclide in WIPP brine. Work that addresses the effect of radiolysis on actinide speciation will be the future focus of this work.

---

[30]R. Stumpe and J. I. Kim, *Laser-Induced Photoacoustic Spectroscopy for Detection of the Chemical Behavior of Actinides in the Natural Aquatic System*, Institute for Radiochemistry of the Technical University of Munich, RCM 02386 (1986).

[31]S. R. Aston, Marine Chem. **8**, 319 (1980).

V. SEPARATION SCIENCE AND TECHNOLOGY

The Division's work in separation science and technology during the past year was mainly concerned with developing methods for removing and concentrating actinides from waste streams contaminated by transuranic (TRU) elements. The objective is to recover valuable TRU elements and lower disposal costs of nuclear waste. The major project in this area involves development of a generic data base and modeling capability for the TRUEX (TRansUranic EXtraction) solvent extraction process. This capability will allow users to design flowsheets for specific waste streams and estimate the cost and space requirements for implementing a site- and feed-specific TRUEX process. It will also be useful as a tool for plant operators to vary, monitor, and control the process once it is in place. As part of this effort, the basic design of the ANL-designed centrifugal contactor is modified as necessary to adapt it for specific TRUEX applications.

Other work in separation science and technology includes the development of (1) a membrane-assisted solvent extraction method for treating natural and process waters contaminated by volatile organic compounds and (2) evaporation technology for concentrating radioactive waste and product streams such as those generated by the TRUEX process.

A. *TRUEX Technology-Base Development*

The TRUEX process extracts, separates, and recovers TRU elements from solutions containing a wide range of nitric acid and nitrate salt concentrations. The extractant found most satisfactory for the TRUEX process is octyl(phenyl)-N,N-diisobutylcarbamoylmethylphosphine oxide, which is abbreviated CMPO. This extractant is combined with tributyl phosphate (TBP) and a diluent to formulate the TRUEX process solvent. The diluent is typically a normal paraffinic hydrocarbon (NPH), either a C_{12}-C_{14} mixture or n-dodecane. The TRUEX flowsheet includes a multistage extraction/scrub section that recovers and purifies the TRU elements from the waste stream, and multistage strip sections that separate TRU elements from each other and the solvent. Our current work is focused on facilitating the implementation of TRUEX processing of defense TRU-containing waste and high-level waste, where such processing offers financial and operational advantage to the DOE community.

1. Improvements to Generic TRUEX Model

The Generic TRUEX Model is a computer program that has been developed to (1) act as a tool for designing TRUEX process flowsheets for specific waste stream compositions, process constraints, and process goals, (2) estimate the space and cost requirements for installing a TRUEX process, and (3) act as a guide to process monitoring and control. This year we released the Generic TRUEX Model (GTM), version 2.4.1, for the Macintosh and IBM-compatible computers. The options available in GTM 2.4.1 are summarized in Table V-1.

The new version of GTM contains many improvements, including the following: Option 1 has bismuth, phosphoric acid, and boric acid added to the possible feed components;

Table V-1. Options Available in GTM 2.4.1

Option 1	Calculate the complete Generic TRUEX Model for a specific feed solution.
Option 2	Calculate the charge balance, density, ionic strength, speciation, and activities (hydrogen, nitrate, and water) of an aqueous feed solution.
Option 3	Calculate oxalic-acid additions to fission-product-containing waste.
Option 4	Calculate distribution ratios for a user-specified aqueous phase, where the organic phase is assumed pre-equilibrated.
Option 5	Calculate distribution ratios for equilibration of user-specified aqueous and organic phases.
Option 6	Conduct flowsheet analysis with user-specified distribution ratios.
Option 7	Generate a TRUEX flowsheet for a specific feed solution.
Option 8	Estimate space and costs for user-specified flowsheet.
Option 9	Estimate solvent degradation for a specific TRUEX process.
Option 10	Generate reports from existing TRUEX flowsheets or space and cost calculations.
FE_Loop	Run multiple flowsheet calculations (Option 7) without using the front-end to input data.
SASPE Independently	Calculate items in Options 2 and 4 without using the front-end to input data.

Option 2 employs new equations that calculate activities (hydrogen, nitrate, and water) at high ionic strengths; Option 5 displays the final aqueous and organic concentrations in distribution ratio calculations for equilibration of user-specified aqueous and organic phases; and Option 9 shows the effect of solvent degradation by calculating the americium distribution ratios at 0.01 and 0.05 M HNO_3 after a user-specified number of processing cycles (rather than single cycle).

Modifications were also made to the module of the GTM that calculates the speciation of certain feed components (Option 2). Originally, this module only calculated the speciation of the cations Fe^{3+}, Al^{3+}, Zr^{4+}; the anions $C_2O_4^{2-}$, SO_4^{2-}, and F^-; and rare earths grouped together as one pseudo component (La^{3+}, Ce^{3+}, Pr^{3+}, Nd^{3+}, Pm^{3+}, Sm^{3+}, Eu^{3+}, Gd^{3+}, and Y^{3+}). The speciation module was expanded so that it now adds the tripositive actinides Am^{3+}, Pu^{3+}, and Cm^{3+} to the rare earth sum. Representing a large number of components as one pseudo component allowed us to use only one mass balance and one distribution ratio equation for all of these elements instead of one for each element. The module will also calculate the speciation of Th^{4+}, UO_2^{2+}, Pu^{4+}, Np^{4+}, Cd^{2+}, and PO_4^{3-}, along with the neutral species $B(OH)_3$.

The GTM now functions with the new version of Microsoft Excel (version 3.0) and under the latest release of the operating systems for the IBM (DOS 5.0) and the Macintosh (System 7). The process for converting the GTM from the Macintosh version to the IBM-PC version was made even easier. The conversion is required since model development for both versions is performed on a Macintosh. All of the code can now be transferred from the Macintosh to the IBM-PC without any changes.

A Microsoft Excel macro was developed to complete multiple runs of the GTM without user intervention. This macro can be used when multiple runs of the GTM need to be completed with variations in (1) the concentrations of components in the feeds, (2) the flow rate to a section, or (3) the components present in a feed stream. Two reports are generated when running this macro, one which contains the flow rates and component concentrations of influent and effluent streams, and another which contains the component concentrations at every stage in the flowsheet.

Future enhancements to the GTM will include treating feed components that are unique to feed-specific and site-specific processes and have not yet been adequately modeled, further improving speciation calculations in handling complexation equilibria in aqueous solutions, and adding stage extraction efficiencies in flowsheet calculations.

2. Development of Data Base and Modeling Capability

The data base generated for developing the GTM contains information (from the literature and our own laboratory measurements) on the solution and extraction behavior of all important feed components over a wide range of possible waste-stream and processing conditions. The GTM contains algorithms for predicting the extractability of chemical species with TRUEX solvent (typically 0.2 M CMPO and 1.4 M TBP in NPH) based on aqueous-phase physicochemical properties, e.g., density, ionic strength, thermodynamic activities. Our recent efforts on expanding the data base and adding extraction models have focused on chemical species from the nuclear waste housed in the single-shell storage tanks at Hanford, WA, and waste generated by the Idaho Chemical Processing Plant (ICPP) from the reprocessing of naval nuclear reactor fuel. The chemical species being investigated are PO_4^{3-}, Bi^{3+}, and Cr^{3+}, which are important constituents in the Hanford storage tanks, and Cd^{2+}, BF_4^-, and $B(OH)_3$, which are found in the ICPP process stream but have not previously been included in the GTM. Discussed below is our experimental and modeling work done on extraction of the phosphate, bismuth, and cadmium species.

The phosphate found in the single-shell tanks at Hanford originates from the $BiPO_4$ process used to separate plutonium from irradiated uranium. The extractability of H_3PO_4 by the TRUEX-NPH solvent at 25°C was determined by measuring the concentration of phosphoric acid in the aqueous and organic phase with acid-base potentiometric titration or use of ^{32}P radiotracer. Figures V-1 and V-2 show the results for H_3PO_4 distribution ratios measured as a function of H_3PO_4 concentration and $HNO_3/NaNO_3$ concentration, respectively. To model these extraction measurements, it is necessary to postulate the formation of an organic-phase

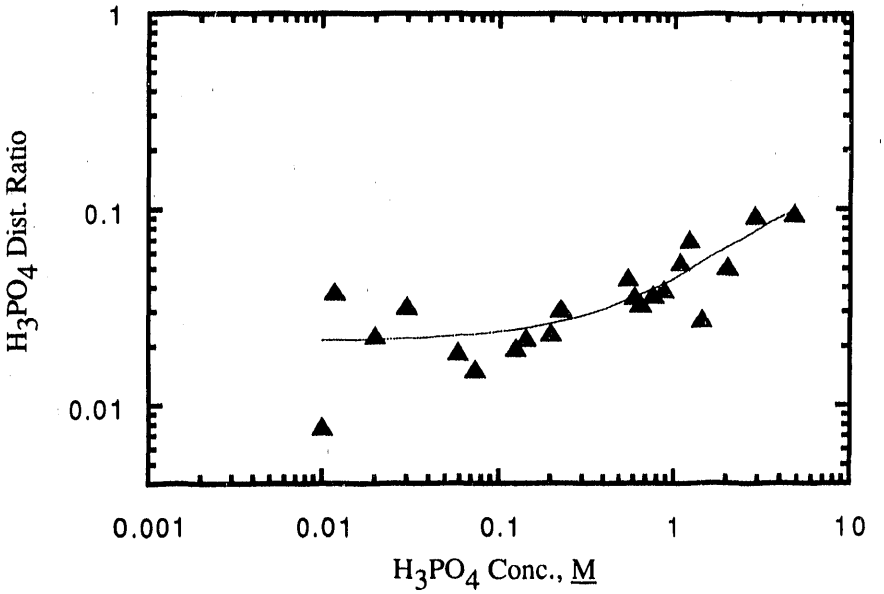

Fig. V-1. Distribution Ratio of H_3PO_4 vs. H_3PO_4 Concentration with TRUEX-NPH Solvent at 25°C. (Curve shows best fit of data.)

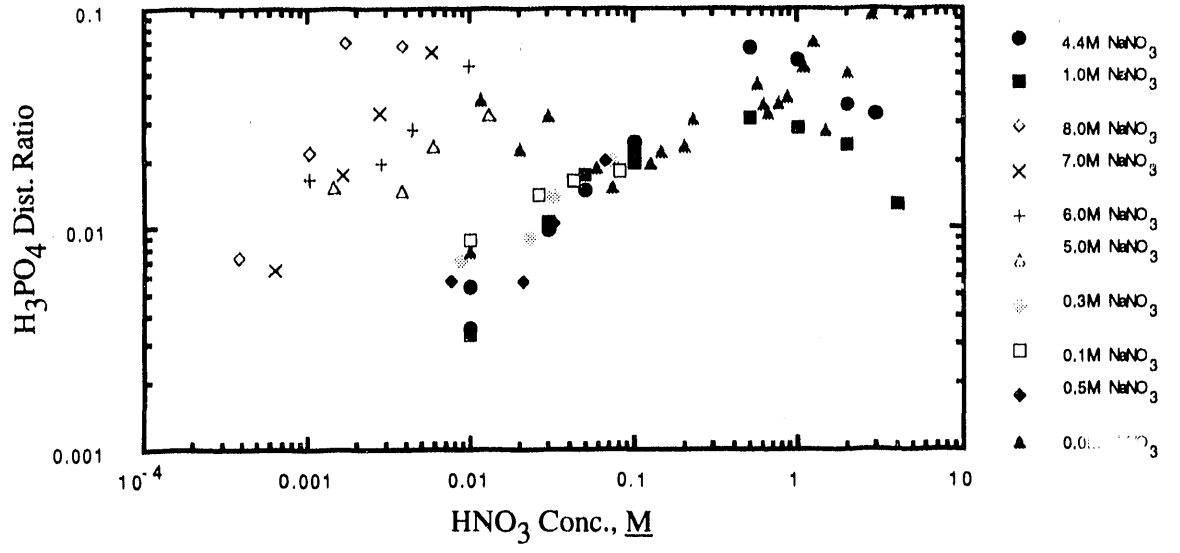

Fig. V-2. Distribution Ratio of H_3PO_4 vs. Concentration of HNO_3 and $NaNO_3$ with TRUEX-NPH Solvent at 25°C

phosphoric acid dimer. The distribution ratio for phosphorus (D_p) derived from these data is given by

$$D_p = \frac{[CMPO_f]\,[TBP_f]}{\{H_2O\}}\,[H_3PO_4]\left[K_1\{H^+\}\{NO_3^-\} + K_2\,[H_3PO_4]\right] \quad (1)$$

where $K_1 = 1.36$; $K_2 = 0.0117$; $[H_3PO_4]$ is the phosphoric acid concentration; $[CMPO_f]$ and $[TBP_f]$ are the concentrations of these extractants not bound with HNO_3 in the organic phase; and braces { } indicate activities of the species.

Bismuth is also found in the Hanford waste as a result of the $BiPO_4$ process. Measurements of Bi^{3+} distribution ratio with TRUEX-NPH at 25°C as a function of nitric acid concentration were obtained from researchers in the ANL Chemistry Division and Pacific Northwest Laboratories. Due to the limited data, we believed that the best way to model the measurements was by correlation with the distribution ratio model for Am^{3+} presently used in the GTM. This model can account for loading of the solvent by HNO_3; activities of H_2O, H^+, and NO_3^-; and aqueous-phase complexation by fluoride, oxalate, phosphate, and sulfate. The correlation gave the following relationship:

$$D_{Bi} = \frac{30}{1 + 7\,\{NO_3^-\}} \cdot D_{Am} \quad (2)$$

Figure V-3 illustrates the good agreement between results calculated with this equation and the experimental data. Much more Bi^{3+} data as a function of high-salt, low-acid conditions (total nitrate ≥ 1 M, total H^+ ≤ 0.05 M), with or without the addition of other species (phosphate, oxalate, sulfate, fluoride), must be collected to better model the extraction of Bi^{3+}.

Cadmium is added as a neutron absorber (due to a large neutron cross section) to dissolver solutions for the naval reactor fuel processed at ICPP. Because of the rather large concentration of cadmium in the waste (0.4 M), even with a rather low distribution ratio, the cadmium concentration in the solvent will be greater than or equal to that of the TRU elements. The extractability of the Cd^{2+} species by TRUEX-NPH at 25°C was determined using ^{109}Cd radiotracers. Cadmium distribution ratios were measured as a function of HNO_3 concentration and $HNO_3/NaNO_3$ concentration. These measurements allowed the determination of stability constants and thermodynamic equilibrium for the system. The equation for calculating D_{Cd} derived from our measurements is

$$D_{Cd} = \frac{1.36\,\{NO_3^-\}^2\,[CMPO_f]}{1 + 2.84\,\{NO_3^-\}} \quad (3)$$

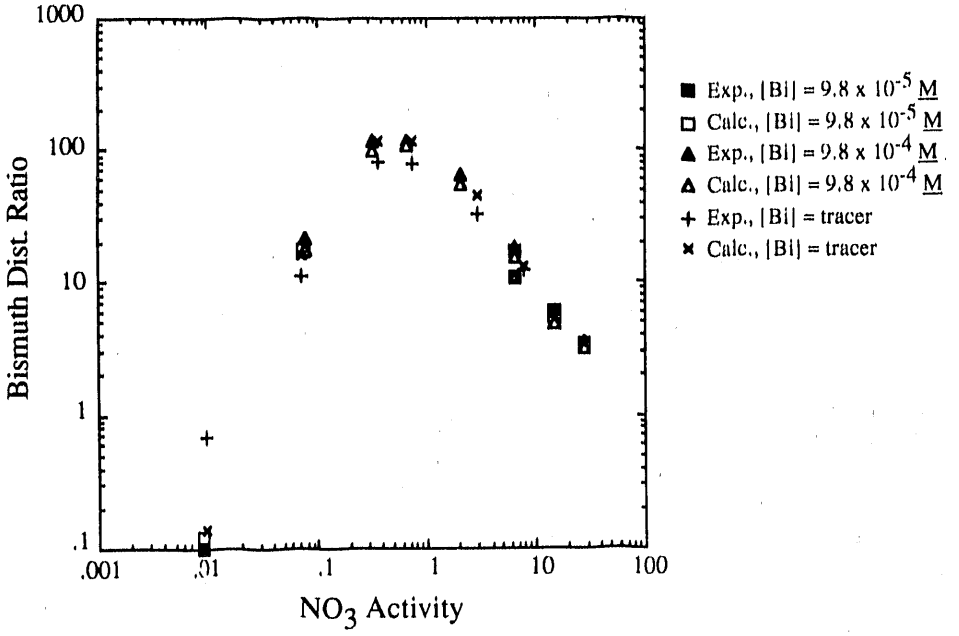

Fig. V-3. Experimental and Calculated Bismuth Extraction Behavior at Bismuth Concentrations of 9.8×10^{-5} M, 9.8×10^{-4} M, and Tracer Levels ($<9.8 \times 10^{-5}$ M) with TRUEX-NPH Solvent at 25°C

Future work will measure the effect on D_{Cd} of aqueous-phase complexants (F^-, $C_2O_4^{2-}$, SO_4^{2-}, and PO_4^{2-}) and temperature.

3. Monitoring and Control of TRUEX Processes

A TRUEX flowsheet designed for a specific application must be optimized for obtaining process goals and "robustness." A robust flowsheet is one that will continue to meet processing goals with wide variations in feed composition and flow rate. As part of an effort to develop a monitoring and control system for the TRUEX process, we have employed the GTM to determine the effect of perturbations in feed compositions and flow rates with regard to meeting the process goals for a typical nuclear waste generated at the Plutonium Finishing Plant operated by Westinghouse Hanford Co. Figure V-4 gives the base-case TRUEX flowsheet developed for this waste with the GTM. The goals set for processing this waste are as follows: ≤10 nCi/mL TRU concentration in the raffinate from the extraction section, <0.3 mol % americium in effluent from the second strip, <1.1 mol % plutonium in the effluent from the first strip, and <0.01% TRU lost in the organic flow exiting the second strip.

In the sensitivity analysis using the GTM, we determined the effect of varying the flow rates and compositions with respect to the base case for the organic extraction feed (DX), the aqueous extraction feed (DF), the aqueous scrub feed (DS), and the aqueous feeds for the first

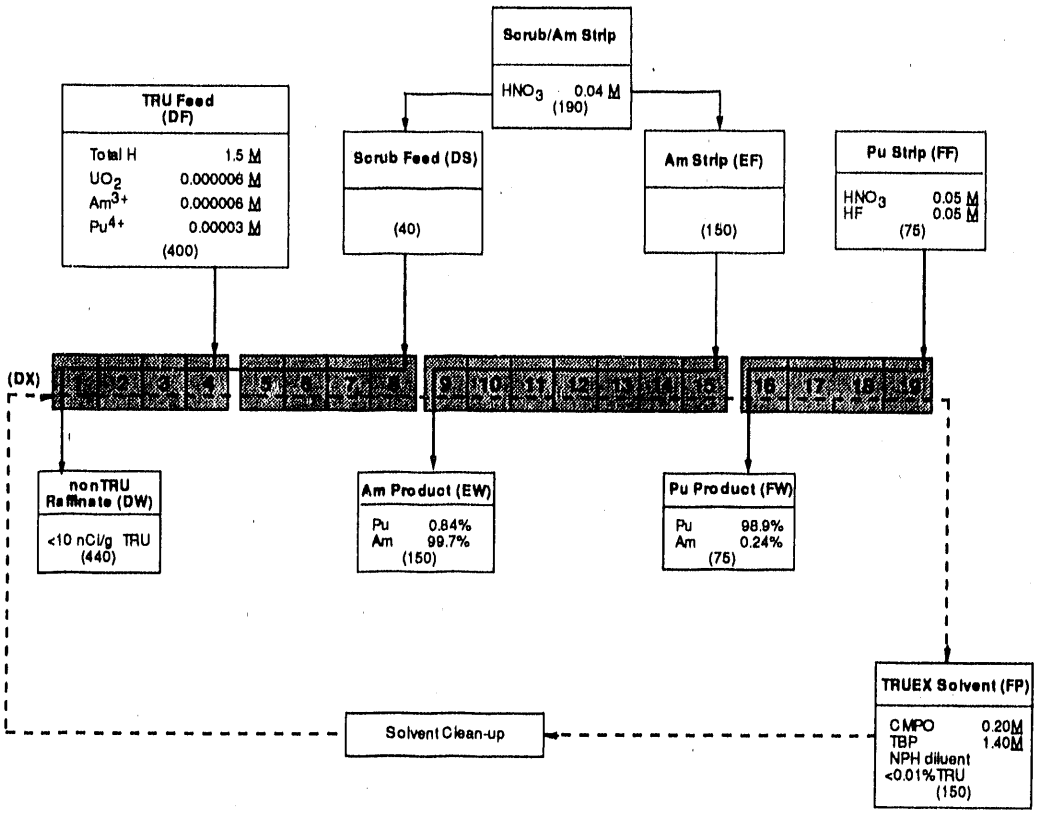

Fig. V-4. Flowsheet for Tests with Synthetic Plutonium Finishing Plant Waste. (Parenthetical entries indicate stream flow rates in mL/min.)

strip (EF) and the second strip (FF). We were particularly concerned with determining when a perturbation in a feed composition or flow rate led to a process goal or goals not being met.

Of all the perturbations analyzed, only one of them, a change in the flow rate for the aqueous extraction feed, resulted in the most important process goal (a TRU concentration in the raffinate of ≤ 10 nCi/mL) being exceeded. But even in this case, the flow rate could be up to four times greater than its base value of 400 mL/min without exceeding the process goals.

The tightest bounds obtained were in the cases of (1) the organic-feed flow rate and (2) the concentration of HNO_3 in the aqueous feed to the scrub and the first strip. For these cases, the upper value could not exceed 1% and 2%, respectively, of the base value before the americium mole percent in the second strip exceeded the process goal of less than 0.3 mol %. The base-case flowsheet can be redesigned to increase the operating range of these two parameters. This can be accomplished by adding more stages in the first strip so that less americium is lost to the second strip. But adding more stages to the first strip causes not only more americium to be stripped, but also more plutonium to be lost to the americium product. To avoid this, one must increase the HNO_3 concentration in the organic solvent that enters the first stage of the americium strip. This can be achieved by increasing the HNO_3 concentration in the scrub feed. Increasing the HNO_3 concentration in this organic solvent increases the distribution ratio for plutonium. For example, the distribution ratio for plutonium in the first stage of the first

strip increases from 120 to ~200 if the HNO_3 concentration in the scrub feed is increased from 0.04 to 0.5 M. A plutonium distribution ratio of 200 will produce a loss of plutonium in the americium product stream of only 0.53 mol %. Since the maximum loss of plutonium in the americium strip was set as 1.1 mol %, an HNO_3 concentration of 0.5 M in the scrub feed will permit changes in the scrub acid concentration significantly larger than the 0.04 M of the first flowsheet.

With the increased acid concentration in the organic solvent entering the first strip, the distribution ratios of americium also increased for the first two stripping stages. As a result, two stages must be added to the first strip to compensate for the lost stages. Since the scrub and americium feeds now have different HNO_3 concentrations, it is not possible to use the same storage tank for both feeds. This is a trade-off that needs to be made in order to obtain a more robust flowsheet.

In sum, the changes in the redesigned flowsheet are (1) 0.5 M HNO_3 feed to the scrub section and (2) two more stages in the first strip section. Note that the feeds to the scrub and the americium strip are now independent. Figures V-5 to V-7 show the effect of changes in the organic-feed flow rate, for both the new and old flowsheets, on the americium mole percent in the second-strip effluent, the plutonium mole percent in the first-strip effluent, and the TRU lost in the organic flow exiting the second strip. The process goals for these parameters are indicated by horizontal lines. (Since the extraction section was not changed, the TRU concentration in the extractant was not affected.) As shown in these figures, increasing the HNO_3 concentration in the scrub and adding two more stages made the flowsheet less sensitive to a perturbation in organic-feed flow rate. The range in which the process goals still hold as the organic flow rate is changed was expanded from between -7% and +1% (old flowsheet) to between -24% and +10% (new flowsheet) of the base organic flow rate. With the new flowsheet, the goal that restricts a decrease in the organic flow rate is the mole percent of the plutonium in the first strip (Fig. V-6); also, the allowable increase in this flow rate is almost equally restricted by the other two goals (Figs. V-5 and V-7).

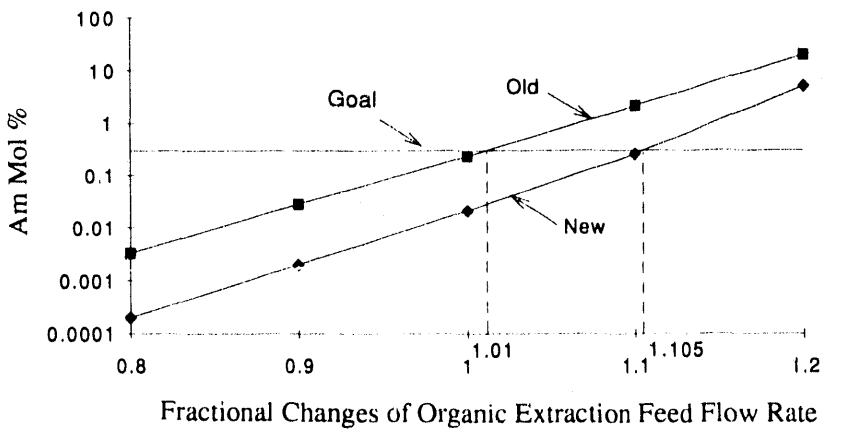

Fig. V-5. Americium Mole Percent in Second-Strip Effluent as Function of Changes in Flow Rate for Organic Extraction Feed. (Flow rates are relative to the base case.)

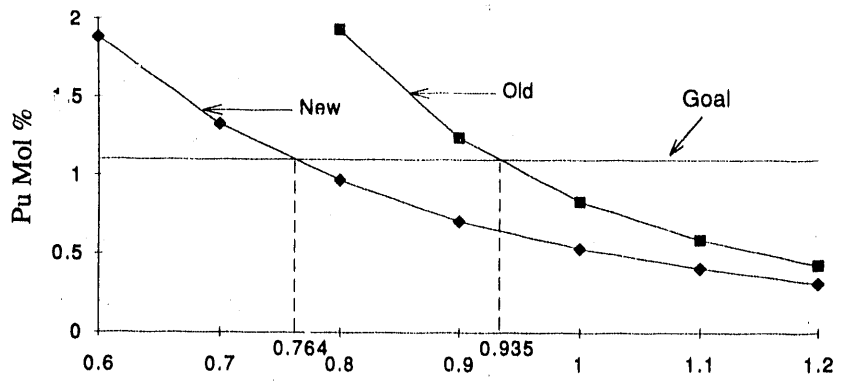

Fig. V-6. Plutonium Mole Percent in First-Strip Effluent as Function of Changes in Flow Rate for Organic Extraction Feed. (Flow rates are relative to the base case.)

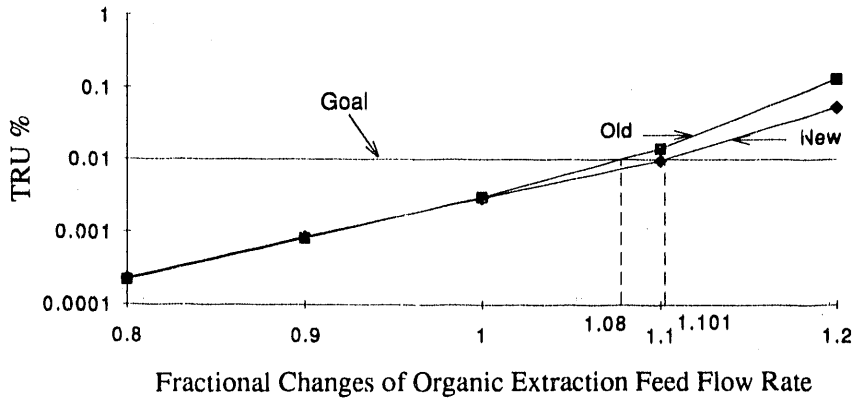

Fig. V-7. Percentage of TRU-α Lost in Organic Flow Exiting Second Strip as Function of Changes in Flow Rate for Organic Extraction Feed. (Flow rates are relative to the base case.)

Another feature of the new flowsheet is that independent changes in the HNO_3 concentration are possible for the feeds to the scrub and first strip. With the old flowsheet, the scrub and the first strip had the same HNO_3 concentration in their feed. As a result, when the HNO_3 concentration was perturbed for the scrub and first strip, the HNO_3 concentration could be decreased by 57% but could only be increased by 2% and still meet process goals. With the new flowsheet, the HNO_3 concentration could be decreased by 99.8% or increased by 187% in the scrub and decreased by 75% or increased by 19.3% in the first strip and still meet process goals. Thus, maintaining the HNO_3 concentration in the scrub feed at 0.5 M will allow wide variation in the extraction section (HNO_3 concentration in the extraction feed and flow rates for both the aqueous and organic feed) without disrupting the operation of the first strip.

The above results illustrate how sensitivity analysis can be used early in the design stage to develop a robust TRUEX flowsheet.

4. Centrifugal Contactor Development

We have been modifying the basic design of the ANL centrifugal contactor as necessary to adapt it for specific solvent extraction processes. A key feature in these design efforts is the use of computational models for (1) the flow of the organic and aqueous phases through the contactor and (2) the vibrational parameters of the spinning motor/rotor combination. This past year, these hydraulic and vibrational models were used to guide the conceptual development of a contactor with increased throughput for a given contactor diameter. This super high-throughput centrifugal contactor (SHTCC) will allow an increase in contactor throughput by a factor of four to eight times, yet keep the unit safe with respect to nuclear criticality by its geometry. Thus, one contactor will be able to handle the process throughput that would otherwise have required four to eight contactors.

When nuclear criticality considerations are important, the rotor diameter for a centrifugal contactor cannot be much greater than 10 cm if each contactor stage is to be criticality safe by geometry. Thus, we are investigating ways to increase contactor throughput by increasing the rotor length and rotational speed. An SHTCC contactor design is being evaluated for the effect that it will have on contactor hydraulics and vibrations. Since the internal hydraulics of the contactor will be different, we will have to modify the weirs for the less-dense and more-dense (organic and aqueous) phases. These modifications will have to be made in such a way that the two-phase dispersion, shown in the separating zone of Fig. V-8, stays within the separating zone over a wide range of flow rates, organic-to-aqueous flow ratios, and expected

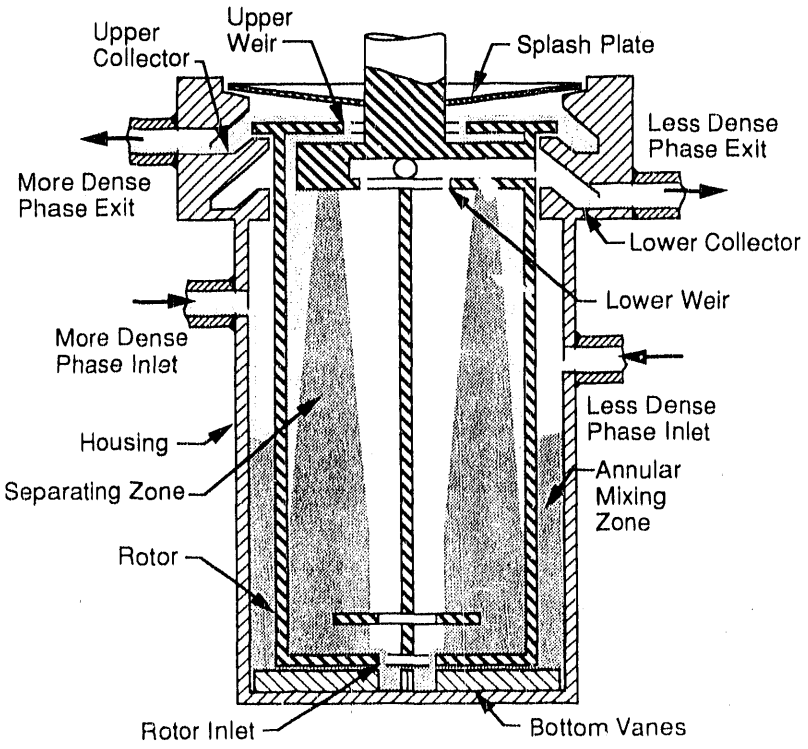

Fig. V-8. Schematic of Centrifugal Contactor

variations in phase density. A vibration analysis showed that the SHTCC rotor will need to operate above its first natural frequency. Use of a steady bearing has been proposed to support the rotor as it passes through its first natural frequency. Several steady-bearing options, shown in Fig. V-9, were tested experimentally using a long 4-cm dia rotor. Normal contactor rotors have a length-to-diameter ratio (L/D) of about 2.5. The SHTCC rotors will have an L/D of 10 or more. The rotor used in the tests had an L/D of 13. The test results were very encouraging when the steady bearing was near the top of the rotor (Option 1). Based on these results, we are planning to build a prototype SHTCC. For this prototype, any of several motor options (also shown in Fig. V-9) could be used to drive the contactor rotor.

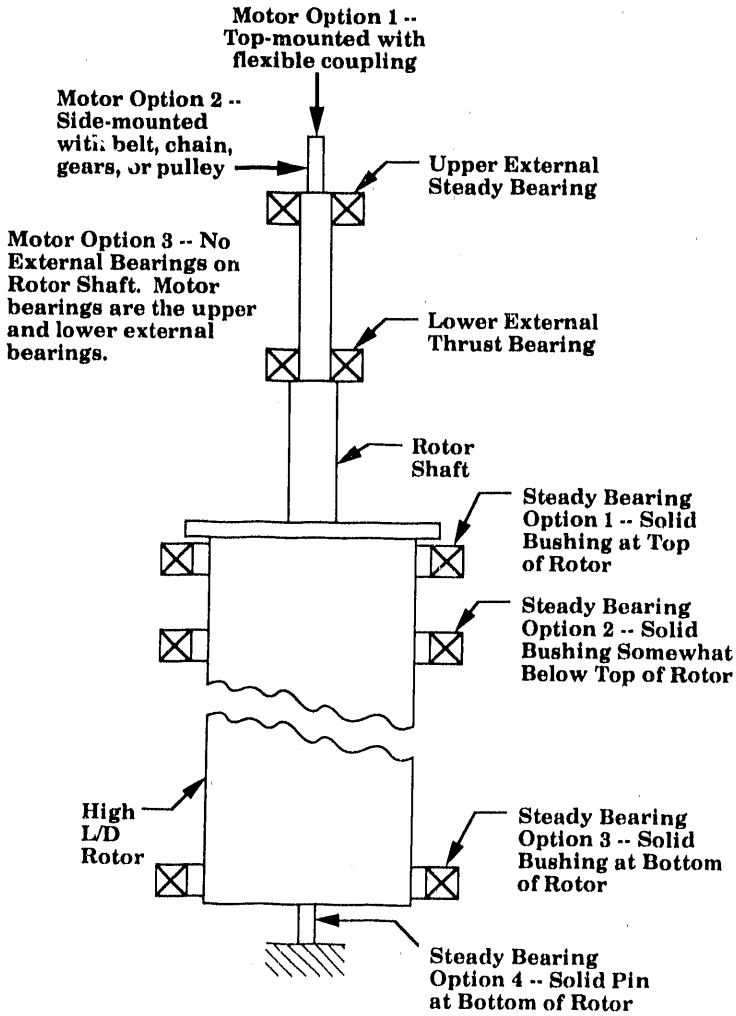

Fig. V-9. Schematic of SHTCC Rotor Showing Motor and Steady-Bearing Options

B. *Treatment of Plutonium Waste Solution by TRUEX Process*

Approximately 200 L of waste solution from the analysis of plutonium samples has accumulated over the past several years at New Brunswick Laboratory (NBL) and ANL. These

solutions, stored in over six-hundred 250 mL bottles, contain varying concentrations of nitric, sulfuric, phosphoric, and hydrochloric acids, as well as U, Pu, Np, and Am. Originally destined for storage at the Idaho National Engineering Laboratory and eventual disposal at the Waste Isolation Pilot Plant in New Mexico, these wastes now appear to have no place that will accept them. In this project, the TRUEX process is being used to convert the bulk of these wastes into non-TRU (low-level) waste. (Our original goal was to reduce the TRU concentration below 10 nCi/mL. However, after the first batch was processed, we were informed that the goal had been changed to a TRU concentration of less than 0.1 nCi/mL.)

Five benefits are expected from this program. First, the treatment of these waste solutions will solve a waste treatment problem at NBL and ANL. Second, the lessons that we learn will benefit others contemplating the installation of a TRUEX facility. Third, this program will give us experience in applying the GTM to designing flowsheets for specific feeds and process goals. Fourth, the data collected will be used to verify GTM predictions. And fifth, this demonstration will show the applicability of using the TRUEX process for treating similar wastes at Rocky Flats Plant, Los Alamos National Laboratory, the Hanford site, and the Idaho Chemical Processing Plant.

The TRUEX solvent extraction process used to generate the non-TRU waste stream and recover the plutonium is being completed in a 20-stage 4-cm centrifugal contactor installed in a glovebox. A TRUEX solvent (0.2 M CMPO, 1.4 M TBP) with n-dodecane diluent will be used in this process. The non-TRU raffinate produced from the TRUEX process will be further processed to make it acceptable for handling by Waste Management Operations in ANL's Plant Facilities and Services (PFS-WMO) by neutralizing the solution with NaOH so that the final pH is between 6 and 9. The plutonium oxalate stream will be further processed by evaporating the solution to dryness, calcining the resulting solids in an oven at 600°C to produce PuO_2, then converting the PuO_2 to plutonium metal. The metal will then be returned to NBL for storage and subsequent shipment to ANL-West, where the recovered plutonium will help fuel the Integral Fast Reactor (Sec. VI).

Several other solutions are generated by the TRUEX process, namely an americium product stream and two solvent wash solutions. The americium stream will be further concentrated and used in future TRUEX verification and laboratory experiments. The solvent wash solutions will most likely be acidified, then recycled to the TRUEX process by mixing it with the feed for the next batch. Recycling these solutions is necessary because the TRU content of this waste will most likely be greater than the 0.1 nCi/mL limit set by PFS-WMO.

During 1990, we developed a flowsheet for treating this waste based upon GTM model runs, centrifugal contactor verification tests, and batch tests using a sample of the actual waste solution (Fig. V-10).[1] Several features of this flowsheet are worth highlighting:

---

[1]M. J. Steindler et al., *Chemical Technology Division Annual Technical Report, 1990*, Argonne National Laboratory Report ANL-91/18, pp. 97-98 (1991).

1. Americium is concentrated by a factor of 80 in its product stream.

2. An added benefit of concentrating the americium is the elimination of the scrub feed solution. A scrub solution is used to strip HNO_3 from the organic phase, which improves the operation of the americium strip section. In this flowsheet, only 3% of the americium strip solution is removed as product (stage 9); the remainder is used to scrub the organic phase (stages 7-8).

3. Plutonium is stripped by oxalic acid under conditions where $Pu(C_2O_4)_2$ will precipitate. This will be a test of how organic-phase precipitates are handled by centrifugal contactors.

4. Carbonate wash solutions are recycled continuously.

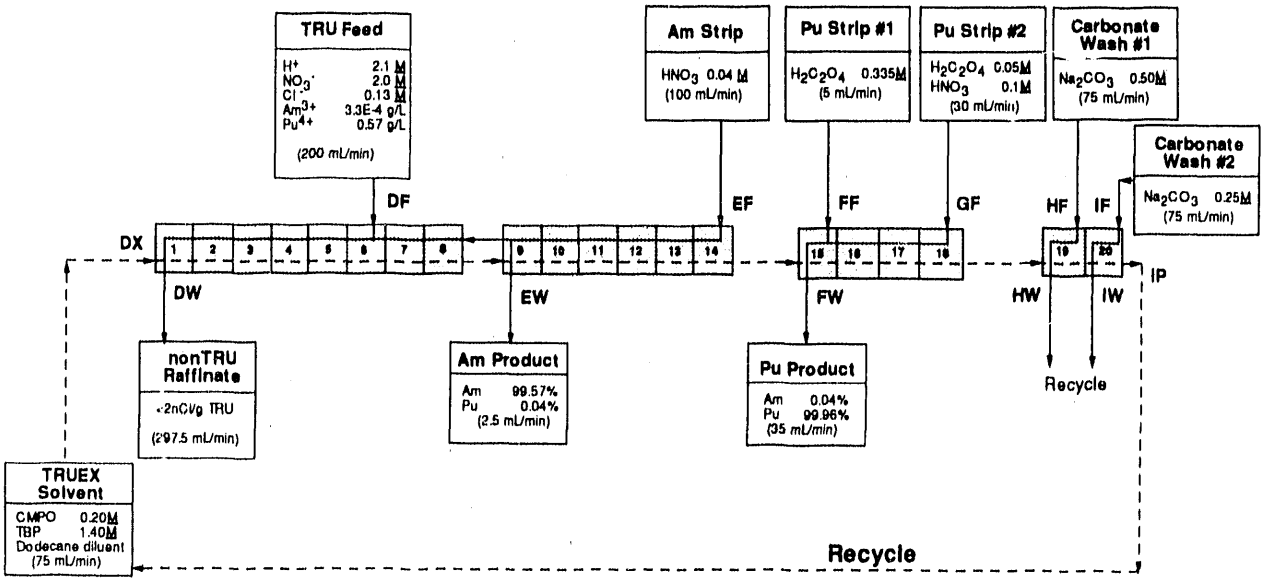

Fig. V-10. Flowsheet for Processing First Batch of Plutonium Waste Solution

On January 3, 1991, the first batch of waste solution, containing 11.7 g plutonium, was processed. The concentration of TRU elements in the waste was reduced by a factor of ~22,000, producing a raffinate with an activity of 2 nCi/mL. The material balance for this batch is summarized in Table V-2. Of the 11.7 g plutonium in the feed solution, 49.6% of the plutonium was recovered in product solutions, and 10.2% was present in various waste solutions. The recovered plutonium, 5.6 g or 48% of the batch, has been converted to PuO_2. About 4.7 g, or 40.2% of the plutonium, was not recovered in any of the process streams.

Concentration of americium and elimination of the separate scrub solution proved to be very successful--no operating problems were evident in this part of the flowsheet. However,

Table V-2. Material Balance for First Batch of Plutonium Waste Solution

Process Stream	Plutonium Mass, g	% of Feed
Feed Solution	11.7	100.0
Products		
Raffinate[a]	0	0
PuO_2	5.6	48
Am Product	0.03	0.3
Miscellaneous	0.15	1.3
Total Product	5.78	49.6
Waste Solutions		
Carbonates	0.14	1.2
Samples	0.4	3.4
Miscellaneous	0.65	5.4
Total Waste	1.19	10.2
Unrecovered Pu[b]	4.73	40.2

[a]Extraction section raffinate that had ~2 nCi/mL alpha activity.
[b]This plutonium is assumed to be contained in centrifugal contactor rotors and other process equipment as a plutonium oxalate precipitate.

precipitation of plutonium oxalate was a significant problem in the plutonium strip section, as indicated by the low PuO_2 recovery (48% of the batch). Because of the difficulty in recovering solids from the process equipment, we believe that a majority of the plutonium not recovered in any of the process streams is present in the centrifugal contactor rotors and housings in the plutonium strip section. In support of this conclusion, about 2 g of plutonium was recovered when the acidified carbonate solutions from solvent cleanup operations were processed. Recycle of the solvent wash solutions (sodium carbonate) was also a success in that a non-TRU raffinate solution was generated.

After processing the first batch, we were notified by PFS-WMO that the waste acceptance criteria had been changed, and these wastes could not be disposed of in their present form. The new criteria lowered the acceptable TRU content by a factor of 1000, from 100 to 0.1 nCi/mL. This change meant that the TRU concentration in our raffinate solution was too high by a factor of 20. With this new criterion, PFS-WMO can process these solutions in its evaporator.

To meet this more stringent goal, we developed the flowsheet shown in Fig. V-11. This flowsheet differs from typical TRUEX flowsheets because we tried to reduce the volume of waste generated. This volume reduction was accomplished by eliminating the americium and plutonium strip sections and recovering these TRU elements in the solvent wash section. The raffinate from the first batch was successfully processed in April 1991; the TRU raffinate

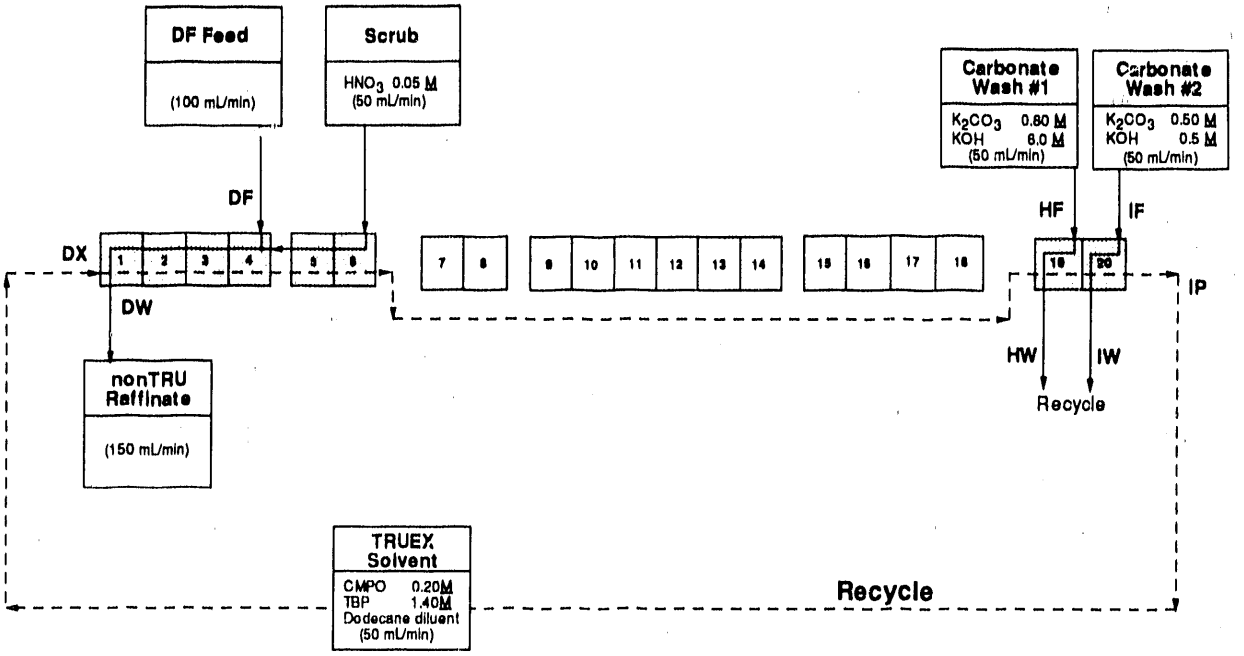

Fig. V-11. Flowsheet for Processing Raffinate from First Batch of Plutonium Waste Solution

concentration for this test was 0.2 nCi/mL (before neutralization). This waste was accepted by PFS-WMO at this slightly higher level than the 0.1 nCi/mL goal.

Approximately 50 L of waste solution was generated from (1) processing of the first batch, (2) centrifugal contactor decontamination efforts, and (3) reprocessing of the first-batch raffinate. On the basis of laboratory tests and calculated results with the GTM, a flowsheet was developed for processing this waste. This flowsheet, shown in Fig. V-12, incorporates several significant improvements over previous flowsheets, including the use of a new plutonium strip solution, 0.28 M $(NH_4)_2C_2O_4$, which eliminates the plutonium oxalate precipitation that occurred in the first test. The flow rate of the plutonium strip feed (FF) was set fairly low to reduce the volume of the plutonium-product stream to be evaporated to dryness. In addition, a scrub feed (DS) was incorporated into the flowsheet to add the required amount of $Al(NO_3)_3$ and thereby (1) increase the distribution ratio of plutonium in the extraction section and (2) strip oxalic acid from the solvent before it entered the americium strip (where it would strip the plutonium with the americium). Processing of this acidified carbonate waste will be completed in 1992.

C. *Treatment of Rocky Flats Plant Waste by TRUEX Process*

A TRUEX flowsheet was developed for recovering TRU (Am and Pu) elements from a nitrate waste stream at the Rocky Flats Plant (RFP). This nuclear waste stream, which can contain as much as 0.001 to 0.01 g plutonium per liter and similar amounts of americium, differs from previous TRUEX feeds in that the acid concentration is very high, 5.0 to 7.5 M HNO_3. The benefits of using the TRUEX process are that (1) the volume of solid TRU waste generated

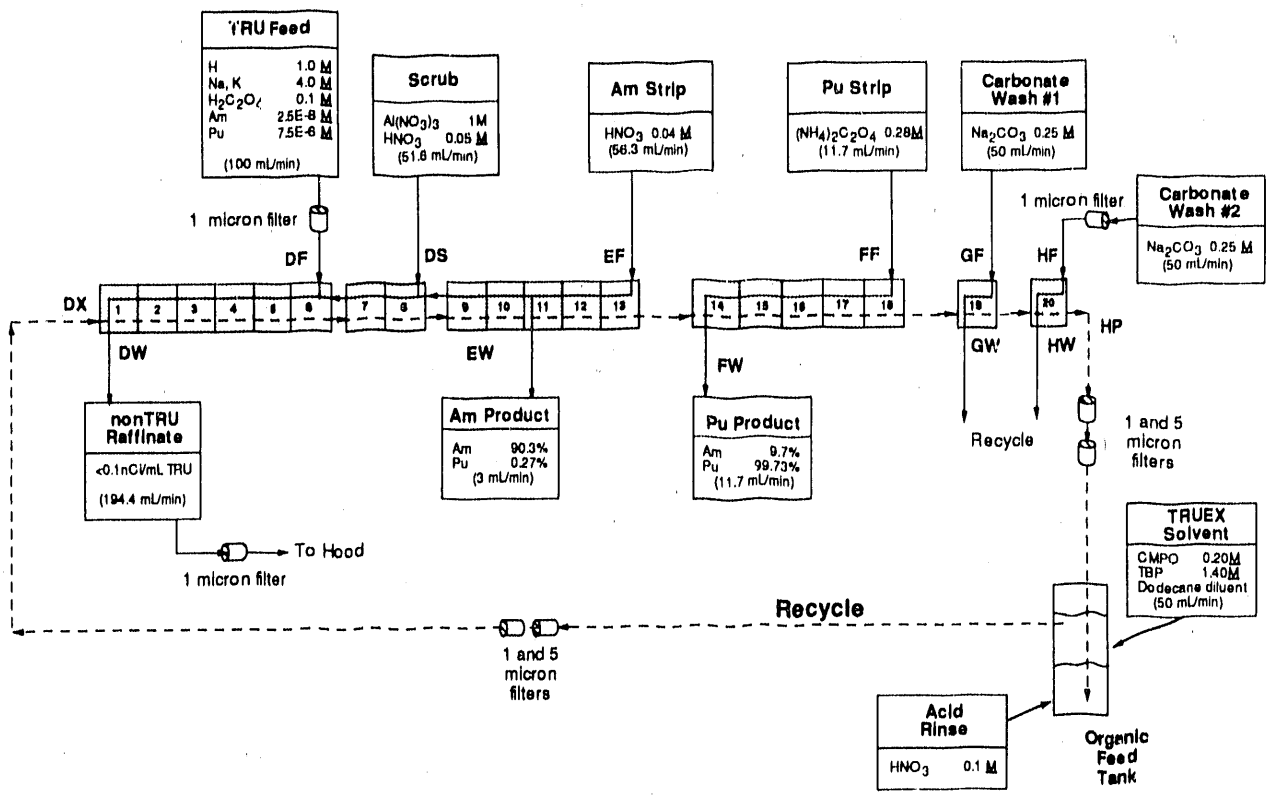

Fig. V-12. Improved Flowsheet for Processing Acidified Carbonate Waste and Second Batch of Plutonium Waste Solution

would be greatly reduced, saving an estimated $5-10 million per year, (2) the recycling of nitric acid from evaporation of this stream would be made easier because the concentration of TRU elements in the feed to the evaporator would be very low, (3) operator exposure to gamma rays from ^{241}Am would be reduced because these elements would be contained within a properly shielded facility and would not be moved into an unshielded waste treatment facility, (4) fewer liquid effluents would have to be recycled because they slightly exceed the discard limits, and (5) hundreds of grams of plutonium would be recovered and recycled.

Our goals in designing this TRUEX process were to (1) keep the concentration of TRU elements in the aqueous raffinate to less than 0.01 nCi/mL, (2) achieve our TRU concentration and recovery goals over the expected range for aqueous feed concentrations, (3) achieve our TRU concentration and recovery goals with variations in the specified feed rates of up to ±10%, (4) address the problems of sending the aqueous raffinate to a process where HNO_3 is recovered and recycled, (5) identify a solvent cleanup process such that the recycled solvent will keep the concentration of the TRU elements in the aqueous raffinate at the required low level, (6) recover the americium in the americium product stream with less than 1% of the plutonium, and (7) allow 0.1% or less of the americium to reach the plutonium strip section.

Using the GTM, we developed the base-case flowsheet shown in Fig. V-13 to meet these process goals. For the extraction section, we calculated that the desired removal of americium

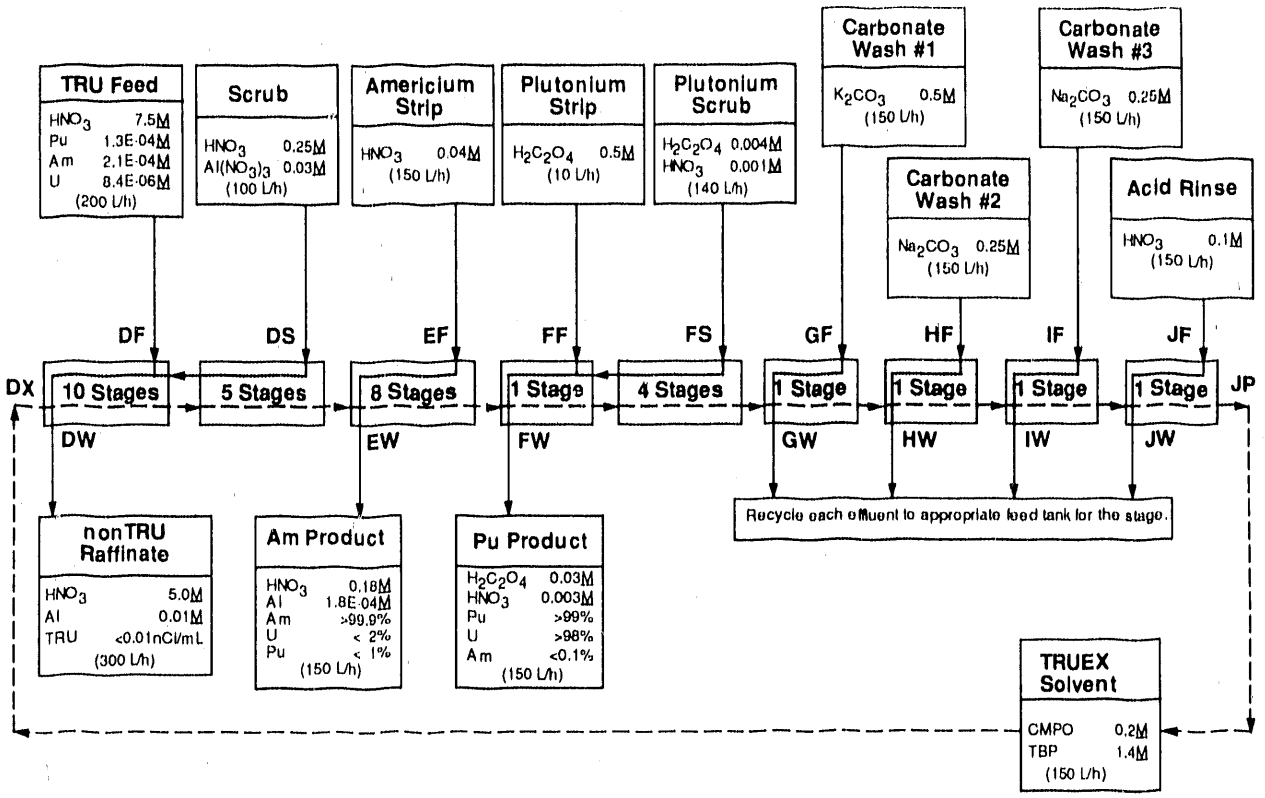

Fig. V-13. Base-Case Flowsheet for Rocky Flats Plant Waste

from the aqueous effluent required eight stages; two stages were added to give the design the desired robustness. For the scrub section, five stages are required to derive the proper low concentration of HNO_3 in the organic phase leaving the scrub section. No additional stages were added because the HNO_3 concentration is balanced between too high a value, which would make americium difficult to strip, and too low a value, which would allow too much plutonium in the americium strip effluent. The americium strip section is required because the solubility of the americium in the oxalic acid used in the plutonium strip section is very low, about 1×10^{-6} M. Maintaining the americium concentration in the plutonium strip section at or below 3×10^{-7} M, well below the solubility limit for americium oxalate, requires six americium strip stages; two strip stages were added to give the design for this section the desired robustness. The key design parameter for the plutonium strip section is to prevent plutonium oxalate from precipitating in the first stage. A model for the solubility of plutonium oxalate was developed and used to arrive at the plutonium strip and scrub sections shown in Fig. V-13. The four separate stages for solvent cleanup reflect a conservative approach based on our experience with solvent cleanup during the plutonium waste runs (Sec. V.B).

Using the GTM, we completed a sensitivity analysis for the flowsheet shown in Fig. V-13. We found that this flowsheet would meet our process goals with the desired robustness. One of the most sensitive parameters is the flow rate of the organic phase, because it passes through all the sections. In some sections, a higher flow rate is better; in others, a lower flow rate is better.

The two limiting cases for organic-phase flow rate are shown in Fig. V-14. Even though the stated goal was ±10% flow variation, the flowsheet was able to tolerate a ±20% flow variation. As a result, the organic and aqueous flows in a section can have a 10% flow variation in the most unfavorable direction and the section goals would still be met.

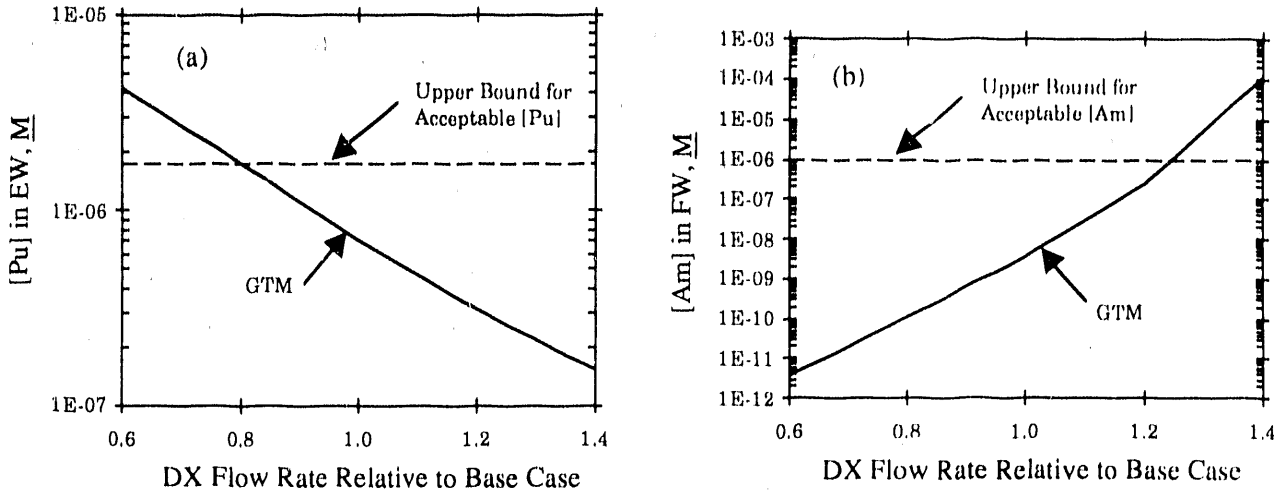

Fig. V-14. Effect of Solvent (DX) Feed Rate on (a) Plutonium Concentration in EW Effluent and (b) Americium Concentration in FW Effluent

An alternative process flowsheet for the RFP waste was developed to concentrate the americium in the americium product effluent by a factor of 50. Further work is needed to optimize this flowsheet and to verify that it meets process goals 2 and 3 above. To achieve this high americium concentration factor, additional stages are required for both the extraction and the americium strip sections. Thus, the alternative flowsheet requires a 40-stage contactor, while the base-case flowsheet requires only a 32-stage unit. In this alternative flowsheet, the rate of americium product withdrawal would depend on the americium concentration in the effluent. Thus, if the amount of americium in the waste stream fed to the TRUEX process is lower than the maximum value expected, the concentration factor can be made even higher.

Other work done in support of the TRUEX flowsheet for the RFP waste was as follows. Chemical information pertinent to a safety analysis for the TRUEX process was assembled. Solvent losses were estimated and ways to minimize these losses were outlined. Possible interactions between the TRUEX process and the HNO_3 recycle process were examined, and it appears that the HNO_3 recycle process can be operated safely.

D. *Decontamination of Groundwaters Containing Volatile Organic Compounds*

Development of a membrane-assisted solvent extraction/membrane-assisted distillation stripping (MASX/MADS) process to recover volatile organic compounds (VOCs) from groundwater is underway. This process will be used to remediate contaminated sites and to

prevent process stream releases of dilute VOCs to the environment. A flow diagram of the MASX/MADS process is given in Fig. V-15. Contaminated groundwater enters the membrane extraction module, where it is contacted with a natural-oil solvent that extracts the pollutants from the groundwater. The membrane material in the module is porous and is used to separate the two liquid phases (oil and water) and provide a large interfacial area for mass transfer. The nonvolatile solvent extracts the VOCs from the water with a distribution ratio that is typically 100-1000. Because of these high distribution ratios, the oil flow rate can be up to 100 times lower than the groundwater flow rate. The MASX unit will be designed so that the groundwater leaves the extraction unit decontaminated to a purity as good as the drinking water standards, so that this water can be safely reintroduced to the environment. At this point, the nonvolatile solvent contains the contaminants recovered from the groundwater, which are in a concentrated form. The maximum concentration of the contaminants in the nonvolatile solvent is determined from the distribution ratio between the water and the solvent and their relative flow rates.

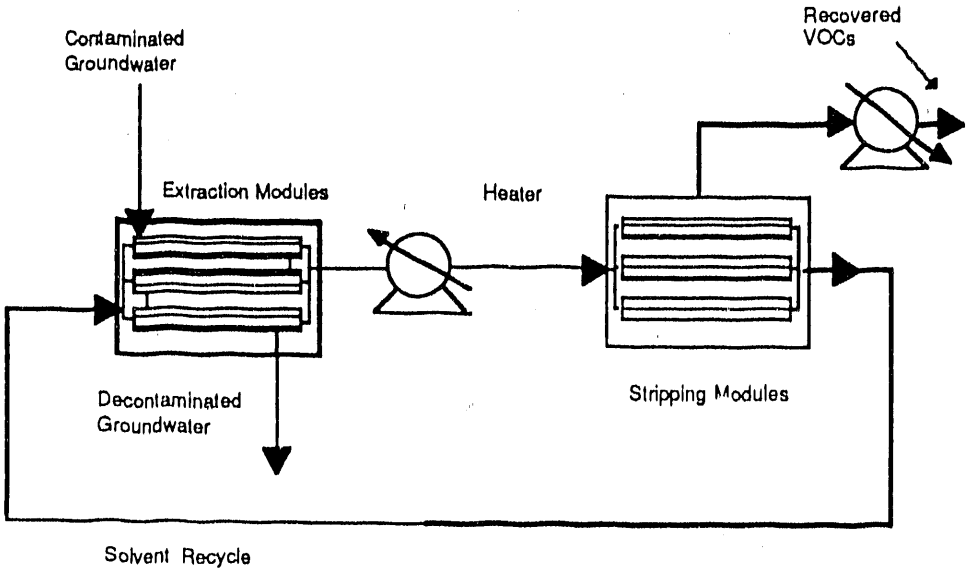

Fig. V-15. Flow Diagram for the MASX/MADS Process

The solvent must be stripped of contaminants before it can be recycled to the extraction modules. This operation is carried out in the MADS unit after the solvent is heated. In this unit, the volatile contaminants are vaporized and recovered in a condenser. In addition to the contaminants, some of the solvent and residual groundwater dissolved in the solvent is recovered in the condenser. The decontaminated solvent is then recycled to the extraction modules. This process is not a conventional distillation step involving multiple stages; it is a one-stage evaporation, but additional stages may have to be added if higher concentrations of VOCs are required for destruction or disposal.

Experimental data to design these units are not available. Performance data required include VOC concentrations in contaminated water and nonvolatile solvents after MASX/MADS treatment. To measure these VOC concentrations, we are developing analytical techniques that

employ a gas chromatograph equipped with a photoionization detector and electrolytic conductivity detector. These analytical techniques are similar to Environmental Protection Agency methods for determining VOC concentrations in environmental and drinking water samples. In addition to VOC concentration, we are measuring distribution ratios of VOCs between water and nonvolatile solvents, membrane wetting properties and stability, and Henry's law constants for various VOCs in both nonvolatile solvents and water over the temperature range of -10°C to 50°C. These measurements will be used to evaluate the feasibility of the MASX/MADS process compared to conventional remediation and pollution control technology.

E. *Advanced Evaporator Technology*

The purpose of this effort is to develop evaporator technology for concentrating radioactive waste and product streams from processes such as TRUEX. Minimizing waste generation requires the installation of equipment for concentrating radioactive waste streams and recycling the decontaminated condensates. A technology that shows a great deal of potential for this application is an evaporator being developed by LICON Inc. (Pensacola, FL).

Initial studies will evaluate this technology for concentrating specific process streams in terms of (1) economic and institutional advantages and disadvantages, (2) effectiveness of this technology in terms of concentrating radioactive product and waste streams and decontamination factors for radionuclides in the overheads, and (3) the effects of this concentration on plant operations. In a collaborative effort, LICON and ANL will (1) design an evaporator specifically for remote operation and (2) in a hot facility at Argonne, test the remote operability and maintenance of this evaporator and other equipment in glovebox, shielded-cell, and canyon facilities. In later stages of this effort, this equipment will be installed in a DOE processing/production plant for actual in-plant demonstration.

A portion of this program is being undertaken by researchers at the University of Illinois, who have completed a literature survey covering work on mixed-phase equilibria (vapor/liquid and vapor/liquid/solid) of aqueous solutions of HNO_3 in the presence of metal nitrate salts. This literature survey is critical to the design and interpretation of our planned experiments to collect necessary data not available in the literature. One of the conclusions reached from the survey is that a circulation apparatus should be used to determine the vapor/liquid equilibrium for the nitric acid-water-nitrate salt system. The Altsheler still,[2] currently manufactured by LUREX Scientific, is considered to be a very precise circulation apparatus. This apparatus reaches equilibrium in about 40 min but has no means of measuring temperature at present. Nevertheless, the Altsheler still may be easily modified to measure the temperature of the vapor and liquid. Owensby[3] has inserted two thermocouples, one for the vapor and one for the liquid phase, through the top of the Altsheler still and successfully tested them. With these considerations in mind, it appears that a modified Altsheler still would be the best choice for our experiments.

---

[2]W. B. Altsheler, E. D. Unger, and P. Kolachov, Ind. Eng. Chem. **43**, 2559 (1951).

[3]G. S. Owensby, C. A. Plant, and W. L. S. Laukhuf, J. Chem. Eng. Data **34**, 213 (1989).

VI. INTEGRAL FAST REACTOR PYROCHEMICAL PROCESS

The Integral Fast Reactor (IFR) is an advanced reactor concept proposed by, and under development at, ANL. Its distinguishing features are that it is a sodium-cooled, pool-type reactor (all the major components, reactor core, pumps, and heat exchangers are in a large sodium-filled pot); it employs a metallic fuel (an alloy of U, Pu, and Zr clad with a stainless steel-type alloy); and it has an integral fuel cycle (discharged core and blanket materials can be processed and refabricated in an on-site facility). The advantages of this concept are (1) an exceptionally high degree of passive safety, resulting from use of a metallic fuel with a sodium coolant and (2) competitive economics, resulting from low costs for reactor construction and fuel recycle.

The CMT Division is responsible for developing the on-site process for recovering Pu and U from the core and blanket fuel, removing fission products from the recycled fuel, and incorporating them into suitable waste forms for disposal. To accomplish this, major efforts are directed toward flowsheet development for the electrorefining process, laboratory experiments on process chemistry, engineering-scale demonstration of the process, and studies of IFR waste treatment and management. The processes developed in this effort will be demonstrated in the Fuel Cycle Facility for the Experimental Breeder Reactor-II (EBR-II) in Idaho. For this demonstration, reprocessed spent fuel will be used to refuel EBR-II for continued operation and to complete the fuel cycle.

A. *Process Flowsheet and Chemistry Studies*

The IFR pyrochemical process flowsheet accepts any mix of spent fuel from the reactor, removes fission products and cladding, and yields a product from which fresh fuel can be fabricated. Details of the process flowsheet, process chemistry, and operation of the electrorefiner have been provided in previous reports in this series. In the IFR electrorefining process, spent fuel in its stainless-steel cladding is chopped into approximately quarter-inch lengths and placed in a basket that is introduced into molten salt (LiCl-KCl) at 500°C in an electrorefining vessel. The basket is connected to a dc power supply and made anodic; nearly pure uranium is removed from the spent fuel by electrotransport to solid cathodes, then the plutonium and any remaining uranium in the feedstock are electrotransported to liquid cadmium cathodes. During electrorefining, noble metal fission products mostly remain in the basket, but some fall as particulate to the bottom of the electrorefiner. The alkali and alkaline earth metals in the spent fuel are oxidized and remain in the electrorefiner salt, as do most of the rare-earth fission products.

Experiments have demonstrated that separation of actinides from all fission products except the rare earths is excellent, but because sufficient quantities of most rare earths remain in the mixed uranium-plutonium product from the liquid cadmium cathode, this product requires remote handling. As fuel batches pass through the electrorefiner, the rare earth level builds up in the product and the salt. Because the radiation level and heat generation due to fission-product decay in the electrorefiner also increase, the electrorefiner salt has to be processed from time to time to remove the rare earths.

To predict the product composition in the liquid cadmium electrode and to design and control the rare-earth removal process, we must first understand the partition of the rare earth and actinide elements between molten salt (where they exist as chloride compounds) and liquid cadmium (where they exist as metals in solution). We are therefore measuring the separation factor for pairs of the rare earth elements up to atomic number 64 (gadolinium) and for neodymium vs. plutonium. These separation factors are being determined by measuring the concentrations of pairs of the rare earth elements in molten LiCl-KCl eutectic salt and liquid cadmium phases at 500°C.

We define the distribution coefficient as the ratio of the weight percent of an element in the salt phase (as the element, not its chloride) to the weight percent of the element in cadmium. Because most of the elements of interest (actinides and most lanthanides) are present in the salt as trichlorides, it is convenient to define the separation factor as the ratio of the distribution coefficients of two (trivalent) elements. When the oxidation state of the chlorides differs from three ($EuCl_2$, for example), we define the separation factor (SF) as having the same form as the equation for the equilibrium constant of the reaction between UCl_3 and the metal, M:

$$UCl_3 + 3/x\ M \rightleftarrows 3/x\ MCl_x + U \qquad (1)$$

That is,

$$SF = \frac{[U]\,[MCl_x]^{3/x}}{[UCl_3]\,[M]^{3/x}} \qquad (2)$$

Unless the chlorides of both elements have the same oxidation state, the distribution coefficient of one element in a pair will depend in a nonlinear fashion on the distribution coefficient of the other element. Nonetheless, this approach allows us to "chain" separation factors and form a self-consistent set of separation factors from measurements on a minimum number of element pairs. Self-consistency is of critical importance for calculations as the separation factor becomes larger than 25, because it soon becomes difficult if not impossible to measure precisely at least one member of the smaller pair of concentrations (for example, the uranium in the salt or the yttrium in the metal for the U-Y pair). By "chaining" more easily measured separation factors, though, we can estimate, for example, the separation factor of the U-Li pair ($\sim 7 \times 10^{12}$), even though it is clearly impossible to measure this separation factor directly.

It is easiest to envision the relative distribution of the elements as the oxidizing state of the system is changed, if the distribution coefficients of all the elements are plotted as a function of the distribution coefficient of one element. In Fig. VI-1, distribution coefficients (calculated from the appropriate separation factors) are plotted against the logarithm of the distribution coefficient of uranium. The separation factors used are the best presently known values; measurement and data analysis are still in progress. A logarithmic scale was used to accommodate the large range of oxidizing conditions from the very reducing state, where the

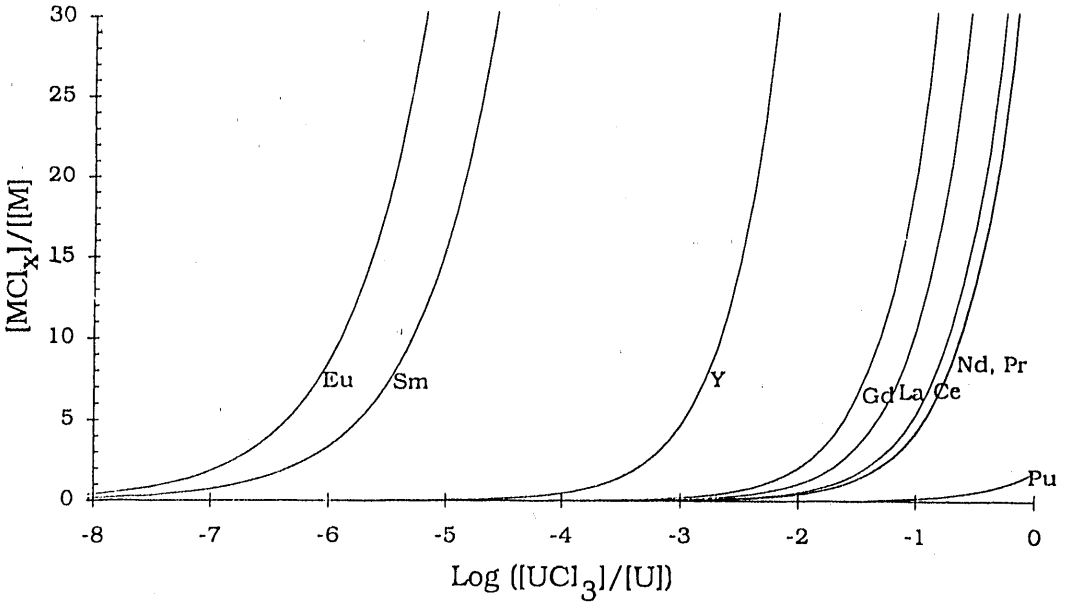

Fig. VI-1. Distribution Coefficients of Selected Elements as a Function of Oxidation State

concentration of UCl_3 is small and only Eu and Sm are present as chlorides, to the highly oxidizing state (relative to the IFR process conditions), where nearly all the rare earth and actinide elements are found in the salt phase.

The behavior of the most metallic (readily oxidized) rare earth elements is of interest in the salt purification steps, where the salt is treated with Li or U in Cd to recover the transuranics and separate them from the rare earths. A computer code has been developed to simulate countercurrent extraction with salt and metal, where no solid phases are formed. This code uses the set of separation factors to calculate the distributions of the rare earth and actinide elements in the extraction process; it is being used in designing the salt-treatment part of the pyroprocess flowsheet (Sec. VI.D.1).

B. *Process Development Studies*

Work in this area included experiments to study zirconium behavior in an electrorefiner and fabrication of a new laboratory-scale electrorefiner for use in process-development experiments.

1. Zirconium Behavior Studies

Zirconium constitutes about 30 vol % of IFR fuel. In the normal transport of uranium to a solid cathode and U-Pu to a liquid cathode, the bulk of the zirconium is not transported but is left in the electrorefiner. With repeated cycles, this zirconium accumulates in the cadmium anode pool.

Laboratory studies were continued to determine the behavior of zirconium in electrorefiner operations and to devise methods for zirconium removal from the cadmium anode pool. Although the site of zirconium deposition during anodic dissolution of the fuel is not altogether clear, examination of our engineering-scale electrorefiner indicated that some, if not all, of the zirconium deposits on the crucible wall.[1] A similar finding was made during examination of laboratory-scale crucibles (15-cm dia) and stirrers used in small-cell tests.[1] To clarify where zirconium deposits, several small electrorefining cells (housed in 5-cm dia crucibles with capacity of ~300 g cadmium) were operated, then their crucibles were cut apart and examined to determine where the zirconium had deposited.

In typical tests, cells of the type Zr/LiCl-KCl-$ZrCl_x$/Cd(Zr) were operated at ~500°C. No uranium was used, and zirconium was transferred electrochemically from a zirconium anode rod to a cadmium pool cathode. The cell electrolyte was prepared by adding $CdCl_2$ to oxidize zirconium metal to $ZrCl_x$ (species not determined). The electrolyte, LiCl-KCl eutectic, contained an estimated 1 wt % Zr. The zirconium anode rod was easily anodized at a current density of 100 mA/cm^2 and low voltage. Visual examination of the cross-sectioned crucibles after the test indicated that the solids had piled up on top of the cadmium pool cathode. The cell stirrer was not adequate to break up this deposit.

In these tests, deposits of $ZrCd_2$ (identified by X-ray diffraction) were found on the zirconium anode rod. Since this formation was likely due to "splashing," in the stirred cell, of cadmium onto the zirconium rod, we needed to determine if the zirconium would be chemically attacked by cadmium. The objectives of the next two tests were to determine (1) how much $ZrCd_2$ would actually be formed, and (2) whether or not the zirconium could be electrochemically removed from this cadmium phase. Results from these two tests revealed the following: (1) 37 g zirconium dissolved in 307 g cadmium over a seven-day period at ~500°C, and (2) the cadmium phase with this much zirconium appeared to be nearly solid at ~500°C. (The solubility of zirconium in liquid cadmium is about 0.2 wt %.[2]) The zirconium from the cadmium phase was transported electrochemically onto a mild steel rod. However, we could not establish whether the cathode product was zirconium metal, a zirconium salt, or a combination of both. A relatively low voltage (<0.3 V) was required to facilitate this transport.

Typical results from the crucible analyses are illustrated in Figs. VI-2 to VI-4. Figure VI-2 shows the cross section of a crucible after zirconium deposition onto cadmium. In this photograph, we see an irregular boundary between the white salt phase and the dark cadmium phase. Before deposition of zirconium, this interface was a flat plane, as expected between two immiscible liquids. Figure VI-3 shows a Cd_2Zr-rich phase on top of a cadmium ingot removed from a crucible, indicating that the upper phase contained solids (Cd_2Zr intermetallic) at the operating temperature (~500°C). This phase was located between the liquid cadmium and the salt (not shown in this photograph). Figure VI-4 shows a zirconium-bearing

---

[1]M. J. Steindler et al., *Chemical Technology Division Annual Technical Report, 1990*, Argonne National Laboratory Report ANL-91/18, pp. 112 and 117 (1991).

[2]I. Johnson, K. E. Anderson, and R. Claypol, in *Chemical Engineering Division Summary Report -- July, August, and September 1960*, Argonne National Laboratory Report ANL-6231, p. 67 (1960).

Fig. VI-2. Cut-up Crucible at End of Test

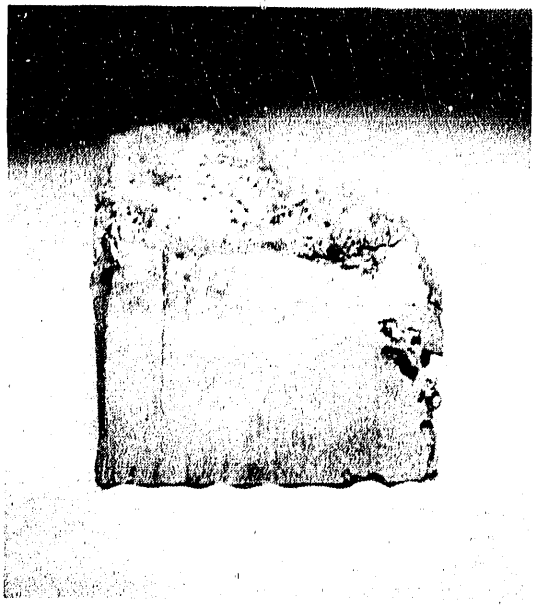

Fig. VI-3.

Cut Section of Product Ingot Showing Cd_2Zr on Top of Cadmium

electrodeposit obtained on an iron cathode from a cell which had a zirconium-rich cadmium anode. The deposit appears to contain some metal crystals encased in salt. Analysis of similar cathode deposits revealed both zirconium metal and a zirconium salt.

This work indicates that zirconium can be electrotransported to a cathode and is readily dissolved by direct attack of cadmium metal or by electrolytic anodic dissolution. Accordingly, these methods should be candidates for removing the fuel-alloy zirconium from the electrorefiner.

Fig. VI-4.

Typical Deposit Obtained with Zirconium

Our next objective is to investigate the removal of zirconium (electrochemically) from the cell at the end of the "drawdown procedure." The drawdown procedure is employed in the IFR electrorefining process to remove most actinides from the salt and metal phases prior to removal of the salt for waste processing. A low concentration of actinides in the cadmium pool permits formation of zirconium chloride species in the salt, a necessary condition for electrotransport of zirconium to a cathode.

2. Laboratory-Scale Electrorefiner

A new, laboratory-scale electrorefiner has been designed and fabricated. The major design change, compared to the electrorefiner in use earlier, is in the cadmium cathode. The new impeller design for the cathode provides for axial as well as rotational motion. Our work with the old design showed that the actinide solids, found in the cathode, tended to build up on the rotating blades of the impeller instead of sinking into the liquid cadmium. The added axial motion should force the solids downward into the cadmium phase. The apparatus was assembled outside a plutonium glovebox and was operated cold, and certain initial deficiencies were found and corrected. The apparatus was then moved into the plutonium glovebox, and further shakedown tests were completed. The electrorefiner is now being loaded with processing reagents (cadmium and LiCl-KCl electrolyte) prior to heatup. After the electrorefiner has been charged with U and Pu, experiments will be conducted to establish process parameters and electrochemistry for transport of these elements to liquid cadmium cathodes.

C. *Engineering-Scale Process Development*

The key steps in the pyrochemical processing of spent fuel are dissolution and product recovery by electrodeposition using either solid or liquid cathodes. Progress made in developing each step is discussed below. Also reported are results from tests of a system to reduce cadmium-aerosol release from the electrorefining process, a device for harvesting the uranium

deposit from a steel cathode, and zirconium behavior. All tests were conducted in our engineering-scale electrorefiner (0.9-m dia crucible).

1. Dissolution of Spent Fuel

Anodic dissolution of chopped, clad U-Zr alloy pins at the engineering-scale level (~10 kg batch size) has become a routine operation. To date, ~200 kg uranium has been anodically dissolved in the engineering-scale electrorefiner. Dissolution of 10 kg batches is typically achieved in less than 30 h. After an anodic dissolution run, the baskets are rotated in the gas phase above the salt in the electrorefiner to reduce the amount of salt on the cladding hulls and basket. Measurements were made to determine the effect of the basket rotation speed on the weight of salt retained in the baskets. Approximately 60, 130, and 144 g of salt were retained on the baskets and hulls at basket rotation speeds of 250, 125, and 0 rpm, respectively. Based on these results and the fact that the maximum basket rotation speed for the system is 250 rpm, this rotation speed is recommended for salt removal from baskets. Future efforts will be directed to the development of improved anodic basket designs for direct transport of dissolved uranium from the basket to a solid cathode and for increased throughput rate.

2. Electrotransport to Solid Cathode

Electrotransport of ~10 kg uranium from a cadmium pool anode to a single mandrel cathode has also become a routine operation. In the most recent electrotransport tests (Runs 43, 45, 51, 52, and 54), 9.5, 9.3, 8.2, 10.0, and 8.6 kg of uranium were electrodeposited on a single mandrel cathode in 37, 26.5, 30, 46, and 30 h, respectively. These and other test results are given in Table VI-1. The optimal operating conditions required to produce a 10 kg uranium deposit have been determined from the test results.

An important operating condition was determined to be adequate salt and cadmium mixing, which is needed to facilitate the electrotransport of uranium from the cadmium anode pool to the solid mandrel cathode. However, the mixing must be controlled after a deposit weight of about 5 kg has been produced to reduce mechanical losses as the weight of the deposit is increased to 10 kg. This is accomplished by turning the salt mixer off halfway through the run and by not using the cadmium mixer.

As shown in Table VI-1, the collection efficiency for the above tests was 39 to 48%. The throughput rate could be nearly doubled by increasing the collection efficiency to about 80%. Future efforts will include tests to increase the collection efficiency.

3. Electrotransport to Liquid Cadmium Cathode

Tests were continued to determine the operating conditions required to electrodeposit 3 kg uranium in a liquid cadmium cathode (LCC). (Since the glovebox in which these tests are carried out is not a plutonium facility, uranium is used as a stand-in for plutonium.) Figure VI-5 is a schematic of the LCC in the engineering-scale electrorefiner. The

Table VI-1. Results from Electrotransport to Single-Mandrel Solid Cathodes

	Run No.				
	43	45	51	52	54
Wt. Uranium Deposit, kg	9.5	9.3	8.2	10.0	8.6
Deposition Rate, kg/h	0.26	0.35	0.27	0.22	0.29
Collection Efficiency, %	39	39	42	42	48
Average Current, A	222	302	219	111[a] 254[b]	200
Time, h	37	26.5	30	25[a] 21[b]	30

[a]Uranium was electrotransported directly from the anodic dissolution baskets to the cathode.
[b]Electrotransport from the cadmium pool anode to the cathode.

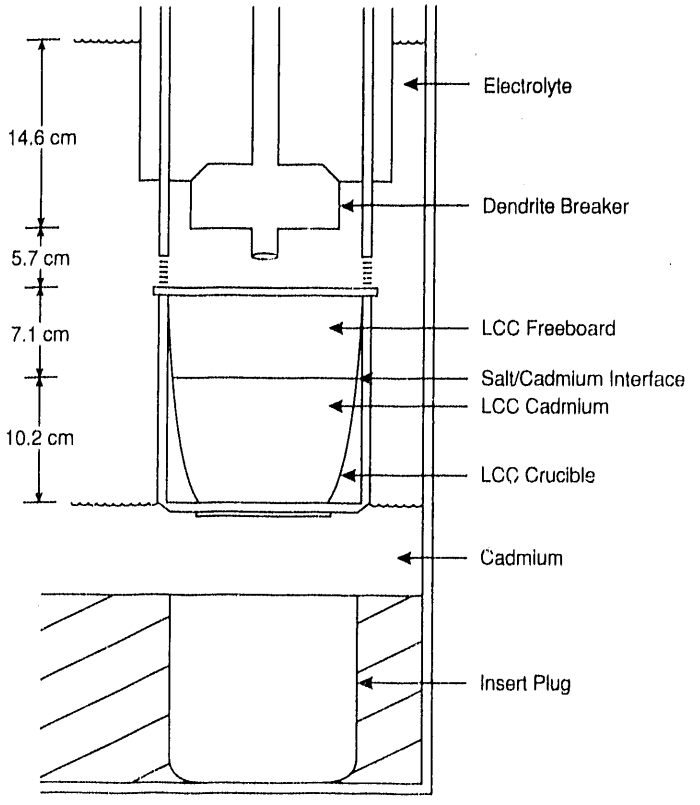

Fig. VI-5. Configuration of Liquid Cadmium Cathode in Engineering-Scale Electrorefiner

tests conducted during this reporting period were designed to determine the effect of the following variables on LCC performance:

1. Cadmium height in LCC crucible
2. Electrode area of LCC
3. Freeboard in LCC crucible
4. Electrode distance between LCC and cadmium anode pool
5. Height of salt above the LCC crucible

One of the conclusions reached from these tests is that electrode area, freeboard of the LCC crucible, and the electrode distance between the LCC and cadmium anode pool have a major effect on the cell resistance. To date, resistance has been measured for reference conditions and then a 20% increase in the electrode area, 50% increase in the freeboard, and 50% increase in the distance between the electrodes. The resistance tripled as a result of the increase in these variables. Further testing is needed to determine the contribution of each variable to this increase in cell resistance.

In one liquid cadmium cathode test (Run AD-LCC-7/7A), uranium was electrotransported directly from the anodic dissolution baskets to the LCC. During the run, the electrodeposition was interrupted after about 250 Ah; the front edge of the dendrite breaker was positioned below the surface of the cadmium in the LCC to compact the uranium dendrites; and the dendrite breaker was then raised above the LCC and rotated at 150 rpm to remove uranium dendrites from the breaker and upper surfaces of the LCC crucible. These operations were repeated until the run was terminated. The average current for this run was 62 A, and the electrodeposition time was 59.4 h.

Based on chemical analysis of samples taken from the LCC product, the product contained 66.8 wt % cadmium, 33.2 wt % uranium, and negligible amounts of salt and zirconium. The weight of uranium in the LCC was 4.2 kg. If similar results can be obtained with U-Pu mixtures (i.e., about 4 kg heavy metal in about 9 kg cadmium), this would meet our goals for the LCC needed for the electrorefiner in the Fuel Cycle Facility. The data from these experiments will be useful in designing the liquid cathode for testing with U-Pu mixtures in the Fuel Cycle Facility.

4. Experiments with Pulsed Liquid Cadmium Cathode

Pulsed current electrodeposition is being explored as an alternative to mechanical means of controlling the growth of dendrite whiskers out into the molten salt from the surface of the liquid cadmium cathode. If successful, this approach will result in a simplified design for the liquid cadmium cathode.

So far, two experiments with this approach have been conducted. In the first (LCC-8), a deposition current of 60 A was applied for 4 s followed by 0.8 s at open circuit. After

1200 Ah, approximately 1.2 kg of uranium was electrodeposited into the cadmium cathode. The current efficiency in this experiment was somewhat low (33%). There was a clean separation between the salt and the metal phases. An autoradiograph of the sectioned product ingot showed that the uranium had settled to the crucible bottom, but not in a compact mass.

In the second experiment (LCC-9), a modified stirrer was used in an attempt to increase the mass transfer of salt to the surface of the liquid cadmium cathode. The stirrer was fabricated from mild steel with four blades pitched at a 45° angle. It was rotated so as to force salt downward to the molten salt/liquid cadmium interface. The pulsed current waveform was also changed to 4 s of deposition current (50 to 100 A) followed by a series of four 20 ms stripping pulses (200 A) spaced 200 ms apart. The stripping pulses were an attempt to anodically dissolve dendrites growing out from the liquid cadmium surface. The current efficiency decreased in this run to 11%, with only 0.5 kg of uranium deposited after 1500 Ah. The autoradiograph of the sectioned product ingot showed that the uranium had settled to the bottom of the crucible and formed a more compact mass than in LCC-8.

The results from these two experiments are inconclusive. Because of high demand for the engineering-scale electrorefiner, the need for more control over some of the experimental variables, and the need to investigate plutonium electrodeposition with liquid cadmium cathodes, further exploration of this approach will be conducted with a smaller scale apparatus in a facility where U-Pu codeposition can be studied.

5. Cover-Gas Treatment System

During testing with the engineering-scale electrorefiner, we observed the release of cadmium aerosols to the glovebox. These aerosols deposit on the interior of the glovebox windows and equipment and could cause problems in the argon cell of the Fuel Cycle Facility if similar releases were to occur. A cover-gas treatment system (CGTS) was developed to reduce such releases from the engineering-scale electrorefiner and, in principle, should be usable with the electrorefiner for the Fuel Cycle Facility. In this system, a portion of the cover gas is withdrawn and passed through a mass transfer unit (MTU) that removes cadmium by vapor condensation. The unit is in the form of countercurrent flow heat exchanger trays, which are fabricated from 5-mm high corrugated internal passages. The gas temperatures are carefully controlled to suppress the onset of homogeneous nucleation and, thus, to prevent formation of cadmium aerosols, which would be very difficult to remove from the gas stream.

In the system, a portion of gas is withdrawn from the cover gas region of the electrorefiner through a heated pipe connecting the electrorefiner to the MTU. The gas is passed through the MTU and then through a gas cooler of similar construction to the MTU. The cleaned gas is returned through the opposite side of the MTU and then back to the electrorefiner close to the prevailing cover gas temperature. A bleed-and-feed subsystem allows one to purge a fraction of the cleaned gas and to maintain a constant cover-gas pressure. Capability exists for obtaining samples of the inlet and exit gas from the MTU. The system can be heated periodically to melt and drain the trapped cadmium from the system at periodic intervals.

The cadmium concentration in the cover-gas space (untreated) above the salt in the electrorefiner was determined to be in the range of 2000-4000 ppm by weight (ppmw). In tests with the CGTS, the MTU achieved very high collection efficiencies (99.38 to 99.99%) for testing periods where stable operation was achieved. The cadmium concentration in the gas exiting the MTU was significantly less than 1 ppmw. At gas recirculation rates of 5×10^{-4} m^3/min (1 scfm), the MTU reduced the cadmium concentration in the electrorefiner from 2000-4000 ppmw to less than 100 ppmw.

The CGTS was regenerated twice by heating the unit and melting the collected cadmium into a collector pot attached to the bottom of the unit. We collected two ingots of cadmium, which together weighed ~17 kg. This compares favorably with an estimated 20-25 kg of cadmium contained in the gas entering the unit based on samples from the inlet gas. The testing of the CGTS has been completed, and the unit is being disassembled.

6. Equipment Testing

Testing of a device to harvest the uranium deposit collected on a steel mandrel cathode in the engineering-scale electrorefiner was continued.[3] The main elements of this device are a machined die mounted on backing plates, which are attached to a unistrut framework, welded to the glovebox floor. A bolted collar is attached to the cathode assembly, and the die is positioned around a clean portion of the cathode mandrel, above the deposit. The mandrel is pulled through the die, and the stripped uranium deposit is collected in a steel basket. During this report period, the main modifications to the device were (1) a screw-actuated harvester that employs a torque device to pull the mandrel out of the uranium deposit and (2) a thin steel cylindrical sleeve to limit the diameter of the harvested deposit.

We tested a torque wrench, an impact wrench, and a modified power pipe threader for their ability to provide the needed stripping force. The impact wrench was not able to strip the uranium deposit from the steel mandrel cathode, while the other two components were. The torque wrench harvested a deposit that weighed 11.1 kg (9.3 kg uranium) and had a composition of 83.5 wt % uranium, 10.4 wt % salt, 0.9 wt % zirconium, and <0.01 wt % cadmium. A maximum force of 15,670 N (3524 lb-f) was needed to strip the deposit. Figure VI-6 shows a side view of the harvested deposit after removal of the steel cylindrical sleeve. The length of this deposit was ~21 cm. The modified power pipe threader stripped a 10.6 kg deposit from the steel mandrel in 51 s.

The above tests have provided sufficient data to design a harvester device for the Fuel Cycle Facility. No further tests of the harvester are planned.

---

[3]M. J. Steindler, *Chemical Technology Division Annual Technical Report, 1990*, Argonne National Laboratory Report ANL-91/18, p. 117 (1991).

Fig. VI-6.

Side View of Harvested Uranium Deposit

7. Zirconium Behavior in the Engineering-Scale Electrorefiner

The investigation of the zirconium behavior in the engineering-scale electrorefiner has continued (see also Sec. VI.B.1). During this report period, samples were taken from deposits that formed on components immersed in the electrorefiner for various periods of time (see Fig. VI-7 for locations). Samples were also taken of molten material trapped on the horizontal surfaces of the salt stirrer assembly when it had to be removed from the electrorefiner for maintenance purposes. The above samples were found to have a relatively high zirconium concentration. This suggests that "unaccounted" zirconium may be accumulating on the interior surfaces of the electrorefiner.

The first component to be removed and sampled was a corrosion rod to which two metal coupons were attached and immersed in the salt and cadmium, as shown in Fig. VI-7. This corrosion rod and coupons had been immersed in the electrorefiner for approximately one year (two 6-month periods). When removed from the electrorefiner, the corrosion rod was covered with a fairly thick deposit. (No significant deposit was observed on the corrosion rod after the first 6-month period.) Figure VI-8 is a photograph of the corrosion rod. Little or no deposit was observed in the lower 5 cm, which was immersed in the cadmium. The deposit was extensive throughout the portion immersed in the salt and decreased to zero above the salt. The deposit varied from about 0.6- to 1.3-cm thick. Samples A1 to A4 were taken from the rod. As shown in Fig. VI-7, the zirconium content of the deposits ranged from 10.1 to 13.8 wt %. The uranium content was about 3 wt % except for sample A1 (<0.01 wt % uranium). The Li and K contents of the deposits correspond to a salt content of about 9 wt %.

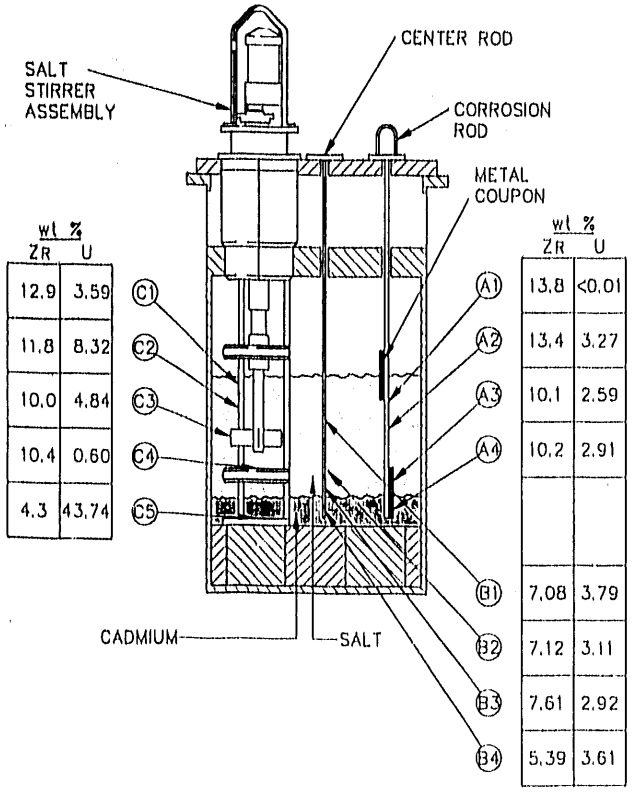

Fig. VI-7.

Analysis Results of Samples Taken from Deposits on Components Immersed in Engineering-Scale Electrorefiner

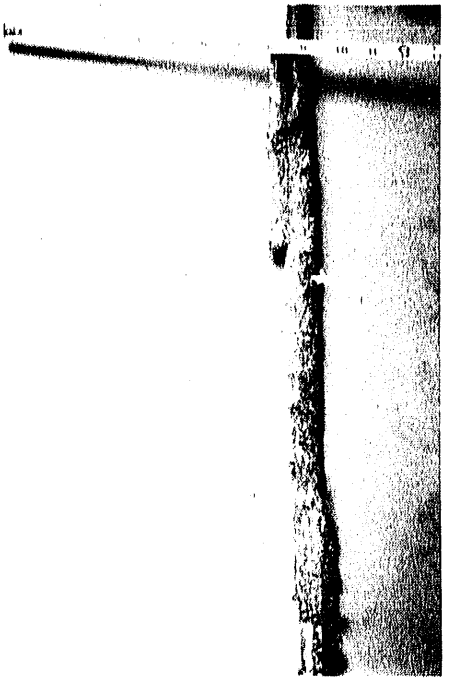

Fig. VI-8.

Corrosion Sample from Engineering-Scale Electrorefiner with Adhering Salt, Uranium, Cadmium, and Zirconium

The second component that was removed and sampled was a center rod used to obtain information on the possible rate of deposit accumulation in the intended location of the stirrer for the Fuel Cycle Facility electrorefiner. This rod had been immersed for two weeks and had only a thin coating on it. Samples B1 to B4 were scraped off the rod. Despite the small amount of material on this rod, these samples also showed a high zirconium content, 5.4 to 7.6 wt %.

The third component to be removed from the electrorefiner was the salt stirrer assembly, which had to be removed to replace its motor. At that time, samples C1 to C5 were obtained. Samples C1 and C2 were deposits that had formed on the support rods; sample C3 was a deposit from the blade of the stirrer; and samples C4 and C5 were obtained from molten material that was trapped on the horizontal top surfaces of the heat baffle and the bottom plug, respectively. These samples also had high zirconium contents, ranging from 4.3 to 12.9 wt %.

The above analyses indicate that deposits containing significant amounts of zirconium had built up on certain components in the electrorefiner. Because the surfaces of these components are at cathode potential during the fuel dissolution process, this behavior is not unexpected. An attempt was made to quantify the amount of zirconium on the interior wall of the electrorefiner. The amount of deposit collected on the corrosion rod and coupons was about 500 g. If a similar deposit thickness to that of the rod and coupons were formed on the inner wall of the electrorefiner, then the amount of zirconium contained in this deposit would be 4-5 kg. This quantity represents a major portion of the 7 kg of zirconium "unaccounted for" during the many tests run with this electrorefiner.

Filtered samples were taken from the cadmium and salt several days after the above components were sampled. The results, shown in Table VI-2, indicate that the cadmium was saturated with zirconium and slightly below the saturation value for uranium. As usual, the salt showed very small amounts of zirconium. Thus, the excess zirconium appears not to be mobile but attaches itself to cathodic surfaces. In a future drawdown run (i.e., electrochemical removal of all uranium present), attempts will be made to electrochemically remove the zirconium from the electrorefiner.

Table VI-2. Zirconium and Uranium Content of Filtered Cadmium Samples[a]

		Wt %	
Sample ID	Phase	Zr	U
S154	Salt	<0.01	6.87
S155	Salt	<0.01	6.73
M210	Cadmium	0.23	1.93
M211	Cadmium	0.22	1.99

[a]Uranium saturation of cadmium, 2.35 wt %; zirconium saturation of cadmium, 0.22 wt %.

D. *Waste Treatment Processes*

Processes are being developed to treat the spent salt and metal from the electrorefiner to recover TRU elements and then to convert the treated salt and metal into disposable high-level waste forms. The spent salt contains the alkali metal, alkaline earth, rare earth, and halide fission products. It also contains small, but significant amounts of uranium and TRU elements. The spent metal consists of cadmium from the electrorefiner pool, which contains zirconium and noble metal fission products, and the cladding hulls. Efforts have been concentrated on developing the processes needed to treat and immobilize salt, and work has been initiated on developing methods for metal waste treatment and consolidation.

The reference flowsheet for treating spent salt and metal was given in the previous annual report.[4] The main process steps are as follows:

1. The spent salt is passed through a multistage, countercurrent extraction process, where it is contacted with a Cd-2.2 wt % U solution. With the proper metal/salt ratio and number of equilibrium stages, more than 99% of the TRU elements is transferred to the metal phase by exchange with uranium, while more than 70% of the rare earths remains in the salt. The TRU-rich metal product is returned to the electrorefiner.

2. Essentially all of the uranium, any residual TRU elements, and most of the rare earths are removed from the salt raffinate by contact with a Cd-0.1 wt % Li alloy in a salt stripping step. The stripped salt contains all of the alkali metal, alkaline earth, and halide fission products; some rare earths (Y, Sm, Eu); and only trace amounts of actinides (<100 nCi/g).

3. The cadmium solution from the salt stripping step is combined with spent metal from the electrorefiner and cladding hulls, and the excess cadmium is removed by distillation and returned to the electrorefiner.

Several techniques are being explored for immobilizing the treated salt and metal and converting them to high-level waste forms. To immobilize and convert the waste salt, it will be sorbed into a zeolite, and the salt-zeolite compound will be hot-pressed into a solid waste form. The metal wastes will be combined with a matrix metal or alloy (e.g., Cu, Ni, Zr-Fe, Al), yet to be selected, and pressed or melted to produce a final waste form.

1. Salt Extraction

A test facility with a high-temperature centrifugal contactor (pyrocontactor) is being developed to separate elements from the rare earths in the IFR fuel cycle. This pyrocontactor is similar to the ANL centrifugal contactors developed for aqueous/organic solutions (Sec. V). The

---

[4]M. J. Steindler et al., *Chemical Technology Division Annual Technical Report, 1990*, Argonne National Laboratory Report ANL-91/18, p. 119 (1991).

development work includes the design, fabrication, and assembly of a pyrocontactor and the associated processing equipment to be housed in an argon-filled glovebox. Experiments will be conducted in this facility to determine the performance and extraction efficiency of the contactor with molten cadmium and chloride salts at 500°C. The ultimate goal is to develop a continuous liquid metal-salt extraction process that uses multistage, countercurrent pyrocontactors to recover the TRU elements from the waste salts produced in the Fuel Cycle Facility.

Progress toward building the test facility is summarized as follows:

1. The pyrocontactor (made of Type 304 stainless steel) was designed and fabricated. A pretest of the contactor at room temperature without liquids was successful.

2. The metal and salt feed tanks will be two horizontal tanks made of Type 304 stainless steel, with ~26.5 L (7 gal) capacity each. These feed tanks, along with their associated heaters and support brackets, were designed. Procurement and fabrication of the tanks and the accessories were initiated.

3. The raffinate and treatment tanks for metals and salts, which have a liquid volume of 26.5 L (7 gal) each, were designed, fabricated, and installed. Shakedown tests are nearly complete.

4. The design work to modify an existing glovebox (1.7-m high, 1.4-m wide, and 4.1-m long) for pyrocontactor testing is complete. Nearly completed is the assembly of this glovebox, including floor wells for the raffinate and treatment tanks, electrical and mechanical feedthroughs, an end plate with electrical fittings, and gas ducts connecting the main purification system. The environmental control system for the glovebox includes a main purification system with pressure-control, emergency-control, and gas-cooling subsystems. This system will provide dry (<15 ppm H_2O) and oxygen-free (<15 ppm O_2) argon at a rate of 0.02 m^3/min (40 cfm) to the glovebox. This system is also nearly assembled.

2. Salt Stripping

A prototype of the salt stripper system to be installed in the Fuel Cycle Facility has been designed and is being fabricated. The system includes the stripper vessel and a pump-and-transfer line to move salt between the engineering-scale electrorefiner and the stripper vessel. The stripper is equipped with an agitator capable of imparting mixing power densities up to 1.4 kW/m^3 (7 hp/1000 gal) in the salt and 5.9 kW/m^3 (30 hp/1000 gal) in the metal phase. Ports for sampling and charging materials and fittings for instrumentation, such as liquid level probes and reference electrodes, are provided.

Several small-scale experiments were done to support development of the salt stripper. In these experiments, the salt from the laboratory-scale electrorefiner (Sec. VI.B) was stripped to recover the heavy metals. In total, 4200 g of molten salt was contacted with Cd-Li

solutions in five stripping runs. The actinides (U, Pu, Am) and rare earths (Ce and Nd) were almost completely removed from the salt solution. Nevertheless, difficulties were encountered in dissolving the reduced actinides and rare earths in the cadmium, probably because the rapid reduction from the salt resulted in the formation of slowly dissolving intermetallic compounds at the salt-metal interface. In two runs, an attempt was made to dissolve the intermetallic compounds by reducing the lithium-addition rate to the metal phase (the Cd-Li was added in three steps rather than one). This completely dissolved the reduction products, but some evidence suggested that the reduction rate exceeded the dissolution rate during certain periods. The intermetallic compounds were also dissolved by raising the melt temperature from 500 to 550°C.

Experiments will be conducted to measure stripping rates as functions of mixing intensity, to assess the effectiveness of various filters, to determine the characteristics of insolubles, and to evaluate the performance of various components and instruments.

3. Salt Immobilization

Although the treated salt will contain only trace amounts of actinides and very small amounts of rare earth fission products, it will contain Cs and Sr and is, therefore, a high-level waste according to the definition in the Code of Federal Regulations (Title 10, Part 60). As such, it must be disposed of in a geologic repository for high-level waste. A waste form that will meet the acceptance criteria for the repository must be developed for the IFR waste salt. Although the exact acceptance criteria have not been specified, some guidance has been obtained from the Waste Acceptance Preliminary Specifications for high-level waste glass being prepared at the Savannah River Site and the West Valley Demonstration Project. Qualitatively, the waste form for IFR waste salt must be strong, leach resistant, and stable with respect to radiation and radiogenic heating. In addition, the process for producing the waste form must be amenable to remote operation and compatible with other IFR pyroprocessing operations.

With these guidelines in mind, it is proposed to use salt-occluded zeolite powders as an immobilization matrix for IFR waste salt. Densified salt-occluded zeolite monoliths, possibly with added strengtheners, have been proposed as the corresponding waste form. The experimental program for testing this concept has been focused on measuring the leach resistance and radiation and thermal stability of salt-occluded zeolites.

a. Leach Resistance

The leach resistance of a waste form is of paramount importance since leaching is the most likely mechanism by which waste will reenter the accessible environment. The leach resistances of zeolite A samples occluded by simulated IFR waste salt were measured at room temperature with deionized water as the leachant. The ratio of the volume of leachant to the mass of solid was 200 mL/g. The duration of the tests was 2, 5, and 25 days. The leachability [L, in units of g/(m^2•day)] was determined from the equation:

$$L = C_i \bullet V/(F_i \bullet SA \bullet d) \qquad (3)$$

where C_i is the concentration of species i in the leachate (g/mL), V is the volume of the leachant (mL), F_i is the fraction of species i in the sample, SA is the surface area (m^2), and d is the duration of the leach test in days. Because the SA was calculated from the literature value for the average particle size (1.39 μm) and from an estimated value of the density (2.10 g/cm^3), these leach test results must be considered preliminary. The leachate was analyzed for strontium by inductively coupled plasma spectroscopy and for cesium by atomic emission spectroscopy.

The leachabilities for Cs and Sr in the short-term (2-5 day) tests averaged about 10^{-3} and 10^{-5} g/(m^2•day), respectively. The leachability for both Cs and Sr in the 25-day test was approximately 10^{-5}g/(m^2•day). Three conclusions were reached from these data: cesium is released more readily than strontium from the zeolite matrix, the leachability for cesium decreases with time, and the leachability for strontium is extremely low and independent of time.

These leachability data compare favorably with the "initial" (i.e., less than 28 days), room-temperature leachabilities given for borosilicate glass, i.e., 10^{-1} to 10^{-3} g/(m^2•day).[5] Also, the same time dependence of leachability is observed in tests with borosilicate glass. However, the differences in the SA/V ratios, i.e., 0.1 cm^{-1} in the borosilicate glass and 50 cm^{-1} for the salt-occluded zeolite, were not considered in this comparison. Notwithstanding, the leachability of the salt-occluded zeolite is well within the range that would be acceptable for repository disposal. These studies are continuing.

b. Radiation and Thermal Stability

The radiation and thermal stability of zeolite A occluded by simulated IFR waste salt have also been investigated. In these tests, three salt-occluded zeolite samples were subjected to one of the following conditions: (1) heated to 200°C (no irradiation); (2) irradiated to 8.0 x 10^8 rad at a dose rate of 0.63 Mrad/h in a gamma facility at room temperature (about 30°C); and (3) irradiated to 9.3 x 10^8 rad at a dose rate of 0.73 Mrad/h and heated to 200°C. After irradiation and/or thermal treatment, the three samples and a baseline sample (no radiation or thermal treatment) were examined with X-ray diffraction and infrared spectroscopy. These samples were also leached in deionized water at room temperature for seven days, and the leachate analyzed for Cs and Sr.

The results of these tests indicated that neither heat nor irradiation affected the crystal structure or the leach resistance of the salt-occluded zeolite. X-ray diffraction and infrared spectra for the four samples were nearly identical, and the leachability results for all of the samples tested were the same within experimental error. The concentrations of Cs and Sr in all of the leachates were at or below detection limits. (The concentrations of Cs and Sr initially present in the salt-occluded zeolite were 1.96 and 0.965 wt %, respectively.) The pH values of the various leachates were also the same within experimental error. It is concluded that, for the conditions tested, the salt-occluded zeolite is stable with respect to radiation and heat.

---

[5]*Environmental Assessment Waste Form Selection for SRP High-Level Waste*, U.S. Department of Energy Report DOE/EA-0179 (July 1982).

c. Literature Review

Salt immobilization methods other than use of zeolites are also being explored, including the conversion of salt into ceramic or vitreous waste forms. A preliminary literature survey indicated that titanates and zirconates would also be attractive alternatives to zeolites. Several areas of concern with respect to these waste forms were addressed. One concern is whether ceramic waste forms could retain the cations predominant in IFR salt waste. Evaluators in several countries are considering a parallel question with respect to PUREX wastes. Some conclude that ceramics would be a superior waste form, while others disagree. Another concern is what processes could be used to extract the cations from the salt and incorporate them into titanates, zirconates, oxides, or silicates. Several reports describe carrying out such processes to prepare materials for various non-nuclear applications. Analysis of such literature will enable an evaluation of the applicability of these candidate waste forms to IFR wastes and help to identify conceptual processes for transforming the salt waste into these forms.

A second literature survey focused on finding insoluble chloride compounds, especially those that occur in nature. It was found that only silicates form complexes with chlorides that are not readily water soluble. One class of highly insoluble chloride-silicate minerals is sodalite, $Na_6[AlO_2]_6[SiO_2]_6 \cdot 2NaCl$, in which the halide salt is an essential constituent. This mineral has a crystal structure with a molecular cage similar to zeolites, and its Al/Si ratio is the same as that for zeolite A. Work to develop techniques for synthesizing monolithic sodalite structures containing IFR waste salt was initiated.

4. Metal Waste Handling

The initial work in this area has been focused on the use of copper as the matrix for immobilizing metal wastes. Because the Environmental Protection Agency (EPA) has identified cadmium as a toxic material, one of the early objectives has been to show that a Cu-Cd waste form would not be classified as a hazardous waste. The main effort has involved the preparation of copper alloy specimens containing Cd and La in a laboratory-scale distillation unit. These have been prepared by dissolving Cu and La in cadmium and distilling off the excess cadmium. During these preparations, data were obtained on cadmium vaporization into a flowing argon stream as a function of cadmium content (50 to 75 wt %), argon flow rate (30 to 500 mL/min), temperature (600 to 800°C), and pressure (atmospheric to 27 kPa). These data will be used to design a waste-metal distillation unit.

We found that the cadmium vaporization rate was primarily controlled by diffusion in the condensed phase and was strongly affected by temperature and surface oxidation. The rate was less affected by pressure or argon flow rate. The cadmium vaporization rate was also determined to be linearly dependent on the vapor pressure of pure cadmium. Assuming ideal solutions, which is a reasonable assumption for a Cu-Cd system, the data can be extrapolated to mixtures with nonvolatile components (e.g., copper) to determine the vaporization flux. With the assistance of computer modeling and the experimental data, a temperature-time profile was developed for a distillation run which optimizes efficiency and prevents splattering and solidification by keeping the effective vapor pressure within a prescribed range. This profile was used in the preparation of Cu-Cd and Cu-Cd-La alloys, but more experiments are needed to gain

a better understanding of the relationship between the vapor pressure and cadmium vaporization from more complex metal mixtures. A conceptual design of a waste-metal distillation unit has been started. Materials of construction and operating parameters have been identified with the knowledge gained from the laboratory-scale tests.

Several Cu-Cd alloys (10 to 80 wt % Cd) have been subjected to the Toxicity Characteristic Leaching Procedure (TCLP), which is used to determine if a waste containing a toxic component is hazardous. The alloy samples specified for the TCLP must be less than 9.5 mm in diameter. These samples are tumbled for 18 h in an acetic acid solution (pH = 5). In the present TCLP tests, the milling of the brittle Cu-Cd alloys produced fine particles, from which cadmium was rapidly leached so that the leachate contained more than 1 mg/L of cadmium, which is considered a threshold hazardous level. However, the test results, when extrapolated to copper alloys with only a few percent cadmium (the expected level in IFR waste forms), indicated that such alloys would pass the TCLP and thus would be considered by the EPA as nonhazardous with respect to cadmium content.

5. Waste Form Assessment

Regulations and publications on acceptance of high-level waste for disposal were reviewed to obtain foresight on requirements for acceptance of IFR waste. The perceptions resulting from this review were that acceptance would probably depend on (1) specifications devised in agreement with the DOE Office of Civilian Radioactive Waste Management (OCRWM) during waste form development and production, (2) judgment by the repository licensee (DOE-OCRWM), and (3) the final waste acceptance specifications that evolve in the repository-licensing process.

To assess the performance of a geologic repository, with particular emphasis on the containment of long-lived radioisotopes such as ^{99}Tc, we reviewed the literature on the release rates of technetium from various waste forms and the behavior of technetium in a geologic environment. The experimental data reported by various investigators indicate that a source term for computer predictive modeling of IFR waste performance may be established if congruent dissolution and congruent leaching are assumed. A number of geochemical and performance assessment codes may be used to calculate a source term for a specific geologic environment and the subsequent migration of technetium through the geosphere. However, because the pyroprocessing of the IFR waste is still in the developmental stage, it is premature to select a performance assessment code at this time. Nevertheless, for conceptual development of an IFR waste form, the EQ3/6 computer code[6] is being acquired to study the interaction of groundwater with the IFR waste form. This code will be used to establish the source term for the important radionuclides present in the IFR waste and to support performance assessment of the IFR waste forms under conditions of geologic disposal.

---

[6]W. L. Bourcier, *Geochemical Modeling of Radioactive Waste Glass Dissolution Using EQ 3/6: Preliminary Results and Data Needs*, Lawrence Livermore National Laboratory Report UCID-21862 (1990).

VII. ACTINIDE RECOVERY

A new technology under development in CMT is a pyrochemical process for recovering actinides, particularly the transuranic (TRU) elements, in spent fuel from a Light Water Reactor (LWR). These elements constitute a valuable energy resource in that they could be used in Integral Fast Reactor (IFR) fuel (see Sec. VI). Moreover, removal of these elements from LWR spent fuel would significantly reduce the quantity of long-lived radioisotopes that would otherwise be disposed in a geologic repository.

Two conceptual processes are being developed in CMT for recovery of TRU elements: a salt transport process and a magnesium extraction process. In both processes, the LWR spent oxide fuel is reduced to metallic components by reaction with calcium metal in a two-phase (liquid metal and molten salt) system. The concentrated TRU product from these processes can be incorporated into the IFR fuel cycle, where it can be purified and fabricated into fuel pins. These high-temperature (~800°C) processes are based on work done at ANL during the 1960s and 1970s.

A. *Flowsheet Development*

Flowsheets have been developed for the salt transport and magnesium extraction processes. These flowsheets are summarized below.

The major steps for both processes are the same: (1) the oxide fuel is declad, (2) the declad fuel is reduced with calcium in the presence of $CaCl_2$-CaF_2 salt, (3) the TRU elements are separated from the uranium and collected in a volatile metal solvent, (4) the TRU elements are recovered by evaporating the metal solvent and cast into an ingot for charging to the IFR electrorefiner, (5) the uranium-rich product is cast into an ingot and stored for later use, and (6) the CaO reduction product is electrochemically decomposed to recover the salt and calcium for recycle.

Removal of the fission products from the TRU-containing ingot is desirable but not necessary because the IFR electrorefining will remove them. In both processes, the alkali and alkaline earth metals are not reduced and remain in the salt. In addition, I, Te, and two rare earths (Sm and Eu) remain in the reduction salt. Approximately 2% of the salt is discarded after each calcium reduction step to control the concentration of these elements. The salt transport and magnesium extraction processes include an extraction step that separates the TRU elements from the less reactive metals. Although these metals would be removed effectively in the IFR electrorefiner, this separation lessens the required cadmium-anode processing. Neither of the processes separates the bulk of the rare earth metals from the TRU elements; therefore, these must be separated in the IFR electrorefiner.

The salt transport process employs a salt extraction step to transfer the TRU elements from a Cu-Mg alloy to a Zn-Mg alloy. The "nobler" (less reactive) metals collect in the Cu-Mg alloy. A portion of this alloy is discarded after recovery of the magnesium by evaporation. The resultant copper-noble metal alloy may be a suitable waste form for disposal in a geologic

repository. Most of the Cu-Mg alloy is recycled to the salt recovery step, where it serves as a cathode to collect calcium. The resultant Mg-Cu-Ca is the reductant for the next reduction step. The Zn-Mg alloy is distilled and recycled, and the remaining TRU elements are cast into an ingot, which contains about equal amounts of TRU elements, rare earth metals, and uranium.

The magnesium extraction process collects the reduced fuel as U-10 wt % Fe alloy. The TRU elements are recovered from this alloy by multiple extractions into a liquid magnesium phase, which is immiscible with uranium. The rare earth metals, some of the nobler metals, and a small amount of uranium also are extracted. The magnesium is distilled from the extract and recycled, and the TRU-rich material is cast into an ingot for charging to the IFR electrorefiner.

Because a portion of the neptunium (~20%) precipitates along with the uranium in the reduction step of the salt transport process, the uranium product is melted and cast in the presence of a $CaCl_2$-CaF_2-UCl_3 salt (halide slagging), which extracts the residual neptunium from the uranium phase. The resultant salt is recycled to the reduction step. Similarly, neptunium is not extracted adequately by the magnesium in the magnesium extraction process; therefore, the U-Fe alloy is also contacted with $CaCl_2$-CaF_2-UCl_3 salt to extract neptunium prior to casting. Again, this salt is recycled to the reduction step.

Laboratory-scale (25-100 g simulated fuel) testing is being done to evaluate each process step for both flowsheets (Sec. VII.C). The objective of this testing is to select the best process for further development.

B. *Materials Development*

The processes for recovering actinides from LWR fuels for use in an IFR require containment vessels, stirrers, filters, and transfer tubing. The stability of materials used in these components is an important factor in determining the success or failure of the candidate process. The demands made on materials are stringent. First, the liquid metal solvents (e.g., Cu-Mg) and the molten calcium and alkaline earth halide salts should not react excessively with the containers and other components. In addition, to allow repeated use of the containers as molds for TRU product solidification, they should not be susceptible to wetting by these metals, salts, or radioactive materials. Second, the materials should withstand high temperatures, should not vaporize appreciably, should be chemically stable, and should possess good mechanical strength and thermal shock resistance in pyrochemical environments pertinent to actinide-recovery processes. Third, the materials should be sufficiently dense or porous, depending on the specific applications, and still have the mechanical integrity needed in the aggressive chemical and thermal environments. Finally, the technology for fabrication of components should allow scaleup from laboratory to commercial size.

The candidate materials for these high-temperature operations can be either refractory metals, ceramics of appropriate compounds, or metal-oxide composites. The ceramic materials being evaluated for their mechanical properties and corrosion resistance include oxides (yttrium oxide, magnesium oxide, chrome spinel, chrome alumina, calcium zirconate, calcium yttrate, calcium titanate), nitrides (aluminum nitride and titanium nitride), carbides (titanium carbide and tantalum carbide), and titanium carbonitride.

During the past year, preliminary corrosion experiments were performed on the above ceramic materials, which were fabricated at ANL in crucible and test coupon shapes, either by cold pressing followed by sintering or by hot pressing. The exceptions to fabrication at ANL were titanium carbide and titanium carbonitride (obtained from Materials and Electrochemical Research Corp.), aluminum nitride (from Technical Ceramics Laboratory), and chrome spinel and chrome alumina (from Carborundum Co.). These corrosion experiments consisted of exposing the materials to molten calcium or molten $CaCl_2$-15 wt % CaF_2 saturated with calcium at 900°C for 26 h. Following the exposure, the materials were cross-sectioned and metallographically prepared for optical and scanning electron microscopy and energy dispersive X-ray analysis.

The results led to several observations. First, severe corrosion occurred in all of the oxide ceramics (in some cases the ceramic completely disintegrated), although corrosion, in general, was less severe in the CaO-based ceramics (i.e., calcium zirconate, calcium yttrate, and calcium titanate) than in single-oxide ceramics. Second, the presence of impurities such as alumina exacerbated corrosion. Third, a reaction layer formed on aluminum nitride but appeared to be protective. Finally, carbide and nitride ceramics may be more promising as container materials than oxide ceramics. Further work is necessary to confirm their long-term chemical stability in the molten-salt and molten-metal environments of interest in the actinide recovery processes.

C. *Laboratory-Scale Testing*

Laboratory-scale testing in an argon-atmosphere glovebox is being conducted to evaluate the process flowsheets. When sufficient experimental data have been obtained, we will select the best process concept for further development. The selection criteria include simplicity of equipment and operation, high TRU recovery, adaptation to large-scale operation, and minimum materials corrosion.

These experiments over the past year have concentrated on the reduction and, where applicable, the extraction steps. The reduction step is essentially the same for both flowsheets and consists of the reaction of calcium with simulated LWR fuel in a $CaCl_2$-CaF_2 salt. The reduced fuel is collected in a metal phase. It is the metal phase and subsequent treatment of this phase which differs for the flowsheets. The simulated LWR fuel (25-100 g) consisted of a mixture of UO_2, PuO_2, NpO_2, CeO_2, Nd_2O_3, Eu_2O_3, Sm_2O_3, ZrO_2, MoO_3, RuO_2, Pd, BaO, SrO, and Cs_2UO_4, with the UO_2 making up ~98% of the total weight.

The experimental results indicate that the reduction of the actinide oxides is quite good, averaging above 99% for both processes. Those fission product oxides whose chlorides are more thermodynamically stable than $CaCl_2$ (i.e., $BaCl_2$, $SrCl_2$, $EuCl_2$, CsCl, and possibly $SmCl_2$) were expected to be converted to the chloride rather than the metal and remain in the salt phase. As expected, Ba, Sr, and Eu fission products remained in the reduction salt, while the Cs and Sm fission products distributed approximately 2/3 to the reduction salt and approximately 1/3 to the metal phase. The Ce and Nd fission products were completely in solution in the metal phases, and the noble metal fission products (Pd, Ru, Zr, and Mo) were reduced and transferred to the metal phase. Because of the low concentrations of these noble metal fission products, we have experienced some difficulty in obtaining reliable chemical analyses. Some of these noble metals

are probably in solution in the metal phases, whereas others are probably precipitated as intermetallic compounds.

The laboratory-scale experiments also included testing the extraction steps in the salt transport and magnesium extraction processes. In the salt transport process, the TRU elements, Ce, and Nd are extracted from the Cu-Mg reduction (donor) alloy with $MgCl_2$, leaving the noble metal fission products and uranium behind. They are subsequently stripped from the $MgCl_2$ using a Zn-Mg (acceptor) alloy. This is a multistep operation requiring a number of donor and acceptor cycles. Experimental results obtained after three cycles indicate that most of the Pu, Am, Ce, and Nd was extracted from the Cu-Mg alloy. The plutonium nearly completely transferred to the Zn-Mg acceptor alloy, whereas portions of the Am, Ce, and Nd were retained in the $MgCl_2$. Since the $MgCl_2$ would be reused in the salt transport process, the Am, Ce, and Nd would represent an in-process inventory. Extraction of the neptunium from the Cu-Mg alloy was complicated because a portion of it precipitated along with the uranium and was unavailable for extraction. A halide slagging step will be required to extract the residual neptunium.

The magnesium extraction process also requires multiple extraction steps. The magnesium is separated from the extracted elements by retorting and is then recycled. Our experimental results obtained after three extractions indicate that Pu and Am are readily extracted, whereas the Np is not. As with the salt transport process, a halide slagging step will be required to extract the remaining neptunium.

Additional laboratory-scale experiments are planned to better define the behavior of the spent fuel components in each process step and the optimum parameters (temperature, composition, agitation, etc.) for each step. For example, experiments will be done to determine the minimum amount of excess calcium required to achieve >99.5% reduction of the oxides, the effect of a second reduction step on achieving >99.9% reduction, and the behavior of the noble metals in the process. In addition, preliminary studies on retorting to recover and consolidate the TRU product are planned.

D. *Development of Calcium/Salt Recovery Method*

An initial step in the pyrochemical processes for recycling LWR actinides to an IFR employs calcium to reduce the oxide fuel. The CaO reduction product dissolves in the $CaCl_2$-CaF_2 molten salt. When the CaO nears saturation, the reduction reaction becomes slow, and the salt must be purified or discarded. To minimize wastes, use of an electrochemical cell with a liquid metal (Zn or Cu-Mg) was proposed to recover the salt and calcium for recycle by converting the CaO back to calcium metal.

Preliminary experiments were undertaken to evaluate the electrolysis of CaO in molten $CaCl_2$-CaF_2. In the electrolysis, the cathode reaction generates calcium in the liquid electrode, and the anode reaction yields CO and CO_2 gas. Thus, the oxygen from the oxide fuel is removed as gas, which can be scrubbed and released. Because the salt and calcium can be recycled, waste is minimized. If zinc is used as the cathode, pure calcium metal is recovered by distilling off the zinc. The Mg-Cu cathode is employed for the flowsheet that uses Mg-Cu-Ca alloy as reductant.

The electrolysis experiments were conducted with a specially designed electrochemical cell in a helium-atmosphere glovebox. The cell vessel was a high-density MgO crucible (ID of 90 mm, depth of 150 mm, and wall thickness of 1.5 mm). This crucible contained the electrolyte, the electrodes, a porous anode shroud, and a stirrer (triangular tungsten paddle). The cathode was a pool of liquid zinc or liquid Cu-Mg alloy with an insulated tungsten electrical conductor. Two different anode designs were used: a carbon or graphite rod and a hollow graphite tube to facilitate collection of product-gas samples. The cell was operated either in a constant-current or constant-voltage mode at 800°C. The cell potential was generally limited to less than 2.7 V, the reversible decomposition potential for $CaCl_2$ with a zinc cathode.

The experimental results demonstrated that the electrochemical cell can recover reduction salt and calcium metal in either a zinc or Cu-Mg liquid metal cathode. The process was reproducible under the established conditions. Current efficiencies were excellent--80% with the zinc cathode and 71% with the Cu-Mg cathode. Initial current densities were 250 mA/cm^2 with the zinc cathode and 170 mA/cm^2 with the Cu-Mg cathode. (Current densities of at least 1 A/cm^2 will be required for a practical processing system.) Both CO and CO_2 were released at the carbon anode. However, no chlorine was detected in samples of effluent gas from the anode. Thus, no $CaCl_2$ was decomposed even when the cell voltage was deliberately increased to 3.4 V.

A major problem encountered in the early experiments was carbon contamination of the molten-salt electrolyte. Carbon particles were dislodged from the anode surface during the electrolysis and as a result of chemical reduction of carbonates, which form by reaction of CO_2 from the anode with CaO in the salt. The accumulation of carbon dust in the electrolyte may cause short circuiting and voltage oscillation. Most important, carbon makes the salt unsuitable for recycling without filtering. Therefore, we developed a porous anode shroud to prevent contamination of the bulk salt with carbon dust.

Experimental work is continuing on development of a porous anode shroud that has good corrosion resistance, adequate porosity with the correct pore size and open fraction, and fabricability in sizes large enough for engineering scale (~20 kg simulated fuel) experiments. Methods are being explored to increase the electrolytic current density to >1 A/cm^2.

E. *Engineering-Scale Testing*

Equipment and facilities are needed to demonstrate recovery of actinides from approximately 20 kg of simulated LWR fuel by the processes presently under development. The processes to be carried out include reduction of the oxide fuel to metal, separation of uranium from the other actinides in suitable forms for storage and eventual use as feed for the IFR, separation of other fission products, and regeneration of the reagents used in the process to minimize waste.

Design of the needed facilities and equipment is underway. The design of an argon-atmosphere glovebox, which will contain most of the equipment, is almost complete. The room in which it will be constructed has been emptied and prepared for equipment installation.

Radiation estimates are being made for the anticipated operations to be performed in this glovebox. The primary radiation sources of concern are (1) neutrons from both spontaneous fission of Pu, Am, and Cm isotopes and alpha/neutron reactions from high-energy alpha particles in low-atomic-number process fluids, and (2) gamma rays from americium isotopes. Fortunately, the concentrations of the most prolific sources of neutrons and gamma rays (Am and Cm) are very low in simulated LWR spent fuel; nevertheless, we are calculating these concentrations to quantify the expected radiation levels. Preliminary calculations indicate that curium levels must be kept very low (~10 mg or less), and americium levels must be kept slightly below the levels expected in LWR spent fuel to meet the allowable personnel dose levels. Local shielding will probably be required in small areas such as the retort, where the product will be consolidated, and around storage areas.

VIII. APPLIED PHYSICAL CHEMISTRY

The program in applied physical chemistry involves studies of the thermodynamic, thermophysical, and transport behavior of selected materials in environments simulating those of fission and fusion energy systems.

A. *Liquidus-Solidus Temperatures and Viscosities of Core-Concrete Mixtures*

Thermophysical properties of core-concrete mixtures are being measured in this research program. Such mixtures are expected to occur during the molten core-concrete interaction (MCCI) phase of severe accidents at light-water nuclear reactors. The MCCI phase is preceded by a series of other phases: loss of coolant, heatup and degradation of the reactor core (urania and its fission products, Zircaloy cladding, control rods, and structural materials), melting of the stainless-steel vessel, and collapse of the hot core debris and melted vessel onto the concrete basemat. A knowledge of the thermophysical properties of the solids, liquids, and gases that exist during the MCCI phase is crucial for understanding and modeling the consequences of the accident. The results of this research will be incorporated in thermal hydraulic codes such as CORCON,[1] which is an integral part of the Source-Term Code Package[2] for the Nuclear Regulatory Commission (NRC). (The amount of a fission product that is released in an accident is called its "source term.") In addition, our experiments are designed to aid researchers in ANL's Reactor Engineering Division in analyzing results from their large-scale (~500 kg) MCCI experiments, which are being performed under international sponsorship (the ACE Consortium).

In earlier experiments,[3] sponsored by the Electric Power Research Institute (EPRI), we conducted source-term measurements of the vaporization of refractory fission products from core-concrete mixtures. Our current experiments are concerned with two other important properties of the core-concrete mixtures: liquidus-solidus temperatures and viscosities. The liquidus-solidus temperatures are being measured by differential thermal analysis (DTA) in a program sponsored by the NRC. (Liquidus temperatures are the onset of solidification; solidus temperatures are the onset of melting.) In our experiments, these temperatures range from 1175 K (solidus) to greater than 2850 K (liquidus), depending on the sample composition. The viscosities are being measured by rotational viscometry in a program sponsored by the ACE Consortium.

---

[1] R. K. Cole, Jr., D. P. Kelly, and M. A. Ellis, *CORCON-Mod2: A Computer Program for Analysis of Molten Core-Concrete Interactions*, U.S. Nuclear Regulatory Commission Report NUREG/CR-3920 (1984).

[2] J. A. Gieseke, P. Cybulskis, H. Jordan, K. W. Lee, P. M. Schumacher, L. A. Curtiss, R. O. Wooton, S. F. Quale, and V. Kogan, *Source Term Code Package*, U.S. Nuclear Regulatory Commission Report NUREG/CR-4587 (1986).

[3] M. F. Roche, L. Leibowitz, J. L. Settle, C. E. Johnson, R. C. Vogel, and R. L. Ritzman, Nucl. Technol. **96**, 96 (1991).

1. Differential Thermal Analysis Experiments

In the previous report in this series,[4] we presented DTA measurements of solidus and liquidus temperatures for three types of concrete (limestone, limestone-sand, and siliceous) and for their mixtures at 27.5 wt % calcined concrete with UO_2-ZrO_2 (1.6:1 mole ratio of UO_2 to ZrO_2). In addition, we presented preliminary curves of liquidus-solidus temperatures for the three concretes with UO_2-ZrO_2.

During this report period, we continued DTA measurements of liquidus-solidus temperatures on concretes and their mixtures with UO_2-ZrO_2. In the experiments, the samples, which weigh up to 20 g, are held in covered molybdenum crucibles (9 cm^3) that rest on a sample thermocouple within a high-temperature furnace cavity. A gas of Ar-3% H_2 (at a pressure of about 0.03 MPa) is added to the furnace cavity to minimize vaporization losses to less than 2% of the sample mass. The output from the sample thermocouple is compared with that from a control thermocouple which drives a furnace, via a programmable power supply, between two temperature limits at a prescribed linear rate (e.g., 1173 to 2673 K limits at a rate of 30 K/min). The peaks in the resulting DTA curves on heating and cooling are related to the liquidus and solidus temperatures.

In recent DTA experiments with samples containing limestone concrete (60 wt %) and UO_2-ZrO_2 (40 wt %), we experienced difficulty in obtaining satisfactory DTA curves because of problems between the sample thermocouple and the crucible base. As a result, new crucibles and lids for use in our DTA experiments were machined from molybdenum rod stock. The base of the crucibles (1.9-cm OD and 3.8-cm height) contains a specially designed thermocouple well (0.5-cm dia and 1-cm height) that provides a high sensitivity to the thermal events occurring in the sample. We derived DTA curves for 6.6 g of an alumina standard (Standard Reference Material 742 from National Institute of Standards and Technology) in one of the new crucibles. The curves, which were computed directly from the sample and control thermocouple signals without any electronic amplification, showed that the new crucibles provide a high level of sensitivity to thermal events; the peaks were easily distinguished from background.

We conducted DTA measurements of the eutectic temperature and composition in the UO_2-CaO system to resolve significant differences in the previously published phase diagrams.[5,6] Our experiments employed the new crucibles, and they were conducted using a carefully controlled atmosphere (flowing Ar-3% H_2 at a pressure of about 0.015 MPa and at a monitored water-vapor concentration of less than 5 ppm). Seven UO_2-CaO samples were tested with urania concentrations of 30 to 60 wt %. Figure VIII-1 is an example of the DTA curves for one of the seven samples (37 mol% UO_2). It shows the eutectic temperature at 2218 K (1945°C). This value is 135 K lower than that given by Alberman et al.[5] and 95 K higher than that given by

---

[4]M. J. Steindler et al., *Chemical Technology Division Annual Technical Report, 1990*, Argonne National Laboratory Report ANL-91/18, pp. 129-132 (1991).

[5]K. B. Alberman, R. C. Blakely, and J. S. Anderson, J. Chem. Soc., p. 1352 (1951).

[6]J. Holc and D. Kolar, J. Solid State Chem. **61**, 260 (1986).

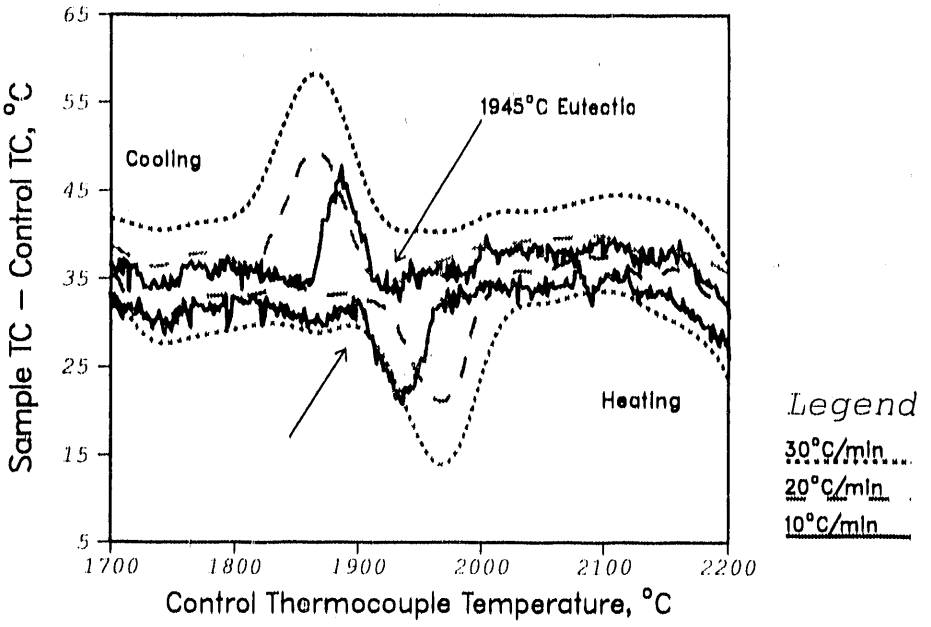

Fig. VIII-1. Curves from Differential Thermal Analysis of 37 mol % Urania-63 mol % Calcia on Heating and Cooling (TC = Thermocouple)

Holc and Kolar.[6] Our confidence in this eutectic temperature (±5 K) is based on measurements with four different sample thermocouples, as well as the alumina-standard calibration. Figure VIII-2 presents eutectic-peak areas vs. sample compositions determined from our DTA curves. The triangle shown in this figure is derived from the compositions for the solid solution (70 mol % UO_2) and eutectic (37 mol % UO_2) given by Holc and Kolar[6]; the height of the triangle is normalized to our data. Our solid-solution and eutectic compositions support the data of Holc and Kolar and do not agree with those of Alberman et al.,[5] who place the solid-solution boundary at 53 mol % UO_2 and the eutectic composition at 45 mol % UO_2. Our revised phase diagram for the UO_2-CaO system is shown in Fig. VIII-3. It was calculated using our eutectic temperature, the composition data of Holc and Kolar,[6] and the chemical thermodynamics program F*A*C*T (product of Thermfact Ltd., Mount-Royal, Quebec, Canada).

Table VIII-1 presents solidus and liquidus temperatures from our earlier DTA experiments[4] on mixtures having a UO_2-ZrO_2 mole ratio of 1.6:1. Also given in this table are preliminary results of solidus and liquidus temperatures calculated by Mignanelli[7] for our sample compositions. The experimental and calculated solidus temperatures presented in Table VIII-1 are in reasonable agreement. The disagreement between experimental and calculated liquidus temperatures appears to be roughly proportional to the amount of calcia in the calcined concrete (72 wt % in limestone, 36 wt % in limestone-sand, 15 wt % in siliceous). We expect that incorporation of our UO_2-CaO phase diagram (Fig. VIII-3) in the thermodynamic data base now being employed by Mignanelli will significantly improve the agreement between our experiments and his calculations.

---

[7]M. A. Mignanelli, Atomic Energy Authority, Harwell, private communication (1991).

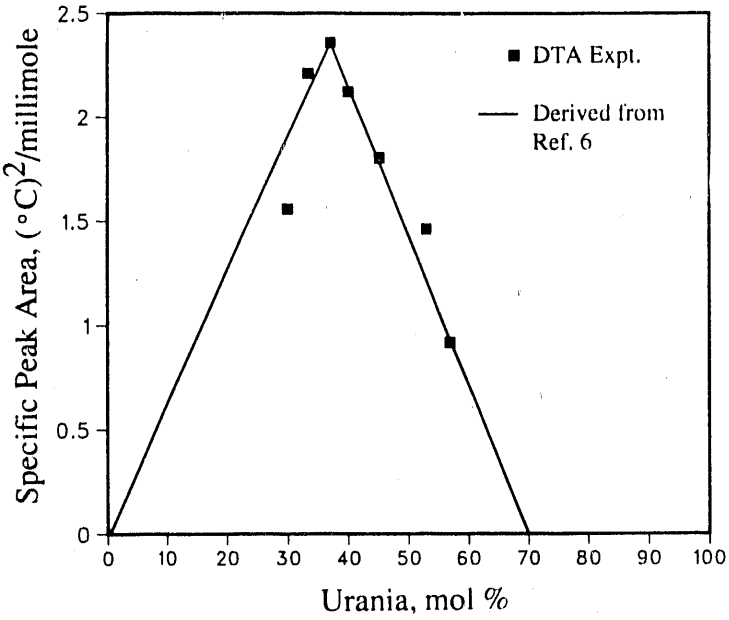

Fig. VIII-2. Areas of 2218 K (1945°C) Eutectic Peaks Derived from DTA Experiments with Urania-Calcia Samples and from Data of Holc and Kolar[6]

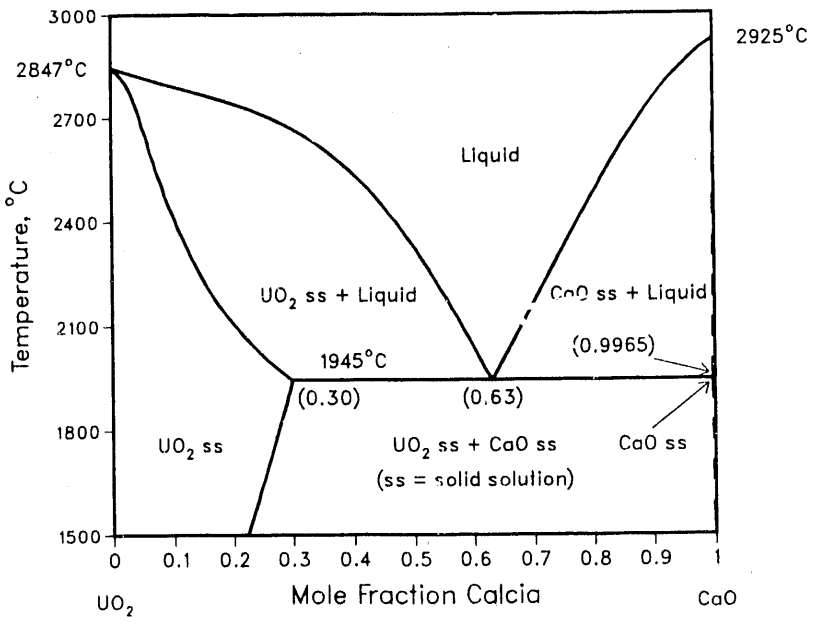

Fig. VIII-3. Phase Diagram for UO_2-CaO System

Table VIII-1. Experimental and Calculated Solidus and Liquidus Temperatures for Mixtures of 27 wt % Concrete with UO_2-ZrO_2 (1.6:1 mole ratio)

Concrete with UO_2-ZrO_2	Solidus Temp., K		Liquidus Temp., K	
	DTA[4]	Calc.[7]	DTA[4]	Calc.[7]
Limestone	1520	1550	>2723	2320
Limestone-Sand	1360	1450	>2638	2490
Siliceous	1412	1434	2549	2395

We plan to continue DTA experiments with additional core-concrete compositions to provide more data for calculation of liquidus-solidus curves.

2. Viscosity Experiments

We have measured the viscosity for eight mixtures of UO_2-ZrO_2 (1.6:1 mole ratio) with calcined concrete: one with siliceous concrete, four with limestone concrete, and three with limestone-sand concrete. The mixtures, which weighed 150 to 200 g and had a volume of about 30 cm^3, were heated to temperatures as high as 2850 K within the hot zone of a molybdenum-tungsten alloy (70Mo-30W) furnace tube. The furnace tube was continuously purged by Ar-3% H_2 gas to ensure retention of the urania in the U^{4+} state. A Brookfield programmable viscometer equipped with a 70Mo-30W alloy spindle that was immersed in the molten sample was employed to measure its viscosity as a function of spindle rotation rate.

Viscosities were measured for a mixture of siliceous concrete (27.5 wt %), urania (56.6 wt %), and zirconia (15.9 wt %) over the temperature range 2004-2595 K. The measured solidus and liquidus temperatures for this particular mixture are 1412 and 2549 K, respectively (see Table VIII-1). Therefore, the viscosity measurements extended from above the liquidus well into the liquidus-solidus temperature range. This sample exhibited Newtonian behavior (a viscosity independent of spindle rotation rate) over the temperature range 2367-2595 K. This behavior is expected of a single phase fluid or a fluid with only a minor volume fraction of solids. However, as the temperature was decreased further into the liquidus-solidus region, the sample exhibited non-Newtonian behavior, called shear thinning (the viscosity decreased significantly with increasing rotation rate). This shear thinning is due to the presence of a significant fraction of undissolved solids at the lower temperatures. The large increase (a factor of about 1000) in viscosity with decreasing temperature is another indication of increasing solids content.

Viscosities were also measured for a mixture of limestone-sand concrete (27.5 wt %), urania (56.6 wt %), and zirconia (15.9 wt %) over the temperature range 2287-2467 K. The measured solidus and liquidus temperatures for this particular mixture are 1360 and >2638 K, respectively (see Table VIII-1). Therefore, these viscosity measurements were conducted on a mixture of solid and liquid within the liquidus-solidus temperature range. The sample exhibited a remarkable degree of shear thinning; the viscosity was approximately

inversely proportional to rotation rate. We attribute the shear thinning to a competition between the shearing force exerted by the spindle and sintering of the solids in the solid-liquid mixture. Indeed, in the absence of stirring, the sample thickened considerably, and a large force was then required to reestablish flow. Viscosity measurements on this sample were extended to temperatures as high as 2850 K. At that temperature, the sample behavior was nearly Newtonian [the viscosity ranged from about 1.2 Pa•s (1.2 x 10^3 centipoise) at 10 rpm to 0.6 Pa•s (0.6 x 10^3 centipoise) at 200 rpm], which indicated that the volume fraction of solids was low. The viscosity measurements indicate that the liquidus temperature is >2850 K. Note that this is a more accurate limit when compared to the DTA value (>2638 K). This improvement is due to the higher temperature capabilities of the viscosity apparatus.

The viscosity of the mixture of limestone concrete (27.5 wt %), urania (56.6 wt %), and zirconia (15.9 wt %) could not be measured because of a large volume fraction of solids, even at temperatures as high as 2850 K. This indicates that the liquidus temperature is much greater than 2850 K (the DTA measurements listed in Table VIII-1 showed it to be greater than 2723 K). Viscosities measurements were possible on mixtures of UO_2-ZrO_2 (1.6:1 mole ratio) with 36 and 60 wt % limestone concrete over the temperature range 2000-2850 K. These data, which are being analyzed, also indicate liquidus temperatures in excess of 2850 K because of the non-Newtonian behavior of the viscosity.

The above viscosity data differ significantly (typically, two orders of magnitude) from the viscosity estimates now being employed in thermal hydraulic codes such as CORCON. Since the viscosity affects heat transfer, release of fission products, and a variety of other important processes in the MCCI phase such as melt spreading and cooling, it is important to have reliable data for incorporation in the codes. We therefore plan to extend this work to provide improved correlations of viscosity versus composition for a broad range of core-concrete mixtures.

B. *Metal Fuel Property Studies*

Measurements and analyses are being performed to provide needed information on the thermodynamic and transport properties of Integral Fast Reactor (IFR) fuel. In 1991, this effort was focused on determining phase relations in the U-Fe-Zr system, measuring thermal conductivity of ternary IFR fuel alloys, and determining the behavior of actinides and lanthanides in IFR alloy systems.

1. Phase Studies of U-Fe-Zr System

An important area in the IFR development is chemical interactions between the U-Pu-Zr fuel and steel claddings (HT9, D9, or Type 316). Cladding integrity could be compromised by formation of liquid phases during fuel irradiation. We have been examining simpler systems than actual fuel-cladding mixtures to clarify phase relations in those systems. We have previously presented our results on the U-Zr[8] and U-Fe systems.[9] We have now

[8]L. Leibowitz, R. A. Blomquist, and A. D. Pelton, J. Nucl. Mater. **167**, 76 (1989).
[9]L. Leibowitz and R. A. Blomquist, J. Nucl. Mater. **184**, 47 (1991).

performed some preliminary DTA experiments of the U-Fe-Zr system. A sample with a composition of 43.8 at. % U-43.5 at. % Fe-12.7 at. % Zr was heated in an yttria crucible at 10 K/min to about 1850 K, after which several heating/cooling cycles were initiated at various rates. The DTA curves derived from these heating/cooling cycles were found to be similar to those previously derived for the U-Fe system.[9] We also compared the U-Fe results with those of Fe-(U,Zr) and HT9-(U,Zr), where U-10 wt % Zr fuel was used for the (U,Zr). (These alloys had roughly the same atomic U/Fe ratio.) A marked peak in the DTA curves for U-Fe was due to a eutectic at 998 K in that binary system. The major peak in the other systems occurred at close to the same temperature; other peaks in the DTA curves were very small. Preliminary phase diagram calculations for the U-Fe-Zr system indicated that the composition of the ternary eutectic is very close to the U-Fe binary edge. Further study and modification of the calculations are in progress, and the results will be reported when complete. We are proceeding with scanning electron microscopy examination of the ternary residues from the DTA experiments and are planning a similar test with a plutonium-containing alloy.

As part of our standard practice, a recalibration of the DTA system was performed during this reporting period. We measured melting points of five high-purity metals (Al, Cu, Ni, Pb, and Sn), including two Standard Reference Materials (SRM) obtained from the National Institute of Standards and Technology (NIST). The standards were SRM 44e (aluminum) and SRM 45d (copper). Several DTA heating and cooling cycles were performed for each material at about 10 K/min. Previous experience revealed essentially no differences between melting points obtained at 1 and 10 K/min. Repeat determinations showed a range of, at most, 3 K. A calibration curve based on these results has been prepared and will be applied to reported values, as done in the past. As an additional improvement to our DTA system, we have acquired a differential scanning calorimetry head for the instrument, which will allow enthalpy measurements to be performed. This device also requires extensive calibration.

2. Thermal Conductivity Studies

Efforts have been initiated to test our thermal conductivity instrument with 1.3-cm (1/2-in.) dia samples of ternary IFR fuel. This device was designed to use 2.5-cm (1-in.) dia samples, which were unavailable for ternary IFR fuel alloys. Discussions with the instrument manufacturer (Holometrix Inc., formerly Dynatech Inc.) indicated that measurements with the smaller diameter samples would be possible with some sacrifice of accuracy. Testing with known materials showed that the thermal conductivity results with the smaller diameter samples were more sensitive to instrument conditions than were prior results with the larger diameter samples. Effort was, therefore, devoted to optimizing the instrument settings, after which measurements were performed over the accessible temperature range. These measurements employed samples of a stainless-steel thermal conductivity standard, SRM 1461, provided by NIST. In these measurements we used the SRM as both the reference and the unknown in our instrument. The goal was to determine how well we could reproduce the NIST data. Figure VIII-4 shows the NIST data as a solid line, the NIST-reported standard deviation as a shaded area, and our measurements as the filled circles. We believe that these results are satisfactory, and that our instrument will provide the necessary thermal conductivity data on ternary IFR fuel alloys when they become available.

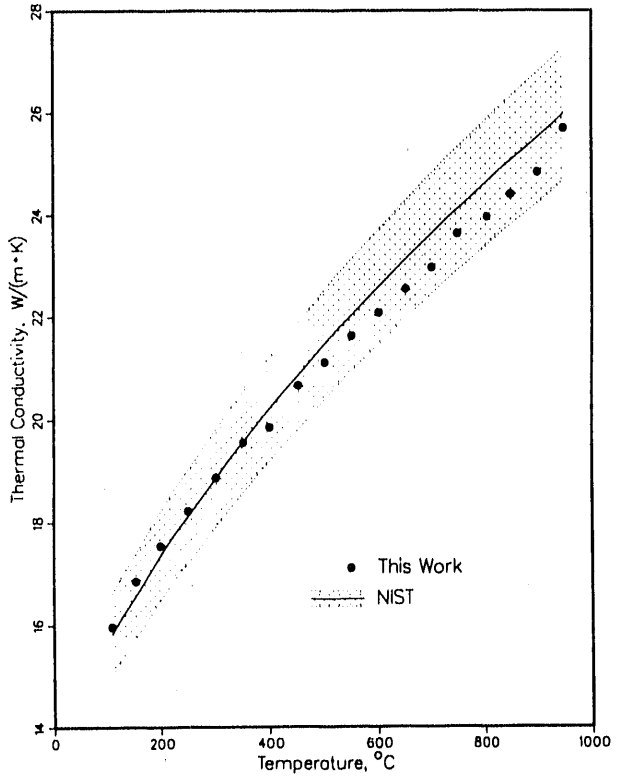

Fig. VIII-4.

Thermal Conductivity vs. Temperature Determined for Standard Reference Material (SRM 1461)

3. Behavior of Actinide and Lanthanide Alloys

Developments in the IFR program have drawn increased attention to the behavior of lanthanides and actinides in IFR fuel. Lanthanides appear to accumulate in the neighborhood of the cladding during irradiation, and the possible significance of this to fuel performance should be understood. The buildup and intentional addition of actinides to fuel also need to be considered. The behavior of the actinide and lanthanide elements during irradiation of IFR fuel, their influence on fuel performance, and the possible interactions between lanthanides and cladding are not easily predicted. In this section, we summarize our analysis of some of the basic chemistry and phase relations among these elements.

It might be expected that the lanthanides and the actinides would be very similar chemically and physically in that both series of elements form by the addition of electrons to an f shell. However, as reported last year,[10] the actinides are not simple analogues of the lanthanides. A great many properties of the actinide elements change markedly between Pu and Am, i.e., the heavier actinides are much more like the lanthanides than are the lighter actinides. This behavior can have important consequences for IFR fuel performance as well as recycling chemistry and should be understood.

---

[10]M. J. Steindler et al., *Chemical Technology Division Annual Technical Report, 1990*, Argonne National Laboratory Report ANL-91/18, pp. 143-144 (1991).

Some of the lanthanide and actinide binary phase diagrams of importance to the IFR program exist in the literature. Others, however, do not. In the absence of experimental data on many important systems of interest, the familiar techniques of thermodynamic modeling and phase diagram optimization cannot be applied. Calculation of phase diagrams is being approached in a variety of ways, but to date no clearly satisfactory approach exists. The ultimate goal of calculating a binary phase diagram from basic properties of the constituent elements has not been reached. Some success has been achieved with various models, but our needs are made more difficult because of the extraordinary complexity of the actinides.

One approach which we followed was to use the model developed by Engel[11] and expanded by Brewer.[12] This model is an extension of the well-known observation that many intermetallic compounds exhibit a strong correlation between the number of electrons per atom and the crystal structure. For our interests, one of the important contributions by Brewer was the application of this model to actinides.

Engel recognized that the crystal structure of metals is highly correlated with the electronic structure. Roughly stated, this correlation is that the body-centered cubic (bcc), hexagonal close packed (hcp), and face-centered cubic (fcc) structures are respectively associated with one, two, and three s and p electrons. Application of these ideas to lanthanides and actinides is complicated because consideration must be given to f electrons. In addition to electronic configuration, other considerations must be dealt with in metallic solutions. For example, differences in atomic size and internal pressure will also influence the free energy of a solution. In general, the free energy is increased by a difference in atomic size except in certain cases, such as in Laves phases, in which higher packing density can be obtained.

Following Brewer, we performed calculations of the phase diagrams for three systems of interest, using the chemical thermodynamics program F*A*C*T. We chose two, Am-Pu and Pu-U, which have been reported in the literature, and one, Am-U, which has not. An important aspect of Brewer's ideas[12] is that the enthalpy of vaporization to be used in the regular solution model is the enthalpy for vaporization from the metal to a vapor of the same electronic state as exists in the condensed phase rather than to the normal (ground state) gas.

From these calculations, we found that the calculated Am-Pu phase diagram was a reasonable representation of the published phase diagram. This was not the case, however, for the calculated and the published Pu-U diagrams. It is not obvious how that calculation can be improved within the framework of Brewer's model. We are, therefore, unsure as to how much confidence we should have in the calculated Am-U diagram. Judging from the availability of d electrons in americium, we anticipate that americium would stabilize the close-packed fcc structure in plutonium, but it is not obvious how americium would interact with the complex structures of uranium. This model and the work that Brewer has already done on actinide

---

[11]N. Engel, ASM Trans. Quart. **57**, 619 (1964).

[12]L. Brewer, "Viewpoints of Stability of Metallic Structures," in *Phase Stability in Metals and Alloys*, eds., P. S. Rudman, J. Stringer, and R. I. Jaffe, McGraw-Hill, New York, p. 39 (1967).

systems could be used to make some reasonable predictions on unknown systems, but further study of this approach is needed.

Another approach to phase diagram calculations, developed chiefly by Kaufman,[13] has been applied to actinide and lanthanide systems by several workers with mixed success. This method is similar in concept to Brewer's in that both begin with the regular solution equations. Application of this model to unknown systems would, therefore, be of unpredictable reliability, particularly with regard to the complex actinides. One of the more extensive applications of Kaufman's ideas has been presented by Selle,[14,15] who calculated binary phase diagrams of the rare earth and actinide systems. Selle has extended the Kaufman method and thereby made possible approximate calculations for systems of interest to our program.

To test Selle's selection of values for stability and interaction parameters, we calculated the phase diagram for the Nd-Y system with these parameters and compared it with the experimentally derived diagram given by Massalski.[16] The computed curves were above the experimental curves for the Nd-Y phase diagram. Nevertheless, for the liquidus-solidus curves, the agreement was fairly good, especially considering that the experimental liquidus is given as uncertain in the Massalski diagram. This difference is greater for the bcc-hcp transformation. Part of this difference is due to the fact that the hcp structures for Nd and Y are slightly different. Since the estimation of the interaction parameters has a large uncertainty, we are not surprised that these small details of the Massalski phase diagram cannot be reproduced by the computations. This simple example probably gives a good indication of the accuracy that can be expected using the Kaufman methods and the parameters for the rare earths and actinides estimated by Selle.

Additional study concerning the influence of lanthanides and actinides on IFR fuel performance is needed. We have investigated some theoretical approaches to phase diagram calculation with mixed success. Our efforts at a combined theoretical and experimental approach to attaining this understanding are continuing.

C. *Fusion-Related Research*

A critical element in development of a fusion reactor is the blanket for breeding tritium fuel. We are conducting experimental and calculational studies with the objective of determining the feasibility of using lithium-containing ceramics (e.g., Li_2O, $LiAlO_2$, Li_4SiO_4, Li_2ZrO_3) as breeder material.

---

[13]L. Kaufman and H. Bernstein, *Computer Calculation of Phase Diagrams*, Academic Press, New York (1970).

[14]J. E. Selle, *Calculation of Intra-Rare Earth Binary Phase Diagrams*, EG&G Rocky Flats Plant Report RFP-4423 (1991).

[15]J. E. Selle, *Calculation of Binary Phase Diagrams Between the Actinide Elements, Rare Earth Elements, and Transition Metal Elements*, EG&G Rocky Flats Plant Report RFP-4450, in press.

[16]T. B. Massalski, Metall. Trans. A **20A**, 1295 (1989).

1. Temperature-Programmed Desorption from $LiAlO_2$

Data on the energetics and kinetics of desorption of $H_2O(g)$ and $H_2(g)$ from the surface of ceramic tritium breeders are needed in the fusion power program for predicting and modeling the release of tritium (in the forms of HTO, T_2O, HT, and T_2) from such breeders. An important issue being addressed is the effectiveness of H_2 as a promoter of tritium release. The temperature-programmed desorption (TPD) technique is well suited to provide such data and has been used in earlier work.[17]

In this report period, TPD experiments were run on $LiAlO_2$ (~0.5 g) that had been pretreated at 923 K for periods of 20 h to 12 days in a helium gas stream containing H_2 at concentrations of 247, 495, and 990 ppm (by volume). After such an exposure, the experimental system was cooled quickly to 473 K while the equilibrating gas composition was maintained. During the TPD run, the temperature was increased from 473 to 1073 K at a rate of 5.6 K/min. The sweep gas during the TPD run was either pure helium or the same He-H_2 mixture that was used in the pretreatment. The composition of the evolved gas was monitored with a mass spectrometer to provide continuous traces for the gases of interest.

a. Experimental

A comparison of the TPD curves for desorption of $H_2O(g)$ from the $LiAlO_2$ showed that the rates and amounts of desorption into He-H_2 mixtures are enhanced substantially over those into pure helium.

We had reported earlier that the desorption process may be related to different kinds of sites on the surface of the $LiAlO_2$.[18] The experimental TPD curves obtained during the past year were deconvoluted to derive values for the kinetic parameters of the contributing subpeaks, which represent the different kinds of sites on the $LiAlO_2$ surface (designated by the labels A, B, C, and D). The method of deconvolution was to synthesize the experimental curve from subpeaks determined for a first-order desorption process, where the desorption rate is given as

$$r = \Sigma \nu_i a_i \exp(-E_{di}/RT) \qquad (1)$$

Here, r is the overall rate of desorption of $H_2O(g)$ in mol/min and is the sum of desorption from the individual types of sites identified by subscript i, ν_i is the pre-exponential term for a given type of site in units of mol H_2O/(min-mol occupied site i), a_i is the amount in moles of H_2O adsorbed on a given type of site at a given time, and E_{di} is the activation energy of desorption from a given type of site in units of kJ/mol. As an example of our method, Fig. VIII-5 shows the calculated subpeaks, the sum of these subpeaks, and the experimental TPD curve derived for a sweep gas of He-495 ppm H_2.

---

[17] A. K. Fischer, Fusion Technol. **19**, 1012 (1991).

[18] J. P. Kopasz, A. K. Fischer, and C. E. Johnson, Adv. Ceram. **27**, 317 (1990).

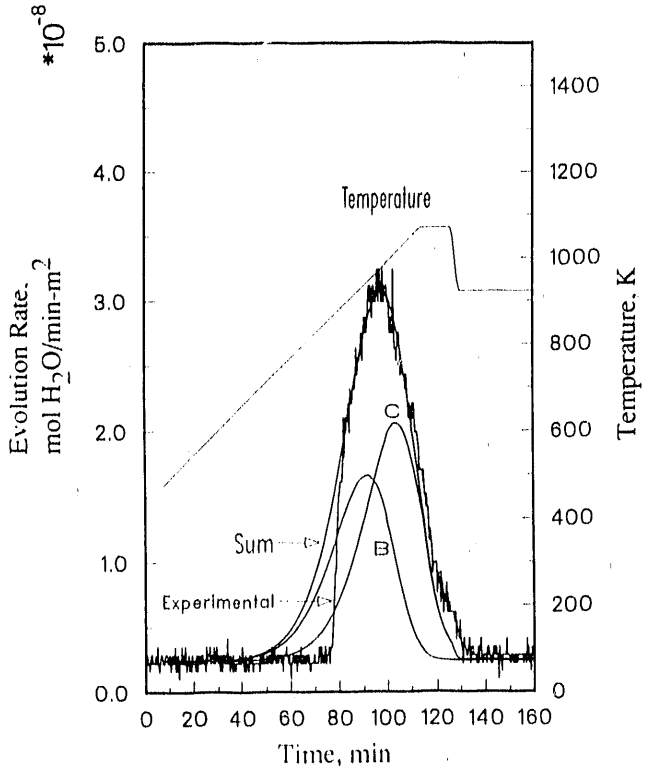

Fig. VIII-5.

Desorption of H_2O from Pretreated $LiAlO_2$ into Helium Sweep Gas Containing 495 ppm H_2. Pretreatment involved exposure to He-495 ppm H_2 for 18 h. Peaks B and C derived from deconvolution of experimental curve.

The activation energies and pre-exponential terms calculated for all runs are shown in Table VIII-2. Consistently, the TPD curves for desorption into He-H_2 mixtures contained two peaks, labeled B and C (Fig. VIII-5), and the curves for desorption into pure helium contained peaks of types C and D. The activation energies of the B, C, and D peaks were determined to be ~96, 117, and 134 kJ/mol, respectively. (In the earlier work, dealing with desorption from samples pretreated at 673 K with 900 ppm H_2, A, B, and C peaks were identified.[17] The A peaks were determined to have a desorption activation energy of 75 kJ/mol.) The data suggest that the H_2 in the sweep gas causes the OH^- population, which is the precursor of desorbed H_2O, to occupy preferentially and to build up in the B and C sites. This leads to an activation energy that is lower than that obtained for pure helium, where the higher activation energy combination of C and D sites is involved. An important point is that the activation energies for specific types of sites do not change significantly with increases in pretreatment time or H_2 level.

From a comparison of the pre-exponential terms for the C peaks in Table VIII-2, one may judge the effect of H_2. The mean values and their standard deviations are $2.22 \pm 1.16 \times 10^5$ mol H_2O/(min-mol occupied site) for pure helium and $8.91 \pm 1.14 \times 10^4$ mol H_2O/(min-mol occupied site) for He-H_2 mixtures. These values are slightly different at the 1σ level. Therefore, the effect of H_2 is to make a small change in the pre-exponential term for the C peak, which is in the direction of reducing the overall desorption rate; however, this effect is overcome by the buildup of substantial coverage in the lower-activation-energy B peak.

Table VIII-2. Kinetic Parameters for First-Order Desorption of H_2O from B, C, and D Sites on $LiAlO_2$.[a] (Symbols and their units of measure are defined in Eq. 1.)

Pretreatment								
Time, H	H_2 in He, ppm	H_2 in He Sweep Gas, ppm	ν_B	E_{dB}	ν_C	E_{dC}	ν_D	E_{dD}
20	247	0	--	--	1.90 E5	118	3.51 E5	135
170	495	0	--	--	1.25 E5	117	9.91 E5	134
20	990	0	--	--	3.51 E5	117	7.51 E5	134
20	247	247	2.22 E4	96	8.82 E4	117	--	--
20	495	495	1.07 E4	92	7.62 E4	117	--	--
20	495	495	1.62 E4	96	8.78 E4	117	--	--
290	990	990	2.75 E4	95	1.04 E5	117	--	--

[a]Temperature increase from 473 to 1073 K.

Some data for the desorption of $H_2(g)$ into pure helium were deconvoluted into subpeaks. The calculated activation energies and pre-exponential terms were similar to those for desorption of H_2O into pure helium. These data are still being analyzed.

b. Application

To apply these results to blanket design and tritium-release modeling, the areas under the H_2O desorption curves, represented by the sums of the B and C peaks or the C and D peaks, were converted to values of fractional surface coverage, θ, on the assumption of 10^{19} sites per square meter of surface. This θ value is for the total evolvable H_2O under the given conditions, either into the He-H_2 mixtures or into pure He. It is distinguished from the θ value that includes all sites which might be covered but did not participate in the desorption processes that were measured. Such sites include those that would have been activated only at temperatures higher than those in the experimental temperature range. The H_2 adsorption process was regarded as dissociative chemisorption, forming surface OH^- groups which combine bimolecularly prior to desorption. Consequently, the OH^- and the H_2O coverage should vary linearly as the square root of the H_2 partial pressure. This linear relationship for the total evolvable H_2O coverage, θ, is shown in Fig. VIII-6 for sweep gases of pure helium and He-H_2 mixtures.

For example, for the desorption rate of H_2O from $LiAlO_2$ at 923 K into a helium stream carrying H_2 in the measured concentration range (which is a prototypic range for a fusion reactor), a steady-state coverage of desorbable H_2O can be derived from Fig. VIII-6. Calculating the desorption rate requires values for a_B and a_C in Eq. 1. These may be calculated from:

$$a_i = 1.66 \times 10^{-5}\, m\sigma_s\theta_i \qquad (2)$$

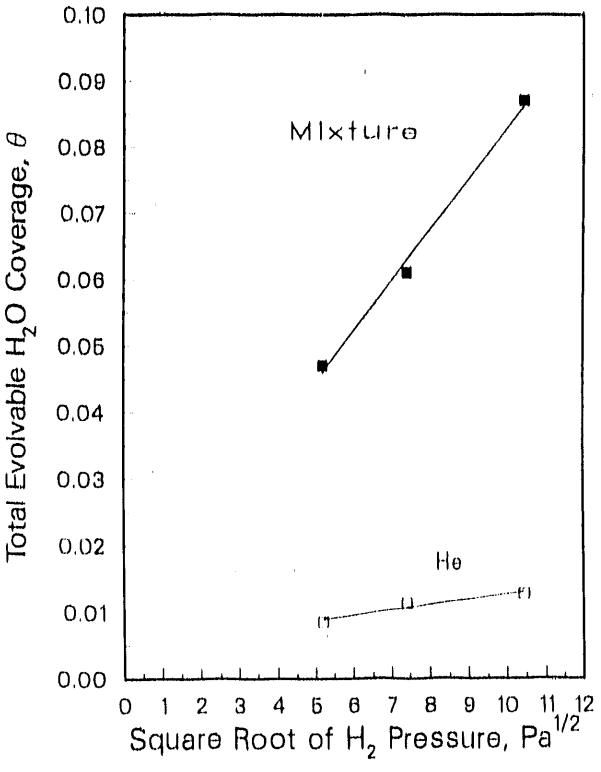

Fig. VIII-6.

Fractional Surface Coverage by H_2O Desorped from Pretreated $LiAlO_2$ into He-H_2 Mixture or Pure Helium Sweep Gas during Temperature Increase from 473 to 1073 K

where m is the mass of the breeder in g, σ_s is the specific surface area in m^2/g, and θ_i is the fractional surface coverage by evolvable H_2O on sites of type i. The factor 1.66×10^{-5} was derived from the assumption of 10^{19} sites/m^2 divided by the Avogadro number, and the last quantity is derived from the curve in Fig. VIII-6 by allocating portions of the indicated total θ to the B and C sites. The exact relationship between B and C site populations still requires study, but for the present purpose, we assume the ratio of B to C sites as approximately 0.5, since the observed ratios ranged from 0.38 to 0.79. That is, 1/3 of the θ from Fig. VIII-6 is assigned to the B peak and 2/3 to the C peak. (For desorptions into pure helium, the ratio of C to D sites is in the range from 0.24 to 1.18.) The desired rate of desorption follows from substitution of the θ_i values into Eq. 2 and then the resulting a_i values into Eq. 1. Future work will deal with H_2/H_2O desorption processes for another candidate breeder material, Li_2O.

2. Lithium Vaporization Behavior of Lithium Ceramics

Lithium oxide mass loss by entrainment of LiOH(g) in the helium sweep gas (vapor transport) is seen as a possible problem under some conditions of fusion reactor operation. The potential problem is greatest for Li_2O breeder material, principally at high temperatures (>1073 K), and less so for the other candidate breeders ($LiAlO_2$, Li_4SiO_4, and Li_2ZrO_3).

To assess the need for further experimental work on lithium losses from Li_2O, the existing studies were placed on a common basis for comparison by expressing the individual data points as a ratio relative to what would be predicted thermodynamically for equilibrium at the same conditions of temperature and H_2O(g) partial pressure. In Fig. VIII-7, the data for inert

conditions, i.e., without complications from corrosion, are presented in a normalized form.[19-21] The principles of the transpiration technique may be applied to explain the data. According to these principles, the apparent vapor density will be constant over a range of sweep-gas flow rates if equilibrium is established. At low flow rates, mass loss rates higher than at equilibrium will be observed because of the additional contribution of diffusional processes to the lithium loss process. At high flow rates, mass loss rates lower than at equilibrium reflect undersaturation of the sweep gas. One of the sets of data (Ref. 19) in Fig. VIII-7 reveals a region of undersaturation but also an equilibrium plateau. The flow rate for a fusion reactor design of current interest, the International Thermonuclear Experimental Reactor (ITER), is marked on Fig. VIII-7. Overall, this plot indicates that flow rates under ITER conditions will be (1) high enough so that diffusional contributions will be negligible and (2) in the range in which one can assume thermodynamic equilibrium conditions. (The other lithium mass loss process, corrosion, follows a parabolic rate law, so that the depth and the duration of the process are limited.) We also concluded that existing studies provide adequate replication for confidence in the thermodynamic analysis, and that further similar studies would not be cost effective.

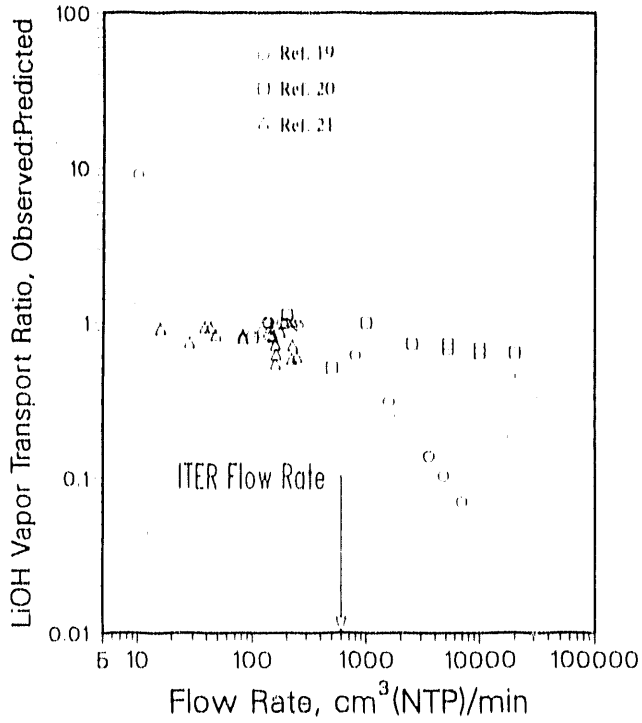

Fig. VIII-7.

Ratio of Observed-to-Predicted LiOH Vapor Transport Rates for Li_2O-H_2O(g)-LiOH(g) System

[19]P. E. Blackburn and C. E. Johnson, Fusion Technol. **19**, 1696 (1991).

[20]T. Kobayashi, T. Suzuki, S. Okazaki, M. Fukuhara, T. Abe, and Y. Tanaka, in *Japanese Contributions to IAEA INTOR Workshop, Phase Two A, Part 3*, Japan Atomic Energy Research Institute Report JAERI-M-87-219 (1988).

[21]M. Tetenbaum and C. E. Johnson, J. Nucl. Mat. **120**, 213 (1984).

On the basis of thermodynamic equilibrium, a conservative expression (i.e., tending to overestimate) for the Li_2O mass loss rate from Li_2O was derived from existing thermodynamic data[22] :

$$\log G = 13.269 + \log V - 2.790 \log T - 9398/T + 0.5 \log p_{H_2O(g)} \quad (3)$$

where G is the rate of loss (g/day), V is the sweep gas flow rate (cm^3/min) at the temperature of interest, T (in K), and p_{H_2O} is the water vapor pressure (atm).

To compare LiOH vaporization loss rates among the different breeders, we calculated the LiOH vapor pressure for a given $H_2O(g)$ partial pressure. The recent determination by Wyers et al.[23] of the standard enthalpy of formation for $Li_2ZrO_3(c)$ was used to estimate its free energy of formation up to 1273 K. The hydrolytic reaction forming LiOH(g) was assumed to be

$$Li_2ZrO_3(c) + H_2O(g) \rightleftharpoons 2LiOH(g) + ZrO_2 \quad (4)$$

with ZrO_2 as a solute at low concentration in Li_2ZrO_3. For the remaining ternary oxide breeders, $LiAlO_2$ and Li_4SiO_4, the assumptions about their hydrolytic reactions were that $Li_2SiO_3(s)$ phase formation occurs in Li_4SiO_4, and that $LiAl_5O_8$ solid-solution formation occurs in $LiAlO_2$. A single set of operating conditions was selected for a common basis of comparison: a temperature of 923 K and a fixed H_2 partial pressure of 100 Pa. The overall system stoichiometry with respect to oxygen and the metallic elements was set exactly by the composition of the parent compound, which thereby established the oxygen activity. At the present time, activity coefficient data for LiOH as a solute are available only for the Li_2O system, thereby enabling calculations for this system to account of this aspect of nonideality. For the other systems, ideal solution behavior was assumed.

The LiOH(g) partial pressures calculated on this basis are 2.0×10^{-4} Pa for Li_2O, 2.7×10^{-5} Pa for Li_4SiO_4, 1.2×10^{-5} Pa for Li_2ZrO_3, and 1.3×10^{-8} Pa for $LiAlO_2$. These results suggest that gaseous entrainment (transport) of LiOH vapor would be greatest for Li_2O and least for $LiAlO_2$; Li_4SiO_4 and Li_2ZrO_3 occupy intermediate positions, but closer to Li_2O than to $LiAlO_2$.

3. Tritium Release Studies

Tritium inventory in ceramic tritium breeding materials is an important issue for fusion reactor designs. To predict the tritium inventory under different conditions, the tritium release from these materials must be understood. We have investigated the tritium release from

---

[22]D. R. Stull and H. Prophet, Project Directors, *JANAF Thermochemical Tables*, 2nd ed., National Bureau of Standards, NSRDS-NBS 37 (June 1971).

[23]G. P. Wyers, E. H. P. Cordfunke, and W. Ouweltjes, J. Chem. Thermodyn. **21**, 1095 (1989).

$LiAlO_2$ in an effort to gain an understanding of the mechanisms involved in tritium release from this class of materials.

Lithium aluminate compares favorably with other candidate solid breeder materials in terms of chemical, mechanical, and irradiation properties; however, tritium release from $LiAlO_2$ is slower than that from Li_2O or Li_2ZrO_3. We have modified $LiAlO_2$ (doped with magnesium or coated with platinum) in an attempt to improve its tritium release and to gain a better understanding of the underlying release mechanism. Single crystals of $LiAlO_2$, Mg-doped $LiAlO_2$, and Pt-coated $LiAlO_2$ were irradiated to produce tritium, and the tritium release was studied using the TPD method. By comparing the desorption data for the altered materials, we hoped that the rate-limiting steps in tritium release could be identified.

An example of the TPD plots obtained in these experiments is shown in Fig. VIII-8. The overlapping peaks indicate that the tritium is released from several states. We investigated the energetics of release from the different states by deconvolution of the observed data into subpeaks. The deconvolution was done using the equation for first-order desorption under conditions of constant-rate heating.[24]

For pure $LiAlO_2$, the activation energies for the five peaks (Fig. VIII-8a) were calculated to be 61, 99, 129, 154, and 174 kJ/mol, which are in good agreement with those previously determined by Botter et al.[25] Roughly 60% of the tritium released was from the peak with an activation energy of 174 kJ/mol.

Doping the lithium aluminate with magnesium changed the activation energies for tritium release slightly and shifted the tritium to peaks with lower activation energies (Fig. VIII-8b). Deconvolution of the TPD plot for the doped $LiAlO_2$ gave peaks with activation energies of 47, 95, 113, 156, and 205 kJ/mol. The peaks corresponding to activation energies of 47 and 95 kJ/mol are increased in intensity relative to the low energy peaks for the pure material. In the doped material, these peaks account for roughly 25% of the tritium released, while for the pure material the corresponding peaks account for only 13% of the released tritium. In addition, the activation energy of 95 kJ/mol is in excellent agreement with the value of 99 kJ/mol reported for the desorption of hydrogen from MgO.[26] This suggests that doping $LiAlO_2$ with magnesium provides low-energy MgO surface sites from which the tritium desorbs.

The TPD plot for $LiAlO_2$ coated with platinum (Fig. VIII-8c) showed peaks corresponding to activation energies of 71, 99, 146, and 177 kJ/mol. The platinum coating shifts the tritium release to peaks with lower activation energies relative to that for the pure material. For the coated material, approximately 40% of the tritium was released from peaks with activation energies below 150 kJ/mol, while for the pure material, only 25% was released from

---

[24]A. W. Smith and S. Aranoff, J. Phys. Chem. **62**, 684 (1958).

[25]F. Botter, J. Mougin, B. Rasneur, S. Tistchenko, and J. Kopasz, "Mechanism of Tritium Release from Lithium Ceramics Irradiated with Neutrons," in *Proceedings of the 16th Symposium on Fusion Technology*, North Holland, New York, p. 924 (1991).

[26]T. Ito, T. Murakami, and T. Tokuda, J. Chem. Soc. Faraday Trans. I, **79**, 913 (1983).

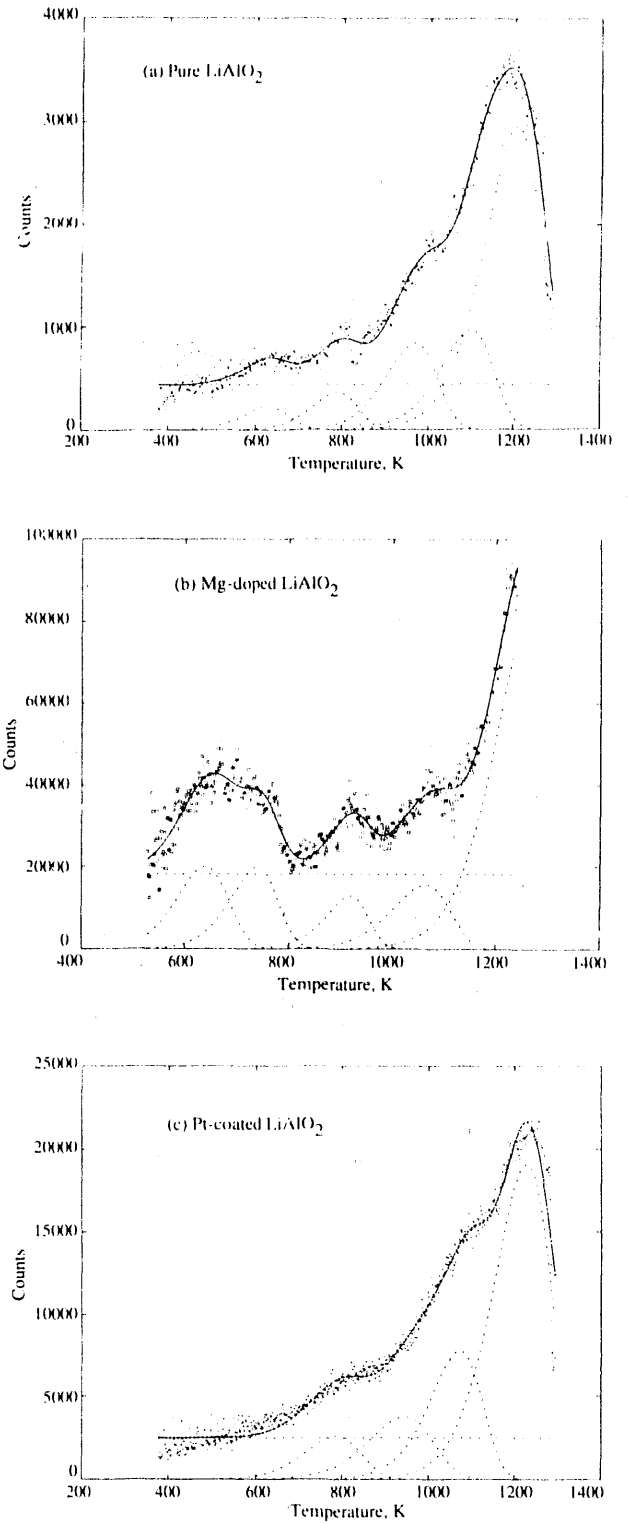

Fig. VIII-8. Temperature Programmed Desorption Plots for Single Crystals (2-mm dia) of (a) Pure $LiAlO_2$, (b) Mg-Doped $LiAlO_2$, and (c) Pt-Coated $LiAlO_2$ at Heating Rate of 0.75 K/min. Dashed curves indicate calculated values for individual peaks; dashed horizontal line indicates baseline; solid curve represents total calculated curve; points represent observed data.

peaks with activation energies below this value. The activation energies of 71 and 146 kJ/mol are in good agreement with the energies reported for the desorption of H_2 and H_2O from platinum.[27,28] The improved tritium release for the platinum-coated material strongly suggests that the rate-controlling step in tritium release from these single-crystal $LiAlO_2$ samples involves the surface and not bulk diffusion. The platinum sputtered on the surface should not affect the bulk properties such as diffusion. Therefore, if diffusion were rate limiting, the platinum coating should have had no effect on the tritium release.

Based on the results of our TPD studies, we developed a tritium release model which focuses on diffusion and simultaneous desorption from several sites and employed this model to calculate in-pile release from $LiAlO_2$. The model contains no adjustable parameters. As input, we used the diffusion coefficient for tritium in $LiAlO_2$ determined by Bruning et al.[29] and desorption coefficients determined by Fischer[30] for material of similar characteristics as the material used in an in-pile test (MOZART, Commissariat a l'Energie Atomique, Institut du Recherche Fondamentale). However, because Fischer does not describe the distribution of tritium between the different kinds of sites, we used the distribution determined for the single crystals.[25] Using these data, which were obtained in laboratory (out-of-pile) experiments, we calculated the expected tritium release for a number of temperature-increase and temperature-decrease tests performed in the MOZART experiment. The agreement between calculated results from our model and the experimentally observed release is quite good. A comparison between our model calculations and the observed data for one of the temperature transients (from 923 to 823 K) is shown in Fig. VIII-9. This level of agreement has not been obtained previously without adjusting some of the input parameters; however, in this case no parameters are changed from the values determined in separate laboratory experiments on $LiAlO_2$.

In the future, we plan to acquire information on the tritium distribution within the solid to give us information on the tritium diffusivity. Isothermal anneals will be performed on irradiated samples for preset times. The samples will then be sectioned and analyzed to provide a tritium profile from which diffusivity can be calculated.

D. *Support Studies for New Production Reactor*

A variety of nuclear materials are used in U.S. nuclear weapons. One of these, tritium, is rare in nature and must be produced in a nuclear reaction to obtain the quantity necessary for

---

[27]P. R. Norton, J. A. Davies, and T. E. Jackman, Surf. Sci. **121**, 103 (1982).

[28]E. Fridell, B. Hellsing, B. Kasemo, S. Ljungstrom, A. Rosen, and T. Wahnstrom, J. Vac. Sci. Technol. **A9**, 2322 (1991).

[29]D. Bruning, D. Guggi, and H. R. Ihle, "The Diffusivity of Tritium in the System Li_2O-Al_2O_3," in *Proceedings of the 12th International Symposium on Fusion Technology*, Pergamon Press, New York, p. 543 (1983).

[30]A. Fischer, "Processes for Desorption from $LiAlO_2$ Treated with H_2 as Studied by Temperature Programmed Desorption," Proc. of Ninth Topical Meeting on Technology of Fusion Energy, Oak Brook, IL, October 7-11, 1990, pp. 1012-1017 (1991).

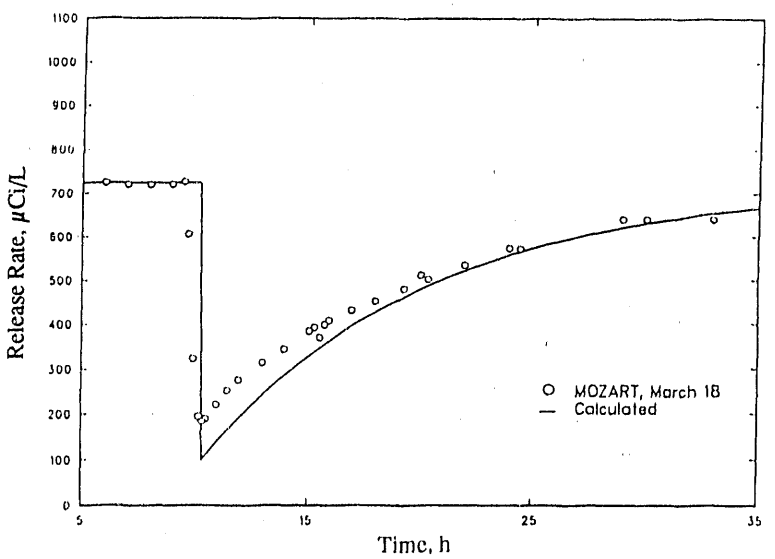

Fig. VIII-9. Calculated and Observed Tritium Release for In-Pile (MOZART experiment) Temperature Decrease from 923 to 823 K with $LiAlO_2$ Material

manufacturing and maintaining nuclear weapons. Since tritium decays radioactively, weapons production requires a constant and reliable source of tritium. The only practical method for producing large quantities of tritium is to irradiate lithium targets with neutrons in a reactor designed for that purpose. The DOE initiated the New Production Reactor (NPR) Program to plan, design, and construct safe and environmentally acceptable new reactor capacity for an assured supply of tritium. In 1991, CMT provided technical support to this program by performing the following: (1) calculational and experimental studies of fission product release from fuel and target in a severe accident and (2) design studies of the modifications needed to a hot cell at ANL-West so that irradiated fuel and target tubes can be handled there with minimal tritium contamination.

The objective of the first support study was to develop a thermodynamic model that would predict the behavior of fuel and target in a severe accident of an NPR that is a heavy water reactor (HWR). As part of this study, we examined earlier pertinent literature and conducted preliminary tests in preparation for transpiration measurements with Al-U fuel, Al-Li target, and fission product simulants exposed to flowing helium mixtures at temperatures up to 1673 K.

The literature analysis focused on the behavior of aluminum at high temperatures. In earlier experiments in which solid and liquid aluminum were oxidized by oxygen and water vapor, Blackburn and Gulbransen[31] established that a thin oxide layer forms on the surface of the aluminum at temperatures of 773 K or more. Thus, a thin oxide film on the molten aluminum may be a barrier to transport of the gaseous aluminum species in the flowing helium

[31]P. E. Blackburn and E. A. Gulbransen, J. Electrochem. Soc. **107**, 944 (1960).

of the transpiration measurements. This oxide film may also act as a barrier to other gases from the fuel, target, and fission products. Blackburn and Gulbransen[31] focused on measurement of oxidation rates of electrochemically polished aluminum in helium gas containing oxygen, oxygen plus water vapor, or hydrogen plus water vapor. At 898 K, the oxide layer reached about 200 Å in 15 min in water vapor, after which the growth of the oxide layer slowed to approximately 6 Å per hour. The oxidation is controlled by the diffusion of aluminum or oxygen through the oxide layer.

The oxide layer may also control the release of fission products from NPR-HWR fuel-target mixtures. To understand the fission product release mechanism, the diffusion of aluminum through the oxide layer must be measured. Further, this measurement must be carried out to establish a baseline for subsequent fission-product release measurements. Measurements of oxidation of aluminum alloys containing 3 wt % Li and 2 wt % Mg (Mg should behave like Ba or Sr) produced oxide layers that were 75 times as thick as the oxide layers on pure aluminum.[32] This finding suggests that Li, U, and the fission products in the fuel and target will enhance the corrosion rate, and this may, in turn, affect the loss of fission products.

Preliminary transpiration tests were undertaken with an ingot prepared by Savannah River Laboratory. This ingot contained Al, U, Ba, C, Ce, Mo, Sr, and Zr but was not entirely representative of irradiated NPR-HWR fuel. (It contained carbon and oxygen impurities and had an excess in the proportion of cesium and deficiencies in the proportions of Mo and Sr. Further, the zirconium content was low by a factor of 45 relative to the barium content.) In the transpiration experiment, the ingot was heated to 1098 K with no significant loss in weight. No change occurred at 933 K, where aluminum melts. The gas in the system was pure helium until the temperature reached 973 K, where 3% water was added. At 1146 K the sample began to increase in weight. The temperature was held at about 1248 K for 4 h, where the sample oxidized at a decreasing rate with time. The curve for weight change versus time suggested formation of a protective oxide layer, as predicted by our literature study. Additional experimental studies on formation of this oxide layer are needed. However, no further work is planned because of budget termination.

In other NPR-related support work, we developed conceptual designs for modifications needed in the Main Cell of the Hot Fuel Examination Facility (HFEF) at ANL-West if it is to be used for handling irradiated fuel and target materials. The conceptual design minimizes possible tritium contamination by use of a defense-in-depth methodology. In this design, the HFEF Main Cell would be provided with a primary enclosure and a system that would recover gaseous tritium releases and particulate residue from cutting operations with irradiated targets. The recovery system would employ particulate filters and a catalyst bed that converts tritium to water. The enclosure would be sized to handle the test-vehicle assembly and disassembly operations associated with the irradiation tests and to accommodate the recovery system. Redundant tritium recovery units would be used to minimize maintenance within the HFEF Main Cell. In addition, the HFEF Main Cell purification system would be modified to recover tritium

---

[32]D. J. Field et al., *High Temperature Oxidation Studies, Aluminum-Lithium Alloys*, eds., T. H. Sanders, Jr. and E. A. Stark, Jr., Metallurgical Society of AIME, New York, p. 325 (1981).

in the event of a failure in the primary enclosure and/or its recovery system. During decommissioning, a secondary enclosure would be constructed around the primary enclosure to prevent contamination and would use the recovery system on the primary enclosure to capture any tritium releases. The tritium atmospheric concentration would be monitored outside the primary and secondary enclosures, outside and inside the HFEF Main Cell, and in the HFEF Main Cell exhaust. Issues that need to be addressed in the future include the training of workers and management in tritium control; the development of appropriate HFEF operating procedures and health physics operating procedures for tritium work; and the development of agreements with Westinghouse Savannah River Site on the required accuracy of tritium measurement and the final disposal site for all waste.

IX. BASIC CHEMISTRY RESEARCH

Basic chemistry research is being pursued in four different areas: catalytic chemistry associated with molecular energy resources; chemistry of superconducting oxides and other materials of basic interest with technological application; interfacial processes of importance to corrosion science, catalysis, and high-temperature superconductivity; and the geochemical processes involved in water/rock interactions occurring in active hydrothermal systems.

A. *Fluid Catalysis*

The aim of this research is to explore new catalytic chemistry and catalytic reaction mechanisms to activate small gaseous molecules (e.g., CO, CO_2, H_2, CH_4, N_2) that often require high temperatures and pressures to produce useful products. Maximal concentrations of reactant gases are achieved by making use of their complete miscibilities with supercritical fluids, which also have the potential to alleviate gas-liquid mixing and catalyst recovery problems typical of many homogeneous catalytic processes. Our current research uses nuclear magnetic resonance (NMR) measurements (multinuclear, dynamic, and magnetochemical) at high temperature and pressure to explore the reactions of dicobalt octacarbonyl, an oxo-process catalyst, under hydroformylation process conditions. The catalytic process had not previously been explored by *in situ* NMR methods at the high pressures and temperatures required for the reaction, and considerable unsuspected chemistry has now been uncovered by this approach. Most noteworthy is that all of the chemical reactions so far investigated have virtually the same activation barrier of 18 ± 2 kcal/mol (75 ± 8 kJ/mol). We suspect that this value reflects the barrier to dissociation of the Co-Co bond in $Co_2(CO)_8$, and that the observed chemistry is actually that of the radical species, $\bullet Co(CO)_4$. In other research directed toward the activation of methane, we have been synthesizing potentially catalytic complexes containing rhodium centers bound to solubilized phthalocyanine ligands. In this approach, methane is activated by means of the rhodium center's ability to form reasonably strong, but still reactive, metal-carbon and metal-hydrogen bonds.

1. Catalytic Chemistry in Supercritical Media

The largest-scale industrial homogeneous catalytic process is the oxo process for the hydroformylation of olefins. In oxo catalysis, olefins are reacted with carbon monoxide and hydrogen in the presence of a soluble catalyst to produce aldehydes and alcohols for use in detergents, plastics, and agricultural products. The reaction is catalyzed by carbonyl and phosphine complexes of cobalt and rhodium, and not surprisingly, much of the development of transition-metal carbonyl chemistry stems from research into the mechanism of the hydroformylation reaction and methods to improve it.

The currently accepted mechanism for oxo catalysis is that proposed by Heck and Breslow,[1] which was supported by a recent *in situ* high-pressure infrared study by Mirbach[2]. Our

---

[1]R. F. Heck and D. S. Breslow, J. Am. Chem. Soc. **84**, 2499 (1962).

[2]M. F. Mirbach, J. Organomet. Chem. **265**, 205 (1984).

own research in oxo catalysis began with the expectation that the reaction, often plagued with gas-liquid mixing problems which limit product selectivity, reaction rate, and catalyst stability,[3] would benefit from the use of supercritical fluid solvents. Although supercritical fluids have seldom been explored for use in homogeneous catalysis, they have properties that could make them nearly ideal for conducting processes, such as hydroformylation, that involve the reactions of gases with liquid substrates. Because only one phase is present in the supercritical system, gas-liquid mixing, which is often rate limiting in liquid solvents, is not a problem for supercritical fluids. In addition, since gases are completely miscible with the supercritical phase, reactive gas concentrations are typically much higher than achievable in normal liquids. In oxo catalysis, carbon monoxide depletion, occurring in the liquid phase because of low solubility and incomplete mixing, results in poor selectivity to the desired linear alcohol/aldehyde product because isomerization steps are favored at low carbon monoxide concentration. Perhaps the greatest benefit that might occur through use of supercritical fluids is increased efficiency of catalyst and product separations that normally are accomplished by energy-intensive distillations. Due to the sharp changes in solubilities of dissolved species with density of the supercritical medium, separations might be easily accomplished by pressure alterations that control fluid density, and, in turn, catalyst or product solubility.

Our preliminary experiments with propylene hydroformylation in supercritical carbon dioxide[4,5] indicated that the catalytic reaction works well in this medium, giving a higher selectivity for linear products than in any liquid solvent. Catalyst solubility and stability and important equilibrium and rate constants were determined[5,6] to be comparable to those for conventional liquid hydroformylation. In the course of this research, we discovered several new dynamic NMR processes occurring under oxo reaction conditions, which we interpreted as stemming from the chemistry of the tetracarbonylcobalt radical. We suspect that such a reactive species, if present, would be involved in hydroformylation catalysis, although the Heck and Breslow mechanism assigns it no role. In this report, we describe our high-pressure NMR observations that have convinced us that not only does this radical chemistry occur, but it also might even be predominant at the high pressures and temperatures required for oxo catalysis.

Our first indication of the tetracarbonylcobalt-radical involvement came from the ^{59}Co NMR spectra in Fig. IX-1. These spectra were initially recorded at varied temperature to measure the enthalpy and entropy changes for the hydrogenation of $Co_2(CO)_8$ to form $HCo(CO)_4$:

$$Co_2(CO)_8 + H_2 \rightleftharpoons 2HCo(CO)_4 \qquad (1)$$

---

[3]R. L. Pruett, *Advances in Organometallic Chemistry*, eds., F. G. A. Stone and R. West, Vol. 17, Academic Press, New York, pp. 1-60 (1979).

[4]M. J. Steindler et al., *Chemical Technology Division Annual Technical Report, 1990*, Argonne National Laboratory Report ANL-91/18, pp. 156-162 (1991).

[5]J. W. Rathke, R. J. Klingler, and T. R. Krause, Organomet. **10**, 1350 (1991).

[6]J. W. Rathke, R. J. Klingler, and T. R. Krause, Organomet., in press.

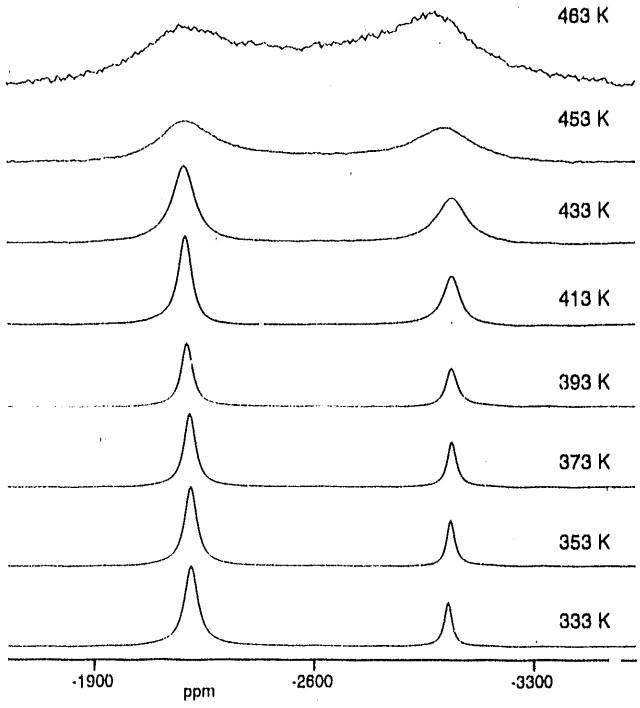

Fig. IX-1.

^{59}Co NMR Spectra Obtained at Temperatures between 333 and 463 K with Supercritical CO_2. The spectra show broadening and merging of the resonances for $Co_2(CO)_8$ (-2000 ppm) and $HCo(CO)_4$ (-3000 ppm). Total pressure (carbon monoxide) is 3600 MPa at 463 K.

Figure IX-1 shows that the resonances for the two species broaden and begin to merge at higher temperatures, indicating the occurrence of a process that is fast on the NMR time scale. At the point of coalescence, ~483 K, the half-life for this process is estimated to be 5×10^{-6} s. If this experiment had been performed with a normal liquid, the line-width alterations would be obscured by large additional line-width changes stemming from temperature-dependent viscosity variations that occur in liquids. For the supercritical system, the viscosity variations are negligible, and the line-width changes in Fig. IX-1 are chemical in origin.

If occurring sufficiently rapidly, reaction 1 could be considered as the source for the broadening and coalescing of the resonances for $HCo(CO)_4$ and $Co_2(CO)_8$. However, it is not nearly fast enough. In addition, if reaction 1 were fast on the NMR time scale, separate ^1H NMR resonances observed for H_2 and $HCo(CO)_4$ would also broaden and coalesce. Experimentally, this is not the case, and the proton spectra remain sharp and essentially stationary even at temperatures where the ^{59}Co resonances have merged.

A two-step process that would cause coalescence in the ^{59}Co spectra without affecting the ^1H spectra is

$$Co_2(CO)_8 \rightleftharpoons 2(CO)_4Co\bullet \qquad (2)$$

$$(CO)_4Co\bullet + HCo(CO)_4 \rightleftharpoons (CO)_4CoH + \bullet Co(CO)_4 \qquad (3)$$

Reaction 2 produces the tetracarbonylcobalt radical by dissociation of the Co-Co bond in dicobalt octacarbonyl. Reaction 3 involves transfer of a hydrogen atom from a molecule of tetracarbonylcobalt hydride to the radical, producing new, but identical, molecules of hydride and radical. Coalescence of the ^{59}Co resonances would result if reactions 2 and 3 occur rapidly. Note that since H_2 is not involved in either reaction, and since the environment of the hydrogen nucleus in $HCo(CO)_4$ is also not altered by either reaction, the proton spectra of the radical and hydride species would remain unchanged as temperature is varied. This observation is in accord with experiment.

Our interpretation requires that reaction 2 be fast on the NMR time scale at temperatures where broadening and merging of the ^{59}Co signals for $Co_2(CO)_8$ and $HCo(CO)_4$ occur. If this is the case, then broadening of the ^{59}Co signal for $Co_2(CO)_8$ should occur even in the absence of $HCo(CO)_4$ due to averaging of the ^{59}Co nuclear environments in the carbonyl dimer and radical species of reaction 2. We have experimentally verified this effect in a carbon monoxide gas phase, which is required to stabilize the metal carbonyl. Line-shape analysis of the broadening of the ^{59}Co resonance for the dissociation of $Co_2(CO)_8$ in this gas phase at varied temperature leads to the Arrhenius plot in Fig. IX-2. The activation energy, 17.3 kcal/mol (72.5 kJ/mol), and the frequency factor, 7×10^{11} s^{-1}, for reaction 2 were derived from this plot. The hydrogen atom transfer process in reaction 3 is expected to have only a small activation barrier, since it is thermoneutral and involves only the breaking, and probably nearly simultaneous reformation, of a relatively weak Co-H bond. From these arguments, one would expect that the two dynamic NMR processes discussed so far, namely, (1) broadening and coalescence of the ^{59}Co resonances for $Co_2(CO)_8$ and $HCo(CO)_4$ and (2) broadening of the ^{59}Co resonance for $Co_2(CO)_8$ in the absence of $HCo(CO)_4$, should have nearly the same activation barrier. This has also been experimentally verified by line-shape analysis, and both processes have barriers near 17 kcal/mol (71 kJ/mol).

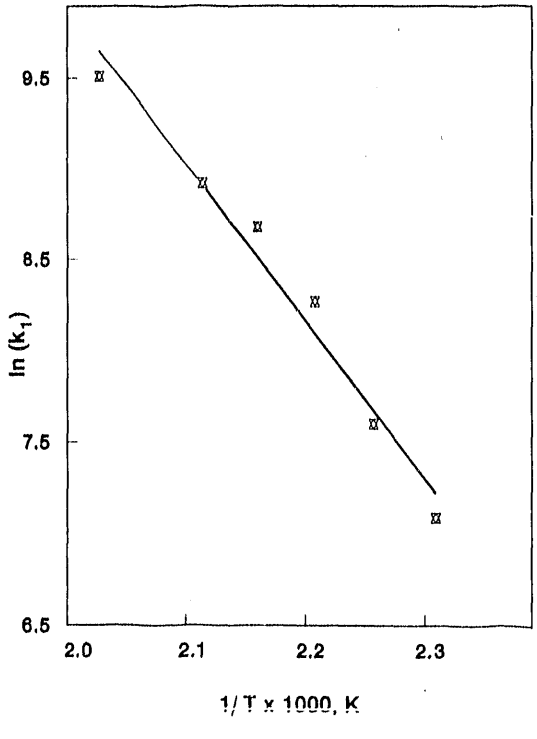

Fig. IX-2.

Arrhenius Plot for Dicobalt Bond Homolysis Derived from ^{59}Co NMR Line-Width Analysis (where k_1 is the first-order rate constant)

The most convincing evidence for the involvement of the tetracarbonylcobalt radical stems from ^{13}C NMR spectral measurements showing a contact shift in the exchange of free CO with coordinated CO in $Co_2(CO)_8$. Figure IX-3 shows ^{13}C NMR spectra for liquid mesitylene solution at varied temperature. As the temperature is increased, individual resonances for CO and $Co_2(CO)_8$ broaden and finally coalesce at approximately 418 K. Two-site exchange analysis of this process gives an activation energy of 19 kcal/mol (80 kJ/mol), which is the same as that for ^{59}Co processes within experimental error. This finding suggests the possibility that CO exchange occurs through the radical, as follows:

$$\bullet Co(CO)_4 + CO^* \rightleftharpoons \bullet Co(CO)_3CO^* + CO \qquad (4)$$

This exchange occurs because of the anticipated high lability for $\bullet Co(CO)_4$, while the measured activation barrier is that for the dissociation of $Co_2(CO)_8$ to form $\bullet Co(CO)_4$ (reaction 2). Thus, all of the ^{59}Co and ^{13}C NMR processes (reactions 2-4) are expected to have the same activation energy because each includes radical formation in reaction 2 as the presumed rate-determining step.

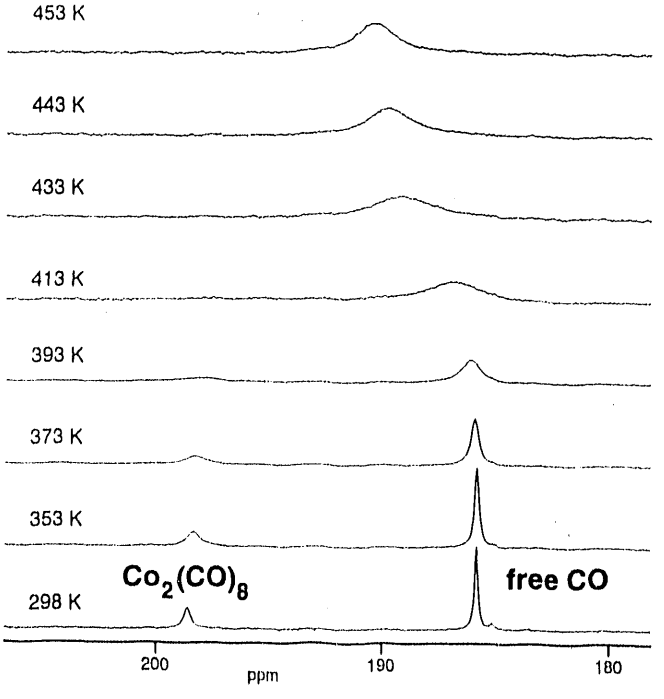

Fig. IX-3.

^{13}C NMR Spectra Obtained at Temperatures between 298 and 453 K with Liquid Mesitylene Solvent. Spectra indicate exchange between free CO and coordinated CO in $Co_2(CO)_8$ and a contact shift in the combined resonance above 393 K.

Further convincing evidence for radical involvement in the CO exchange process is that the combined resonance resulting from coalescence of the signals for $Co_2(CO)_8$ and CO is shifted in Fig. IX-3 to progressively lower values as the temperature is raised above 413 K. The measured shifts, $\delta\upsilon$, are too large to be other than contact shifts, which indicate radicals in NMR spectra. As expected, analysis of the temperature dependence of the contact shift, Fig. IX-4, yields an enthalpy change of 19.1 ± 1 kcal/mol (80.0 ± 4 kJ/mol). Thus, the formation of the

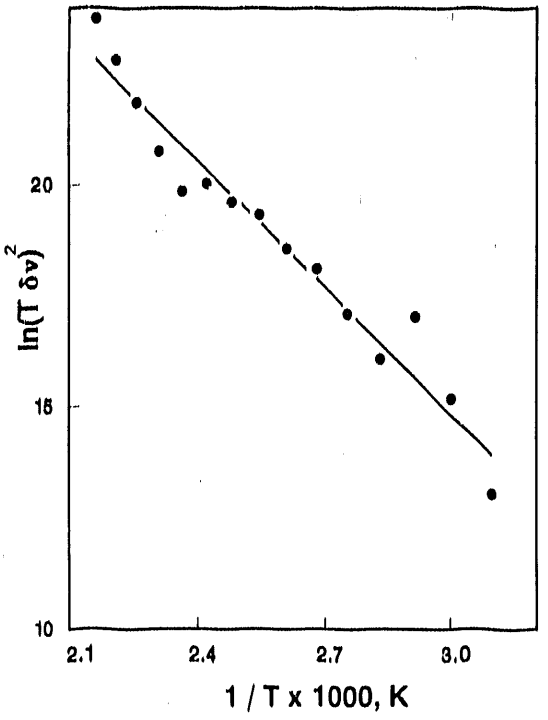

Flg. IX-4.

Temperature Dependence of ^{13}C Contact Shift ($\delta\nu$) for Carbon Monoxide in Presence of $Co_2(CO)_8$ in Liquid Mesitylene Solvent

radical responsible for the contact shift involves, within experimental error, the same energy as the CO exchange and the two ^{59}Co processes described earlier.

Carbon monoxide exchange in $Co_2(CO)_8$ had been investigated by Breitschaft and Basolo using ^{14}C tracer studies[7] and, more recently, by Roe using a low-temperature magnetization transfer NMR technique.[8] Both publications favored a non-radical mechanism involving dissociation of carbon monoxide from $Co_2(CO)_8$, based on the observed zero-order dependence on CO concentration and first-order dependence on $Co_2(CO)_8$ concentration. However, a free-radical mechanism including rate-limiting dissociation of $Co_2(CO)_8$ to form $\bullet Co(CO)_4$ (reaction 2), followed by rapid exchange of $\bullet Co(CO)_4$ with CO (reaction 4), is not only consistent with the observed concentration dependences, but also the only mechanism in accord with the observed contact shift and dynamic NMR data presented here.

When it became evident that $\bullet Co(CO)_4$ is an important reactive intermediate, we began to explore techniques to measure and identify radicals at high temperatures and pressures. We have developed a high-pressure NMR method for measuring volumetric magnetic susceptibilities in the gas phase and in supercritical fluids. If the magnetic moment of the radical is known or can be calculated, volumetric susceptibility measurements yield radical concentrations, and thus, equilibrium constants and thermodynamic parameters associated with the radical can be calculated. Our preliminary measurements indicate that $Co_2(CO)_8$ is approximately 10% dissociated at 473 K and 3700 MPa in carbon monoxide, in reasonable accord with estimates from our dynamic NMR measurements. Radicals can also be identified by

[7]S. Breitschaft and F. Basolo, J. Am. Chem. Soc. **88**, 2702 (1966).
[8]D. C. Roe, Organomet. **6**, 942 (1987).

their contact shifts, which for coordinated liquids can be calculated from hyperfine coupling in electron paramagnetic resonance spectra. Although the contact shift can seldom be measured by direct NMR observation of the radical, conditions can generally be found for fast ligand exchanges with the radical for metal carbonyl catalysis at sufficiently high pressures and temperatures. The contact shift can be calculated from the NMR spectra of the ligand under fast exchange conditions if the concentrations of the radical and ligand are known.

In future activities we intend to further explore the hydroformylation mechanism using high-pressure NMR techniques to determine if $\bullet Co(CO)_4$ is involved in the olefin coordination and dihydrogen activation steps. The finding that CO exchange occurs through this radical indicates that both are reasonable possibilities. In addition, we intend to begin exploration of a Shell Oil catalyst and a commercial rhodium-based catalyst for potential use in supercritical CO_2 solvent.

2. Hydrocarbon Activation Chemistry

The principal objective of this project is to study the activation and functionalization of hydrocarbons by soluble metallophthalocyanines. We have previously shown[4,9] that at 473 K hydrocarbons are activated by the Rh-Rh bonded dimer, $[(R_8Pc)Rh]_2$, where R_8Pc^{2-} is the dianion of 1,4,8,11,15,18,22,25-octapentylphthalocyanine ($R = C_5H_{11}$). A radical mechanism, initiated by the homolysis of the rhodium dimer to give $(R_8Pc)Rh\bullet$ radical, was proposed to explain our observations. We have continued our study to define the scope of this activation process and to elucidate the mechanism of the reaction.

We have found that at 453 K the rhodium dimer catalyzes the H-D exchange reaction between D_2O and both the aromatic and the alkyl hydrogens of the R_8Pc^{2-} ligand, resulting in the $(R_8Pc)RhD$ complex. The catalytic radical chain mechanism involving the H-D exchange between D_2O and the alkyl hydrogens was determined to be

$$[(R_8Pc)Rh]_2 \rightleftharpoons 2(R_8Pc)Rh\bullet \tag{5}$$

$$(R_8Pc)Rh\bullet + (R_8Pc)RhRh(R_7Pc\text{-}CH_2CH_2CH_2CH_2CH_3) \rightleftharpoons (R_8Pc)RhH$$

$$+ (R_8Pc)RhRh(R_7Pc\text{-}\underset{\text{I}}{\dot{C}HCH_2CH_2CH_2CH_3}) \tag{6}$$

$$(R_8Pc)Rh\bullet + \text{I} \rightleftharpoons (R_8Pc)RhH + (R_8Pc)RhRh(R_7Pc\text{-}\underset{\text{II}}{CH{=}CHCH_2CH_2CH_3}) \tag{7}$$

---

[9]M. J. Chen and J. W. Rathke, "Hydrogen and Methane Activation Studies Using Soluble Rhodium Phthalocyanine Dimers," Abstracts of XIVth Int. Conf. Organometallic Chemistry, Detroit, MI, August 19-24, 1990, p. 177 (1990).

$$(R_8Pc)Rh\bullet + II \rightleftharpoons (R_8Pc)RhH + \underset{III}{(R_8Pc)RhRh(R_7Pc\text{-}CH{=}CH\text{-}CHCH_2CH_3)} \quad (8)$$

$$(R_8Pc)Rh\bullet + III \rightleftharpoons (R_8Pc)RhH + \underset{IV}{(R_8Pc)RhRh(R_7Pc\text{-}CH{=}CH\text{-}CH{=}CHCH_3)} \quad (9)$$

$$(R_8Pc)Rh\bullet + IV \rightleftharpoons (R_8Pc)RhH + (R_8Pc)RhRh(R_7Pc\text{-}CH{=}CH\text{-}CH{=}CH\text{-}\dot{C}H_2) \quad (10)$$

$$(R_8Pc)RhH + D_2O \rightleftharpoons (R_8Pc)RhD + DHO \quad (11)$$

Note that I represents a benzylic radical and would also facilitate the H-D exchange of the aromatic hydrogens with D_2O.

Further studies of the $(R_8Pc)RhH$ complex revealed the existence of two stable isomers, the monomeric $(R_8Pc)RhH$ and the dimeric $(R_8PcH)Rh\text{-}Rh(R_8Pc)H$. The later may be envisioned as a complex generated from the heterolytic splitting of H_2 by $[(R_8Pc)Rh]_2$, with the H^- ion bonded to one of the pyrrolic nitrogens and the H^+ ion bonded to the Rh of the other $(R_8Pc)Rh$ macrocycle. These two hydrido complexes may be interconverted by simply changing the solvent:

$$(R_8PcH)RhRh(R_8Pc)H \underset{C_6H_6}{\overset{THF}{\rightleftharpoons}} 2(R_8Pc)RhH \quad (12)$$

where THF is tetrahydrofuran solvent.

We have also prepared and isolated $(R_8Pc)LRh\bullet$ radicals, where L represents trimethylphosphine and tributylphosphine, via

$$(R_8PcH)RhRh(R_8Pc)H + 2L \rightarrow 2(R_8Pc)LRhH \rightarrow 2(R_8Pc)LRh\bullet + H_2 \quad (13)$$

$$[(R_8Pc)Rh]_2 + 2L \rightarrow [(R_8Pc)Rh]_2L + L \rightarrow 2(R_8Pc)LRh\bullet \quad (14)$$

Formation of the intermediates, $(R_8Pc)LRhH$ and $[(R_8Pc)Rh]_2L$, has been confirmed by their ^1H and ^{31}P NMR spectra. These radicals are generated at room temperatures and do not react with CO, H_2, C_2H_4, or other hydrocarbons in refluxing benzene. The contrast between the inert phosphine-coordinated $(R_8Pc)LRh\bullet$ radical and the highly reactive four-coordinated $(R_8Pc)Rh\bullet$

radical suggests that the reactivity of the $(R_8Pc)Rh\bullet$ radical may be fine-tuned with an axial ligand.

Because of the difficulty in preparing and characterizing soluble phthalocyanine complexes, the catalytic chemistry of metallophthalocyanines has hardly been explored. We have shown that Rh-phthalocyanine complexes may duplicate some of the catalytic activities of Rh-porphyrin complexes.[10,11] It seems reasonable to expect this similarity to extend further. Utilizing the higher thermal stability of phthalocyanines, we will examine some of the higher temperature reactions at which metalloporphyrins are unstable. The effect of various axial ligands on the catalytic activity of the five-coordinated $(R_8Pc)LRh\bullet$ radical will also be a topic of our continuing studies.

B. *Materials Chemistry*

Our goal in this effort is to perform experimental and theoretical studies that lead to a basic understanding of materials chemistry. Our major focus in the past year was on determining the properties of high-critical-temperature (T_c) superconducting oxides and determining and applying quantum chemical methods for calculation of energies of clusters and molecules containing first-, second-, and third-row elements.

1. Studies of High-T_c Superconductors

We are investigating the properties of high-T_c superconducting oxides by use of electromotive force (emf) and X-ray diffraction measurements and molecular orbital calculations.

a. Structural Transitions and Thermodynamic Behavior

These studies explore the structural, nonstoichiometric, and thermodynamic behavior of high-T_c superconducting oxide systems as a function of oxygen partial pressure, oxygen stoichiometry, and temperature by means of a coulometric titration technique, where the oxygen content is varied by small, well-defined amounts. The objective of our current measurements is to determine the effect of ionic size of Ln (= Y, Gd, and Nd) on the immiscibility and structural transitions of the $LnBa_2Cu_3O_x$ system.

Our previous emf measurements on the $YBa_2Cu_3O_x$ system[12] indicated a miscibility gap centered at x = 6.65 with a consolute temperature of 473 K (200 ± 50°C). Knowledge of the presence and extent of such a miscibility gap is important for optimal preparation of high-T_c materials. The results of extensive emf measurements of oxygen

---

[10]A. E. Sherry and B. B. Wayland, J. Am. Chem. Soc. **112**, 1259 (1990).

[11]R. S. Paonessa, N. C. Thomas, and J. Halpern, J. Am. Chem. Soc. **107**, 4333 (1985).

[12]M. Tetenbaum, L. A. Curtiss, B. Tani, B. Czech, and M. Blander, "Oxygen Stoichiometry, Structural Transitions, and Thermodynamic Behavior of the $YBa_2Cu_3O_x$ System," *Physics and Material Science of High Temperature Superconductors*, eds., R. Kossowsky et al., NATO ASI Series E, Vol. 181, Kluwer Academic Publishers, Netherlands, pp. 279-296 (1990).

fugacities as a function of oxygen stoichiometry in the $NdBa_2Cu_3O_x$ system over the temperature range of 673-923 K indicated that, if a miscibility gap is present, it occurs at a much lower temperature and a higher value of x than was found for the $YBa_2Cu_3O_x$ system. Our current results did not show the slight hysteresis at 673 K in the composition range x = 6.65-6.85 observed in our earlier measurements with $NdBa_2Cu_3O_x$.[13] The relative locations of the miscibility gap for $YBa_2Cu_3O_x$ and the presumed miscibility gap for $NdBa_2Cu_2O_x$ are consistent with the effects of ionic radii on the composition dependence of T_c for these systems found by Veal et al.[14] For values of x > 6.5, partial pressures of oxygen above $NdBa_2Cu_3O_x$ were found to be higher than for the $YBa_2Cu_3O_x$ system. We also determined that rapid changes of partial molar entropies and enthalpies of solution of oxygen in $NdBa_2Cu_3O_x$ occur as x approaches the stoichiometric composition 6.00, indicating important structural transformations and order-disorder effects in the region x = 6.15-6.00 (for example, see Fig. IX-5).

In related work, a model has been developed for the $YBa_2Cu_3O_x$ system with x > 6.5. This model represents the thermodynamic properties and miscibility gaps in terms of a binary mixture of orthorhombic phase I (x = 7.0) and a coulombically ordered orthorhombic phase II. The coulombic ordering explains the composition at the consolute temperature in the miscibility gap of the $YBa_2Cu_3O_x$ system.

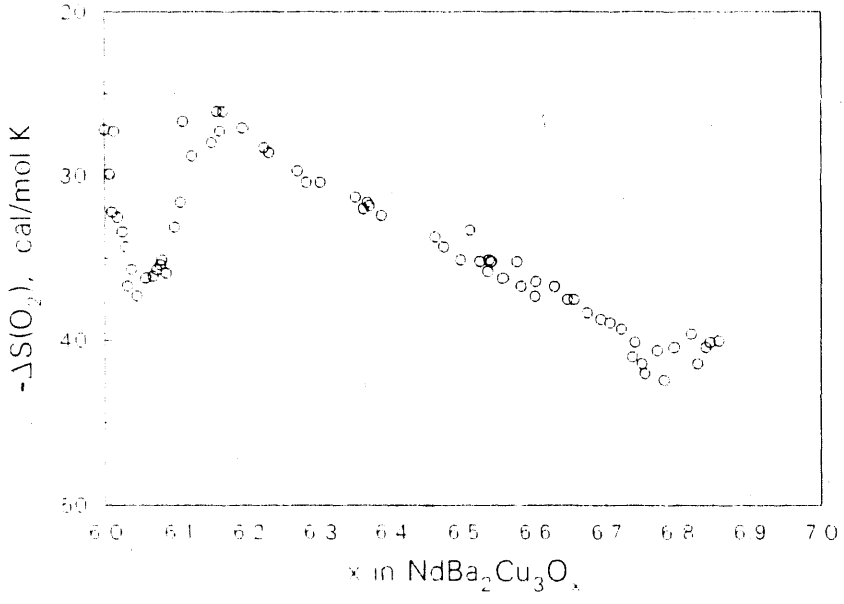

Fig. IX-5. Partial Molar Entropy of Solution of Oxygen, $\Delta\bar{S}(O_2)$, in $NdBa_2Cu_3O_x$

[13]M. Tetenbaum, P. Tumidajski, I. D. Bloom, D. L. Brown, and M. Blander, "Thermodynamic Behavior of High-T_c Oxide Systems via EMF and Related Measurements," in *New Physical Problems in Electronic Materials*, eds., M. Borissov et al., World Scientific Publishing Co., Singapore, pp. 259-280 (1991).

[14]B. W. Veal, A. P. Paulikas, J. W. Downey, H. Clavs, K. Vanderwoort, G. Tomlins, H. Shi, M. Jensen, and L. Morss, Physica C **97**, 162 (1989).

In the future we plan to investigate the nonstoichiometric behavior of the $GdBa_2Cu_3O_x$ and $Tl_2Ba_2CuO_6$ systems in collaboration with the ANL Materials Science Division. In addition, we will collaborate with the ANL Materials Science Division in attempting to confirm the miscibility gap deduced from our emf measurements in $YBa_2Cu_3O_x$, and we will continue to model the thermodynamic measurements of the $YBa_2Cu_3O_x$, $NdBa_2Cu_3O_x$, and related systems which exhibit strong nonideal solution behavior.

b. Phase Development Studies of High-T_c Superconducting Ceramics

The purpose of this research is to examine the factors that influence growth and stability of high-T_c phases in the lead-doped Bi-Sr-Ca-Cu-O system. The work is being conducted as part of a collaborative research agreement with American Superconductor Corp. (ASC). The ultimate goal is to determine the synthesis and processing parameters that have the greatest effect on the critical current properties of metal-sheathed high-T_c conductors.

The growth and stability of $(Bi_{2-x}Pb_x)Sr_2Ca_2Cu_3O_y$ (Bi-2223) phase fabricated into the form of silver-sheathed wires are being investigated by a combination of X-ray diffraction (XRD), scanning electron microscopy (SEM), energy dispersive X-ray analysis (EDX), and transmission electron microscopy (TEM). At ASC, silver tubes loaded with Bi-2223 precursor powders are processed into high-T_c wires by established metallurgical techniques. At ANL the wires are treated in a specially designed equilibration apparatus at selected temperatures (1083-1123 K), gas-phase oxygen concentrations (7.5% and 20%), and times (10 to 6000 min). Heating and cooling procedures included slow heating (~10 K/min), rapid heating (~100 K/min), slow cooling (~10 K/min), and rapid quenching (using liquid gallium or silicone oil). From these studies, it is possible to determine the ranges for time, temperature, oxygen partial pressure, and oxide composition wherein the precursor powder $(Bi_{2-x}Pb_x)Sr_2CaCu_2O_y$ (Bi-2212) transforms to Bi-2223.

We found that fractional conversion (Bi-2212 → Bi-2223) versus time data show excellent conformance to a kinetic model given by Carter[15] for a reaction taking place at the interface between spherical particles and a fine powder or a fluid. The results obtained to date for wires having Bi-2212 + $CaCuO_2$ as the representative starting phase mix show two distinct kinetic regimes. The more rapid of these regimes occurs between 5 and 80% conversion of Bi-2212 to Bi-2223 (at 1098 K and 7.5% O_2) and may involve a liquid-phase reactant. The slower regime (85 to 100% conversion of Bi-2212 to Bi-2223) is believed to involve only solid-state reactants. We are using SEM/EDX and TEM/EDX analyses to investigate the evolution of the Bi-2223 macrostructure (1 to 100 μm range) and microstructure (1 to 1000 nm).

[15]R. E. Carter, J. Chem. Phys. **34**, 2010 (1961).

2. Quantum Chemical Studies

a. Application of Accurate Quantum Mechanical Method

The Gaussian-2 (G2) theoretical procedure, developed in a collaborative effort with researchers at AT&T Bell Laboratories and Carnegie Mellon University, is a highly accurate general method for determining dissociation energies, ionization potentials, electron affinities, and proton affinities.[16] During the past year we have applied it to calculations concerning molecular interactions with surfaces and properties of silicon hydrides.

In work related to the electron stimulated desorption (ESD) studies of methanol on a Al(111) surface by researchers in the ANL Chemistry Division, we have used G2 theory to investigate the properties of a number of species that they are able to detect during ESD. An important finding of our theoretical work was that the literature value for the ionization potential of the methoxy radical is in error by about 3.5 eV because of an incorrect assignment of the photoelectron spectra.[17,18] In addition, the theoretical results have shown that the established experimental C-H bond dissociation energy[19,20] of methanol is in error. This has also been confirmed by an independent theoretical effort of Bauschlicher et al.[21]

We have used G2 theory to investigate the silicon hydrides, Si_2H_n(n = 0-6) and $Si_2H_n^+$(n = 0-7).[22] The thermodynamic properties of silicon hydrides are of fundamental interest, as well as of technological importance in the semiconductor industry. The resulting G2 energies were used to calculate appearance potentials and ionization potentials. The results are in general agreement with the recent photoionization study of Rusic and Berkowitz,[23] supporting their observation of the species Si_2H_2, Si_2H_3, Si_2H_4, and Si_2H_5 for the first time. Atomization energies of the neutral Si_2H_n species were calculated and used to derive enthalpies of formation. These enthalpies of formation are in agreement with the values derived by Ruscic and Berkowitz[23] for Si_2H_n(n = 2-5) and $Si_2H_n^+$(n = 2-6) and those of Boo and Armentrout[24] for Si_2H^+ and Si_2^+. The structures of some of the neutrals and cations, including $Si_2H_3^+$, Si_2H_2, $Si_2H_2^+$, Si_2H, and Si_2H^+, are characterized by unusual hydrogen bridges between the silicon atoms, illustrated in Fig. IX-6. This is in contrast to the analogous carbon systems in which only $C_2H_3^+$ has a bridging structure (single hydrogen bridge).[25]

---

[16]L. A. Curtiss, K. Raghavachari, G. W. Trucks, and J. A. Pople, J. Chem. Phys. **94**, 7221 (1991).
[17]L. A. Curtiss, L. D. Kock, and J. A. Pople, J. Chem. Phys. **95**, 4040 (1991).
[18]J. M. Dyke, J. Chem. Soc., Faraday Trans. II, **83**, 69 (1987).
[19]D. M. Golden and S. W. Benson, Chem. Rev. **69**, 125 (1969).
[20]S. Lias et al., J. Phys. Chem. Ref. Data **17**, Suppl. 1 (1988).
[21]C. Bauschlicher, S. Langhoff, and S. P. Walch, J. Chem. Phys. **96**, 450 (1991).
[22]L. A. Curtiss, K. Raghavachari, P. W. Deutsch, and J. A. Pople, J. Chem. Phys. **95**, 2433 (1991).
[23]B. Ruscic and J. Berkowitz, J. Chem. Phys. **95**, 2407 (1991).
[24]B. H. Boo and P. B. Armentrout, J. Am. Chem. Soc. **109**, 3549 (1987).
[25]L. A. Curtiss and J. A. Pople, J. Chem. Phys. **88**, 7405 (1988); **91**, 2420 (1989).

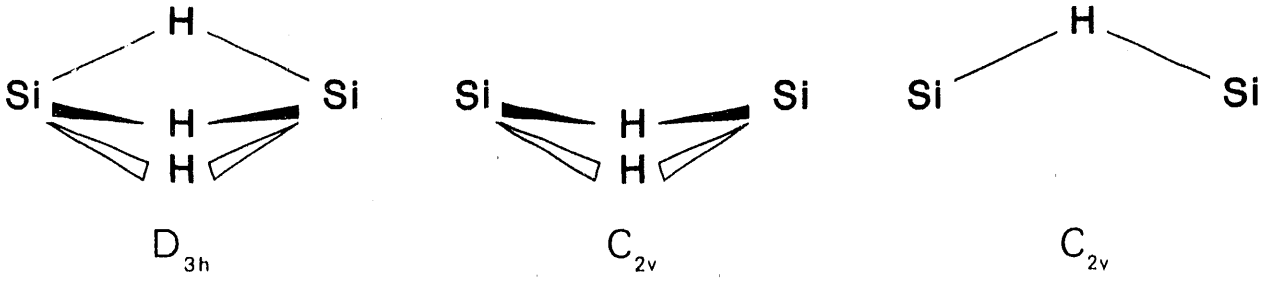

Fig. IX-6. Illustration of Hydrogen Bridging Structures for $Si_2H_3^+$ (left), Si_2H_2 and $Si_2H_2^+$ (center), and Si_2H^+ (right)

b. Metal Halide Complexes

A comparative study of $MAlF_4$ complexes (M = H, Li, Na) using *ab initio* molecular orbital theory, including correlation effects, has been carried out in collaboration with the Central Institute of Inorganic Chemistry (Berlin, Germany). These complexes have relevance to applications in high-temperature industrial processes, catalysis, chemical synthesis, and metal halide lamps. The three structures illustrated in Fig. IX-7 were investigated. Edge- and corner-bridged $HAlF_4$ structures were found to be nearly equal in energy (0.4 kJ/mol), with the results being quite sensitive to inclusion of correlation effects. We also found that the $LiAlF_4$ complex has an edge-bridged structure, the edge- and face-bridged structures of $NaAlF_4$ are of nearly equal stability, and the $HAlF_4$ complex is much less stable than the alkali complexes. The latter finding may be one of the reasons for the difficulties in observing this molecule.[26]

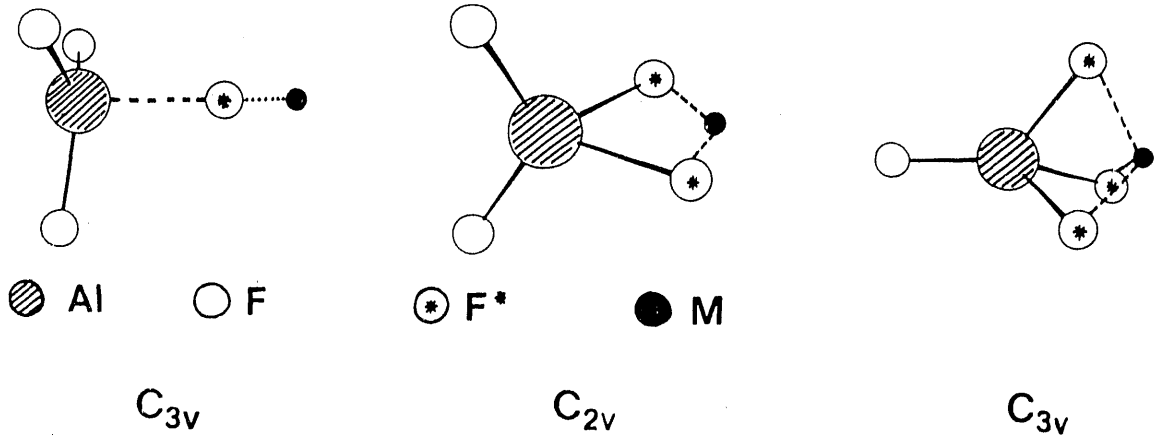

Fig. IX-7. Illustration of $MAlF_4$ Structures: Corner-Bridged (left), Edge-Bridged (center), and Face-Bridged (right)

[26]D. Menz, L. Kolditz, K. Heide, C. Schmidt, Ch. Kunert, Ch. Mensing, H. G. V. Schnering, and W. Honle, Z. Anorg. Allg. Chem. **551**, 231 (1987).

c. Future Work

We plan to further refine G2 theory so that it can handle molecules and clusters of larger size. We will also make use of new advances in computer technology, including the new Reduced Instruction Set Computers (RISC) and supercomputers such as the CRAY at the National Energy Research Supercomputing Center. The refined theory and new computer technology will be applied to the modeling of reactions occurring in molecular sieve materials and continued studies of metal atom clusters.

C. *Interfacial and Corrosion Science*

This research program consists of experimental and theoretical studies that focus on interfacial processes of importance to electrochemical and corrosion science, catalysis, and high-temperature superconductivity. The experimental work has three thrusts: (1) investigations of interface structure and dynamics over a wide range of temperatures, using novel procedures based largely on the integration of spectroscopic, X-ray scattering, and electrochemical techniques, (2) exploration of novel catalysis schemes employing molecular sieve materials, and (3) studies of phase evolution/stability in high-T_c superconducting oxide systems. Paralleling semiempirical and *ab initio* theoretical research is carried out to support and extend all of the above experimental pursuits.

1. Interface Structure and Dynamics

The interaction of metals and metal oxides with aqueous media is a phenomenon that has been studied extensively because of the many technologically important applications of water as a coolant, an electrolyte, or a solvent. The overall goal of this research effort is to provide experimental information against which theoretical models of the metal/water and metal oxide/water interface can be tested over a wide range of temperatures. The research program that we have established to reach this goal couples *in situ* surface-sensitive spectroscopic methods with interfacial electrochemical techniques and with theory. The experimental studies are proceeding along two concurrent lines. One involves the use of optical and X-ray spectroscopies to probe the structure and composition of the metal or metal oxide surface and the interfacial solution layer; the second is concerned with transient electrochemical measurements of electron transfer processes. All of this experimental work is closely coupled with a first-principles theoretical effort.

a. Spectroelectrochemical Studies of Aqueous Corrosion

This research has for its objective the elucidation of the interrelationship between the structural and transport properties of metal/solution interfaces and the mechanisms of interfacial reactions in aqueous solution environments. Electrochemical, laser Raman, infrared (IR), and X-ray techniques are employed to make *in situ* determinations of the composition of surface films on metals, the structure of the interface region, and the rates and mechanisms of the interfacial processes involved in the corrosion of metals.

The composition and structure of the passive film formed on nickel in a 0.1 M NaOH and 0.15 M NaCl solution were established by *in situ* surface-enhanced Raman spectroscopy (SERS) using an electrodeposited silver overlayer on a nickel substrate. We showed that (1) the film is composed of both $Ni(OH)_2$ and NiO, most probably in a bilayer structure with NiO closer to the metal, and (2) NiO is not formed as a consequence of a $Ni(OH)_2$ dehydration, but rather the two phases form independently. These results are significant not only for an improved fundamental understanding of the structure of passive films, but also because of their relevance to nickel-based batteries and electrochromic devices.

During this period, we also used *in situ* SERS to determine the composition of the near-monolayer corrosion film formed on chromium. Chromium in air and in aqueous solution is always coated by a layer of Cr_2O_3. At more positive potentials (>0 V vs. standard calomel electrode) in 0.15 M NaCl solution, we find evidence for the further oxidation of Cr(III) to Cr(VI), resulting in the formation of soluble chromate.

In collaboration with Memphis State University, we explored the use of attenuated total internal reflection/Fourier transform infrared (ATR/FTIR) spectroscopy to study passive films on metals. A search was made for the Ni-O and O-H vibrations of $Ni(OH)_2$ on the anodized surface of a ~150 Å nickel film deposited on a germanium ATR plate. We were not successful in detecting these vibrations due to the inadequate power of our conventional IR source, but we believe that the use of the high-powered IR radiation generated by a synchrotron would greatly facilitate this type of experiment. Accordingly, plans are being made to conduct such experiments at the National Synchrotron Light Source (NSLS) at Brookhaven National Laboratory.

b. Electrode Kinetic Studies

This research concentrates on gaining an understanding of the kinetic and mechanistic aspects of heterogeneous charge-transfer reactions in aqueous solutions for a wide range of temperatures. Heterogeneous charge transfer is an essential chemical reaction in aqueous corrosion studies and many energy-related technologies, such as batteries for electrical vehicles, large-scale fuel cells for primary electrical power generation, and photoelectrochemical energy production (e.g., water splitting). The kinetic measurements are carried out by relaxation techniques that employ galvanostatic, coulostatic, or potentiostatic pulse transients; ac impedance measurements; and rotating-disk electrodes combined with computerized data-evaluation methods. Method development is an integral part of this study, partly because little prior experimental work has been done at high temperatures, and partly because reaction rates at higher temperatures are much faster than ones normally measured at room temperature. The method development has included advances in experimental laboratory technique, measurement theory, and numerical data-evaluation procedures.

During the past year, we extended our experimental/theoretical charge transfer studies to the Cu^{2+}/Cu^0 electrode reaction in aqueous solution, which consists of two consecutive electron transfers followed by the incorporation of the copper adatom into the metal lattice. There were two reasons for choosing this reaction: (1) copper deposition has been identified as one of the most troublesome cathodic reactions occurring during corrosion in cooling systems of

light water nuclear reactors, and (2) this system provides an interesting challenge for the extension of our electron transfer theory methods (Sec. IX.C.1.c) to an ion for which the Jahn-Teller distortion of the hydration shell must be accounted.

We conducted preliminary experimental measurements on Cu^{2+}/Cu^{0} in perchloric acid solution at room temperature and have essentially reproduced some kinetic results reported in the literature.[27] However, the results of our numerical modeling of the transient response of this reaction indicate that the earlier conclusion predicting that the fast step of the reaction sequence is 1000 times faster than the rate-determining step was based on unjustified assumptions and will have to be reevaluated. As part of the preparation for this study, we developed a computer code that can solve the partial differential equations describing the system more efficiently than our previous code. To date, we have achieved about one order of magnitude improvement in computational speed. The numerical technique that we are utilizing (Keller's Box Method[28]) has never been applied to electrochemical reactions but appears to be applicable to a wide variety of problems in electrochemistry. The use of the improved code will be essential in the future, since it will permit us to carry out the required large-scale simulations needed in the evaluation of data from transient kinetic measurements of electron transfer at metal/solution and metal oxide/solution interfaces.

c. Theoretical Studies

The purpose of this research is to investigate electron transfer processes that are important in high-temperature electrochemical processes. This theoretical study uses a combination of molecular dynamics and molecular orbital methods to study electron transfer at an electrode/electrolyte interface. The work is being done in collaboration with the Corrosion Institute at the University of Minnesota, which is carrying out the molecular dynamics simulations and is developing algorithms for calculating electron transfer rates from the classical trajectories of the reactants. Molecular orbital calculations are performed in CMT to determine the potentials employed in the molecular dynamics calculations and to provide insights into electronic effects. The theoretical studies are closely coupled with the experimental studies in Sec. IX.C.1.b.

During the past year, we continued our effort to develop the theoretical model for Cu^{2+} in water necessary for studying the Cu^{2+}/Cu^{0} electron transfer reaction. Information from X-ray diffraction indicates that the Jahn-Teller distortion of the waters in the first solvation shell about the divalent cation is significant.[29] Our molecular dynamics code for modeling the solvation of the ferrous and ferric ions has been modified to include the Jahn-Teller effect. For this purpose, we used the pair potential for the interaction of Cu^{2+} with a water molecule derived from previous *ab initio* calculations. This is the first time that the Jahn-Teller effect has been incorporated into a molecular dynamics simulation of a solvated ion. Preliminary investigations

---

[27]E. Mattson and J. O'M. Bockris, Trans. Faraday Soc. **55**, 1586 (1959).

[28]H. B. Keller, "A New Difference Scheme for Parabolic Problems," in *Numerical Solution of Partial Differential Equations*, ed., B. Hubbard, Vol. 2, Academic Press, New York, pp. 327-350 (1971).

[29]M. Magini et al., *X-Ray Diffraction of Ions in Aqueous Solutions: Hydration and Complex Formation*, CRC Press, Boca Raton, LA (1987).

with this molecular dynamics code have focused on how time scales (such as rotation of the solvation shell, transitions between degenerate distortions, and vibrations of the first coordination shell) vary with parameters in the Jahn-Teller potential. The following conclusions have been made: on the longest time scales, the structure of the solvation shell is rotationally invariant; on intermediate time scales, the shell exhibits cubic (O_h) symmetry; and on the shortest scales, it shows the Jahn-Teller distortion (D_{4h}).

In closely related work, *ab initio* molecular orbital calculations have been used to examine the stability of Cu^0 in a water environment. The interaction energy of Cu^0 with a water molecule has been the subject of some disagreement. We have carried out new high-level calculations which indicate that the interaction energy is only about 0.2 eV. In addition, the calculated shift in the HOH bending vibration frequency is in good agreement with experimental results for this complex in a low-temperature argon matrix.[30] Theoretical studies were also carried out with additional water molecules added to the complex to simulate the liquid. These calculations also indicated a very weak binding of the water molecules to the neutral atom. These results will be used in our development of a model for studying the Cu^{2+}/Cu^0 electron transfer reaction.

d. Synchrotron Radiation Studies of Immersed Interfaces

Adsorbed layers and surface films at metal/solution and oxide/solution interfaces can range in thickness from less than a monolayer to many hundreds of monolayers. In recent years, extensive research has been done on the development of methods to investigate such interfaces. The most promising methods for determining structural properties are based on the use of X-rays, because of the ideal match of X-ray wavelengths to the desired dimensional information and the ability of X-rays to probe interfaces that are buried within condensed phases. In collaboration with the ANL Materials Science Division, we have developed a novel experimental technique that permits *in situ* X-ray investigations of immersed interfaces under uniform potential control. In the longer term, it is expected that our X-ray studies of immersed interfaces will make extensive use of the unique capabilities afforded by the Advanced Photon Source (APS) under construction at ANL.

During the past year, a series of combined X-ray and electrochemical measurements was made on thin copper films (~250 Å) supported on Si(100). These room-temperature measurements were carried out in borate buffer solution using the transmission-type X-ray electrochemical cell fabricated and tested in 1990.[31] In the past year, a methodology was developed for analyzing the observed fluctuations in the X-ray reflectivity patterns as a function of potential. This methodology employs the Fresnel laws of classical optics, modified to include the effect of correlated roughness between pairs of interfaces. The changes in scattering density at the copper/electrolyte interface during anodic and cathodic treatments of the copper films were found to be consistent with the formation and reduction of a copper oxide layer on the surface of

---

[30]J. W. Kaufman, R. N. Hauge, and J. L. Margrave, J. Phys. Chem. **89**, 3541 (1985).

[31]M. J. Steindler et al., *Chemical Technology Division Annual Technical Report, 1990*, Argonne National Laboratory Report ANL-91/18, p. 175 (1991).

the film. The thickness of the oxide layer and the underlying metal film, as well as interfacial roughness parameters, were determined as a function of potential. The results indicate that the copper film surface redensifies during reduction cycles but becomes progressively rougher with repeated oxidation/reduction cycles. These results represent first-of-a-kind X-ray reflectivity measurements on immersed, electrochemically controlled metal films.

While thin metal-film electrodes have proven highly useful for studies of passive film structure and growth dynamics by the X-ray reflectivity/electrochemical method, they do not exhibit the long-term stability required for detailed investigations of the electrical double layer. To circumvent this problem, we have begun to investigate the interfacial stability and behavior of noble-metal single crystals. The first phase of these investigations has involved X-ray reflectivity measurements on Pt(111) electrodes as a function of potential. During a series of oxidation and reduction cycles with Pt(111) in cesium fluoride solution, we found that the initially flat surface completely recovered its original morphology after reduction of the oxide film formed at potentials up to 500 mV (vs. Ag/AgCl electrode in 3 M KCl) but irreversibly roughened after oxidation at potentials exceeding 500 mV. Charge calculations from voltammetric measurements indicated that the critical oxygen coverage necessary to induce surface disorder is approximately one monolayer.

Preliminary results were obtained from an investigation aimed at determining the width and concentration distribution of the electrochemical double layer formed at the Pt(111) interface in cesium fluoride electrolyte. The intensity of reflected X-rays at a fixed momentum transfer was found to depend on the applied potential. This observation has been attributed to alteration of the concentration profile of cesium ions in the interfacial region as the electrode is polarized negative of the potential of zero charge. Such alterations are a signature of the reconstruction of the double layer following a voltage change.

The application of X-ray techniques to problems in interfacial and electrochemical science will be expanded in future years to include a wider variety of studies that take full advantage of the APS, such as X-ray Raman spectroscopy, X-ray imaging/microscopy, and X-ray absorption techniques. The emphasis of this work will continue to be on interface structure and dynamics utilizing the time resolution capabilities that will be afforded by the APS.

2. Research on Molecular Sieve Materials

Recent advances in the synthesis of novel molecular sieve materials have opened new vistas for product-selective catalysis of fuels and chemical feedstocks. This research is focused on studies of the mechanisms of sieve formation in gel media and the catalytic properties of the framework structures produced therefrom.

a. Theoretical Studies of Molecular Sieves

Ab initio molecular orbital theory continues to be employed for investigating the Bronsted acid strengths of ZSM-5 zeolites. We are studying TSi_nO_m clusters (T = Si, Al) tied off with hydrogens to determine the dependence of acid-site properties on cluster size. Although there have been many studies of acid sites using cluster fragments to represent the

zeolite framework, this is the first systematic study of the dependence of the results on cluster size. Clusters containing up to 25 oxygen atoms, 7 silicon atoms, and 1 aluminum atom have been used in this study. We have found the proton affinities to exhibit a surprisingly slow convergence with cluster size [variation of up to 126 kJ/mol (30 kcal/mol) with addition of a new coordination shell of silicons or oxygens]. This is due to long-range electrostatic effects. However, the calculated results for clusters with Si-O-Si and Si-O-Al central bridges indicate that, despite this slow convergence of the proton affinity, the use of small clusters to study the effects of substitutions in the Si-O-T bridge should be valid.

In contrast to proton affinities, the OH stretching frequency does not depend on cluster size. While the well depth at the bridging oxygen is sensitive to long-range electrostatic fields, the curvature of the potential energy surface apparently remains quite constant. The calculated OH stretching frequencies (3499-3623 cm^{-1}) are in agreement with experimental values (3609 cm^{-1}).[32] Finally, geometry relaxation effects in the clusters were found to be important for calculating both the vibrational frequencies and proton affinities.

In collaboration with Valparaiso University, we have calculated the electronic structure and X-ray absorption cross section as a function of energy in the near-edge region for cluster models of the local environment of oxygen in silica sodalite and its related aluminosilicate version. We are using these results to determine the effects of cluster size and the presence of aluminum (with a charge-balancing proton) on the oxygen 1s ionization energy and to assign features in measured X-ray absorption near edge spectra (XANES). Three clusters of increasing size are being used to model the local environment of oxygen in sodalite: (1) H_3SiOTH_3, (2) $(OH)_3SiOT(OH)_3$, and (3) $Si_7TO_8H_{16}$, where T = Si, Al. (The T = Al clusters include a charge-balancing proton attached to the central oxygen atom.) *Ab initio* molecular orbital calculations of oxygen 1s ionization energies were used to help determine input parameters for the local density approximation calculations of electronic structure, which were the basis for determining the X-ray absorption cross section. The calculated cross sections for the medium-size cluster, $(OH)_3SiOAl(OH)_3$, indicate a considerable influence of aluminum and the charge-balancing proton on the structure of the 1s absorption edge. Work is in progress on the larger cluster ($Si_7TO_8H_{16}$).

In future work on molecular sieves we plan to use the TSi_nO_m clusters to investigate the effect of substitution of metal atoms (T) on the acid strength of the oxygen site. The characteristics (vibrational frequency, charge, and proton affinity) of the bridging OH group will be studied as a function of substitution of a Si site by B, Ga, Ti, and Fe. The effect of geometry changes will be included, and the results will be correlated with infrared spectroscopic studies of the O-H stretching frequencies. In addition, we will also use these clusters to investigate the interactions of molecules such as NH_3 and C_2H_4 with the acid site. This will include determining properties which are difficult to derive experimentally, such as the equilibrium structures, barrier to proton transfer, and barriers to hopping from one acid site to another.

---

[32] J. Datka, M. Boczar, and P. J. Rymarowicz, J. Catal. **114**, 368 (1988).

b. Studies of Catalysis by Molecular Sieve Materials

In this research effort, we seek to gain new understanding of the catalytic activity and product selectivity demonstrated by molecular sieve cage networks of medium pore size (4 to 8 Å). Infrared spectroscopy is used in conjunction with gas chromatography to provide detailed information on structure-composition-reactivity relationships for a variety of light hydrocarbon reactions on selected aluminosilicate and aluminophosphate framework systems. The emphasis of this work in recent years has been on development of a molecular sieve-based catalyst with two functions: converting methane into higher hydrocarbons (C_{2+}) and providing selective control of the product mix.

During the past year, transition metal-sulfur clusters have been synthesized in cages of molecular sieve materials. The molybdenum-sulfur-loaded molecular sieve, Mo_xS_y/Y zeolite, exhibited detectable catalytic activity for methane coupling in a reducing environment at temperatures of 575 to 700 K. When CH_4/H_2 mixtures were fed to a packed-bed reactor containing Mo_xS_y/Y zeolite at 625 K, small but detectable quantities of ethane, ethylene, propane, and propylene, plus traces of C_4 and C_5 hydrocarbons, were found downstream of the reactor. There was no evidence for co-production of carbon oxides, indicating that the C_{2+} selectivity is near 100%. The mechanism by which this methane activation catalysis is believed to occur involves pairs or groups of coordinatively unsaturated molybdenum ions in trimeric clusters.

Infrared spectroscopic studies of the Mo_xS_y/Y revealed a strong chemisorption of CO at temperatures up to 525 K, which was not present in any closely related materials, such as MoO_3/Y, H-Y, or neat MoS_2 powder. Activation of the catalyst with H_2/He at 625 K prior to CO adsorption enhanced the CO binding.

When Mo_xS_y/Y was treated with H_2 at 625 K, purged with helium to remove gaseous H_2, then exposed to methane, only trace amounts of C_{2+} products were detected. If, however, H_2 was fed to the reactor along with the methane or was fed in after methane exposure, much greater quantities of C_2H_6, C_2H_4, C_3H_6, C_3H_8, and C_4H_{10} were detected. Gas chromatographic results of an experiment where the H_2-activated Mo_xS_y/Y was exposed to CH_4, purged of excess gaseous CH_4, then treated with H_2 are given in Fig. IX-8. In similar experiments where CO was used in place of CH_4, the C_{2+} product mix was dominated by C_3H_6 and C_3H_8.

Studies of the effect of temperature (575 to 725 K) on the fractional conversion of CH_4/H_2 mixtures to C_{2+} hydrocarbons with Mo_xS_y/Y zeolite indicated that the optimum temperature is around 625 K. Rehydrogenation of the reaction intermediates back to methane (as opposed to C_{2+} hydrocarbons) increased with increasing temperature beyond 625 K. Also, the fractional conversion of CH_4/H_2 mixtures increased with increasing contact time in the catalyst bed, and no CO or CO_2 (above background levels) was detected in any of the CH_4/H_2 experiments. Taken collectively, the results to date show that conversion of CH_4 to C_{2+} hydrocarbons over Mo_xS_y/Y in the presence of H_2 occurs with high selectivity (near 100%) but at a low conversion rate. The Mo_xS_y/Y material retains its activity over many cycles and is

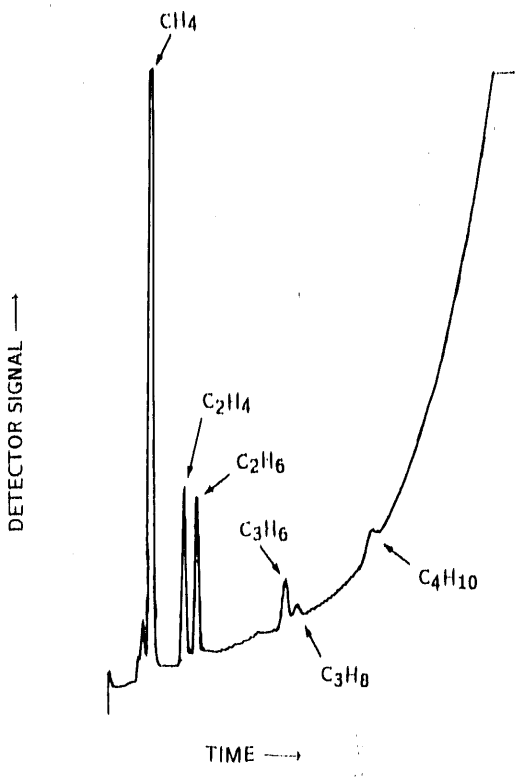

Fig. IX-8.

Gas Chromatogram of Products Trapped after Sequential Exposure of Mo_xS_y/Y to H_2, UHP (ultra high purity) He, CH_4, UHP He, and finally H_2 at 625 K

insensitive to treatment with H_2S, but can be regenerated with H_2S if it is exposed to oxygen or H_2O. Blank methane activation experiments with MoO_3-loaded Y zeolite, using the same procedures that gave clear evidence of C_{2+} products over Mo_xS_y/Y, did not produce any detectable hydrocarbons other than unreacted methane. This establishes the need for the catalyst to be in a sulfided form. The plan for future work in this area is to develop methane activation catalysts that facilitate higher conversion rates to C_{2+} products.

3. Preparation of High-T_c Films by Alloy Oxidation

The objective of this research effort is to develop methods for the preparation of high-T_c superconducting ceramic films by oxidation of liquid alloy precursors. In this effort, we have prepared textured high-T_c films of $YbBa_2Cu_3O_{7-\delta}$ supported on single-crystal ($SrTiO_3$ and MgO) and polycrystalline (MgO) substrates by oxidation of a liquid precursor alloy. For this preparation, the substrates were coated by dipping them into a molten alloy ($YbBa_2Cu_3$, mp 1143 K), withdrawing them from the melt, then oxidizing the adhering liquid alloy layer to the corresponding oxide phase, i.e., $YbBa_2Cu_3O_{7-\delta}$. The oxidized films, typically 10-μm thick for single-crystal substrates and 20-μm thick for polycrystalline substrates, had smooth surfaces and exhibited a uniform coloration.

These samples were analyzed by XRD and SEM. We found that the XRD patterns of the film surfaces on the single-crystal and polycrystalline substrates are dominated by the {001} peaks of orthorhombic $YbBa_2Cu_3O_{7-\delta}$. Moreover, the lattice parameters for the film on the polycrystalline MgO are essentially the same as those obtained on the single-crystal substrate,

presumably due to the similar synthesis/processing conditions. A peak located at $2\theta = 33^{\circ}$, corresponding to the most intense peak of randomly oriented $YbBa_2Cu_3O_{7-\delta}$, appears for both types of samples but is slightly more prominent for films on polycrystalline substrates. Small amounts of impurity phases, mainly $BaCuO_2$ and Yb_2BaCuO_5, are also present (more in the case of polycrystalline substrates than single crystals).

The results obtained with the polycrystalline MgO substrates demonstrated that textured films can be produced without exclusive use of single-crystal substrates. The resulting films show preferential c-axis orientation, which is most probably due to rapid anisotropic crystallization of $YbBa_2Cu_3O_{7-\delta}$ caused by a tendency of all available MgO facets to nucleate a-b plane growth in preference to a-c or b-c plane growth. It is possible that the rapid oxygen diffusion and phase formation, occurring at kinetically favorable liquid metal/solid oxide phase boundaries, facilitate this anisotropic growth.

Films on the single-crystal $SrTiO_3(100)$ and MgO(100) grew in a regular rectangular pattern of platelets (dimensions of ~15 x 15 μm each), corresponding to the {001} surface of $YbBa_2Cu_3O_{7-\delta}$. Some cracks were observed in the SEM surface view, and separations among the platelets were systematically present. For films on polycrystalline MgO substrates, the a-b plane growth platelets were still present, confirming a growth pattern favoring the {001} planes of orthorhombic $YbBa_2Cu_3O_{7-\delta}$. However, the platelet dimensions (typically ~4 x 4 μm) were about four times smaller than those observed for films nucleated on MgO(100) and were completely randomly oriented in terms of a- and b-axes direction, even though the c-axis platelets were predominantly perpendicular to the substrate surface. The randomly oriented a-b platelets are believed to be a consequence of the polycrystalline nature of the substrate.

The superconducting transitions for the best films prepared in this study begin at around 80 K, which is below the 90 K value normally observed for $YbBa_2Cu_3O_{7-\delta}$. Approximate critical current densities (J_c) were also determined for several samples [at 56 K and zero field for films on $SrTiO_3(100)$ and MgO(100) and at 50 K and zero field for films on polycrystalline MgO substrates]. The critical current was obtained from the inflection point in the current vs. voltage curve and yielded low J_c values: ~1000 A/cm^2 and ~500 A/cm^2 for films on single-crystal $SrTiO_3$ and MgO, respectively, and ~130 A/cm^2 for the film on polycrystalline MgO.

The somewhat low T_c value for as-prepared samples is most probably due to incomplete oxygenation of the orthorhombic $YbBa_2Cu_3O_{7-\delta}$, caused by slow oxygen diffusion along the c-axis, i.e., relative to that in the a- and b-axes directions. The low J_c values are undoubtedly caused by the crack development observed in the SEM micrographs of the film surface. Thinning of the liquid alloy layer prior to oxidation (to produce thinner films of the high-T_c oxide) should help to alleviate crack formation.

D. *Geochemistry*

The geochemistry research program includes efforts in two general areas: (1) geochemistry and evolution of hydrothermal systems associated with volcanic areas and (2) isotopic and molecular geochemistry of petroleum in sedimentary basins. The approach being taken is to

investigate specific problems through detailed chemical and isotopic analyses of rock, mineral, water, gas, and oil sampled from appropriate, well-characterized field areas. Potential applications of this work are in nuclear waste management; geothermal energy development; and exploration for minerals, oil, and natural gas.

1. Radium Geochemistry and Isotopy of Thermal Waters in Yellowstone National Park, Wyoming

The extent of radioactive disequilibrium among members of the ^{238}U and ^{232}Th decay series can be exploited for many applications in the earth and environmental sciences. For example, Krishnaswami et al.[33] proposed that measurements of actinide-series isotopes in groundwater can be used to estimate *in situ* adsorption-desorption rate constants and retardation factors. However, insufficient data are available to evaluate such applications thoroughly. For example, while numerous studies have been performed on uranium isotope behavior in groundwater, relatively few studies have been performed on radium isotope behavior. Therefore, we chose to characterize the behavior of radium isotopes in the Yellowstone hydrothermal system, which affords a wide range of contrasting physical and chemical conditions in which to observe this behavior. Radium isotopes are unlikely to be fractionated by chemical processes because of their relatively small mass difference.

Three of the four radium isotopes in the uranium and thorium decay series were considered in this study: ^{226}Ra (half-life = 1602 yr) in the ^{238}U series, ^{228}Ra (half-life = 5.75 yr) in the ^{232}Th series, and ^{224}Ra (half-life = 3.64 d) in the ^{232}Th series. All of these radium isotopes are produced by α-decay of longer-lived thorium isotopes. The most abundant radium isotope is ^{226}Ra, which exceeds 99 at. % of natural radium. The second most abundant radium isotope is ^{228}Ra. The $^{228}Ra/^{226}Ra$ ratio in groundwater is related to the Th/U ratio in the radium source and is, therefore, a potential indicator of aquifer compositional characteristics and water-rock interactions on long (from decades to thousands of years) time scales. The $^{224}Ra/^{228}Ra$ ratio is an indicator of water-rock interaction kinetics on shorter (from days to years) time scales. A close chemical analog for radium is barium, because they are both alkaline earth elements having similar ionic radii. The Ra/Ba ratio in groundwater provides evidence pertaining to the source and input of Ra and Ba.

Radium concentrations and isotope activity ratios were measured for water from 29 thermal springs throughout and immediately north of Yellowstone Park, and from the U.S. Geological Survey's drill hole (Y-10) at Mammoth Hot Springs. These measurements were made by γ-spectrometry at ANL, following quantitative extraction of the radium onto a radium-selective ion exchange resin. Temperature and pH of the waters were measured on site using an electronic meter. Concentrations of Al, B, Ba, Ca, Fe, K, Li, Mg, Mn, Na, Si, and Sr were also measured by use of an inductively coupled plasma with atomic emission spectrometry at ANL.

---

[33] S. Krishnaswami, W. C. Graustein, K. K. Turekian, and J. F. Dowd, Water Resour. Res. **18**, 1633 (1982).

The radium concentrations were determined to range from <0.2 to 37.9 dpm/kg (corresponding to $<10^{-15.3}$ to $10^{-12.8}$ molal). The lowest radium concentrations were found in boiling neutral-chloride waters from the Upper and Norris Geyser Basins, and the highest were found in Ca-HCO_3-SO_4 waters from Soda Butte and Mammoth Hot Springs. As shown in Fig. IX-9, the $^{228}Ra/^{226}Ra$ activity ratios for the thermal waters ranged from 0.26 to 14.2. All ratios less than 0.7 occurred with Ca-HCO_3-SO_4 waters at and north of Mammoth Hot Springs and at Soda Butte, and all ratios for neutral-chloride and acid-sulfate-chloride waters were from 0.99 to 14.2. The $^{224}Ra/^{228}Ra$ activity ratios ranged from 0.73 to 3.1, with the highest values being from waters having relatively low pH (3.2 to 4.5).

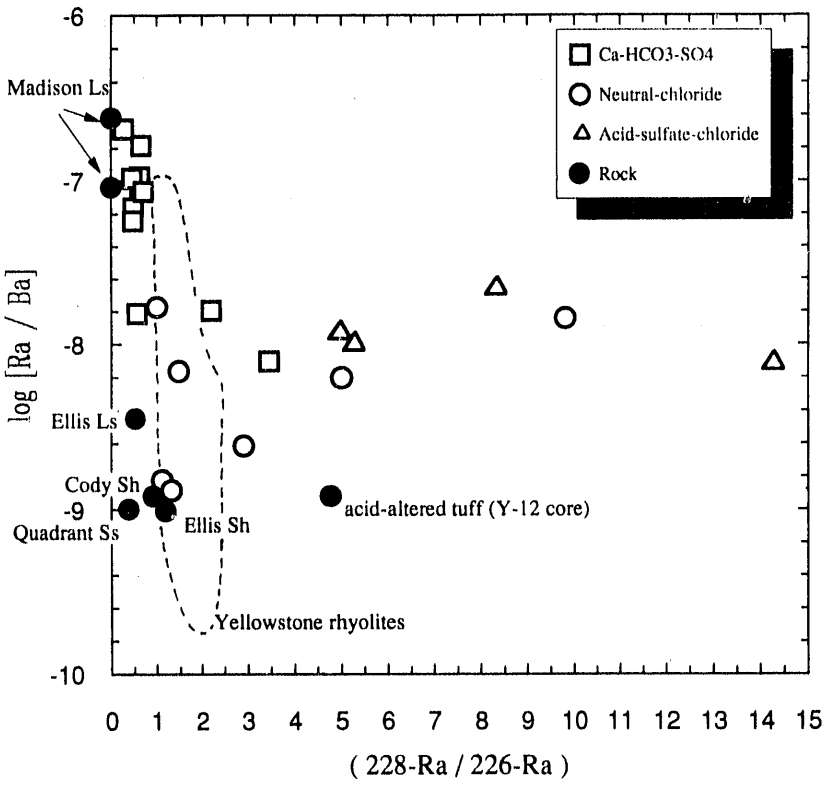

Fig. IX-9. Measured Values of Ra/Ba Molal Concentration Ratio vs. $^{228}Ra/^{226}Ra$ Activity Ratio for Yellowstone Thermal Waters (open symbols) and Calculated Values for Sedimentary Rock Samples (filled symbols). The rock values were calculated from measured U/Ba and Th/U ratios, assuming radioactive equilibrium. Also shown (within dashed line) is the field of calculated values for 31 samples of unaltered Yellowstone rhyolites.

One of the principal conclusions from this study is that the concentrations of radium in Yellowstone thermal waters are correlated with the solubilities of barite, anhydrite, and calcite at aquifer temperatures in most of the areas studied. The most likely control of dissolved radium is its substitution for barium in trace amounts of barite solid solution. Waters significantly

undersaturated with barite at aquifer temperatures were found only within the Upper Geyser Basin, where aquifers include altered vitrophyric rhyolite containing abundant zeolite minerals. In these waters, radium concentrations are influenced by zeolite-water ion exchange.

Another conclusion from this study is that the Ra/Ba and $^{228}Ra/^{226}Ra$ ratios of Yellowstone thermal waters are correlated with the U/Ba and Th/U ratios of the aquifer rocks, respectively (Fig. IX-9). This is consistent with a model in which (1) Ra and Ba are supplied to water mostly by bulk dissolution of aquifer rock, and (2) chemical equilibration of water with rock is rapid relative to the decay of ^{226}Ra in different thermal areas. The relatively high $^{228}Ra/^{226}Ra$ ratios in some thermal waters, compared to those expected of aquifer rocks, implied excess contributions of ^{228}Ra, possibly from surficial concentrations of ^{232}Th within the aquifer rocks or from α-recoil. If α-recoil is responsible for most excess ^{228}Ra, this would have significant implications with respect to the kinetics of water-rock interaction. The mechanism generating the excess ^{228}Ra cannot be clarified without additional details regarding the distribution of thorium within the aquifer rocks. Plans for future work include characterizing the micron-scale distribution of thorium within aquifer rocks.

We also found that excess ^{224}Ra is nearly ubiquitous in Yellowstone thermal waters; the $^{224}Ra/^{228}Ra$ ratios can be used to estimate travel time from aquifer to spring in some areas of thermal water discharge; and they can also be used to estimate average linear velocity in such cases if aquifer depth is known (e.g., ≥ 1 m/h for thermal water at Mammoth Hot Springs). Larger scale chronometric applications of radium isotopes (especially ^{226}Ra and ^{228}Ra) may be precluded by the relatively rapid chemical equilibration in hydrothermal systems.

2. Origin and History of Petroleum: Compound-Specific Isotopic Evidence

With the acquisition of a new gas chromatography/isotope ratio mass spectrometer (GC/IRMS) instrument, we have embarked on a program of research that will exploit the unique capabilities of this instrument for compound-specific carbon isotopic analysis in studying petroleum geochemistry. This research will address fundamental questions regarding the origin and history of petroleum. Examples of such questions include: the relation between source rock quality and the depositional environment; the relation between oil composition and source rock type; the nature of chemical changes that occur within organic matter during diagenesis and catagenesis; the effects of migration, mixing, and biodegradation on oil composition; and the validity of oil-source rock and oil-oil correlations. A number of suites of well-characterized petroleum samples have been acquired for this research from collaborating scientists at major oil companies, the U.S. Geological Survey, the Illinois Geological Survey, and several universities. Each sample suite was selected to address one or more of the fundamental questions noted above.

Before initiating analyses of samples, we devoted considerable effort toward establishing an accurate and reproducible GC/IRMS analysis procedure. A mixture of n-alkanes of known carbon isotopic composition was prepared to test the accuracy and reproducibility of the instrument. Repeated analysis of this mixture over a period of about six months has shown the instrument to reproduce the known values accurately with a precision of better than 0.6 parts per thousand. Several experiments were performed to determine whether isotopic fractionation of hydrocarbon compounds occurs during standard fractional separation of oils (into saturate,

aromatic, polar, and asphaltene fractions) with open-column silica gel chromatography. The results of this experiment indicated that the isotope ratios of compounds in the n-alkane mixture did not change during this separation procedure. Another experiment was performed to test the ability of the GC/IRMS system to accurately measure carbon isotope compositions of n-alkanes in complex mixtures. To simulate a natural (unresolved high background) crude oil sample, a biodegraded saturate fraction was mixed in different proportions with the n-alkane mixture mentioned above. Analysis results from these mixtures reproduced the n-alkane values accurately within analytical uncertainty. Thus, we have demonstrated our ability to analyze carbon isotopic compositions of n-alkanes in crude oils and in fractions of crude oils accurately and precisely using GC/IRMS. Further work remains to extend the ability to branched and cyclic alkanes as well as aromatic compounds.

3. New Facilities

This year we purchased a high-purity germanium detector and associated hardware for gamma spectrometry. This system is based on a 122%-efficient detector having good resolution (1.8 keV at 1.33 MeV), and we are setting it up in an underground counting room with additional low-background Pb, Cd, and Cu shielding. This system will be used primarily for low-level actinide-series measurements.

X. ANALYTICAL CHEMISTRY LABORATORY

The Analytical Chemistry Laboratory is a full-cost-recovery service center, with the primary mission of providing a broad range of analytical chemistry support services to the scientific and engineering programs at ANL. In addition, the ACL conducts a research program in analytical chemistry, works on instrumental and methods development, and provides analytical services for governmental, educational, and industrial organizations. The ACL handles a wide range of analytical problems, from routine standard analyses to unique problems that require significant development of methods and techniques.

The ACL is administratively within CMT, its principal client, but provides technical support for most of the technical divisions and programs at ANL. The ACL has four technical groups--Chemical Analysis, Instrumental Analysis, Organic Analysis, and Environmental Analysis--which together include about 50 technical staff members.

The Chemical Analysis Group uses wet-chemical and instrumental methods for elemental, compositional, and isotopic analyses of solid, liquid, and gaseous samples and provides specialized analytical services. The Instrumental Analysis Group uses nuclear counting techniques in radiochemical analyses over a wide range of sample types, from environmental samples with low radioactivity to samples with high radioactivity that require containment. Other types of analyses use X-ray diffraction and fluorescence of solids, inert gas fusion of metals, and neutron activation of either liquids or solids. The Organic Analysis Group uses a number of complementary techniques to separate and to quantitatively and qualitatively analyze, at the trace level, complex organic mixtures and compounds, including toxic substances, fossil-fuel residues and emissions, environmental pollutants, biologically active compounds, pesticides, and drugs. Organic Analysis Group personnel also develop methods for such purposes as detecting organic compounds remotely with Fourier transform infrared (FTIR) spectrometers and performing rapid on-site analyses for organic constituents. The Environmental Analysis Group performs analyses for the inorganic constituents of environmental, hazardous waste, and coal samples.

The majority of the ACL technical accomplishments are contained in previous sections of this report and in similar reports of other ANL divisions. Selected accomplishments are also summarized here.

Engineering Studies of Pyrochemical Processes for Integral Fast Reactor (IFR) Fuels

In the electrorefining of uranium and plutonium fuels for the IFR, metallic fuel pins (U, Pu, Zr) are dissolved in a molten cadmium anode. The actinide elements are electrochemically transported through a halide-salt electrolyte to the cell cathode, where they are collected as a metallic deposit. Engineering-scale studies of this electrorefining process are being conducted in CMT (Sec. VI.C) to develop models that can predict the recovery of U and Pu, as well as the decontamination of these elements from fission-product elements and process materials. The ACL has contributed to this effort by determining elements of interest in samples from the cadmium anode, the halide-salt electrolyte, and the cathode product. Special dissolution

procedures are followed for each type of sample matrix, and separation schemes based on solvent extraction and ion exchange are used to isolate the desired elements from matrix components and, subsequently, to separate these elements. Uranium and plutonium concentrations in IFR samples are measured with an inductively coupled plasma/atomic emission spectroscopy (ICP/AES) instrument configured to analyze radioactive solutions. The mass spectrometric isotope dilution (MSID) technique is used whenever higher precision and accuracy than attainable with ICP/AES are required.

Samples were analyzed for zirconium by ICP/AES. Zirconium constitutes about 30 vol % of the IFR fuel and will be anodically dissolved in the electrorefiner during fuel reprocessing. Our analyses of components from the engineering-scale electrorefiner, after completion of uranium electrotransport experiments, provided insight to the fate of zirconium in the system. In addition, chemical analyses for various electrorefiner experiments helped demonstrate the concept of using a liquid cadmium cathode for obtaining a Pu-U mixture from spent IFR fuel.

Analyses in support of experiments dealing with IFR waste (Sec. VI.D) continued. Electrolytic salts containing small amounts of actinides (U, Pu, Am) were stripped of their heavy metals by reaction with lithium in Cd-Li solutions at ~500°C. Analytical data from ICP/AES measurements showed sufficient reduction of actinides to allow disposal of these salts as a non-TRU waste.

Distribution studies of Nd and Pu in the cadmium metal-salt system were undertaken to understand their behavior in the pyrochemical process. The MSID method was used for the measurement of both Nd and Pu. From the data collected, distribution coefficients for these elements were determined over several orders of magnitude in metal and salt phases.

Competitive Exchange Experiments in IFR Chemical and Engineering Support Studies

Pyrochemical reprocessing of fuel in the IFR concept is based on the partitioning of chemical constituents from the spent metal fuel between molten cadmium and a molten LiCl-KCl eutectic. In one of the Chemical Engineering and Support Studies being conducted for the IFR (Sec. VI.A), researchers are using competitive exchange techniques to determine separation factors for elements of special interest, especially the lanthanides and alkaline-earth metals. These experiments start with two metals of interest, such as Y and Sm, dissolved in the cadmium phase or distributed between the salt and cadmium phases, depending on the relative activity of the metal pair. Then, successive additions of cadmium chloride or another metal chloride are made to change the relative amounts of these metals in each phase. Both cadmium and salt phases are sampled in each step of the experiment, and the metal concentrations determined in the samples are used to compute the separation factor. Analytical support for these studies includes analysis of the salt and metal phases to determine not only the elements involved in the competitive exchange, but also a variety of other parameters related to mass-balance checks and conditions prevailing during each experiment.

In most cases, each salt phase is analyzed to determine Li, K, Cd, and the pertinent rare earths by ICP/AES and chloride by silver-chloride gravimetry. Each cadmium metal sample is similarly analyzed to determine Li, K, the rare earths, and Cl. Cadmium in the metal samples is

measured by titration with ethylenediaminetetraacetic acid. Many salt samples are tested for the presence of species oxidizable by ferric ion according to a procedure developed for measuring concentrations of divalent rare earths (Sm^{2+}, Eu^{2+}), which were present in some past experiments.

During FY 1991, approximately 130 salt-phase or cadmium-phase samples were analyzed for this project. Competitive-exchange studies between rare earths were extended to include characterization of separation factors between the rare earths and selected other elements. Experiments involved element pairs containing yttrium with cerium and yttrium with samarium. The Y-Sm experiment provided separation factors for the pair. Because lithium was transferred from the salt to the metal phase in these experiments, information was also obtained on the Li-Sm pair. Recently, measurements were begun to obtain similar information on the Sm-Eu-Li-Ba-Sr system. Preliminary results from samples associated with these experiments suggest the presence of unanticipated species in the salt phase. Methods for the qualitative and quantitative determination of these species are being investigated in the ACL.

X-ray Diffraction of Zeolite Materials

Zeolites are candidate materials for immobilizing IFR waste salt (Sec. VI.D.3). X-ray diffraction (XRD) is a useful analytical technique for identifying phase changes resulting from the effects of dehydration procedures, equilibration temperatures, and salt compositions on the crystal structure of zeolites equilibrated with molten simulated IFR salt. This technique was used to identify non-zeolitic decomposition products that were formed during the equilibration of zeolite with molten salt under different experimental conditions. The XRD data were used for estimating the amount of non-zeolitic material in samples containing mixtures of salt-occluded zeolite and non-zeolitic material. Relative compositional estimates were made from peak-height ratios determined for the major non-overlapped intensity peak of each phase. This is a reasonable approximation since the structures of the zeolites are not known completely. The XRD technique is being used to screen new starting materials and to determine phase stability by correlating changes in crystal structure with different experimental conditions.

Phase Composition/Solubility Studies on Equilibrated Mixtures of LiCl and KCl in Water

The LiCl-KCl eutectic electrolyte used in the electrorefining step of the IFR pyroprocess is inherently hygroscopic, and the possibility exists that this electrolyte could absorb water in the event of an earthquake and resulting destruction of the reprocessing facility. Conceivably under certain conditions, neutrons could be moderated by the diluted electrolyte and lead to criticality.

Researchers in CMT are studying the equilibrium compositions of solid and liquid phases in mixtures of LiCl, KCl, and water at 8 to 10 temperatures ranging from 1 to 40°C above the dew point (in air of fixed absolute humidity) in each of four discrete experiments. The purposes of this work are to (1) understand the relationship among temperature, humidity, and the compositions of all solid and liquid salt-containing phases, (2) provide some of the data necessary to evaluate worst-case scenarios for the possibility of criticality, and (3) develop a facility design that precludes such criticality.

The ACL has thoroughly characterized 33 samples in support of this work. The samples included both LiCl/KCl solutions obtained from the equilibration studies and salts that separated from these solutions when equilibrium was reached under experimental conditions. The water and residue (salt) contents of each sample were determined, as well as the chemical composition of each residue. The amount of residue available for compositional analysis was generally small, ranging from 100 to 500 mg.

Water content was determined as weight loss on heating to a temperature of 350°C. The residue from the water determination was weighed and dissolved in water to provide a weighed solution from which weight aliquots were taken for determining Cl, K, and Li content. Chlorine, which is present as chloride, was determined gravimetrically as AgCl. After determination of the chloride content, the K and Li contents were calculated based on mass and charge balances and the knowledge that only K, Li, and Cl are present in the residue. Using the calculated values, we were able to take aliquots of an optimum size for the K and Li determinations.

Potassium content was measured in the aliquots by a semi-micro gravimetric procedure as potassium tetraphenylborate. In a few cases where the amount of potassium available was insufficient for a gravimetric determination, the potassium content was measured by ICP/AES. Lithium content was measured by thermal ionization mass spectrometry (TIMS), using an isotope dilution technique with a ^{6}Li spike.

Results from these measurements have allowed an accurate accounting of the salt components in the liquid and solid phases that occur under various salt/water equilibrium conditions. The data have provided information on not only the extent of water absorption by the eutectic salt, but also the compositional changes that occur as the brine produced by water absorption becomes saturated, with re-separation of a solid phase. Empirical correlation and theoretical interpretation of the results are expected to benefit from the accuracy and completeness of the analytical measurements performed for this project.

Procedures for Determining Uranium and Uranium Isotopes in High Silica Soils

High silica soils present a special challenge to the analyst determining total uranium and uranium isotopes for environmental monitoring and remediation studies because quantitative recovery of the uranium requires complete dissolution of resistant siliceous mineral phases. This past year, the ACL developed and implemented procedures which provide (1) complete dissolution of high silica soils without time-consuming fluoride/pyrosulfate fusions of the sample, (2) convenient measurement of total uranium by laser kinetic phosphorimetry, and (3) efficient isolation of uranium from the dissolved sample for isotopic analysis by TIMS. These procedures take advantage of ACL experience in dissolution chemistry, recent ANL advancements in actinides separation technology, and the capabilities of existing ACL instrumentation.

Complete dissolution of silica-bearing materials is accomplished by placing the sample (typically 0.25 g) in a Teflon-lined pressure vessel (Parr Decomposition Vessel) with a mixture of nitric and hydrofluoric acids and then heating overnight at moderate temperature (150°C). The solution from the Parr Decomposition Vessel is evaporated to dryness, and the residue is

redissolved in dilute nitric acid for direct introduction to a Kinetic Phosphorescence Analyzer, which measures total uranium. The unused portion of this same solution is again taken to dryness and treated with sulfuric acid to remove fluoride, which inhibits separation of aluminum from uranium in subsequent operations (AlF_3 follows uranium in the column-extraction chromatographic process, although uncomplexed aluminum does not). The treated residue is dissolved in 2 N nitric acid and passed through a U/TEVA•Spec chromatographic column to isolate a pure uranium fraction for TIMS determination of the isotopic composition.

Performance of the procedures has been monitored under actual production conditions by analyzing a high silica matrix standard, NBS* Standard Reference Material (SRM) 4353 ("Rocky Flats Soil Number 1"). This laboratory control standard (LCS) was processed with each batch of field samples. Over a period of nine months, during which almost 200 soils and 18 laboratory control samples were analyzed, the LCS data showed an average recovery for total uranium of 96.8%, and a standard deviation of 4.5%, relative to the 3.15 μg U per g soil reference value. Isotopic data for ^{234}U and ^{238}U agree with NBS reference values within the uncertainty of the TIMS measurements. Results for ^{235}U indicate a slight nonuniformity in the distribution of this isotope in SRM 4353 when 0.25 g samples are used but, on average, are consistent with the ^{235}U concentration (uncertified) shown on the NBS certificate.

Battery Program

The ACL technical support to battery-testing programs in CMT was continued. The ACL staff took part in the examination of 20 aqueous and high-temperature batteries tested at the Analysis and Diagnostics Laboratory (Sec. I.C). These examinations helped identify existing and potential failure mechanisms of the hardware components and correlate changes in performance with changes in the morphology and composition of the electrodes. The information obtained from these studies permitted accurate assessment of the technical progress in battery research. It also provided a better definition of additional R&D needs. Individual reports were prepared for each of the batteries examined and were forwarded to the battery developers and to personnel associated with the program for review.

Analysis of a Novel Neutron Absorber

A new material to absorb neutrons has been developed at ANL to withstand high temperatures and is now in use at the Intense Pulsed Neutron Source (IPNS). The material was created by specialists in the Materials and Components Technology Division and consists of ^{10}B-enriched boron metal sandwiched between two copper plates.

Analysts in the ACL developed a procedure for accurately determining the total ^{10}B content in samples of known surface area. Results from this determination allow calculation of a density factor, i.e., atoms of ^{10}B per unit area of material, which provides a measure of the

*National Bureau of Standards, which has been recently renamed National Institute of Standards and Technology (NIST).

neutron absorption capacity of the material. This density factor is an important parameter for evaluating the suitability of the material for use in IPNS.

The ^{10}B was determined by an MSID technique using boric acid of natural isotopic composition (NBS SRM 951) as the boron spiking agent. Sample preparation prior to the MSID determination of ^{10}B required special care and use of a novel method for separating boron from copper in the nitric-acid matrix obtained from dissolving each sample. To prevent boron pickup from the dissolution apparatus and to avoid losses of boron by volatilization, each sample was dissolved in a quartz reflux apparatus. An insoluble silica residue (from SiO_2 impurity in the boron metal used in fabricating the sample material) was isolated and separately analyzed to determine the small amount of boron that the residue contained. The separation of boron from copper nitrate and nitric acid was accomplished with a mixed-bed ion-exchange system, which yielded an eluate of boric acid in water. This solution was readily analyzed for boron by MSID. The results for all the materials analyzed demonstrated a ^{10}B density that met IPNS specifications.

Study of N_2O Emissions from Fluidized-Bed Combustor

Nitrous oxide emissions from the ANL fluidized-bed combustor (FBC) were studied by a CMT researcher (Sec. II.A.4). The objective of this study was to determine the effect of various parameters on the production of N_2O, which is considered to be one of the gases contributing to the greenhouse effect and the depletion of the ozone layer. The ACL work for this study included setting up a gas chromatography (GC) system to measure N_2O concentrations by direct on-line sampling of the FBC stack gas, periodically calibrating the GC, and calculating measured N_2O concentrations using the generated calibration curves. The level of N_2O emissions from the FBC appeared consistent with other reported FBC measurements and is significant when compared with N_2O emissions from other types of combustors.

Environmental Monitoring Program

During FY 1991, the ACL prepared approximately 600 environmental water samples in support of the Environmental Monitoring Program at ANL-East. Metals determinations on these digested samples by flame or furnace atomic absorption spectrophotometry were subsequently performed by personnel from the Environment, Safety, and Health Division (ESH). During this same period, the ACL also analyzed 180 wastewater samples, collected by ESH personnel from the ANL-East site, for oil and grease.

National Acid Precipitation Assessment Program (NAPAP)

Analytical support for the NAPAP continued this year. Limestone and marble briquettes, exposed to a variety of atmospheric conditions at a number of sites throughout the country, are brought to ANL for sampling and analysis. Over the past few years, hundreds of specimens have been analyzed for anions (fluoride, chloride, nitrate, and sulfate) by ion chromatography, and a smaller number have been analyzed by ICP/AES for metal cations. Little change in cation concentrations was found to occur following exposure at the test sites. However, substantial

elevations in sulfate and nitrate were found, and they have provided a quantitative measure of attack by atmospheric sulfur and nitrogen oxides. Anion measurements were performed on approximately 260 specimens during FY 1991.

Molten Corium Concrete Interaction (MCCI) Studies

In MCCI experiments at the Reactor Engineering Division, mixtures of uranium oxide, zirconium, steel, representative fission-product elements, and concrete are heated to temperatures simulating reactor meltdown conditions. The objectives are to study vaporization behavior of the elements present and to understand the release of refractory fission products during a degraded-core accident. Samples of solidified melt, aerosols collected by impaction or on filters, and gases are examined to study interaction and transport of the simulated reactor materials. Analytical support for these studies involves application of a wide variety of measurement techniques and requires considerable flexibility in approaching the analytical problems that arise from changes in the materials that are brought together in going from one test to the next. The concretes that have been used in particular experiments have included common limestone/sand aggregate, mixtures of different sized limestone, highly siliceous concretes (common in Europe), and serpentine-aggregate concrete imported from Russia. In some tests, volatile fission product metals (e.g., In, Te, Ag) were added to the corium simulation and had to be accounted for in methods used to dissolve and analyze sample materials from each test.

Typically, the solidified melt and aerosol samples are analyzed for Ag, Al, Ba, Ca, Ce, Cr, Cu, Fe, K, La, Mg, Mn, Mo, Na, Ni, Ru, Si, Sn, Sr, U, W, Zn, and Zr by ICP/AES; for Si by atomic absorption spectrophotometry (AAS) or gravimetry; for anions by ion chromatography (often following pyrohydrolytic decomposition of the sample to isolate halides); and for miscellaneous elements such as S or C by appropriate methods. X-ray diffraction (XRD) measurements are often made to identify particularly interesting phases in selected samples. Gas samples are analyzed by mass spectrometry.

In FY 1991, we analyzed samples from three large-scale MCCI tests, which produced approximately 150 samples. These tests involved a limestone/sand concrete, a mixed limestone concrete, and a combination serpentine-siliceous concrete. Dissolving MCCI melts and aerosols for multielement analysis by ICP/AES is always challenging, and ACL has devised a repertoire of dissolution schemes for these samples, including closed-vessel procedures in a Parr Decomposition Vessel or Carius tube, microwave procedures, fusion procedures with lithium tetraborate or sodium carbonate as flux, and other special techniques. For these recent tests, the dissolution procedures were often guided by XRD analyses, which identified undissolved phases and helped select alternative or followup approaches to dissolving these phases.

Results from past MCCI experiments indicated that silicon is present in certain aerosols as silicon metal and SiC, in addition to SiO_2. It is believed that most of the silicon comes off the MCCI melt as SiO gas, which disproportionates during aerosol formation to Si plus SiO_2. For carbonate concretes (i.e., those containing limestone), CO is present in the gas phase and reacts with SiO to form SiC. To test for these reactions, ACL began this past year to devise a procedure for determining the distribution of silicon among the three forms (Si metal, SiO_2, and SiC) in selected aerosol specimens. Preliminary work has demonstrated that silicon metal can be

selectively dissolved in dilute sodium hydroxide and measured by ICP/AES. Determinations of SiO_2 and SiC in synthetic mixtures of the compounds have been fairly successful whenever the SiO_2 had been selectively dissolved with hydrofluoric acid. However, with authentic aerosols, the phase structure of the SiC is sometimes of a nature that it dissolves in HF as well. Work is underway to develop a method for differentiating SiC from SiO_2 in these aerosols. One promising approach is based on the expectation that carbon in these aerosols is all present as SiC. If this is so, the SiC can be estimated from a total carbon determination, and the SiO_2 calculated by difference.

ANL Geoscience Programs

Analytical measurements were performed by the ACL in support of geoscience programs at ANL and at several universities in the Midwest. These measurements included characterization of groundwater samples by analysis for cations with ICP/AES or AAS techniques; measurement of anion concentrations (F^-, Cl^-, NO_2^-, SO_4^{2-}, Br^-, I^-) by ion chromatography; determination of pH, alkalinity, or other properties by classical methods; and isotopic measurements by TIMS. These techniques were applied to thermal waters from Yellowstone National Park; borehole brines from the Illinois Basin; and thermal waters, gases, steam condensates, and gas-sampling absorber solutions from volcanoes in Colombia, Ecuador, and Papua, New Guinea. The data generated by analysis of such samples (almost 300 were processed during FY 1991) have provided information about the age of geological formations, processes and mechanisms that produced the formations, and the movement of groundwater in the formations, both in geologic and modern times.

Radium Measurements

Radium isotopes were measured in a variety of geochemically significant matrices (groundwaters, brines, soils, and rocks) for a CMT program (Sec. IX.D). Radium determination in groundwaters requires that a large volume of water be passed through ~200 cm^3 of special radium-selective resin. For convenience in handling and shipping, this operation was performed in the field, and only the resins were shipped to ANL. Upon arrival at ANL, each resin was sealed into a metal can and γ-counted with a NaI detector. If ^{224}Ra determination was requested, the sample was analyzed before a significant amount of the ^{224}Ra had decayed (half-life = 3.6 days). For samples requiring only ^{226}Ra and ^{228}Ra determinations, the canned resins were allowed to age until ^{226}Ra reached equilibrium with its daughter ^{222}Rn (half-life = 3.825 days), which was then measured. The time allowed before analysis was at least 30 days.

Some of the brine samples had activity levels that were sufficiently high to employ direct canning of 200 cm^3 samples without use of the radium-selective resin. The lower limits of detection for ^{226}Ra and ^{228}Ra by the least squares method of data analysis on canned samples counted with a NaI detector are ~6 and 8 pCi, respectively.

Rock samples were analyzed by the above direct canning method. Where rocks were too small to fill the can, they were introduced into the can with NaCl (table salt) as a filler to maintain the same counting geometry.

Several samples of minerals and volcanic rock from South America were dissolved and analyzed for ^{226}Ra using the radon emanation method. Because of very low levels, the radium could not be determined by NaI γ-counting followed by least squares analysis of the data.

These analytical results will be used to (1) determine the behavior of radium isotopes in groundwater and brine and (2) estimate the age of some of the minerals where the ratios of radium isotopes are determined.

Analysis of Environmental Samples

The ACL provided analytical services to a variety of environmental monitoring, characterization, and remediation projects administered by the Environmental Research (ER) and Energy Systems (ES) Divisions and programs at other DOE facilities (Rocky Flats Plant and Idaho National Engineering Laboratory). Samples processed during FY 1991 included 198 waters, 305 soils/sediments, and 335 miscellaneous matrix samples (air, filters). These samples were analyzed according to protocols described in the Contract Laboratory Program Statements of Work from the Environmental Protection Agency (EPA), the methods described in EPA document SW-846,[1] or other appropriate procedures.

Environmental analyses provided by the ACL include determination of inorganic constituents (metals, anions, cyanide, sulfide, total dissolved and suspended solids), organic compounds (volatiles, semivolatiles, polychlorinated biphenyls/pesticides, phenolics, oil and grease), and radionuclides (gamma emitters, actinides).

Rocky Flats Plant Environmental Restoration Program

The ACL was requested to perform radiochemical analyses in support of the Rocky Flats Plant (RFP) Environmental Restoration Program. To date, the laboratory has received over 200 samples requiring assays for gamma emitters (e.g., Cs, Ra, and Th), Pu, Am, U, and Sr. In addition, gross alpha/beta measurements are in progress. Many determinations have been completed, and some data have been reported. New methods have been developed that allow for increased efficiency (factor of two less time for Sr and Am preparation for counting), lower analytical costs, and minimization of waste (factors of two or more less volume). Additionally, various ACL staff members have served as technical advisors to the RFP program managers as they developed the statement of work and the technical requirements for this program.

Determination of Americium by Extraction Chromatography

The determination of americium in environmental samples is crucial to those individuals responsible for effluent monitoring from facilities employing radioactive substances in their operations. However, the traditional analytical methods employed by most laboratories are

---

[1]U.S. Environmental Protection Agency, *Test Methods for Evaluating Solid Waste*, EPA Document SW-846, U.S. EPA Office of Solid Waste and Emergency Response, Washington, DC (November 1986).

extremely lengthy and manpower-intensive. More important, these traditional methods are often plagued by low and sporadic chemical yields.

In a collaborative study with the Chemical Separations Group of the Chemistry Division and the Environmental Monitoring Group of the ESH Division, we have developed a method to analyze environmental samples for americium utilizing extraction chromatography. This type of chromatography employs an extractant coated onto an inert support material. Extraction chromatography allows for the specificity of solvent extraction with the convenience of column chromatography. Our method has dramatically increased chemical recoveries (factor of two in some cases) and sample throughput (two times as many samples) and significantly decreased generated waste (a factor of thirty).

Development of an Interlaboratory Performance Evaluation Program

In collaboration with the DOE's Radiological and Environmental Sciences Laboratory (RESL) and Environmental Measurements Laboratory (EML), who serve as lead laboratories, ANL is developing and implementing a comprehensive Interlaboratory Performance Evaluation Program (IPEP) for the DOE EM-531 Laboratory Management Branch (LMB). The program is designed to provide information on the quality of radiological and non-radiological analytical data being produced by all laboratories on which DOE is relying for sample analysis in environmental restoration and waste management. The ACL is assisting the two lead DOE laboratories in the development of the program requirements and strategies for implementation, especially in the non-radiological portions of the program. The ACL is also developing the strategies for compiling and analyzing the performance evaluation data and for monitoring to assure that needed corrective actions are taken.

Radiochemical Analysis of the Experimental Boiling Water Reactor (EBWR) Vessel

The EBWR facility was first put into operation at ANL in 1956 as a test reactor to demonstrate the feasibility of operating an integrated power plant with a direct-cycle, boiling-water reactor as its heat source. The EBWR was operated at the 20-MW (thermal) power level from its startup in December 1956 to December 1962, after which the output was increased to the 100-MW (thermal) level. After five years of successful operation at the higher power level, the EBWR was shut down in December 1967. All nuclear fuel was then removed, all liquids were drained from the process systems, and the facility was placed in a dry lay-up status. The facility was subsequently declared surplus and entered into the DOE Surplus Facilities Management Program. Decommissioning and decontamination (D&D) were begun in 1986. The current objectives are to remove all contaminated material from the containment building, clean up the facility to prescribed release levels, and eventually open the building to unrestricted use.

Since detailed operating records of the EBWR are no longer available, ANL could not calculate the activation or radiological inventory of the reactor components or the reactor vessel. Because this information was needed to perform the D&D, an acceptable alternative method of radiological assessment of the reactor vessel was developed, which involved experimentally characterizing samples extracted from the reactor vessel wall. These samples consisted of cores

of carbon steel (A212, Grade B) with a thin layer of 304 stainless steel spot welded to the inner surface of the vessel.

After 24 years of dry lay-up status, short-lived radionuclides could be ignored in the assessment; the remaining radionuclides of interest were ^{14}C, ^{55}Fe, ^{59}Ni, ^{63}Ni, ^{60}Co, ^{93}Mo, and ^{94}Nb. The radioactivity of the EBWR reactor vessel was assessed using a combination of measured values and theoretical calculations based on the chemical composition of the alloy and the measured radioactivity values. The ACL performed detailed chemical and radiological measurements to determine ^{60}Co, ^{55}Fe, and ^{63}Ni in seven reactor vessel core samples, and performed theoretical calculations to assess radioactivity values for ^{14}C, ^{59}Ni, ^{93}Mo, and ^{94}Nb based on the measured ^{63}Ni values. In all, 70 analytical measurements of the seven core-drilled samples were made for ^{60}Co assessments, along with 12 additional analytical measurements for ^{55}Fe and 12 for ^{63}Ni. These analytical data enabled ANL to obtain the total radiological assessment of the EBWR reactor vessel.

FTIR Analysis of Semivolatiles in Soils

The objective of this program is to develop a method that utilizes FTIR spectroscopy to characterize, in the field, soil samples contaminated with explosives or selected volatile and semivolatile organic species. In the first year of the program, we determined that contaminants in soil samples could be thermally desorbed into a heated long-path infrared cell, and that explosives such as trinitrotoluene (TNT) could be detected at levels corresponding to 40-80 ppm in soil. The FTIR method will eliminate the problem that the certified extraction methods have with binding of the TNT to the soil. Field analyses by the FTIR method can be done in minutes.

The past year's effort was directed to field testing the FTIR method on TNT-containing samples obtained from the bioremediation of the Joliet Arsenal and to expanding the analytes to include volatile organic compounds. We ordered new equipment that will be able to contain and desorb 1 g of soil containing explosives. The new equipment is designed specifically for this type of sample. We anticipate analysis of Joliet Arsenal samples to begin in the spring of 1992. The acetone method used by Jenkins[2] to extract high explosives is also being investigated as a means to lower our current detection levels from 40-80 ppm to 4-8 ppm. Initial work shows the extraction to work well. However, the degree to which the detection level will be lowered cannot be determined until the arrival of the new equipment.

To apply the method to volatile organic compounds, eight organic compounds were selected for FTIR analysis. This number will be increased to 16 in FY 1992. Early work has shown that analytical conditions for the desorption of volatile compounds differ from those for semivolatile compounds, and that the volatile compounds studied in these experiments can be detected at approximately 50 ppm in soils. Quantitative accuracy for measurement of these

---

[2]T. F. Jenkins, *Development of Simplified Field Method for the Determination of TNT in Soil*, U.S. Army Corps of Engineers Report USATHAMA CRTHA-TS-CR-90125, Special Report 90-38 (November 1990).

compounds exceeds that obtained previously for TNT and the dinitrotoluene isomers due to better peak resolution.

This technology is applicable for site characterization and site remediation and could play a significant role in the cleanup of the Joliet Arsenal and other areas contaminated by explosives.

Remote Detection of Agent-Related Chemicals Using FTIR

The objective of this project is to determine the feasibility of using passive-remote FTIR spectroscopy to detect chemical agents and their related precursors and degradation products. Prior work demonstrated that agent-related chemicals released at low parts per million levels could be detected when measured against low-sky and brick-wall backgrounds. Two-component mixtures were also analyzed by this method. Our results indicated no problem with false positives or negatives. In the past year, we extended our experimental work to include complex multicomponent mixtures (methanol, isopropanol, dimethylmethyl phosphonate, and diethyl malonate), all with overlapping infrared peak absorbances.

The experimental work was done in the laboratory using a Nicolet 6000 FTIR spectrometer modified to be a passive-remote instrument. The source and inlet optics were replaced with custom-designed optics, which focus with a beam width of 2.5 cm at a distance of 2 m from the target. Chemical releases of the multicomponent mixtures were performed using a special apparatus designed for this project. The FTIR data were analyzed using classical least squares (CLS) and partial least squares (PLS) algorithms. We found that quantitative analysis employing a well-characterized standard set was normally within 20% of the released concentration using PLS. The CLS algorithm outperformed the PLS algorithm when a partial set of standards was used.

We concluded that FTIR spectroscopy shows much promise for remote detection of organics. This method has potential use for other environmental applications, such as compliance monitoring of air toxics released in the atmosphere.

Monitoring of Incinerator Effluent for Organic Analytes

The objective is to monitor incinerator effluent from different feeds and to correlate the feed content with stack effluent by qualitatively and quantitatively analyzing the effluent. This work is a collaborative study with the Energy Systems Division. In FY 1990, an experimental incinerator was constructed, and an FTIR spectrometer was coupled to it. In addition, a library of the FTIR spectra of interest was collected.

In FY 1991, the analytical instrument was used to identify the effluent from methane, toluene, and chlorobenzene burns. To test the analytical equipment, the incinerator was deliberately run under non-optimum temperature and gas-flow conditions. The upset was easily detectable using the FTIR method. The primary products of incomplete combustion were methane and benzene, regardless of the feed.

The objective of future work is to use the analytical instrument at a DOE incinerator and ultimately develop an EPA-certified method for using FTIR spectroscopy as a continuous emission monitor.

Detection of Illegal Drug Laboratories

The Drug Enforcement Administration is exploring new technologies for detecting illegal drug laboratories. The objective of this project is to perform chemical releases of drug-related solvents at field sites so that analytical equipment can be tested. We are responsible for releasing known quantities of chemicals emitted by typical illegal drug laboratories and evaluating test results obtained at the release site by all participating organizations. Equipment evaluated to date includes spectrometers based on ion mobility, FTIR, forward-looking infrared (FLIR), and fluorescence LIDAR (LIght Detection and Ranging).

Computer Generation of Reporting Forms for Volatile Organic and PCB/Pesticide Environmental Analyses

Numerous samples received by the ACL require reporting results on forms specified by the EPA Contract Laboratory Program. In the past, calculations were done by the analyst, and several forms were filled out manually. We have developed the capability to generate these forms electronically for volatile organic compound determinations performed on a Hewlett-Packard gas chromatograph/mass selective detector (GC/MSD) and for PCB/pesticide determinations performed on a Hewlett-Packard GC. Work on this project was done in collaboration with the ANL Electronics Department. By automating this activity, a significant time savings has been realized. A larger portion of the analyst's time can now be spent performing other tasks.

Quality Assurance for Headspace Gas Analysis in the Waste Isolation Pilot Plant (WIPP) Experimental Waste Characterization Program

The objective of the Experimental Waste Characterization Program, which is a key component of DOE's WIPP project, is to characterize volatile organic gases and permanent and low-molecular-weight hydrocarbon gases present in drums containing mixed (radioactive and hazardous) waste. These drums are to be placed in bins, which will go into DOE's long-term mixed waste storage facility (WIPP) in Carlsbad, NM. The ACL participated in a multiorganizational effort (headed by EG&G Idaho) for writing DOE's Quality Assurance Program Plan (QAPP) and Sampling and Analysis Guidance Manual for the WIPP Experimental Waste Characterization Program. These documents were prepared to meet requirements of both EPA and DOE and were designed to assist laboratories in producing reliable and well-documented data. The QAPP establishes the sampling and analysis requirements, and the guidance manual is a compilation of recommended methods that ensure compliance with the QAPP. Both documents are designed to ensure that the quality assurance objectives are met.

The ACL had lead responsibility for establishing analytical laboratory requirements for the analysis of headspace samples to determine permanent and low-molecular-weight hydrocarbon gases in waste bins and drums that are to be sent to the WIPP site. The recommended methods

are mass spectrometry for all the analytes or gas chromatography for all the analytes except combined nitrogen oxides, for which spectrophotometry is recommended. Quality control checks are used both in the field and in the laboratory to assure acceptable performance. Field quality control samples include field reference standards, field duplicates, field blanks, and manifold blanks. Laboratory quality control samples consist of calibration verifications, laboratory control samples, laboratory blanks, and laboratory duplicates. Complete documentation is required, and each laboratory performing headspace gas analysis must participate in the WIPP-QAPP Performance Demonstration Program.

Analysis of WIPP Samples by the Solid Adsorbent Method

To determine the 29 target volatile organic compounds (VOCs) specified in the QAPP, we have established an analytical system that consists of a Tekmar solid adsorbent inlet and the Hewlett-Packard GC/MSD. A constant sample flow, regulated by a mass flow controller, passes through the solid adsorbent trap at ambient temperature. The preconcentrated sample is then desorbed into the GC for separation and is detected by the MSD. This system can identify and quantitate all the target compounds, including alcohols and ketones, in a single run. With this method, a sample can be analyzed in approximately 30 min. Since the installation of the new GC/MSD was completed, we have performed the analyses required for method validation with accuracy and precision required by WIPP; certified cleaned canisters as acceptable for use in the characterization program (all impurities below required limits); and analyzed WIPP VOC Performance Demonstration (PD) samples and obtained results on the PDs that qualify the ACL to do sample analyses in the characterization program. In addition, 35 sample canisters from the WIPP site laboratory in Carlsbad, NM, were analyzed.

We are working to extend the existing calibration range to eliminate the need for serial dilutions of field samples before analysis.

Canister Cleaning and Certification for the WIPP

An important concern in the analytical scheme for measuring the composition of headspace gases over radioactive wastes for the WIPP project is the maintenance of sample integrity. To avoid changes in the composition of gases from the time samples are collected until they are analyzed in the laboratory, the samples are contained in specially treated stainless steel canisters with electropolished interiors. These canisters, sold under the trade name "SUMMA," are used by all of the laboratories participating in the WIPP Project. To obtain uniformity in the condition of canisters employed for sample collection, a decision was made to establish a Central Canister Cleaning Facility at ANL for cleaning and certifying the canisters between uses.

In this facility, up to 16 canisters can be heated simultaneously while they are flushed with humid air. They can then be baked out overnight while being pumped with an oil-free molecular drag pump to a pressure of ~1.3 mPa (~1 x 10^{-5} torr). The canisters are then leak tested on the same vacuum manifold. One canister from each batch is filled with clean humid air, and the contents are analyzed with a GC/MS. This analysis allows the batch to be certified based on the results of the test canister.

To date, ~250 canisters have been cleaned and certified for return to outside laboratories. An additional 250 have been cleaned for our own laboratory use.

Quantitation of Volatile Organic Compounds in Headspace Gas for the WIPP Project

The role of the ACL in this project is to serve as one of the participating laboratories in an effort to determine VOCs contained in the headspace of waste drums that will be shipped to the WIPP site for burial. The VOC analyses being conducted are based on procedures given in the WIPP Sampling and Analysis Guidance Manual and provide quantitative data on 24 target compounds, excluding alcohols and ketones, that are of particular interest to the project. Target compounds include aromatic hydrocarbons, chlorinated aliphatic hydrocarbons, and diethyl ether.

Gas samples are drawn from the waste drums into evacuated stainless steel canisters, which are then shipped to participating laboratories for analysis. Our analytical procedure involves pressurizing these canisters, then extracting aliquots into an intermediate laboratory canister, to which we add an internal standard. An aliquot of 300 mL is then drawn from the laboratory canister and passed through a trap cooled to -100°C, which retains the target compounds. The target compounds are released from the trap and swept into a GC/MS set up for separation and quantitative analysis. Quantitation of each target compound is based on a relative response factor for the area count of a characteristic fragment ion and the area count of an internal standard characteristic ion. We are able, with this technique, to quantitate the target compounds over a concentration range from less than 1 ppmV to 1000 ppmV in the headspace gas.

Analysis of Waste-Drum Headspace Gases for the WIPP

In addition to the analyses performed for other volatile organic compounds (see previous sections), gas samples withdrawn from waste drums in the WIPP Experimental Waste Characterization Program require compositional analysis to determine permanent gases and low-molecular-weight hydrocarbons (methane through propane). Volume-percent concentrations of each of ten target-analyte gases (H_2, N_2, O_2, Ar, CO, CO_2, NO_x, CH_4, C_2H_6, and C_3H_8) are to be measured. Our method for these determinations is based on mass spectrometry using a magnetic-sector, gas-analysis mass spectrometer having moderate resolution. Problems with the mass spectrometer (new to ACL in FY 1991) impeded development of detailed procedures, but these problems were eventually resolved. Instrument stability and sensitivity have been demonstrated to meet program requirements regarding precision and detection limits for measuring the gases of interest. Results of a recent (October 1991) performance demonstration exercise have indicated that inaccuracies occur for a few of the target gases in certain mixtures. The causes of these inaccuracies and means for eliminating them are being investigated.

Supercritical Fluid Extraction/Gas Chromatography for Analysis of Organic Compounds

Supercritical fluid extraction (SFE), which employs a supercritical fluid such as carbon dioxide as the extractant, has been used for extraction for organic compounds from soil samples.

As compared to the other methods of extraction of soil samples (Soxhlet and sonication), SFE can be performed rapidly and does not produce liquid waste.

To perform efficient analysis of organic compounds extracted from soil samples, we have interfaced an SFE apparatus to a GC system. Supercritical carbon dioxide was used for most of the extractions; however, modifiers such as methanol, when added to the supercritical carbon dioxide extractant, improve the efficiency of the SFE process.

Evaluation has begun on the ability of an SFE/GC instrument to separate a mixture containing several high-molecular-weight aromatic hydrocarbons. Data on optimum extraction time and temperature and effectiveness of modifiers were obtained. In addition, preliminary data were obtained on the performance of a flame ionization detector coupled to an SFE/GC.

Analysis of Environmental Samples for the U.S. Department of Agriculture

Contamination of both soil and groundwater with chloroform and carbon tetrachloride at a former grain storage facility (in Waverly, NE) operated by the U.S. Department of Agriculture (USDA) has led to a collaborative effort between the Environmental Research (ER) Division and the ACL. Chloroform and carbon tetrachloride, classified as possible carcinogens, were commonly used as grain fumigants in the 1950s and 1960s by the USDA and companies that operated grain storage facilities in Nebraska. A groundwater extraction and air-stripping system, operated at the Waverly site by a team from the ER Division, is used to remove contaminants from the aquifer and contain the spread of contaminated groundwater that once supplied drinking water to Waverly residents. For the past three years, soil gas and groundwater samples have been taken monthly and sent to the volatile organics laboratory of the ACL for analysis to monitor the progress of the site cleanup. Soil gas samples, collected on charcoal tubes and carbotraps, and groundwater samples are analyzed according to protocols from the U.S. EPA and Standard Operating Procedures written by the ACL. Tests show that the level of carbon tetrachloride in the aquifer has been reduced from 4000 parts per billion (ppb) to 100 ppb. Although these results indicate some success, more work needs to be done to get the contaminant level for carbon tetrachloride below the federal health standard of 5 ppb.

Environmental Assessment Study for Contaminants at Hohenfel Training Area Site, Germany

An exploratory study was conducted at the Hohenfel Training Area site in Germany to assess environmental effects of the troop training exercises by U.S. Armed Forces. Plants, leaves, grass, and soil samples were collected from areas within the site and submitted for determination of two components that have the potential to be contaminants in the training field. The major component of interest was fog oil, a petroleum product used to create an artificial battlefield fog. The second component of interest was 2-chlorobenzaldehyde, a compound found in tear gas used in training exercises. Thirty-three soil samples and 27 plant samples were extracted with organic solvent by sonication. The concentrated extract was analyzed by GC with flame ionization detection. Selected samples were also analyzed by GC/MS. Because there is no certified method for the determination of these compounds, procedures were developed following the protocol of U.S. EPA certified methods. Because very complex chromatograms

were obtained from both soil and plant samples, ratio and subtraction techniques were applied to the data. No fog oil or 2-chlorobenzaldehyde was detected in the soil or plant samples.

FTIR Microscopy

Fourier transform infrared microscopy has contributed to the organic analytical support offered by the ACL. Recent samples analyzed include unknown residues on gold wire, stainless steel, and ceramic surfaces. Individual crystals and inclusions in crystals have been studied. Powders and liquids were analyzed on salt disks after appropriate sample preparation. Selected solid samples have been analyzed by dissolving the solid and analyzing a thin film of residue prepared from the solution. Polymers and other samples containing organic components have been successfully analyzed and functional groups identified.

New Capabilities within ACL

New capabilities of the ACL established in FY 1991 include a laboratory to prepare radioactive environmental samples for analysis, new photoprocessing equipment, a microwave digestion system, an automated carbon/hydrogen/nitrogen analyzer, a new mass spectrometer for organic analysis, and the facilities and procedures to analyze radioactive samples by the Toxicity Characteristic Leaching Procedure.

XI. R&D PROGRAM COORDINATION OFFICE

The R&D Program Coordination Office in CMT is assisting DOE in establishing and maintaining a national program of applied R&D in the environmental restoration and waste management area. The objective of the applied R&D is to improve the efficiency, safety, and timeliness of environmental cleanup activities so that DOE can meet the 30-year environmental compliance and cleanup goals for its facilities.

Currently available technology is not adequate to assess environmental contamination, take permanent remedial action, and eliminate or minimize the environmental impact of future operations. Technical resources to address these shortcomings exist within the DOE system and the private sector, but the involvement of the private sector in attaining permanent and cost-effective solutions has been limited. Thus, this Office is providing technical and management oversight to assist private-sector contractors in performing R&D on new technologies needed for DOE to meet its compliance and cleanup goals. It is also providing this same oversight to research at Hazardous Substance Research Centers co-funded by DOE and the Environmental Protection Agency (EPA).

A. *Private-Sector Contracts*

On behalf of DOE's Office of Technology Development (OTD), ANL is managing R&D projects in four general areas: groundwater contamination, soil remediation, site characterization, and containment of contamination. After a competitive procurement, 15 contracts were awarded, with initiation dates of October 1990 and completion dates ranging from July 1991 through May 1992. The selected projects and contractors are as follows:

- Groundwater Cleanup

  1. Remove radionuclides, heavy metals, and organics from contaminated groundwater using chemical binding/filtration/cold vaporization techniques (Atomic Energy of Canada, Ltd.).

  2. Develop vapor-phase bioreactor that will degrade trichloroethylene (TCE) and other chlorinated hydrocarbons in groundwater (Envirogen, Inc.).

  3. Remove volatile organic compounds (VOCs) from groundwater with a combined air stripping/membrane vapor separation system (Membrane Technology and Research, Inc.).

  4. Evaluate the AlgaSORB process of Bio-Recovery Systems for removing radionuclides, heavy metals, and inorganic and/or organic ions from groundwater (Science Application International Corp.).

- Soil Cleanup

5. Develop a soil washing/vitrification system that will reduce and stabilize soil contaminated with radionuclides, heavy metals, and inorganic and/or organic ions (Duratek Corp.).

6. Investigate electrokinetic effects in the treatment of contaminated soils, sludges, and lagoon sediments (Electro-Petroleum, Inc.).

7. Investigate the effectiveness of composting to destroy explosives and other hazardous organics in soil, sediment, and sludges (IIT Research Institute).

- Site Characterization

8. Develop hardware and software for three-dimensional site characterization using three minimally invasive measurement techniques -- cone penetrometry, synergistic electromagnetic mapping technology, and reflection seismology (Applied Research Associates, Inc.).

9. Develop and test hydraulically installed multisampling lysimeter for use in a vadose zone (Bladon International, Inc.).

10. Develop technique that will allow the rapid emplacement of membrane instrumentation and sampling apparatus in a punched or drilled hole (Science and Engineering Associates, Inc.).

11. Develop a mobile fiber optic Raman spectrograph for *in situ* site characterization and monitoring (EIC Laboratories, Inc.).

12. Develop a surface acoustic wave microsensor for subsurface detecting VOCs (University of Michigan).

13. Develop a bulk soil assay system that uses gamma ray imaging (Nuclear Diagnostic Systems, Inc.).

14. Investigate use of hydrogeological seismic profiling by high-resolution shear wave reflection and conventional compressional wave technology (Paul C. Rizzo Associates, Inc.).

- Containment

15. Investigate the fixation of heavy metals through *in situ* reduction followed by injection of a silica solution to immobilize the resulting metal hydroxides (Sizemore Technical Services, Inc.).

Technical accomplishments for selected projects are summarized below.

Atomic Energy of Canada (AECL) has conducted bench-scale tests of its process for decontaminating groundwater. Since the bench-scale tests demonstrated the feasibility of this process, AECL built a pilot-plant-scale unit to optimize the process using simulated waste solutions and then field tested it with groundwater contaminated by ^{90}Sr (280 MBq). The field test resulted in 84% removal of the ^{90}Sr. Efforts are underway to improve this removal efficiency.

In tests of its bench-scale vapor-phase bioreactor, Envirogen found that 80-90% of very low levels of TCE (parts per million) sparged from groundwater could be initially degraded, but the degradation efficiency of this bioreactor rapidly declined with time. However, intermittent addition of small amounts of lactic acid was found to restore the bioreactor's capability. This minor process modification markedly extends the operation time of the bioreactor.

Membrane Technology and Research constructed a three-stage membrane system and combined it with an air stripper for treating VOC-contaminated groundwater. Laboratory tests with TCE-contaminated groundwater indicated that the air stripper/membrane system performs satisfactorily. However, the exact extent of this TCE removal is still being determined.

Duratek developed soil washing and vitrification techniques for the remediation of soils at contaminated DOE sites. Tests of glasses fabricated with contaminated soil from a DOE site (Weldon Springs, MO) indicated that Duratek's techniques can be used to produce waste glasses with high soil loadings that meet the leachability requirements of DOE and EPA. The leachability of these glasses compares favorably with that for reference designs of high-level nuclear waste glasses.

Using shear wave seismic technology, Rizzo Associates surveyed the subsurface hydrogeologic features in the Cooke Crossroads area (near Charleston, SC). This area was chosen for study because it has relatively uncomplicated marine sediments and sand lenses within a thick clayey unit, which are difficult to detect by conventional technology. The results showed much higher resolution of subsurface features than ever observed previously (~0.3 m resolution). Comparison of the observed features with borehole data from the U.S. Geological Survey is underway.

Applied Research Associates demonstrated its cone penetrometer technology in determining the VOCs in arid soils and underground storage tanks at the Westinghouse Hanford site.

Science and Engineering Associates (SEA) is developing a membrane system for supporting the walls of a well or other hole to be used in lieu of traditional pipe and grout systems for site characterization and monitoring. The membrane system can also carry sampling apparatus to specific depths and orientations within the hole to sense conditions, passively collect groundwater samples, or extract samples to the surface. During 1991, the contractor developed the system materials and mechanics, developed passive sorbent collectors, and devised a mechanism for extracting water through the membrane wall. In a field demonstration of the

technology, SEA successfully emplaced and tested two membrane systems with lengths up to 74 m at Sandia National Laboratories. In addition, the system is being routinely used to monitor tritium in groundwater at Lawrence Livermore National Laboratory, where emplaced passive sorbent collectors adsorb water for an hour or so, are retrieved to the surface, and taken to the laboratory for counting.

As a consequence of this effort, EIC Laboratories and SEA have signed a memorandum of understanding for the joint development of an optical system that will be used for the *in situ* detection of excitation and fluorescence of hydrocarbons through the SEA membrane system. This collaborative effort, not funded by DOE, is a direct result of communications between the two organizations fostered by their OTD-funded R&D contracts.

In addition to the above technology demonstrations, ten more are in the discussion or planning stages.

B. *Hazardous Substance Research Centers*

Through a memorandum of understanding, DOE and EPA are co-sponsoring research at five Hazardous Substance Research Centers (HSRCs). These centers are located in different regions of the country, with each center covering two federal EPA regions. Each center is located at a main participant university but consists of a consortium of several universities in the region. These centers are the Northeast HSRC, Great Lakes and Mid-Atlantic HSRC, South/Southwest HSRC, the Great Plains/Rocky Mountain HSRC, and the Western Region HSRC. The basic mission of the HSRCs is to study all aspects of the manufacture, use, transportation, disposal, and management of hazardous waste. Research at the centers includes projects on biotechnology for waste remediation; pollutant transport mechanisms; chemical and thermal destruction of organics; and remediation of contaminated soils, groundwater, sediments, and dredged material. Twelve proposals were selected for DOE funding in FY 1990, and eight in FY 1991.

The R&D Program Coordination Office in CMT manages the DOE-funded HSRC program and serves as the technical and administrative interface between DOE/EPA and the centers. Under DOE directive, the R&D Program Coordination Office prepared a Proposal Evaluation Plan to fund university research through HSRCs. The key elements of the plan are development of a two-stage review strategy, assembly of review panels of experts, and development of a proposal tracking system.

The first stage of the review process is a comprehensive technical review, where several appropriate evaluation criteria are used, numerical scores are assigned, and written comments are provided on the proposals. The two most important criteria are (1) the scientific/technical merit of the proposal and (2) the relevance to DOE technology development needs in environmental restoration and waste management. The second stage entails a review that allows DOE to make funding decisions on various projects. The R&D Program Coordination Office also assembled a proposal review committee, from which individual panels are established for reviewing specific proposals. During the past year, approximately 80 research proposals received from all centers

were considered by review panels, and recommendations were passed onto DOE for funding decisions.

Research highlights for two of the HSRC projects initiated in FY 1990 are described below.

The goal of the first project (Stanford University) is to evaluate, in the field, the rate and extent of degradation of chlorinated aliphatic compounds in groundwater or soil when exposed to bacteria containing toluene oxygenase enzyme. Recent studies have indicated that microorganisms containing the toluene monooxygenase (TMO) or toluene dioxygenase (TDO) enzyme can oxidize chlorinated aliphatic compounds, such as TCE, by a co-metabolism process similar to biodegradation by methanotrophs with methane monooxygenase (MMO). The toluene oxygenases can be induced by several primary substrates, including phenol. This field study is being conducted at the Moffett Field Naval Air Station in California, where the MMO system has already been evaluated. The present study with the TMO and TDO systems is being conducted in the same manner as the previous study with the MMO system so that the results can be directly compared. In the present study, phenol and oxygen are dissolved in recycled groundwater along with TCE, dichloroethylene (DCE), and vinyl chloride, and then this groundwater is introduced into a confined aquifer that is about 4 m below the surface, as well as 1.2-m deep and 6-m long. The growth of a native phenol-degrading population and the rate and extent to which the introduced chlorinated compounds are removed are continuously monitored by automatic extraction of groundwater from monitoring wells and an on-site analysis. The first season of field testing evaluated the effectiveness of this *in situ* bioremediation method with regard to TCE, cis-DCE, and trans-DCE removal. Effective degradation of TCE and cis-DCE was achieved (greater than 80%), but trans-DCE degradation was limited (less than 40%). These preliminary results indicate that this *in situ* bioremediation method has promise for implementation at several DOE sites where past operations have resulted in contamination by chlorinated organics.

The goal for the second project (Tufts University) is to develop a new contamination detection tool for *in situ* groundwater testing. Current well monitoring is typically done on a quarterly basis, is expensive, and requires purging the well. *In situ* sensors would not only provide data all of the time or on demand, but also would reduce the cost and eliminate purge-water disposal problems. To date, a fiber optic sensor that is sensitive to environmentally significant levels of VOCs has been developed. This sensor employs a chemical indicator (a vapor-absorbing polymer) with fluorescence properties. A portable field sensor has been constructed and field tested at a site contaminated with jet fuel (JP4). The sensor's response correlated well with laboratory measurements using a photoionization detector probe. Expansion of this sensor's capabilities to other compounds and/or its use in combination with other down-hole sensors currently under development will yield a sensor array capable of monitoring all of the commonly encountered groundwater pollutants at DOE sites.

XII. COMPUTER APPLICATIONS

The Computer Applications Group assists CMT staff in many aspects of computer-related activities, including (1) information management systems and data-base development, (2) office automation, (3) laboratory data acquisition and control, (4) computer modeling and simulation studies, (5) small and large computer system networking, (6) post-analysis of experimental results, (7) graphics applications, (8) computer security, (9) computer operating system maintenance, (10) procurement of automatic data processing equipment, and (11) advisory, educational, and consulting services.

The Computer Applications Group has the responsibility for software maintenance and development for several major minicomputer data acquisition systems, the Division's Local Area VAX cluster consisting of twelve VAXs, and both Macintosh and IBM-compatible personal computer (PC) networks. The Group also provides hardware maintenance of various small systems and peripherals, including the Division's extensive terminal communications system and local area networks.

We continue to support data acquisition and control systems that use traditional 16-bit minicomputers [e.g., Digital Equipment Corp. (DEC) PDP-11 minicomputers] and newer systems that use personal computers and VMS-based and UNIX-based workstations, which often operate together in a networked environment.

An example is our work in support of the Analysis and Diagnostics Laboratory (ADL). For over a decade, this facility has tested a wide variety of battery systems (see Sec. I.C), some of which require unusual charging and discharging regimes. Significant effort was devoted to improving the DEC LSI-11 software used to control simulated driving profile discharges in battery tests. Driving profile discharge can now be terminated on the basis of a battery's ability to sustain a minimum specific power level, and performance reports are now produced when a battery appears not to be able to sustain loads of 79, 67, or 50 W/kg. These recent changes in the LSI-11 software have required a major reorganization of the data structures and memory allocation scheme in the LSI-11 microprocessor. In addition, new software in the PDP-11 data acquisition minicomputer for the ADL automatically produces data summary files as a battery test progresses. The summary data are then transmitted to a VAXstation and converted to a form designed for use with a PC-based spreadsheet program for analysis, tabulation, and plotting. Other ADL advances include the development of a new test control data structure for PDP-11 data acquisition software that operates in parallel with the old Test Control Table (TCT). This "extended TCT" allowed the many dozens of processing tasks formerly used by the ADL to be replaced by only three pairs of tasks, thus resulting in a significant decrease in the effort needed for the maintenance and modification of system software.

During the past year, we worked with the Analytical Chemistry Laboratory (ACL, Sec. X) on several tasks. One task involved the development of procedures, which run on a Hewlett-Packard minicomputer, for the automatic generation of forms specified by the Contract Laboratory Program of the Environmental Protection Agency. These forms, which were previously filled out manually, are used with volatile organic compound determinations

performed on a Hewlett-Packard gas chromatograph/mass selective detector (GC/MSD) and with PCB/pesticide determinations performed on a Hewlett-Packard GC. We also developed a new system (utilizing a modification of VAX-based GAMANAL code together with a data base) for automatic collection and presentation of quality assurance data obtained with a gamma spectrometer. Moreover, we are participating in the development of a data base system for the Interlaboratory Performance Evaluation Program, which is designed to provide information on the analytical data being produced by laboratories on which DOE is relying for sample analysis in environmental restoration and waste management. Other support to the ACL included quality-assurance-related enhancements to its job-control data-base system through the use of computer-assisted bar code and sample-tracking capabilities.

The Division's VAX 6320 continues to provide the primary computing resources for the CMT's diverse computing needs (see Fig. XII-1). Principal upgrades during the year included acquisition of 3 gigabytes of additional disk storage. Other members of CMT's VAX cluster are providing computing cycles for the Materials Chemistry Group (Sec. IX.B), for scientific workstation applications and program development, and for laboratory automation as replacements for older 16-bit PDP-11 computer systems.

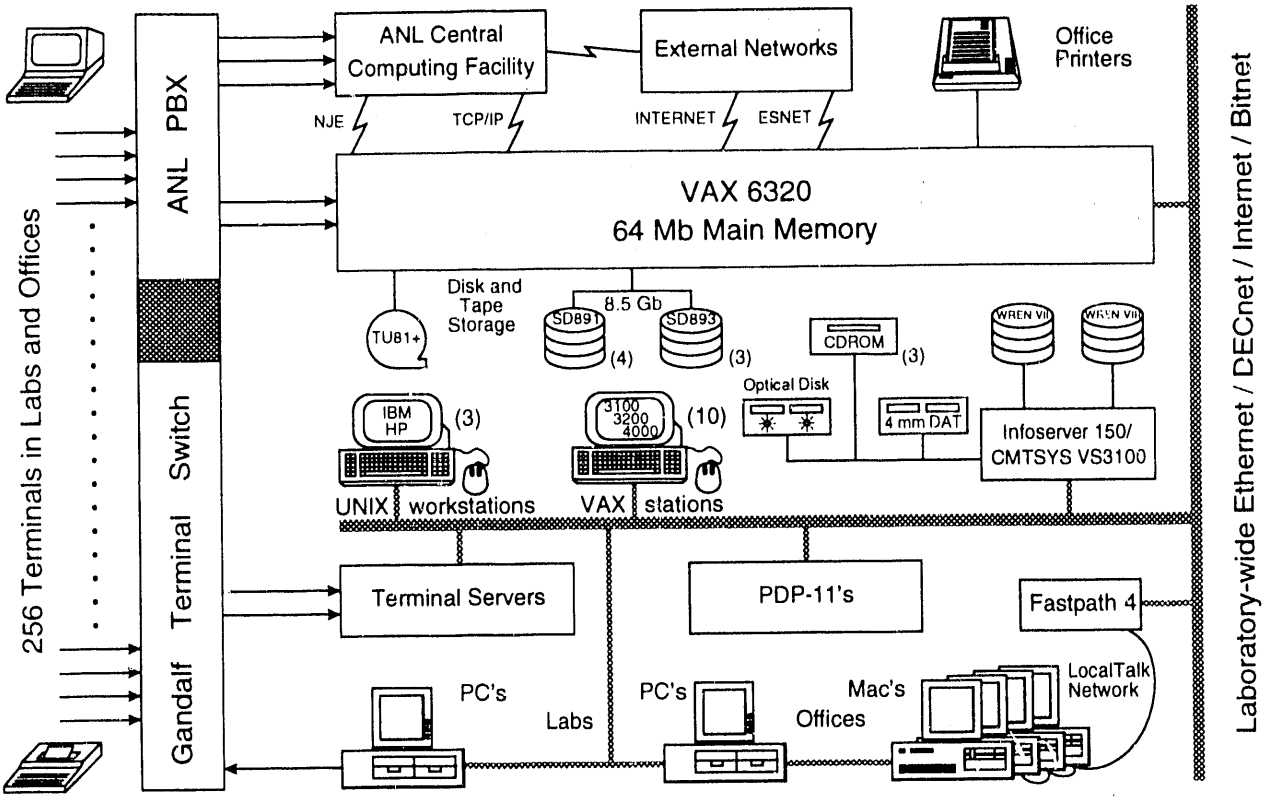

Fig. XII.-1. Block Diagram of CMT Computing Facilities

Computer networks continue to grow in importance in the Laboratory's computing environment. Connection of CMT's VAX to the Laboratory-wide Ethernet permits access to local resources, such as the Computing and Telecommunications Division's (CTD) Cray and

VAX cluster, and to external networks, such as ESNET (DOE energy sciences), the National Sciences Foundation network (NSFNET), and Internet, through use of TCP/IP software. This software supports electronic mail, general file transfer capabilities, and interactive log-ins to other systems on the network, including all CTD computers. Heavy use of these networks has led to some reliability problems, which should be resolved when ANL upgrades the Laboratory-wide Ethernet backbone to a fiber-optic (FDDI) system in the near future. This will increase network throughput between ANL buildings 100-fold.

Personal computers connected to Ethernet are able to use CMT's VAX as a file and/or print server via DEC's PATHWORKS for DOS network software. This is particularly useful for those systems that are now employed for administrative and graphics applications and for other PC systems which rely on the VAX for data analysis. PATHWORKS offers support for Microsoft Windows and the X-Windows standard, which enables a PC user to "window" into several applications running on one or more nodes on the network. Installation of DEC's PATHWORKS for Macintosh software on the VAX provides many of the same file, print, and windows services to the CMT Macintosh community. We expended considerable effort during this past year to support PC network integration and have designed and implemented mechanisms and procedures for network application setup, access, and security.

We also continue to provide programming support for general CMT needs. During the past year, a forms-based data-base application was implemented and used to aid in the preparation of DOE Field Work Proposals. In addition, the VAX-based chemical inventory system (which allows CMT staff to enter, update, examine, and report information regarding chemicals used in their work) was improved by the implementation of additional reporting capabilities and maintenance functions. Applications for tracking performance milestones, calibrations of measuring and test equipment, and the results of safety walk-through inspections were also implemented.

XIII. ADDENDUM.

CHEMICAL TECHNOLOGY DIVISION PUBLICATIONS --- 1991

The Division's publications and oral presentations for 1991 were entered into a bibliographic data base. The pages that follow are a printout of this information sorted into six categories: (1) journal articles, books, and book chapters, (2) patents, (3) ANL progress and topical reports, as well as contributions to reports published by organizations other than ANL, (4) abstracts and papers published in proceedings of conferences, symposiums, workshops, etc., (5) oral presentations at scientific meetings and seminars not referenced in the fourth category, and (6) papers accepted for publication but not yet published.

Chemical Technology Division Publications — 1991

A. Journal Articles, Books, and Book Chapters

Stable Isotope Geochemistry of Organic Matter Alteration in Animikie Basin Sediments within the Thermal Aureole of the Duluth Complex
T. A. Abrajano, B. D. Holt, and G. R. Dyrkacz
Organ. Geochem. **17**(4), 477–482 (1991)

Thermal-Hydraulic Model of a Monolithic Solid Oxide Fuel Cell
S. Ahmed, C. C. McPheeters, and R. Kumar
J. Electrochem. Soc. **138**(9), 2712–2718 (1991)

Synthesis of Ceramic Superconductors under Low Oxygen Pressure
U. Balachandran, R. B. Poeppel, J. E. Emerson, M. T. Lanagan, C. A. Youngdahl, and S. A. Johnson
Bull. Mater. Sci. **14**(2), 185–188 (1991)

Synthesis/Characterization and Novel Applications of Molecular Sieve Materials
R. L. Bedard, T. Bein, M. E. Davis, J. Garces, V. A. Maroni, and G. D. Stucky, eds.
MRS Symposium Proceedings Series, Vol. 233, Materials Research Society, Pittsburgh, PA (1991)

Lithium Mass Transport in Ceramic Breeder Materials
P. E. Blackburn and C. E. Johnson
Fusion Technol. **19**, 1696–1700 (1991)

Solid State Synthesis of $Bi_2Sr_2CaCu_2O_x$ Superconductor
I. Bloom, J. M. Frommelt. M. C. Hash, M. T. Lanagan, C.-T. Wu, and K. C. Goretta
Mater. Res. Bull. **26**(12), 1269–1276 (1991)

Mechanism of Tritium Release from Lithium Ceramics
F. Botter, S. Titchenko, M. Briec, and J. P. Kopasz
Fusion Eng. Des. **17**, 49–54 (1991)

FLIBE Chemistry Studies
R. G. Clemmer, D.-K. Sze, P. E. Blackburn, E. H. Van Deventer, and V. A. Maroni
Fusion Technol. **19**, 1612–1618 (1991)

Yields and Kinetic Energy Distributions of Sputtered Neutral Copper Clusters
S. R. Coon, W. F. Calaway, J. W. Burnett, M. J. Pellin, and D. M. Gruen
Surf. Sci. **259**, 275–287 (1991)

Bonding of a Water Molecule to a Copper Atom
L. A. Curtiss and E. Bierwagen
Chem. Phys. Lett. **176**(5), 417–422 (1991)

A Contracted Bromine Basis Set for Use in Calculation of Molecular Energies
L. A. Curtiss and R. C. Binning
Int. J. Quantum Chem. **40**, 781–787 (1991)

Predicted Proton Affinities of H_3SiO^-, H_3SiOH, $H_3SiOSiH_3$, and $H_3SiOAlH_3^-$
L. A. Curtiss, H. Brand, J. B. Nicholas, and L. E. Iton
Chem. Phys. Lett. **184**(1–3), 215–220 (1991)

Temperature Dependence of the Heterogeneous Ferrous-Ferric Electron Transfer Reaction Rate: Comparison of Experiment and Theory
L. A. Curtiss, J. W. Halley, J. Hautman, N. C. Hung, Z. Nagy, Y.-J. Rhee, and R. M. Yonco
J. Electrochem. Soc. **138**(7), 2032–2041 (1991)

Energies of CH_2OH, CH_3O, and Related Compounds
L. A. Curtiss, L. D. Kock, and J. A. Pople
J. Chem. Phys. **95**(6), 4040–4043 (1991)

A Re-examination of the Be-OH_2 Complex
L. A. Curtiss and J. A. Pople
Chem. Phys. Lett. **185**(1,2), 159–164 (1991)

Theoretical Study of Methyl Hypofluorite (CH_3OF) and Related Compounds
L. A. Curtiss and J. A. Pople
J. Chem. Phys. **95**(11), 7962–7964 (1991)

Theoretical Study of Si_2H_n (n = 0–6) and $Si_2H_n^+(O_2)$ (n = 0–7): Appearance Potentials, Ionization Potentials, and Enthalpies of Formation
L. A. Curtiss, K. Raghavachari, P. W. Deutsch, and J. A. Pople
J. Chem. Phys. **95**(4), 2433–2444 (1991)

Gaussian-2 Theory for Molecular Energies of First- and Second-Row Compounds
L. A. Curtiss, K. Raghavachari, G. W. Trucks, and J. A. Pople
J. Chem. Phys. **94**(11), 7221–7230 (1991)

The Hydration of Borosilicate Waste Glass in Liquid Water and Steam at 200°C
W. L. Ebert, J. K. Bates, and W. L. Bourcier
Waste Manage. **11**, 205–221 (1991)

The Sorption of Water on Obsidian and a Nuclear Waste Glass
W. L. Ebert, R. F. Hoburg, and J. K. Bates
Phys. Chem. Glasses **32**(4), 133–137 (1991)

Analytical Chemistry of PCBs
M. D. Erickson
Lewis Publishers, Chelsea, MI (1991)

Electrochemical and Optical Techniques for the Study and Monitoring of Metallic Corrosion
M. G. S. Ferreira and C. A. Melendres, eds.
NATO-ASI Series, Series E: Applied Sciences, Vol. 203, Kluwer Academic Publishers, Dordrecht, Netherlands (1991)

Helium Processing for Deuterium/Helium Burns in ITER's Physics Phase
P. A. Finn and D.-K. Sze
Fusion Eng. Des. **18**, 15–18 (1991)

Conceptual Design Description for the Tritium Recovery System for the U.S. ITER Li_2O/Be Water Cooled Blanket
P. A. Finn, D.-K. Sze, and R. G. Clemmer
Fusion Technol. **19**, 1589–1594 (1991)

Processes for Desorption from $LiAlO_2$ Treated with H_2 as Studied by Temperature Programmed Desorption
A. K. Fischer
Fusion Technol. **19**, 1012–1017 (1991)

Desorption of H_2O and H_2 from Steel and $LiAlO_2$ by Temperature Programmed Desorption
A. K. Fischer and C. E. Johnson
J. Nucl. Mater. **179–181**, 812–815 (1991)

Chemisorption Effects on the Dynamics of Germanium Clusters and Ultrathin Films
J. Fortner and J. S. Lannin
Surf. Sci. **254**, 251 (1991)

U. S. Solid Breeder Blanket Design for ITER
Y. Gohar, H. Attaya, M. C. Billone, C. Lin, C. E. Johnson, S. Majumdar, D. Smith, A. Raffray, A. Badawi, Z. Gorbis, A. Ying, and M. A. Abdou
Fusion Technol. **19**, 1538–1545 (1991)

Selectivity, Specificity, and Sensitivity in the Photoionization of Sputtered Species
D. M. Gruen, W. F. Calaway, M. J. Pellin, C. E. Young, D. R. Spiegel, R. N. Clayton, A. M. Davis, and J. D. Blum
Nucl. Instrum. Methods **B58**, 505–511 (1991)

Chemical and Carbon Isotopic Alteration of Organic Matter during Stepped Combustion
B. D. Holt and T. A. Abrajano
Anal. Chem. **63**, 2973–2978 (1991)

Oxygen Isotope Fractionation for Understanding the Sulphur Cycle
B. D. Holt and R. Kumar
Chapter 2 in *Stable Isotopes in the Assessment of Natural and Anthropogenic Sulphur in the Environment*, eds., H. R. Krouse and V. A. Grinenko, John Wiley & Sons, New York, pp. 27–41 (1991)

Ceramic Breeder Materials
C. E. Johnson
Ceram. Int. **17**, 253–258 (1991)

Ceramic Breeder Materials
C. E. Johnson
Ceramics Today—Tomorrow's Ceramics, pp. 3029–3039 (1991)

Research and Development Status of Ceramic Breeder Materials
C. E. Johnson
J. Nucl. Mater. **179–181**, 42–46 (1991)

Fabrication, Properties, and Tritium Recovery from Solid Breeder Materials
C. E. Johnson, T. Kondo, N. Roux, S. Tanaka, and D. Vollath
Fusion Eng. Des. **16**, 127–139 (1991)

Thermodynamic Studies of Zeolites: Clinoptilolite
G. K. Johnson, I. R. Tasker, R. Jurgens, and P. A. G. O'Hare
J. Chem. Thermodyn. **23**, 475–484 (1991)

Composition and Spectral Characteristics of Ambient Aerosol at Mauna Loa Observatory
S. A. Johnson and R. Kumar
J. Geophys. Res. **96**(D3), 5379–5386 (1991)

Homogeneous Catalytic Hydrogenation of Carbon Monoxide
R. J. Klingler and J. W. Rathke
Progress in Inorganic Chemistry, Vol. 39, ed., S. J. Lippard, John Wiley & Sons, New York, pp. 113–180 (1991)

Enhanced Tritium Transport and Release by Solids Modification
J. P. Kopasz, S.-W. Tam, and C. E. Johnson
J. Nucl. Mater. **179–181**, 816–819 (1991)

Thermodynamics and Phase Equilibria of the Iron-Uranium System
L. Leibowitz and R. A. Blomquist
J. Nucl. Mater. **184**, 47–52 (1991)

Thermodynamic Modeling of the Phase Equilibria of the Plutonium-Uranium System
L. Leibowitz, R. A. Blomquist, and A. D. Pelton
J. Nucl. Mater. **184**, 59–64 (1991)

A New Model for Solvent Extraction in Columns
R. A. Leonard, M. C. Regalbuto, D. B. Chamberlain, and G. F. Vandegrift
Sep. Sci. Technol. **25**(13–15), 1689–1707 (1990)

The Experimental Hydration of Obsidian as a Function of Relative Humidity and Temperature
J. J. Mazer, C. M. Stevenson, W. L. Ebert, and J. K. Bates
Am. Antiq. **56**(3), 504–513 (1991)

Laser Raman Spectroscopy for *In-Situ* Analysis of Corrosion Films on Metals
C. A. Melendres
Application of Surface Analysis Methods to Environmental/Material Interactions, eds., D. R. Baer, C. R. Clayton, and G. D. David, Vol. 91–7, Electrochemical Society, Pennington, NJ, pp. 159–181 (1991)

Laser Raman Spectroscopy: Principles and Applications to Corrosion Studies
C. A. Melendres
Electrochemical and Optical Techniques for the Study and Monitoring of Metallic Corrosion, eds., M. G. S. Ferreira and C. A. Melendres, NATO-ASI Ser. **203**, Kluwer Academic Publishers, Dordrecht, Netherlands, pp. 355–388 (1991)

On the Breakdown of Passivity of Iron by Thiocyanate
C. A. Melendres, J. Acho, and R. L. Knight
J. Electrochem. Soc. **138**(3), 877–878 (1991)

Effect of Thiocyanate on the Corrosion and Passivation Behavior of Copper and Iron: Laser Raman Spectroscopy and Photoelectrochemical Studies
C. A. Melendres, T. J. O'Leary, and J. Solis
Electrochim. Acta **36**(3/4), 505–511 (1991)

Specular X-ray Reflection for the "In-Situ" Study of Electrode Surfaces
C. A. Melendres, H. You, V. A. Maroni, Z. Nagy, and W. Yun
J. Electroanal. Chem. Interfacial Electrochem. **297**, 549–555 (1991)

Effect of Double-Layer Structure on the Determination of Corrosion Rates from Electrochemical Measurements
Z. Nagy and R. E. Hawkins
J. Electrochem. Soc. **138**(4), 1047–1050 (1991)

Cell Design for *In-Situ* X-ray Scattering Study of Electrodes in Transmission Geometry
Z. Nagy, H. You, R. M. Yonco, C. A. Melendres, W. Yun, and V. A. Maroni
Electrochim. Acta **36**, 209–212 (1991)

Superexchange-Pathway Model for Long-Distance Electronic Couplings
C. A. Naleway, L. A. Curtiss, and J. R. Miller
J. Phys. Chem. **95**(22), 8434–8437 (1991)

Battery Construction, Testing, and Materials
P. A. Nelson and T. D. Kaun
Molten Salt Techniques, Vol. 4, eds., R. J. Gale and D. G. Lovering, Plenum Publishing Co., London, England, pp. 229–266 (1991)

Magnetic and Structural Properties of Fe in Single Crystals of $YaBa_2Cu_{3-x}Fe_xO_{7-\delta}$
L. Nunez, R. D. Rogers, G. W. Crabtree, V. Welp, K. Vandervoost, A. Umezawa, and Y. Fang
Phys. Rev. B: Condens. Matter **44**, 4526 (1991)

Speciation of Pu(VI) in Near-Neutral Solutions via Laser Photoacoustic Spectroscopy
S. Okajima, D. T. Reed, J. V. Beitz, C. S. Sabau, and D. L. Bowers
Radiochim. Acta **52/53**, 111–117 (1991)

Determination of Cadmium in Blood, Plasma, and Urine by Electrothermal Atomic Absorption Spectrophotometry after Isolation by Anion-Exchange Chromatography
D. P. Peterson, E. A. Huff, and M. H. Bhattacharyya
Anal. Biochem. **192**, 434–440 (1991)

Fundamentals of the Chemical Behavior of Select Welding Fluxes
A. Polar, J. E. Indacochea, and M. Blander
Weld. J., 15s–19s (1991)

The Energy of N_2H_2 and Related Compounds
J. A. Pople and L. A. Curtiss
J. Chem. Phys. **95**(6), 4385–4388 (1991)

Propylene Hydroformylation in Supercritical Carbon Dioxide
J. W. Rathke, R. J. Klingler, and T. R. Krause
Organomet. **10**(5), 1350–1355 (1991)

A Simultaneous Comparison of Four Se Hollow Cathode Lamps Used in Graphite Furnace Atomic Absorption Spectroscopy
G. D. Rayson and D. A. Bass
Appl. Spectrosc. **45**(6), 1049–1050 (1991)

Alpha Particle-Induced Formation of Nitrate in the Cm-Sulfate Aqueous System
D. T. Reed and D. L. Bowers
Radiochim. Acta **51**, 119–125 (1990)

The Isotopic Analysis of Sulphur and Oxygen
C. E. Rees and B. D. Holt
Chapter 3 in *Stable Isotopes in the Assessment of Natural and Anthropogenic Sulphur in the Environment*, eds., H. R. Krouse and V. A. Grinenko, John Wiley & Sons, New York, pp. 43–64 (1991)

Approximate Solutions for Nonlinear Diffusion-Reaction Equations Using the Maximum Principle: The Effects of Pellet Geometry
M. C. Regalbuto, W. Strieder, and A. Varma
Chem. Eng. Sci. **46**(12), 3317–3319 (1991)

Vaporization of Strontium, Barium, Lanthanum, and Uranium from Mixtures of Urania, Zirconia, Steel, and Concretes at 2150 and 2400 K
M. F. Roche, L. Leibowitz, J. L. Settle, C. E. Johnson, R. C. Vogel, and R. L. Ritzman
Nucl. Technol. **96**, 96–116 (1991)

Direct Comparison of the Preparation and Structural Features of Crown Ether and Polyethylene Glycol Complexes of $NdCl_3 \cdot 6H_2O$
R. D. Rogers, A. N. Rollins, R. F. Henry, J. S. Murdock, R. D. Etzenhouser, S. E. Huygen, and L. Nunez
Inorg. Chem. **30**, 4946 (1991)

The Sibelius Experiment: Study of the Irradiation Behavior of Beryllium/Ceramic and Beryllium/Steel Compacts
N. Roux, M. Briec, M. Bruet, T. Flament, C. E. Johnson, M. Masson, A. Terlain, and F. Tournebize
J. Nucl. Mater. **179–181**, 827–830 (1991)

Evaluation of Gas Chromatography/Matrix Isolation-Infrared Spectroscopy for the Quantitative Analysis of Environmental Samples

J. F. Schneider, K. R. Schneider, S. E. Spiro, D. R. Bierma, and L. F. Sytsma

Appl. Spectrosc. **45**(4), 567–571 (1991)

New Evidence on the Long Valley Hydrothermal System from Wells, Fluid Sampling, Electrical Geophysics, and Age Determinations of Hot Spring Deposits

M. L. Sorey, G. Suemnicht, N. C. Sturchio, and R. Sundquist

J. Volcan. Geotherm. Res. **48**, 229–264 (1991)

Mechanisms of Selenium Vaporization with Palladium Modifiers Using Electrothermal Atomization and Mass Spectrometric Detection

D. L. Styris, L. J. Prell, D. A. Redfield, J. A. Holcombe, D. A. Bass, and V. Majidi

Anal. Chem. **63**, 508–517 (1991)

Possible Design Modification of ITER Fuel Cycle

D.-K. Sze, P. A. Finn, J. Anderson, J. R. Bartlit, and R. Sherman

Fusion Technol. **19**, 1601–1606 (1991)

ARIES-I Tritium System

D.-K. Sze, S.-W. Tam, M. C. Billone, and A. M. Hassanein

Fusion Technol. **19**, 1674–1679 (1991)

Tritium Percolation through Porous Ceramic Breeders—A Random Lattice Approach

S.-W. Tam and V. Ambrose

Fusion Eng. Des. **17**, 43–48 (1991)

Investigations of Hydrogen/Li_2O Surface Interactions via Quantum Chemical Cluster Methods

S.-W. Tam, J. Wright, L. A. Curtiss, and C. E. Johnson

J. Nucl. Mater. **179–181**, 859–862 (1991)

Thermodynamic Behavior of High-T_c Oxide Systems via EMF and Related Measurements

M. Tetenbaum, P. Tumidajski, I. Bloom, D. L. Brown, and M. Blander

New Physical Problems in Electronic Materials, eds., M. Borissov, N. Kirov, J. M. Marshall, and A. Vavrek, World Scientific Publishing Corp., New Jersey, pp. 259–280 (1991)

TRUEX Process Solvent Cleanup with Solid Sorbents

P.-K. Tse, L. Reichley-Yinger, and G. F. Vandegrift

Sep. Sci. Technol. **25**(13–15), 1763–1775 (1990)

Sterically Crowded Organometallic Influence of Complexation upon Conformation of Hexa(pheylethyl) Benzene

M. J. Zaworotko, S. J. Sturge, L. Nunez, and R. D. Rogers

Organomet. **10**, 1806–1810 (1991)

B. Patents

Activation of Methane by Transition Metal-Substituted Aluminophosphate Molecular Sieves
L. E. Iton and V. A. Maroni
Patent No. 5,068,485, issued November 26, 1991

Apparatus for Supporting Contactors Used in Extracting Nuclear Materials from Liquids
R. A. Leonard and R. C. Frank
Registration No. H914, DOE Case No. S-67,795, issued May 7, 1991

Method of Bonding Metals to Ceramics
V. A. Maroni
Patent No. 5,010,053, issued April 23, 1991

Apparatus and Process for the Electrolytic Reduction of Uranium and Plutonium Oxides
D. S. Poa, L. Burris, R. K. Steunenberg, and Z. Tomczuk
Patent No. 4,995,948, issued February 26, 1991

Toroids as NMR Detectors in Metal Pressure Probes and in Flow Systems
J. W. Rathke
Patent No. 5,045,793, issued September 3, 1991

Conductive Ceramic Composition and Method of Preparation
J. L. Smith and E. H. Kucera
Patent No. 5,008,163, issued April 16, 1991

Fabrication of Dual Porosity Electrode Structure
J. L. Smith and E. H. Kucera
Patent No. 4,992,341, issued February 12, 1991

Process and Apparatus for Recovery of Fissionable Materials from Spent Reactor Fuel by Anodic Dissolution
Z. Tomczuk, W. E. Miller, R. D. Wolson, and E. C. Gay
Patent No. 5,009,752, issued April 23, 1991

C. Reports

Unsaturated Glass Testing for DOE Program in Environmental Restoration and Waste Management Annual Report, October 1989–September 1990

J. K. Bates, C. R. Bradley, J. P. Bradley, N. L. Dietz, W. L. Ebert, J. W. Emery, T. J. Gerding, J. C. Hoh, J. J. Mazer, and J. E. Young

ANL-90/40 (January 1991)

Engineering Evaluation/Cost Analysis for the Proposed Removal of Contaminated Materials at the Elza Gate Site, Oak Ridge, Tennessee

J. S. Devgun et al.

U.S. Department of Energy Report DOE/OR/23701.3 (1991)

Derivation of Uranium Residual Radioactive Material Guidelines for the Elza Gate Site

J. S. Devgun, J.-J. Cheng, and C. Yu

Argonne National Laboratory Report prepared for U.S. Department of Energy (February 1991)

Guidelines to Achieve Seals with Minimal Leak Rates for HWR-NPR Coolant System Components

P. A. Finn

ANL-90/29 (March 1991)

Analytical Chemistry Laboratory Progress Report for FY 1991

D. W. Green, R. R. Heinrich, D. G. Graczyk, P. C. Lindahl, and A. S. Boparai (with contributions from ACL Staff)

ANL/ACL-91/1 (December 1991)

Nuclear Technology Programs Semiannual Progress Report, April–September 1989

C. E. Johnson, G. F. Vandegrift, J. K. Bates, R. D. Pierce, T. A. Abrajano, K. A. Barnthouse, B. M. Biwer, P. E. Blackburn, R. A. Blomquist, D. J. Chaiko, D. B. Chamberlain, L. S. H. Chow, R. G. Clemmer, C. J. Conner, J. M. Copple, A. A. DiFilippo, W. L. Ebert, P. A. Finn, A. K. Fischer, D. R. Fredrickson, T. J. Gerding, L. R. Greenwood, M. A. Internoscia, R. J. Jaskot, G. K. Johnson, I. Johnson, J. P. Kopasz, J. Kwasny, A. B. La'O, L. Leibowitz, R. A. Leonard, J. J. Mazer, F. C. Mrazek, T. P. Mulcahey, S. Okajima, D. S. Poa, J. L. Reed, D. T. Reed, M. C. Regalbuto, L. Reichley-Yinger, M. F. Roche, J. Sedlet, W. B. Seefeldt, J. L. Settle, S. M. Smidt, J. E. Stangel, D.-K. Sze, S.-W. Tam, I. R. Tasker, L. E. Trevorrow, E. H. Van Deventer, E. Veleckis, M. O. Wasserman, A. B. Woodland, D. J. Wronkiewicz, and J. E. Young

ANL-91/26 (August 1991)

Nuclear Technology Programs Semiannual Progress Report, October 1988–March 1989

C. E. Johnson, J. K. Bates, G. F. Vandegrift, R. D. Pierce, K. A. Barnthouse, B. M. Biwer, R. A. Blomquist, D. L. Bowers, D. J. Chaiko, D. B. Chamberlain, L. Chow, R. G. Clemmer, C. J. Conner, J. M. Copple, A. Crabtree, W. L. Ebert, P. A. Finn, A. K. Fischer, D. R. Fredrickson, T. J. Gerding, L. R. Greenwood, J. C. Hoh, A. Intasorn, M. A. Internoscia, G. K. Johnson, I. Johnson, T. R. Johnson, J. P. Kopasz, J. D. Kwok, A. B. La'O, L. Leibowitz, R. A. Leonard, J. J. Mazer, F. C. Mrazek, T. P. Mulcahey, K. Orlandini, E. R. Orth, D. S. Poa, J. B. Rajan, D. T. Reed, M. C. Regibuto, L. Reichley-Yinger, M. F. Roche, J. Sedlet, W. B. Seefeldt, N. Simonzadeh, J. E. Stangel, W. E. Streets, D.-K. Sze, S.-W. Tam, I. R. Tasker, L. E. Trevorrow, P.-K. Tse, E. H. Van Deventer, E. Veleckis, M. O. Wasserman, and J. F. Wright

ANL-90/16 (December 1990)

Geochemical Investigations of Hydraulic Connections Between the Corwin Springs Known Geothermal Resources Area and Adjacent Parts of Yellowstone National Park
Y. Kharaka, R. Mariner, T. Bullen, B. M. Kennedy, and N. C. Sturchio
In Chapt. F: *Effects of Potential Geothermal Development in the Corwin Springs Known Geothermal Resources Area, Montana, on the Thermal Features of Yellowstone National Park*, ed., M. L. Sorey, U.S. Geological Survey, Water-Resources Investigations Report 91-4052, pp. F1–F38 (1991)

Improved Treatment/Disposal of Reactive Metals. Phase II: Technical Research and Development
R. Kumar and J. E. Helt
ANL-91/21, DOE/HWP-92 (May 1991)

Alkali Vapor Removal Activities
S. H. D. Lee and W. M. Swift
Int. Gas Turbine and Aeroengine Technology Report for 1991, Int. Gas Turbine Institute, p. 22 (1991)

Studies of Corrosion Using a Combination of X-ray Scattering and Electrochemical Techniques
V. A. Maroni, H. You, C. A. Melendres, and Z. Nagy
ANL/APS-TM-9 (1991)

Temperature Effects on Waste Glass Performance
J. J. Mazer
ANL-91/17 (February 1991)

Materials Performance in the Atmospheric Fluidized-Bed Cogeneration Air Heater Experiment
K. Natesan, W. F. Podolski, D. Y. Wang, F. G. Teats, W. Gerritsen, A. Stewart, and K. Robinson
ANL-91/4 (February 1991)

Geologic Setting of the Corwin Springs Known Geothermal Resources Area— Mammoth Hot Springs Area in and Adjacent to Yellowstone National Park
K. L. Pierce, K. Adams, and N. C. Sturchio
In Chapt. C: *Effects of Potential Geothermal Development in the Corwin Springs Known Geothermal Resources Area, Montana, on the Thermal Features of Yellowstone National Park*, ed., M. L. Sorey, U.S. Geological Survey, Water-Resources Investigations Report 91-4052, pp. C1–C37 (1991)

Practical Superconductor Development for Electrical Power Applications, Annual Report for FY 1991
R. B. Poeppel, K. C. Goretta, U. Balachandran, I. Bloom, Y. S. Cha, S. E. Dorris, J. T. Dusek, J. E. Emerson, K. E. Gray, M. C. Hash, J. R. Hull, J. S. Kallend, R. T. Kampwirth, M. A. Kirk, D. S. Kupperman, M. T. Lanagan, V. A. Maroni, R. L. McDaniel, D. J. Miller, J. J. Picciolo, J. L. Routbort, J. P. Singh, and C. A. Youngdahl
ANL-91/28 (October 1991)

Component Cost Analysis for Compressed Natural Gas Vehicles
J. B. Rajan and R. R. Sekar
ANL/ESD/TM-18 (June 1991)

Transportation Technology
D. Santini, M. Mintz, A. Vyas, and J. B. Rajan
Limiting Net Greenhouse Gas Emissions in the United States: Volume I: Energy Technologies, U.S. Department of Energy Report DOE/PE-0101, pp. 6.1–6.35 (September 1991)

Chemical Technology Division Annual Technical Report, 1990
M. J. Steindler et al.
ANL-91/18 (May 1991)

Dissolution Characteristics of Mixed UO_2 Powders in J-13 Water under Saturated Conditions
E. Veleckis and J. C. Hoh
ANL-91/8 (March 1991)

Parametric Effects on Glass Reaction in the Unsaturated Test Method
A. B. Woodland, J. K. Bates, and T. J. Gerding
ANL-91/36 (December 1991)

Leaching Action of EJ-13 Water on Unirradiated UO_2 Surfaces under Unsaturated Conditions at 90°C: Interim Report
D. J. Wronkiewicz, J. K. Bates, T. J. Gerding, E. Veleckis, and B. S. Tani
ANL-91/11 (July 1991)

D. Abstracts and Proceedings Papers

Can Isotopically Distinct Components of Carbonaceous Materials Be Resolved by Stepped Combustion?
T. A. Abrajano and B. D. Holt
Abstracts with Programs, Geological Soc. of America Annual Meeting, San Diego, CA, October 21–24, 1991, Vol. 23, p. A150 (1991)

Modeling Studies of a Monolithic Solid Oxide Fuel Cell
S. Ahmed, R. Kumar, H. Walden, and K. P. Barr
Proc. of the 26th Intersoc. Energy Conversion Eng. Conf., Boston, MA, August 4–9, 1991, Vol. 3, pp. 594–599 (1991)

Quantitation of Volatile Organic Compounds in the Headspace over Transuranic Waste by Gas Chromatography/Mass Spectrometry
D. V. Applegate, G. A. Baudino, G. K. Gosztola, G. T. Reedy, Y. Tsai, and A. S. Boparai
Abstracts of the 32nd ORNL-DOE Conf. on Analytical Chemistry in Energy Technology, Gatlinburg, TN, October 1–3, 1991, p. 60 (1991)

Quality Assurance for Headspace Gas Analysis in the WIPP Experimental Waste Characterization Program
D. A. Bass, P. C. Lindahl, J. Arvizu, M. Connolly, J. Connolly, K. Knudtsen, and M. J. Duff
Abstracts of the 32nd ORNL-DOE Conf. on Analytical Chemistry in Energy Technology, Gatlinburg, TN, October 1–3, 1991, pp. 47–48 (1991)

Disposal of Vitrified Waste in an Unsaturated Environment
J. K. Bates
Proc. of the Second Annual Int. High-Level Radioactive Waste Management Conf., Am. Nucl. Soc., Las Vegas, NV, April 28–May 1, 1991, Vol. 1, pp. 700–707 (1991)

Mechanistic Interpretation of Glass Reaction: Input to Kinetic Model Development
J. K. Bates, W. L. Ebert, J. P. Bradley, and W. L. Bourcier
Proc. of the Second Annual Int. High-Level Radioactive Waste Management Conf., Am. Nucl. Soc., Las Vegas, NV, April 28–May 1, 1991, Vol. 1, pp. 720–727 (1991)

The Role of Surface Layers in Glass Leaching Performance
J. K. Bates, W. L. Ebert, J. J. Mazer, J. P. Bradley, C. R. Bradley, and N. L. Dietz
Mater. Res. Soc. Symp. Proc. **212**, 77–88 (1991)

Pyrometallurgical Processing of Integral Fast Reactor Metal Fuels
J. E. Battles, W. E. Miller, and E. C. Gay
Proc. of the Third Int. Conf. on Nuclear Fuel Reprocessing and Waste Management, RECOD '91, Sendai, Japan, April 14–18, 1991, Vol. 1, pp. 342–347 (1991)

Sealants Research for SOFC
I. Bloom, S. E. Dorris, M. C. Hash, F. G. Teats, and M. Krumpelt
Proc. of the Third Annual Fuel Cells Contractors' Review Meeting, ed., W. J. Huber, DOE/METC-91/6120, October 1991, p. 139 (1991)

Intermediate Temperature Electrolytes for SOFC
I. Bloom, M. C. Hash, J. D. Pullockaran, J. P. Zebrowski, and M. Krumpelt
Proc. of the Third Annual Fuel Cells Contractors' Review Meeting, ed., W. J. Huber, DOE/METC-91/6120, October 1991, p. 117 (1991)

In Pile Tritium Release from Lithium Ceramics and the Influence of Surface Processes
M. Briec, J. P. Kopasz, S. Casadio, and H. Werle
Proc. of the 16th Symp. on Fusion Technol., London, U.K., September 3–7, 1990, pp. 857–861 (1991)

Preliminary Results of Laboratory Studies of Repository Chemistry for the Waste Isolation Pilot Plant
L. H. Brush, D. Grbic-Galic, D. T. Reed, X. Tong, R. H. Vreeland, and R. E. Westerman
Mater. Res. Soc. Symp. Proc. **212**, 893–900 (1991)

Effects of Composition Variations on Microstructure and Chemical Durability of West Valley Reference Glass
A. C. Buechele, X. Feng, H. Gu, I. S. Muller, W. Wagner, and I. L. Pegg
Mater. Res. Soc. Symp. Proc. **212**, 141–152 (1991)

Redox State Effects on Microstructure and Leaching Properties of West Valley SF-12 Glass
A. C. Buechele, X. Feng, H. Gu, and I. L. Pegg
Ceram. Trans. **23**, 85–94 (1991)

Comparison of Costs, Emissions, and Waste Products for an 80-MW CFBC Burning Mine-Run and Washed Coals
M. K. Clemens and W. F. Podolski
Proc. of the 11th Int. Conf. on Fluidized-Bed Combustion, Montreal, Canada, April 21–24, 1991, Vol. 2, pp. 923–924 (1991)

The Role of Laboratory Analog Experiments in Assessing the Performance of Waste Package Materials
J. C. Cunnane and J. K. Bates
Mater. Res. Soc. Symp. Proc. **212**, 885–892 (1991)

Determination of On-Stream Destruction Removal Efficiency Using Fourier Transform Infrared Spectroscopy
J. C. Demirgian, Z. Mao, M. MacIntosh, and C. A. Wentz
Proc. of the 1991 Incineration Conf. on Thermal Treatment of Radioactive, Hazardous Chemical, Mixed and Medical Wastes, Knoxville, TN, May 13–17, 1991, pp. 563–570 (1991)

Waste Management and Environmental Compliance Aspects of a Major Remedial Action Program
J. S. Devgun and N. J. Beskid
Proc. of the Waste Management '91 Conf., Tucson, AZ, February 24–28, 1991, Vol. 2, pp. 639–644 (1991)

The Importance of Secondary Phases in Glass Corrosion
W. L. Ebert and J. K. Bates
Mater. Res. Soc. Symp. Proc. **212**, 89–98 (1991)

Mechanistic Effects of Deuteration of the Aqueous Corrosion of Nuclear Waste Glasses
X. Feng, L. Fu, T. K. Choudhury, I. L. Pegg, and P. B. Macedo
Mater. Res. Soc. Symp. Proc. **212**, 49–56 (1991)

The Effect of Redox State on the Chemical Durability of West Valley Glasses
X. Feng, I. S. Muller, I. L. Pegg, P. B. Macedo, J. Seghal, I. Joseph, and L. D. Pye
Ceram. Trans. **23**, 501–508 (1991)

Effect of pH on the Leaching Mechanism of Nuclear Waste Glasses
X. Feng, I. L. Pegg, Q. Yan, X. Mao, and P. B. Macedo
Ceram. Trans. **23**, 95–104 (1991)

Actinide Consumption: Nuclear Resource Conservation without Breeding
W. H. Hannum, J. E. Battles, T. R. Johnson, and C. C. McPheeters
Proc. of the 53rd Annual Meeting of the Am. Power Conf., Chicago, IL, April 29–May 1, 1991, Vol. 53–II, p. 1308 (1991)

Development of Prototype Sealed Bipolar Lithium/Sulfide Cells
T. D. Kaun, M. J. Duoba, W. Johll, V. Luong, F. C. Mrazek, D. Palkon, and D. Simon
Proc. of the 26th Intersoc. Energy Conversion Eng. Conf., Boston, MA, August 4–9, 1991, Vol. 3, pp. 417–422 (1991)

Quality Assurance Program Plan for the Waste Isolation Pilot Plant Experimental-Waste Characterization Program
K. Knudtsen, B. Marron, J. Arvizu, M. Connolly, J Connolly, D. A. Bass, P. C. Lindahl, B. Draper, F. Dooley, and M. Duff
Abstracts of the 32nd ORNL-DOE Conf. on Analytical Chemistry in Energy Technology, Gatlinburg, TN, October 1–3, 1991, pp. 18–19 (1991)

ANL's Development of Conductive Ceramic Components for MCFC
G. H. Kucera and A. P. Brown
Proc. of the Third Annual Fuel Cells Contractors' Review Meeting, ed., W. J. Huber, DOE/METC-91/6120, October 1991, pp. 53–58 (1991)

Pressurized Fluidized-Bed Combustion of Illinois High-Sodium/High-Chlorine Coal and Its Derived Char
S. H. D. Lee, F. G. Teats, and E. L. Carls
Proc. of the CRSC/EPRI First Int. Conf. on Chlorine in Coal, eds., J. Stringer and D. D. Banerjee, Chicago, IL, October 9–11, 1989, Coal Science and Technology, Elsevier, Amsterdam, Vol. 17, pp. 275–294 (1991)

U.S. DOE Applied Environmental R&D Initiatives for Private Sector Involvement in Dealing with Environmental Restoration and Waste Management
S. C. T. Lien, S. S. Borys, and M. D. Erickson
Proc. of the Conf. on Hazardous Waste Research, Manhattan, KS, May 21–22, 1990, Vol. 1 (1991)

Research and Development for DOE Environmental Restoration and Waste Management
S. C. T. Lien, K. Hain, S. S. Borys, D. Bugielski, and M. D. Erickson
Proc. of the National Research and Development Conf. on the Control of Hazardous Materials, Anaheim, CA, February 20–22, 1991, Vol. 1, pp. 356–365 (1991)

An Interlaboratory Performance Evaluation Program for DOE's Environmental Restoration and Waste Management Programs
P. C. Lindahl, W. E. Streets, S. Morton, T. F. Gesell, D. C. Bogen, and D. Bottrell
Abstracts of the 32nd ORNL-DOE Conf. on Analytical Chemistry in Energy Technology, Gatlinburg, TN, October 1–3, 1991, pp. 4–5 (1991)

Selective Oxidation of Hydrocarbons by Cobalt-Substituted Aluminophosphate Molecular Sieves
V. A. Maroni and L. E. Iton
Mater. Res. Soc. Symp. Proc. **233**, 37–43 (1991)

Fuel Cell Powered Vehicle Development Programs
J. F. Miller
Proc. of the SAE Topical Technical Conf. on Fuel Cells for Transportation, Arlington, VA, November 4–5, 1991

Centered Extrapolation Methods for Electrochemical Simulation
M. Minkoff and Z. Nagy
Extended Abstracts, 179th Electrochem. Soc. Meeting, Washington, DC, May 5–10, 1991, Vol. 91–1, pp. 907–908 (1991)

Applicability of DC Relaxation Techniques to Multistep Reactions
Z. Nagy, N. C. Hung, K. C. Liddell, M. Minkoff, and G. K. Leaf
Extended Abstracts, 180th Electrochem. Soc. Meeting, Phoenix, AZ, October 13–18, 1991, Vol. 91–2, pp. 1093–1094 (1991)

Error Analysis of the Polarization Resistance Technique
Z. Nagy and J. M. Wesson
Extended Abstracts, 179th Electrochem. Soc. Meeting, Washington, DC, May 5–10, 1991, Vol. 91–1, pp. 73–74 (1991)

Modeling of Lithium-Sulfide Batteries for Electric Vehicles and Hybrid Vehicles
P. A. Nelson and T. D. Kaun
Proc. of the 26th Intersoc. Energy Conversion Eng. Conf., Boston, MA, August 4–9, 1991, Vol. 3, pp. 423–428 (1991)

Sputtering of Molecules from ZnS, CdS, and FeS_2
S. Nikzad, W. F. Calaway, M. J. Pellin, D. M. Gruen, C. E. Young, and T. A. Tombrello
Mater. Res. Soc. Symp. Proc. **201**, 93–95 (1991)

Trace Surface Analysis Using Ion and Photon Desorption with Resonance Ionization Detection
M. J. Pellin, C. E. Young, W. F. Calaway, K. R. Lykke, P. Wurz, and D. M. Gruen
Proc. of the Laser Ablation Mechanisms and Applications Conf., Springer Series in Chem. Phys., Oak Ridge, TN, April 8–10, 1991, p. 63 (1991)

Recycle of Light Water Reactor Actinides to an Integral Fast Reactor
R. D. Pierce, J. P. Ackerman, G. K. Johnson, T. P. Mulcahey, and D. S. Poa
Proc. of the Third Int. Conf. on Nuclear Fuel Reprocessing and Waste Management, RECOD '91, Sendai, Japan, April 14–18, 1991, Vol. 1, pp. 336–341 (1991)

A Study of Parameters Influencing Metal Wastage in Fluidized Bed Combustors
W. F. Podolski, R. W. Lyczkowski, E. Montrone, J. Drennen, Y. H. Ai, and B. T. Chao
Proc. of the 11th Int. Conf. on Fluidized-Bed Combustion, Montreal, Canada, April 21–24, 1991, Vol. 2, pp. 609–618 (1991)

The Atmospheric Fluidized-Bed Cogeneration Air Heater Experiment
W. F. Podolski, K. Natesan, W. Gerritsen, A. Stewart, K. Robinson, H. Domian, and W. Roczniak
Proc. of the 11th Int. Conf. on Fluidized-Bed Combustion, Montreal, Canada, April 21–24, 1991, Vol. 2, pp. 1047–1056 (1991)

Corrosion of Copper-Based Materials in Irradiated Moist Air Systems
D. T. Reed and R. A. Van Konynenburg
Mater. Res. Soc. Symp. Proc. **212**, 317–325 (1991)

Effect of Ionizing Radiation on the Waste Package Environment
D. T. Reed and R. A. Van Konynenburg
Proc. of the Second Annual Int. High-Level Radioactive Waste Management Conf., Am. Nucl. Soc., Las Vegas, NV, April 28–May 1, 1991, Vol. 2, pp. 1396–1403 (1991)

Migration of Radionuclides in Geologic Media: Fundamental Research Needs
D. T. Reed, F. J. Wobber, and J. M. Zachara
Mater. Res. Soc. Symp. Proc. **212**, 765–776 (1991)

Internal U-Series Systematics in Pumice from the 13-Nov-1985 Eruption of Nevado Del Ruiz, Columbia
S. Schaefer, N. C. Sturchio, M. Murrell, and S. Williams
Abstracts with Programs, Geological Soc. of America Annual Meeting, San Diego, CA, October 21–24, 1991, Vol. 23, p. A73 (1991)

Microbeam Titanium Isotopic Analyis by Resonance Ionization Mass Spectrometry
D. R. Spiegel, M. J. Pellin, W. F. Calaway, J. W. Burnett, S. R. Coon, C. E. Young, D. M. Gruen, A. M. Davis, and R. N. Clayton
Proc. of the XXII Lunar and Planetary Science Conf., Houston, TX, March 18-22, 1991, pp. 1303–1304 (1991)

Radium Geochemistry and Isotopy of Thermal Waters and Travertines, Yellowstone National Park, Wyoming
N. C. Sturchio, J. K. Bohlke, and F. Markun
Abstracts with Programs, Geological Soc. of America Annual Meeting, San Diego, CA, October 21–24, 1991, Vol. 23, p. A74 (1991)

Thermodynamic Behavior of High-T_c Oxide Systems via EMF and Related Measurements
M. Tetenbaum, P. Tumidajski, D. L. Brown, and M. Blander
Proc. of the Second Int. Conf. on Rare Earth Development and Applications, Beijing, China, May 29–31, 1991, Vol. 2, pp. 523–528 (1991)

1991 (February–June) Eruption of Colima Volcano, Mexico
S. N. Williams, S. De La Cruz-Reyna, F. Nunez-Cornu, Y. Sano, and N. C. Sturchio
Abstracts with Programs, Geological Soc. of America Annual Meeting, San Diego, CA, October 21–24, 1991, Vol. 23, p. A396 (1991)

Formation and Characterization of Sulfide Clusters in Molecular Sieve Zeolite Materials
M. Winterer, L. E. Iton, S. A. Johnson, and V. A. Maroni
Mater. Res. Soc. Symp. Proc. **233**, 201–206 (1991)

Effects of Alpha and Gamma Radiation on Glass Reaction in an Unsaturated Environment
D. J. Wronkiewicz, J. E. Young, and J. K. Bates
Mater. Res. Soc. Symp. Proc. **212**, 99–106 (1991)

X-ray Reflectivity Study of Cu/Solution Electrochemical Interface
H. You, C. A. Melendres, Z. Nagy, V. A. Maroni, and W. Yun
Extended Abstracts, 180th Electrochem. Soc. Meeting, Phoenix, AZ, October 13–18, 1991, Vol. 91–2, p. 1114 (1991)

E. Papers Presented at Scientific Meetings

Stable Isotope Evidence for Mixing of Waters in the Depositional Environment Banded Iron Formations
T. A. Abrajano and B. D. Holt
Presented at the AGU-MSA Spring Meeting, Baltimore, MD, May 28–June 1, 1991

Modeling of Tritium Behavior in Ceramic Breeder and Beryllium Multiplier Materials
M. C. Billone, H. Attaya, Y. Gohar, J. P. Kopasz, C. E. Johnson, and S.-W. Tam
Presented at the Fifth Int. Conf. on Fusion Reactor Materials, Clearwater, FL, November 17–22, 1991

Ordered Ionic Liquids
M. Blander
Presented at the Institut für Physikalische Chemie und Elektrochemie, Universität Karlsruhe, Germany, November 28, 1991

Origin of Meteorites as Condensates from a Solar Nebula
M. Blander
Presented at the Institut für Planetologie, Universität Muenster, Germany, November 5, 1991

A Possible Origin of EII Chondrites from a High Temperature-High Pressure Solar Gas
M. Blander, L. Unger, A. D. Pelton, and G. Ericksson
Presented at the 54th Annual Meeting of the Meteoritical Soc., Monterey, CA, July 21–26, 1991

A Possible Origin of EII Chondrites from a High Temperature-High Pressure Solar Gas
M. Blander, L. Unger, A. D. Pelton, and G. Ericksson
Presented at the University of Hawaii, June 6–7, 1991

Alternative SOFC Materials
I. Bloom, M. C. Hash, J. D. Pullockaran, J. P. Zebrowski, and M. Krumpelt
Presented at the EPRI/GRI Fuel Cell Contractors' Review Meeting, New York, March 20–21, 1991

Oxide-Ion Conductivity of Bi-Al-O and Related Compounds
I. Bloom, M. C. Hash, J. P. Zebrowski, and M. Krumpelt
Presented at the Eighth Int. Conf. on Solid State Ionics, Lake Louise, Canada, October 20–26, 1991

Evaluation of Supercritical Fluid Extraction/Gas Chromatography/Matrix Isolation-Infrared Spectrometry for Analysis of Organic Compounds
A. S. Boparai, D. R. Bierma, and D. V. Applegate
Presented at the 42nd Pittsburgh Conf. and Exposition on Analytical Chemistry and Applied Spectroscopy, Chicago, IL, March 4–8, 1991

Analysis of Complex Mixtures by Gas Chromatography/Matrix Isolation Infrared Spectroscopy
A. S. Boparai and J. F. Schneider
Presented at the Eighth Triangle Chromatography Symp. and Instrument Exhibit, Raleigh, NC, May 16, 1991

Shaping Particles for Ultramicrotomy
C. R. Bradley, N. L. Deitz, and J. K. Bates
Presented at the Fall Meeting of the Materials Research Soc., Boston, MA, December 2–6, 1991

Computational Studies of Acid Sites in Zeolites
H. Brand, L. A. Curtiss, and J. Nicholas
Presented at the XXIV Midwest Theoretical Chemistry Conf., DeKalb, IL, May 16–18, 1991

Laboratory and Bin-Scale Tests of Gas Generation for the Waste Isolation Pilot Plant
L. H. Brush, M. A. Molecke, A. R. Lappin, R. E. Westerman, X. Tong, J. N. P. Black, D. Grbic-Galic, R. E. Vreeland, and D. T. Reed
Presented at the Organization for Economic Cooperation and Development/Nuclear Energy Agency (OECD/NEA) Workshop on Gas Generation and Release in Radioactive Waste Repositories, Aix-en-Provence, France, September 23–26, 1991

Observation and Characterization of Clusters Ejected during Argon Ion Bombardment of Polycrystalline Copper
W. F. Calaway, S. R. Coon, D. R. Spiegel, J. W. Burnett, M. J. Pellin, M. J. White, and D. M. Gruen
Presented at the 17th Department of Energy Surface Science Conf., Pleasanton, CA, October 15–18, 1991

Surface Analysis by Resonance Ionization of Sputtered Atoms (SARISA)
W. F. Calaway, C. E. Young, M. J. Pellin, J. W. Burnett, J. E. Whitten, S. R. Coon, D. M. Gruen, D. R. Spiegel, A. M. Davis, and R. N. Clayton
Presented at the Joint Meeting of the Federation of Analytical Chemistry and Spectroscopy Societies and Pacific Conf. on Chemistry and Spectroscopy, Anaheim, CA, October 6–11, 1991

Application of Aqueous Biphasic Extraction to Waste Treatment
D. J. Chaiko
Presented at Los Alamos National Laboratory, Los Alamos, NM, January 22–23, 1991

Aqueous Biphasic Extraction
D. J. Chaiko
Presented at Battelle Pacific Northwest Laboratory, Hanford, WA, November 12, 1991

Combined Physical and Biochemical Treatment of Uranium Contaminated Soils
D. J. Chaiko
Presented at the Uranium Soils ID Meeting, Cincinnati, OH, October 17, 1991

Partitioning of Polymeric Plutonium in Microemulsion Based Solvent Extraction Systems
D. J. Chaiko
Presented at the 15th Annual Actinide Separations Conf., Charleston, SC, June 17–21, 1991

Beneficiation of Plutonium Residues by Ultrafine Grinding and Aqueous-Two Phase Extraction
D. J. Chaiko, R. Mensah-Biney, C. J. Mertz, and A. Rollins
Presented at the Seventh Symp. on Separation Science and Technology for Energy Applications, Knoxville, TN, October 20–24, 1991

Beneficiation of Plutonium Residues Using Aqueous Biphasic Extraction
D. J. Chaiko, R. Mensah-Biney, C. J. Mertz, and A. Rollins
Presented at the Summer AIChE National Meeting, Pittsburgh, PA, August 18–21, 1991

Concentration of Radioactive Streams by Evaporation
D. B. Chamberlain, L. Nunez, and G. F. Vandegrift
Presented at the Summer AIChE National Meeting, Pittsburgh, PA, August 18–21, 1991

Unusual Tautomerism of a Hydridorhodium Phthalocyanine
M. J. Chen, J. W. Rathke, and R. J. Klingler
Presented at the Gordon Research Conf. on Organometallic Chemistry, Newport, RI, July 15–19, 1991

Development of a Pyrochemical Actinide Extraction Apparatus
L. S. H. Chow, R. A. Leonard, and T. R. Johnson
Presented at the 11th Annual Pyrochemical Workshop, Oak Brook, IL, November 11–14, 1991

Power Sources for Electric Vehicles
C. C. Christianson
Presented at the Energy and Transportation Conf., Grand Rapids, MI, April 1991

Environmental Assessment and EV Battery Readiness Working Groups
C. C. Christianson and J. Ohi
Presented at DOE's Annual Automotive Technology Development Contractors' Coordination Meeting, Dearborn, MI, October 28–30, 1991

Determination of Volatile Organics in Soils Utilizing Fourier Transform Infrared Spectroscopy
M. Clapper-Gowdy and J. C. Demirgian
Presented at the Amoco/University Poster Session, Naperville, IL, October 4, 1991

Identification of Colloids in Nuclear Waste Glass Reactions
J. C. Cunnane and J. K. Bates
Presented at the 93rd Annual Meeting of the Am. Ceram. Soc., Cincinnati, OH, April 28–May 2, 1991

Computational Studies of Acid Sites in Zeolites
L. A. Curtiss, H. Brand, J. Nicholas, and L. Iton
Presented at the Int. Symp. on *Ab Initio* Methods in Quantum Chemistry, Ames, IA, May 9–11, 1991

Battery Testing at ANL
W. H. DeLuca
Presented at the EPRI Transportation Program Technical Working Group Meeting, Palo Alto, CA, January 22, 1991

Status and Results of EPRI Battery Test and Development Project at Argonne National Laboratory
W. H. DeLuca
Presented at the EPRI Program Review Committee Meeting, Chattanooga, TN, March 5, 1991

Key Battery Test Result at Argonne National Laboratory
W. H. DeLuca, K. R. Gillie, J. E. Kulaga, J. A. Smaga, A. F. Tummillo, and C. E. Webster
Presented at DOE's Annual Automotive Technology Development Contractors' Coordination Meeting, Dearborn, MI, October 28–30, 1991

Performance and Life Evaluation of Advanced Battery Technologies for Electric Vehicle Applications
W. H. DeLuca, K. R. Gillie, J. E. Kulaga, J. A. Smaga, A. F. Tummillo, and C. E. Webster
Presented at the Soc. of Automotive Engineers Int. Meeting on Future Transportation Technol., Portland, OR, August 5–8, 1991

Status and Results of EPRI Battery Test and Development Project at Argonne National Laboratory
W. H. DeLuca and J. A. Smaga
Presented at the EPRI Program Review Committee Meeting, Argonne National Laboratory, August 22–23, 1991

Rapid Field Characterization of Soil Samples for Hazardous Components by Fourier Transform Infrared Spectroscopy

J. Demirgian and M. Clapper

Presented at the 42nd Pittsburgh Conf. and Exposition on Analytical Chemistry and Applied Spectroscopy, Chicago, IL, March 4–8, 1991

Remote Detection of Organics Using Fourier Transform Infrared Spectroscopy

J. C. Demirgian and S. M. Spurgash

Presented at the Second Int. Symp. on Field Screening Methods for Hazardous Wastes and Toxic Chemicals, Las Vegas, NV, February 12–14, 1991

Role of Risk Assessment in Remediation of Contaminated Sites

J. S. Devgun

Presented at the 11th Annual Meeting of the Int. Assoc. for Impact Assessment, Champaign, IL, June 7–11, 1991

PCB Toxic Equivalent Factors—Significance for the Utilities

M. D. Erickson

Presented at the EPRI 1991 PCB Seminar, Baltimore, MD, October 8–11, 1991

Standard Method for Toxic PCB Congener Analysis

M. D. Erickson

Presented at the EPRI 1991 PCB Seminar, Baltimore, MD, October 8–11, 1991

Toxic PCB Congener Analysis: Recommendation for a Standard Method

M. D. Erickson

Presented at the Dioxin '91 Conf., Research Triangle Park, NC, September 23–27, 1991

R&D Activities at DOE Applicable to Mixed Waste

M. D. Erickson, J. S. Devgun, N. J. Beskid, and J. Brown

Presented at the HAZMAT South Meeting, Emerging Technologies for Hazardous Waste Management, Am. Chem. Soc., Atlanta, GA, October 1–3, 1991

Determination of Uranium and Uranium Isotopes in High Silica Soils by Laser Kinetic Phosphorimetry and Thermal Ionization Mass Spectrometry

A. M. Essling, R. W. Bane, and D. G. Graczyk

Presented at the 37th Annual Conf. on Bioassay, Analytical and Environmental Radiochemistry, Ottawa, Canada, October 7–11, 1991

Effect of pH on the Leaching Mechanism of Nuclear Waste Glasses

X. Feng, I. L. Pegg, Q. Yan, X. Mao, and P. B. Macedo

Presented at the 93rd Annual Meeting of the Am. Ceram. Soc., Cincinnati, OH, April 28–May 2, 1991

Sealing Systems for a Heavy Water Reactor

P. A. Finn

Presented at the Fourth Am. Nucl. Soc. National Topical Meeting on Tritium Technology in Fission, Fusion, and Isotopic Applications, Albuquerque, NM, September 30–October 4, 1991

Helium Processing for Deuterium/Helium Burns in ITER's Physics Phase

P. A. Finn and D.-K. Sze

Presented at the Second Int. Symp. on Fusion Nuclear Technology, Karlsruhe, Germany, June 2–7, 1991

Modification of a Shielded Cell to Handle Tritium
P. A. Finn and J. P. Webb
Presented at the Fourth Am. Nucl. Soc. National Topical Meeting on Tritium Technology in Fission, Fusion, and Isotopic Applications, Albuquerque, NM, September 30–October 4, 1991

Temperature Programmed Desorption from $LiAlO_2$ Treated with H_2
A. K. Fischer
Presented at the Fifth Int. Conf. on Fusion Reactor Materials, Clearwater, FL, November 17–22, 1991

Electrical Conductivity and Thermopower Properties of Liquid Semiconducting Alloys
J. Fortner, M.-L. Saboungi, and J. E. Enderby
Presented at the Am. Phys. Soc. Meeting, Cincinnati, OH, March 18–22, 1991

Overview of DOE's Field Screening Technology Development Activities
C. W. Frank, T. D. Anderson, C. Cooley, K. Hain, S. C. T. Lien, R. L. Snipes, and M. D. Erickson
Presented at the Second Int. Symp. on Field Screening Methods for Hazardous Wastes and Toxic Chemicals, Las Vegas, NV, February 12–14, 1991

ITER Blanket and Shield Studies for High Aspect Ratio Design Option
Y. Gohar, H. Attaya, M. C. Billone, C. E. Johnson, J. P. Kopasz, S. Majumdar, R. Mattas, and D. Smith
Presented at the 14th IEEE/NPSS Symp., San Diego, CA, September 30–October 3, 1991

Analytical Laboratory Management—Interlaboratory Performance Evaluation Program
D. W. Green
Presented at the Ninth DOE Analytical Managers Meeting, Kansas City, MO, September 10–12, 1991

Alkali Monitoring for Direct Coal-Fired Turbine Combustors
W. J. Haas, D. E. Eckels, S. H. D. Lee, W. M. Swift, L. H. Cowell, M. D. Stephenson, and R. T. LeCren
Presented at the Eighth Annual Coal-Fired Heat-Engines and Gas Stream Cleanup Systems Contractors' Review Meeting, Morgantown, WV, July 16–18, 1991

Lithium/Metal Sulfide Technology Status
G. L. Henriksen and J. Embrey
Presented at DOE's Annual Automotive Technology Development Contractors' Coordination Meeting, Dearborn, MI, October 28–31, 1991

TRUEX Processing of Plutonium Analytical Waste Solutions at Argonne National Laboratory
J. C. Hutter, D. B. Chamberlain, E. H. Van Deventer, G. F. Vandegrift, D. R. Fredrickson, R. A. Leonard, J. A. How, M. A. Tranovich, and D. L. Bowers
Presented at the Summer AIChE National Meeting, Pittsburgh, PA, August 18–21, 1991

Decontamination of Groundwater Using Membrane-Assisted Solvent Extraction
J. C. Hutter and G. F. Vandegrift
Presented at the 201st National Meeting of the Am. Chem. Soc., Atlanta, GA, April 14–19, 1991

Fabrication, Properties, and Tritium Recovery from Solid Breeder Materials
C. E. Johnson, T. Kondo, N. Roux, S. Tanaka, and D. Vollath
Presented at the Second Int. Symp. on Fusion Nuclear Technology, Karlsruhe, Germany, June 2–7, 1991

Extraction Processes in the Actinide Recovery Progam
G. K. Johnson, T. P. Mulcahey, R. D. Pierce, D. W. Warren, and E. J. Wesolowski
Presented at the 11th Annual Pyrochemical Workshop, Oak Brook, IL, November 11–14, 1991

Salt Transport for Actinide Recovery
G. K. Johnson, R. D. Pierce, T. P. Mulcahey, and D. W. Warren
Presented at the Tenth Annual Pyrochemical Workshop, Charleston, SC, January 28–31, 1991

Actinide Chemistry
I. Johnson
Presented at the 11th Annual Pyrochemical Workshop, Oak Brook, IL November 11–14, 1991

Introduction to IFR Pyrochemical Processes
I. Johnson
Presented at the IFR Technology Series Meeting, Argonne National Laboratory–West, October 24, 1991

Observations of Variations in the Chemistry of Atmospheric Aerosol in Real Time
S. A. Johnson and R. Kumar
Presented at the Am. Assoc. for Aerosol Research Meeting, Traverse City, MI, October 7–11, 1991

Waste Management in IFR Fuel Cycle
T. R. Johnson and J. E. Battles
Presented at the Waste Management Conf., Tucson, AZ, February 24–28, 1991

High Performance Bipolar Electric Vehicle Battery
T. D. Kaun
Presented at the State of Illinois Review of Technology Challenge Grants Meeting, Argonne National Laboratory, February 20, 1991

High-Pressure NMR Studies of Catalytic Processes in Supercritial Medium
R. J. Klingler and J. W. Rathke
Presented at the Amoco-Argonne Coal Chemistry Distinguished Seminar Series, Naperville, IL, June 10, 1991

Hydroformylation Catalysis in Supercritical Media
R. J. Klingler and J. W. Rathke
Presented at the Gordon Research Conf. on Organometallic Chemistry, Newport, RI, July 15–19, 1991

Nucleophilic Hydrogen Activation
R. J. Klingler and J. W. Rathke
Presented at the Third DOE/BES Organometallic Chemistry and Homogeneous Catalysis Research Conf., Madison, WI, June 3–5, 1991

Applying Lessons Learned from Laboratory Experiments to Modeling of In-Pile Tritium Release Experiments
J. P. Kopasz and C. E. Johnson
Presented at the U.S.-Japan Workshop on Ceramic Breeder Materials Interactions, Clearwater, FL, November 22–23, 1991

Tritium Release from Lithium Aluminate, Can It Be Improved?
J. P. Kopasz and C. E. Johnson
Presented at the Fifth Int. Conf. on Fusion Reactor Materials, Clearwater, FL, November 17–22, 1991

Investigation of Tritium Release and Retention in Lithium Aluminate
J. P. Kopasz, S. Tistchenko, and E. Botter
Presented at the Third Int. Symp. on Fabrication and Properties of Lithium Ceramics, Cincinnati, OH, April 28–May 3, 1991

Chemical Detoxification of Trichloroethylene and 1,1,1-Trichloroethane in a Microwave Discharge Plasma Reactor at Atmospheric Pressure

T. R. Krause

Presented at the Southern California Edison/South Coast Air Quality Management Seminar Series on Advanced Technologies for the Destruction of Air Toxics, Los Angeles, CA, December 4, 1991

Chemical Detoxification of Trichloroethylene and 1,1,1-Trichloroethane in a Microwave Discharge Plasma Reactor at Atmospheric Pressure

T. R. Krause and J. E. Helt

Presented at the Emerging Technologies for Hazardous Waste Management Symp., Atlanta, GA, October 1–3, 1991

Oxo Chemistry in Supercritical Carbon Dioxide

T. R. Krause, J. W. Rathke, and R. J. Klingler

Presented at the Annual AIChE Meeting on Supercritical Fluids, Los Angeles, CA, November 17–22, 1991

Development of MCFC Alternative Components

G. H. Kucera and A. P. Brown

Presented at the EPRI/GRI Fuel Cell Contractors' Review Meeting, New York, March 20–21, 1991

Multifuel Reformer R&D

R. Kumar

Presented at DOE's Annual Automotive Technology Development Contractors' Coordination Meeting, Dearborn, MI, October 28–30, 1991

Alkali Sorber (RABSAM)

S. H. D. Lee and W. M. Swift

Presented at the 11th Annual Gasification and Gas Stream Cleanup Systems Contractors' Review Meeting, Morgantown, WV, August 13–15, 1991

A Fixed Granular-Bed Sorber for Measurement and Control of Alkali Vapors in PFBC

S. H. D. Lee and W. M. Swift

Presented at the 11th Int. Conf. on Fluidized-Bed Combustion, Montreal, Canada, April 21–24, 1991

Computer Evaluation of Solvent Extraction Flowsheets

R. A. Leonard, M. C. Regalbuto, and G. F. Vandegrift

Presented at the Seventh Symp. on Separation Science and Technology for Energy Applications, Knoxville, TN, October 20–24, 1991

Stagewise Calculations in Solvent Extraction Processes

R. A. Leonard, M. C. Regalbuto, and G. F. Vandegrift

Presented at the 15th Actinide Separations Conf., Charleston, SC, June 17–21, 1991

Vibrations in Rotating Equipment

R. A. Leonard, M. O. Wasserman, and G. F. Vandegrift

Presented at the Summer AIChE National Meeting, Pittsburgh, PA, August 18–21, 1991

The Centrifugal Contactor as a Concentrator in Solvent Extraction Processes

R. A. Leonard, D. G. Wygmans, M. J. McElwee, M. O. Wasserman, and G. F. Vandegrift

Presented at the Seventh Symp. on Separation Science and Technology for Energy Applications, Knoxville, TN, October 20–24, 1991

Waste Form Development for IFR Waste Salt
M. A. Lewis and T. R. Johnson
Presented at the 11th Annual Pyrochemical Workshop, Oak Brook, IL, November 11–14, 1991

Remediation Technology Needs and Applied R&D Initiatives
S. C. T. Llen, R. S. Levine, N. J. Beskid, J. S. Devgun, M. D. Erickson, and S. L. Webster
Presented at the Environmental Remediation '91 Conf., Pasco, WA, September 8–11, 1991

Synthesis of C-Oriented $YbBa_2Cu_4O_{7-\delta}$ Thick Films on Single and Polycrystalline Substrates by Oxidation of Liquid-Alloy Precursors
J. S. Luo, N. Merchant, V. A. Maroni, D. M. Gruen, K. H. Sandhage, and C. A. Craven
Presented at the Fall Meeting of the Materials Research Soc., Boston, MA, December 2–6, 1991

A Study of Parameters that Influence Growth and Stability of the $(Bi_{2-x}Pb_x)Sr_2Ca_2Cu_3O_y$
J. S. Luo, N. Merchant, V. A. Maroni, K. H. Sandhage, G. N. Riley, and W. L. Carter
Presented at the Fall Meeting for the Materials Research Soc., Boston, MA, December 2–6, 1991

Studies of Corrosion Using a Combination of X-ray Scattering and Electrochemical Techniques
V. A. Maroni
Presented at the Applications of Synchrotron Radiation to Chemical Engineering Science Symp., Argonne National Laboratory, April 22–23, 1991

X-ray Scattering Studies of Electrochemical Interfaces
V. A. Maroni, H. You, C. A. Melendres, Z. Nagy, R. M. Yonco, and D. J. Zurawski
Presented at the DOE/BES Corrosion Contractors Meeting, Upton, NY, September 19–20, 1991

AEM Analyses of SRL 131 Altered as a Function of SA/V
J. J. Mazer, J. K. Bates, B. M. Biwer, and C. R. Bradley
Presented at the Materials Research Soc. Meeting, Strasbourg, France, November 4–7, 1991

Mechanism of Clay Formation on Tektites: Natural Weathering vs. Laboratory Alteration
J. J. Mazer, J. K. Bates, C. R. Bradley, and C. M. Stevenson
Presented at the 28th Annual Meeting of the Clay Minerals Soc., Houston, TX, October 7–10, 1991

Molecular Water Diffusion in Obsidian and Tektite Glasses between 110 and 230°C
J. J. Mazer, J. K. Bates, C. R. Bradley, and C. M. Stevenson
Presented at the Geological Soc. of America Annual Meeting, San Diego, CA, October 21–24, 1991

Obsidians and Tektites: Natural Analogues for Water Diffusion in Nuclear Waste Glasses
J. J. Mazer, J. K. Bates, C. M. Stevenson, and C. R. Bradley
Presented at the Materials Research Soc. Meeting, Strasbourg, France, November 4–7, 1991

Development of Materials for Containment of Actinide Recycle Processes
C. C. McPheeters, P. S. Maiya, and D. S. Poa
Presented at the 11th Annual Pyrochemical Workshop, Oak Brook, IL, November 11–14, 1991

Pyrochemical Processing of LWR Spent Fuel for Recovery of Actinide Elements
C. C. McPheeters and R. D. Pierce
Presented at the Summer AIChE National Meeting, Pittsburgh, PA, August 18–21, 1991

On the Composition of the Passive Film on Nickel: A Surface Enhanced Raman Spectroelectrochemical Study
C. A. Melendres and M. Pankuch
Presented at the 180th Electrochem. Soc. Meeting, Phoenix, AZ, October 13–18, 1991

X-ray and Light Scattering Studies of Electrode Surfaces and Interfaces
C. A. Melendres, H. You, Z. Nagy, V. A. Maroni, W. Yun, and M. Pankuch
Presented at the NATO Advanced Studies Institute on Structure and Properties of Surfaces and Interfaces, Porto Caras, Greece, August 18–30, 1991

Interfacial Reactions of $YbBa_2Cu_4O_7$ Films Prepared by Oxidation of a Liquid Alloy Precursor on Oriented Oxide Substrates
N. Merchant, R. Mohemad, S. Sinha, D. M. Gruen, J. S. Luo, V. A. Maroni, K. H. Sandhage, and C. A. Craven
Presented at the Spring Meeting of the Materials Research Soc., Anaheim, CA, April 29–May 3, 1991

Electric Autos
J. F. Miller
Presented at the Division of Educational Programs Meeting, Introduction to Research at Argonne, Argonne National Laboratory, June 12, 1991

Liquid Cathodes Used in Electrorefining of IFR Metal Fuel
W. E. Miller, E. C. Gay, and Z. Tomczuk
Presented at the 11th Annual Pyrochemical Workshop, Oak Brook, IL, November 11–14, 1991

Pyrochemical Processing of LWR Spent Fuel for Recovery of Actinide Elements
T. P. Mulcahey, R. D. Pierce, G. K. Johnson, D. Poa, and M. Vest
Presented at the 15th Actinide Separations Conf., Charleston, SC, June 17–21, 1991

Electrowinning of Calcium/Plutonium
T. P. Mulcahey, D. S. Poa, R. D. Pierce, G. K. Johnson, and D. W. Warren
Presented at the 11th Annual Pyrochemical Workshop, Oak Brook, IL, November 11–14, 1991

Developmental Status and System Studies of the Monolithic Solid-Oxide Fuel Cell
K. M. Myles
Presented at the Second Int. Symp. on Solid Oxide Fuel Cells, Athens, Greece, July 2–5, 1991

Application on the Monolithic Solid-Oxide Fuel Cell to Space Power Systems
K. M. Myles and S. K. Bhattacharyya
Presented at the Eighth Symp. on Space Nuclear Power Systems, Albuquerque, NM, January 6–10, 1991

Argonne National Laboratory Electric Vehicle Program
K. M. Myles, C. C. Christianson, G. L. Henriksen, P. A. Nelson, W. H. DeLuca, and D. R. Vissers
Presented at the U.S. Advanced Battery Consortium Technical Advisory Board Meeting, Detroit, MI, April 19, 1991

Briefing on ANL Battery R&D Capabilities
K. M. Myles, P. A. Nelson, C. C. Christianson, D. R. Vissers, G. L. Henriksen, and W. H. DeLuca
Presented at the U.S. Advanced Battery Consortium Technical Advisory Committee Meeting, Argonne National Laboratory, June 3, 1991

X-ray Reflectivity Studies of Metal/Solution Interphase
Z. Nagy, C. A. Melendres, H. You, W. Yun, D. J. Zurawski, R. M. Yonco, and V. A. Maroni
Presented at the Gordon Research Conf. on Electrochemistry, Ventura, CA, January 21–25, 1991

In-Situ Examination of Electrodes by Synchrotron X-ray Radiation
Z. Nagy, C. A. Melendres, H. You, W. Yun, D. J. Zurawski, R. M. Yonco, and V. A. Maroni
Presented at the 33rd IUPAC Congress, Budapest, Hungary, August 17–22, 1991

Materials for FBC Cogeneration Systems
K. Natesan and W. E. Podolski
Presented at the First Int. Conf. on Heat Resistant Materials, Lake Geneva, WI, September 22–26, 1991

Modeling of Sodium/Nickel Chloride Batteries for Electric Vehicles
P. A. Nelson and J. Prakash
Presented at the 180th Electrochem. Soc. Meeting, Phoenix, AZ, October 13–18, 1991

Application of Photoacoustic Spectroscopy to the Detection of Uranyl (UO_2^{2+}) in Aqueous Systems
S. Okajima and D. T. Reed
Presented at the 201st National Meeting of the Am. Chem. Soc., Atlanta, GA, April 14–19, 1991

Pyrochemical Recovery of Actinides from Spent LWR Fuel
R. D. Pierce, G. K. Johnson, T. P. Mulcahey, D. S. Poa, and M. A. Vest
Presented at the Partitioning of Actinides and Fission Products Workshop, Mito-City, Japan, November 19, 1991

Calcium Electrowinning for Salt Recycle
D. S. Poa, G. K. Johnson, T. P. Mulcahey, and R. D. Pierce
Presented at the Tenth Annual Pyrochemical Workshop, Charleston, SC, January 28–31, 1991

Electrochemical Recovery of Pyrochemical Reduction Salt
D. S. Poa, G. K. Johnson, T. P. Mulcahey, and R. D. Pierce
Presented at the 180th Electrochem. Soc. Meeting, Phoenix, AZ, October 13–18, 1991

Parametric Study of N_2O Emissions from Fluidized Bed Combustors
W. E. Podolski
Presented at the Ninth Annual Illinois Coal Development Board Contractors' Technical Meeting, Urbana, IL, July 30–August 1, 1991

Comparison of Costs, Emissions, and Waste Products for an 80-MW CFBC Burning Mine-Run and Washed Coals
W. E. Podolski and M. K. Clemens
Presented at the Ninth Annual Illinois Coal Development Board Contractors' Technical Meeting, Urbana, IL, July 30–August 1, 1991

Development of Advanced Nickel Chloride Electrodes
J. Prakash, L. Redey, I. Bloom, and D. R. Vissers
Presented at the 180th Electrochem. Soc. Meeting, Phoenix, AZ, October 13–18, 1991

Correlation between Capacity and Surface Area of Ni/$NiCl_2$ Electrode
J. Prakash, L. Redey, and D. R. Vissers
Presented at the 180th Electrochem. Soc. Meeting, Phoenix, AZ, October 13–18, 1991

Investigation of Ni/$NiCl_2$ Processes
J. Prakash, L. Redey, and D. R. Vissers
Presented at the 179th Electrochem. Soc. Meeting, Washington, DC, May 5–10, 1991

Catalytic Reactions in Supercritical Fluids and Methane Activation
J. W. Rathke, M. J. Chen, and R. J. Klingler
Presented at the Third DOE/BES Organometallic Chemistry and Homogeneous Catalysis Research Conf., Madison, WI, June 3–5, 1991

Modeling of Sulfide Capacities in Binary Slags
R. G. Reddy, H. Hu, and M. Blander
Presented at the Metall. Soc. Annual Meeting, New Orleans, LA, February 17–21, 1991

Characterization of Active Materials and Electrodes for Battery R&D
L. Redey
Presented at the 179th Electrochem. Soc. Meeting, Washington, DC, May 5–10, 1991

Dynamic-Performance Measurements of Battery Cells for Electric Vehicle and Other Applications
L. Redey
Presented at the 180th Electrochem. Soc. Meeting, Phoenix, AZ, October 13–18, 1991

Electrochemical and Neutron Diffraction Measurements of PdD Cathodes
L. Redey, K. M. Myles, F. J. Rotella, J. W. Richardson, G. P. Felcher, L. R. Hittermann, and R. Kleb
Presented at the 180th Electrochem. Soc. Meeting, Phoenix, AZ, October 13–18, 1991

Application of High-Sensitivity Laser Techniques to Actinide Speciation Studies
D. T. Reed
Presented at the University of Illinois, Urbana, IL, February 26, 1991

Application of High-Sensitivity Laser Techniques to Actinide Speciation Studies
D. T. Reed
Presented at EG&G Rocky Flats, Rocky Flats, CO, January 23, 1991

Application of High-Sensitivity Laser Techniques to Speciation and On-Line Detection of Actinides
D. T. Reed
Presented at Westinghouse Savannah River Company, Aiken, SC, May 21, 1991

Critical Evaluation of the Applicability of High-Sensitivity Laser Spectroscopic Techniques to the Detection and Speciation of Metal Ions in Groundwater Systems
D. T. Reed and S. Okajima
Presented at the 201st National Meeting of the Am. Chem. Soc., Atlanta, GA, April 14–19, 1991

Brief Survey of the Separation of Metal Ions and Organic Species from the Environment
D. T. Reed, I. R. Tasker, and G. F. Vandegrift
Presented at the 201st National Meeting of the Am. Chem. Soc., Atlanta, GA, April 14–19, 1991

Progress in Assessing the Effect of Ionizing Radiation on the Anticipated Waste Package Environment at the Yucca Mountain Potential Respository Site
D. T. Reed and R. A. Van Konynenburg
Presented at the Focus '91 Nuclear Waste Packaging Conf., Am. Nucl. Soc. and Am. Soc. Mater., Las Vegas, NV, September 29–October 2, 1991

Progress in Evaluating the Corrosion of Candidate HLW Container Metals in Irradiated Air-Steam Mixtures
D. T. Reed and R. A. Van Konynenburg
Presented at the Focus '91 Nuclear Waste Packaging Conf., Am. Nucl. Soc. and Am. Soc. Mater., Las Vegas, NV, September 29–October 2, 1991

Viscosities of Core-Concrete Mixtures
M. F. Roche, D. V. Steidl, L. Leibowitz, J. K. Fink, and B. R. Sehgal
Presented at the ACE-TAC Meeting, Electric Power Research Institute, Palo Alto, CA, November 4–8, 1991

Viscosities of Core-Concrete Mixtures
M. F. Roche, D. V. Steidl, L. Leibowitz, J. K. Fink, and B. R. Sehgal
Presented at the ACE-TAC Meeting, Argonne National Laboratory, June 10–14, 1991

Properties and Performance of Tritium Breeding Ceramics
N. Roux, C. E. Johnson, and K. Noda
Presented at the Fifth Int. Conf. on Fusion Reactor Materials, Clearwater, FL, November 17–22, 1991

TRU's and Strontium in Soils
L. L. Smith
Presented at the 37th Annual Conf. on Bioassay, Analytical, and Environmental Radiochemistry, Ottawa, Canada, October 7–10, 1991

Analysis of Potential Contamination by Fog Oil in Soils and Plants
C. T. Snyder
Presented at the 14th Analytical Chemistry Laboratory Technical Meeting, Argonne National Laboratory, April 9, 1991

Development of an Interlaboratory Performance Evaluation Program (IPEP) for the Department of Energy's Environmental Restoration and Waste Management Programs
W. E. Streets, P. C. Lindahl, S. Morton, T. F. Gesell, D. C. Bogen, C. Sanderson, and D. Bottrell
Presented at the 37th Annual Conf. on Bioassay, Analytical, and Environmental Radiochemistry, Ottawa, Canada, October 7–11, 1991

Hydrothermal System of Purace Volcano, Columbia
N. C. Sturchio
Presented at the University of Iowa, Iowa City, IA, March 29, 1991

Radium Isotope Geochemistry of Yellowstone Thermal Waters and Travertines
N. C. Sturchio
Presented at the University of Oklahoma, Norman, OK, February 20, 1991

Release Criteria and Pathway Analysis Methods for Radiologically Decontaminated Sites
G. Subbaraman, R. J. Tuttle, B. M. Oliver, and J. S. Devgun
Presented at the Environmental Remediation '91 Conf., Pasco, WA, September 8–11, 1991

PFBC Evaluation of Illinois Limestones for Reducing SO_2 and HCl Emissions
W. M. Swift and S. H. D. Lee
Presented at the Ninth Annual Illinois Coal Development Board Contractors' Technical Meeting, Urbana, IL, July 30–August 1, 1991

Some Issues in Two-Dimensional Modeling of Tritium Transport
S.-W. Tam
Presented at the Third Int. Workshop on Modeling Tritium Behavior in Ceramic Fusion Blankets, Karlsruhe, Germany, June 10–11, 1991

Tritium Percolation through Porous Ceramic Breeders—A Random Lattice Approach
S.-W. Tam and V. Ambrose
Presented at the Second Int. Symp. on Fusion Nuclear Technology, Karlsruhe, Germany, June 2–7, 1991

Tritium Transport in Lithium Ceramics Porous Media
S.-W. Tam and C. E. Johnson
Presented at the Fifth Int. Conf. on Fusion Reactor Materials, Clearwater, FL, November 17–22, 1991

In Search of a Universal Matrix Modifier
L. B. TenKate
Presented at the 14th Analytical Chemistry Laboratory Technical Meeting, Argonne National Laboratory, April 9, 1991

Spent Fuel Test Material Selection Considerations for Performance Assessment Testing
T. A. Thornton, J. C. Cunnane, and M. K. Manaktala
Presented at the Int. High-Level Radioactive Waste Management Conf., Am. Nucl. Soc., Las Vegas, NV, April 28–May 3, 1991

Electrorefining of Metallic Fuel from a Cadmium Anode
Z. Tomczuk, J. P. Ackerman, R. D. Wolson, and W. E. Miller
Presented at the 180th Electrochem. Soc. Meeting, Phoenix, AZ, October 13–18, 1991

Solubility of $FeCl_2$ in Molten NaCl-$AlCl_3$
P. J. Tumidajski and M. Blander
Presented at the Third Annual Int. Symp. on Molten Salt Chemistry and Technology, Paris, France, July 16–20, 1991

Fundamental and Applied Aspects of Actinide Electrodeposition at Liquid Metal Electrodes
J. L. Willit, Z. Tomczuk, E. C. Gay, and W. E. Miller
Presented at the 180th Electrochem. Soc. Meeting, Phoenix, AZ, October 13–18, 1991

Effects of Alpha and Gamma Radiation on Glass Reaction in an Unsaturated Environment
D. J. Wronkiewicz
Presented at Argonne National Laboratory, August 2, 1991

X-ray Reflectivity Study of Cu-Solution Electrochemical Interface
H. You, C. A. Melendres, Z. Nagy, V. A. Maroni, and W. Yun
Presented at the Am. Phys. Soc. Meeting, Cincinnati, OH, March 18–22, 1991

X-ray Reflectivity Study of the Cu/Solution Electrochemical Interface
H. You, C. A. Melendres, Z. Nagy, V. A. Maroni, and W. Yun
Presented at the Second Int. Conf. on Surface X-ray and Neutron Scattering, Bad Honnef, Germany, June 25–28, 1991

In-Situ X-ray Reflectivity Study of Copper/Solution Electrochemical Interface in Transmission Geometry
H. You, C. A. Melendres, Z. Nagy, W. Yun, and R. M. Yonco
Presented at the Annual National Synchrotron Light Source Users' Meeting, Upton, NY, May 21–22, 1991

X-ray Reflectivity Studies of the Electrode/Solution Interphase
H. You, C. A. Melendres, Z. Nagy, D. J. Zurawski, R. Chiarello, W. Yun, R. M. Yonco, and V. A. Maroni
Presented at the Annual National Synchrotron Light Source User's Meeting, Upton, NY, May 21–22, 1991

X-ray Reflective Studies of the Metal/Solution Interphase
H. You, Z. Nagy, C. A. Melendres, D. J. Zurawski, R. P. Chiarello, H. K. Kim, R. M. Yonco, and V. A. Maroni
Presented at the Workshop on Structural Effects in Electrocatalysis and Oxygen Electrochemistry, Cleveland, OH, October 29–November 1, 1991

In-Situ X-ray Scattering Study of Oxide Growth at Pt(111)/Solution Interface

H. You, D. J. Zurawski, Z. Nagy, R. P. Chiarello, and H. K. Kim

Presented at the Materials Research Soc. Meeting, Boston, MA, December 2–6, 1991

F. Papers Accepted for Publication

Low-Temperature Vapor Alteration of Glass under Potential Storage Conditions
J. K. Bates
To be published in *Radioactive Waste Management and the Nuclear Fuel Cycle*, Special Issue on the Yucca Mountain Project

Colloid Formation during Waste Form Reaction: Implications for Nuclear Waste Disposal
J. K. Bates, J. P. Bradley, A. Teetsov, C. R. Bradley, and M. Buchholtz ten Brink
To be published in Science

Issues Affecting the Prediction of Glass Reacivity in an Unsaturated Environment
J. K. Bates, W. L. Ebert, X. Feng, and W. L. Bourcier
To be published in The Special Issue of J. Nucl. Mater.

Comparison of Leach Behavior between Fully Radioactive and Simulated Nuclear Waste Glasses through Long-Term Testing. Part 2. Reacted Layer Analysis
J. K. Bates, X. Feng, C. R. Bradley, and E. C. Buck
To be published in the Proc. of Waste Management '92

A Possible Origin of EH Chondrites from a High Temperature-High Pressure Solar Gas
M. Blander, L. Unger, A. Pelton, and G. Ericksson
To be published in J. Sci.

Unusual Tautomerism Involving Proton Migration between Metal and Pyrrolic Nitrogen in a Hydridorhodium Phthalocyanine Complex
M. J. Chen and J. W. Rathke
To be published in J. Chem. Soc. Chem. Comm.

Binding Energies and Electron Affinities of Small Silicon Clusters
L. A. Curtiss, P. W. Deutsch, and K. Raghavachari
To be published in J. Chem. Phys.

A Comparison of Glass Reaction at High and Low S/V
W. L. Ebert and J. K. Bates
To be published in the Proc. of the 1992 Int. High-Level Radioactive Waste Management Conf.

PCB Analysis: Status and Challenges
M. D. Erickson
To be published in Chemosphere

Comparison of Leach Behavior between Fully Radioactive and Simulated Nuclear Waste Glasses through Long-Term Testing. Part 1. Solution Analyses
X. Feng and J. K. Bates
To be published in the Proc. of the 1992 Int. High-Level Radioactive Waste Management Conf.

Temperature Programmed Desorption from $LiAlO_2$ Treated with H_2
A. K. Fischer
To be published in J. Nucl. Mater.

Thermodynamic Studies of Mordenite, Dehydrated Mordenite, and Gibbsite
G. K. Johnson, I. R. Tasker, H. E. Flotow, P. A. G. O'Hare, and W. S. Wise
To be published in Am. Mineral.

Hydrogen Activation by Soluble Metal Oxide Complexes
R. J. Klingler, T. R. Krause, and J. W. Rathke
To be published in Am. Chem. Soc. Symp. Ser.

Oxo Chemistry in Supercritical Carbon Dioxide
R. J. Klingler, T. R. Krause, and J. W. Rathke
To be published in Am. Chem. Soc. Symp. Ser.

Thermodynamics for the Hydrogenation of Dimanganese Decacarbonyl
R. J. Klingler and J. W. Rathke
To be published in Inorg. Chem.

Catalytic Effect of Under-Potential Deposited Layers on the Ferrous/Ferric Outer-Sphere Electron Transfer Reaction
Z. Nagy L. A. Curtiss, N. C. Hung, D. J. Zurawski, and R. M. Yonco
To be published in J. Electroanal. Chem. Interfacial Electrochem.

Error Analysis of the Polarization-Resistance Technique for Corrosion-Rate Measurements
Z. Nagy and J. M. Wesson
To be published in J. Electrochem. Soc.

Velocity Distribution and Yield Measurements of Fe Ejected from FeS_2 during Ion Bombardment
S. Nikzad, W. E. Calaway, C. E. Young, M. J. Pellin, D. M. Gruen, T. A. Tombrello, and R. M. Housley
To be published in Phys. Rev. B

Crystal Structure of $PrCl_3$ [15-Crown-5] Prepared via Electrocrystallization
L. Nunez and R. D. Rogers
To be published in J. Cryst. Spec. Rec.

Thermodynamics for the Hydrogenation of Diobalt Octacarbonyl in Supercritical Carbon Dioxide
J. W. Rathke, R. J. Klingler, and T. R. Krause
To be published in Organomet.

Corrosion of Copper-Based Materials in Gamma-Irradiated Air/Water Vapor Systems
D. T. Reed
To be published in the Proc. of the National Association of Corrosion Engineers Annual Conf. and Corrosion Show

Radiolytic Formation of Ammonia in Oxygen-Containing Systems
D. T. Reed, V. Swayambunathan, and R. A. Van Konynenburg
To be published in Radiat. Phys. Chem.

Ab Initio MO Calculations of High Temperature Gaseous Fluorine Complexes $MAlF_4$ (M = H, Li, Na): A Comparative Study Using Different Basis Sets
G. Scholz and L. A. Curtiss
To be published in Theochem.

Boron-Lithium Relationships in Rhyolites and Associated Thermal Waters of Young Silicic Calderas
D. M. Shaw and N. C. Sturchio
To be published in Geochim. Cosmochim. Acta

The Heat of Formation of Formaldimine
B. J. Smith, J. A. Pople, L. A. Curtiss, and L. Radom
To be published in Aust. J. Chem.

Radium Geochemistry and Isotopy of Thermal Waters, Yellowstone National Park, Wyoming
N. C. Sturchio, J. K. Bohlke, and F. Markun
To be published in Geochim. Cosmochim. Acta

X-ray Reflectivity Study of the Copper/Water Interface in a Transmission Geometry under In-Situ Electrochemical Control

H. You, C. A. Melendres, Z. Nagy, V. A. Maroni, W. Yun, and R. M. Yonco

To be published in Phys. Rev. B

X-ray Reflectivity Studies of the Metal/Solution Interphase

H. You, Z. Nagy, C. A. Melendres, D. J. Zurawski, R. P. Chiarello, R. M. Yonco, H. K. Kim, and V. A. Maroni

To be published in *X-ray Methods in Corrosion and Interfacial Electrochemistry*, eds., A. J. Davenport and J. G. Gordon, The Electrochemical Soc. Softbound Proc. Ser., Pennington, NJ

Distribution for ANL-92/15

Internal:

J. P. Ackerman
J. G. Asbury
J. K. Bates
J. E. Battles
N. J. Beskid
P. R. Betten (5)
M. Blander
I. D. Bloom
A. S. Boparai
R. L. Breyne
F. A. Cafasso
E. L. Carls
D. J. Chaiko
D. B. Chamberlain
Y. I. Chang
C. C. Christianson
J. C. Cunnane
D. W. Dees
W. H. DeLuca
H. Drucker
B. D. Dunlap
W. L. Ebert
M. D. Erickson
F. Y. Fradin
S. D. Gabelnick
E. C. Gay
T. J. Gerding
D. G. Graczyk
D. W. Green
D. M. Gruen
J. E. Harmon (2)
R. R. Heinrich
J. E. Helt
G. L. Henriksen
C. E. Johnson
T. R. Johnson
T. D. Kaun
T. R. Krause
M. Krumpelt
G. H. Kucera
R. Kumar
J. R. LaFevers
J. Laidler
S. H. D. Lee
L. Leibowitz
R. A. Leonard
M. A. Lewis
P. C. Lindahl
M. J. Lineberry
R. F. Malecha
V. A. Maroni
C. C. McPheeters
J. F. Miller
W. E. Miller
K. M. Myles
P. A. Nelson
R. D. Pierce
J. W. Rathke
L. Redey
D. T. Reed
D. K. Schmalzer
A. Schriesheim
W. B. Seefeldt
M. A. Slawecki
J. A. Smaga
D. L. Smith
M. J. Steindler (100)
L. M. Stock
N. C. Sturchio
W. M. Swift
S.-W. Tam
C. E. Till
Z. Tomczuk
G. F. Vandegrift
D. R. Vissers
S. Vogler
D. C. Wade
L. C. Walters
R. W. Weeks
C. L. Wilkinson
J. L. Willit
R. D. Wolson
ANL Patent Dept.
ANL Contract File
TIS Files (3)

External:

DOE-OSTI, for distribution per UC-400 and -500 (107)
ANL Libraries (2)
Manager, Chicago Operations Office, DOE
D. L. Bray, DOE-CH
J. Haugen, DOE-CH
J. O. Hunze, DOE-CH
A. L. Taboas, DOE-CH/AAO

Chemical Technology Division Review Committee Members:
S. Baron, Brookhaven National Laboratory, Upton, NY
D. L. Douglas, Consultant, Bloomington, MN
N. Jarrett, Noel Jarrett Associates, Lower Burrell, PA
J. G. Kay, Drexel University, Philadelphia, PA
J. Stringer, Electric Power Research Institute, Palo Alto, CA
J. B. Wagner, Arizona State University, Tempe, AZ
R. G. Wymer, Oak Ridge National Laboratory, Oak Ridge, TN
R. D. Alkire, University of Illinois, Urbana, IL
K. F. Barber, USDOE, Div. of Electric and Hybrid Propulsion, Washington, DC
J. Batchelor, USDOE, Office of Fossil Energy, Germantown, MD
T. F. Bechtel, USDOE, Morgantown Energy Technology Center, Morgantown, WV
D. N. Bennion, Brigham Young University, Provo, UT
S. E. Berk, USDOE, Office of Fusion Energy, Germantown, MD
E. Beyma, USDOE, Office of Fossil Energy, Germantown, MD
J. R. Birk, Electric Power Research Institute, Palo Alto, CA
D. F. Bowersox, Los Alamos National Laboratory, Los Alamos, NM
J. Braunstein, Oak Ridge National Laboratory, Oak Ridge, TN
J. J. Brogan, USDOE, Div. of Energy Utilization Research, Washington, DC
S. A. Butter, USDOE, Office of Basic Energy Sciences, Washington, DC
E. J. Cairns, Lawrence Berkeley Laboratory, Berkeley, CA
M. H. Campbell, Westinghouse Hanford Co., Richland, WA
K. A. Chacey, USDOE, Office of Waste Management, Germantown, MD
A. A. Chesnes, USDOE, Office of Conservation and Renewable Energy, Washington, DC
S. W. Chun, USDOE, Pittsburgh Energy Technology Center, Pittsburgh, PA
M. O. Cloninger, Yucca Mountain Project Office, Las Vegas, NV
S. P. Cowan, USDOE, Office of Waste Operations, Germantown, MD
J. Cuttica, Gas Research Institute, Chicago, IL
H. T. Davis, University of Minnesota, Minneapolis, MN
M. C. Dionisio, USDOE, Office of Technology Development, Washington, DC
E. Dowgiallo, USDOE, Office of Transportation Technologies, Washington, DC
M. Duff, USDOE, Office of Waste Operations, Germantown, MD
L. P. Duffy, USDOE, Office of Environmental Restoration, Washington, DC
H. Feibus, USDOE, Office of Fossil Energy, Germantown, MD
A. P. Fickett, Electric Power Research Institute, Palo Alto, CA
C. W. Frank, USDOE, Office of Technology Development, Germantown, MD
E. Gillis, Electric Power Research Institute, Palo Alto, CA
R. Goldstein, Electric Power Research Institute, Palo Alto, CA
Government Documents Department, University of California, Berkeley, CA
R. Guidotti, Sandia National Laboratories, Albuquerque, NM
K. Hain, USDOE, Office of Technology Development, Germantown, MD
K. L. Heitner, USDOE, Office of Transportation Technologies, Washington, DC
D. Hooie, USDOE, Morgantown Energy Technology Center, Morgantown, WV
W. Huber, USDOE, Morgantown Energy Technology Center, Morgantown, WV
G. L. Hunt, EG&G Idaho, Inc., Idaho Falls, ID
L. C. Ianniello, USDOE, Office of Basic Energy Sciences, Germantown, MD

L. J. Jardine, Lawrence Livermore National Laboratory, Livermore, CA
E. F. Johnson, Princeton University, Princeton, NJ
R. D. Kelley, USDOE, Office of Basic Energy Sciences, Germantown, MD
J. J. Kelly, Electrodex Laboratories, Inc., Willingboro, NJ
R. Kost, USDOE, Div. of Electric and Hybrid Propulsion, Washington, DC
A. R. Landgrebe, USDOE, Advanced Utility Concepts Division, Washington, DC
M. Lankford, USDOE, Office of Technology Development, Washington, DC
B. Lee, Institute of Gas Technology, Chicago, IL
L. Little, USDOE, Nevada Operations Office, Las Vegas, NV
J. E. Lytle, USDOE, Office of Waste Management, Washington, DC
N. J. Magnani, Sandia National Laboratories, Albuquerque, NM
M. J. Mayfield, USDOE, Morgantown Energy Technology Center, Morgantown, WV
F. R. McLarnon, Lawrence Berkeley Laboratory, Berkeley, CA
L. G. O'Connell, Electric Power Research Institute, Palo Alto, CA
R. A. Osteryoung, State University of New York, Buffalo, NY
P. G. Patil, USDOE, Div. of Electric and Hybrid Propulsion, Washington, DC
G. Patton, USDOE, Office of Technology Development, Washington, DC
C. E. Pax, USDOE, Office of Fossil Energy, Germantown, MD
L. Petrakis, Brookhaven National Laboratory, Upton, NY
S. T. Picraux, Sandia National Laboratories, Albuquerque, NM
W. M. Polansky, USDOE, Office of Basic Energy Sciences, Germantown, MD
R. Price, USDOE, Office of Fusion Energy, Germantown, MD
G. Rudins, USDOE, Office of Fossil Energy, Germantown, MD
A. J. Salkind, Rutgers University, Piscataway, NJ
L. A. Salvador, USDOE, Morgantown Energy Technology Center, Morgantown, WV
R. L. San Martin, USDOE, Renewable Energy, Washington, DC
P. S. Schaus, Westinghouse Hanford Co., Richland, WA
L. H. Schwartz, National Institute of Standards and Technology, Gaithersburg, MD
A. W. Searcy, Lawrence Berkeley Laboratory, Berkeley, CA
R. Sehgal, Electric Power Research Institute, Palo Alto, CA
R. W. Shivers, USDOE, Office of Conservation, Washington, DC
J. S. Siegel, USDOE, Office of Fossil Energy, Germantown, MD
W. A. Siegel, USDOE, Div. of Electric and Hybrid Propulsion, Washington, DC
M. I. Singer, USDOE, Office of Fossil Energy, Germantown, MD
F. D. Stevenson, USDOE, Office of Basic Energy Sciences, Germantown, MD
J. P. Strakey, USDOE, Pittsburgh Energy Technology Center, Pittsburgh, PA
R. Swaroop, Electric Power Research Institute, Palo Alto, CA
G. P. Turi, USDOE, Office of Environmental Restoration, Germantown, MD
J. A. Turi, USDOE, Office of Waste Operations, Germantown, MD
G. E. Voelker, USDOE, Office of Technology Development, Washington, DC
G. Weiner, Westinghouse Research Labs., Pittsburgh, PA
M. P. Whelan, Gas Research Institute, Chicago, IL
R. P. Whitfield, USDOE, Office of Environmental Restoration, Washington, DC
B. Wilcox, Defense Advanced Research Projects Agency, Arlington, VA
K. Yeager, Electric Power Research Institute, Palo Alto, CA
M. Tokiwai, CRIEPI FBR Division, Tokyo, JAPAN

END

DATE FILMED

7/2/92